Preparing Main Group Metal Clusters from Organoaluminium Reagents; New Possibilities in Alkali Activated Polymer-Crosslinking

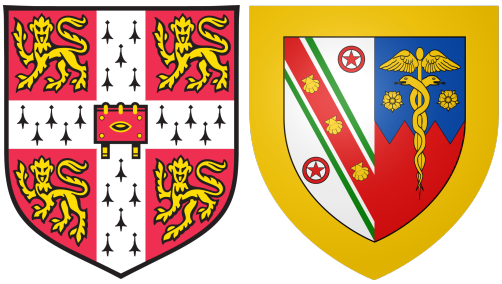

University of Cambridge

Department of Chemistry

Thea-Luise Precht

Darwin College

This dissertation is submitted for the degree of

Doctor of Philosophy

June 2018

Preparing Main Group Metal Clusters from Organoaluminium Reagents; New Possibilities in Alkali Activated Polymer-Crosslinking

Thea-Luise Precht, Department of Chemistry, University of Cambridge

The reactions of carboxylic acids with organoaluminium reagents were studied, which led to the formation of novel aluminium compounds. The reactions of ortho-functionalised derivatives of benzoic acid with trivalent aluminium organyls AlR_3, led to the formation of different Al-based molecular clusters, depending on the nature of R, the reaction stoichiometry and the character of the benzoic acid derivative. The obtained compounds were characterised in the solid state by X-ray diffraction methods and two main motifs were observed. When the acid and AlR_3 reacted in a one-to-two stoichiometry the obtained products, $[^{i}Bu_4Al_2(\mu\text{-}O_2CC_6H_4\text{-}2\text{-}\mu\text{-}O)]_2$, $[(Me_2Al)_2(\mu\text{-}O_2CC_6H_4\text{-}2\text{-}\mu\text{-}NH)]_2$, $[(^{i}Bu_2Al)_2(\mu\text{-}O_2CC_6H_4\text{-}2\text{-}\mu\text{-}NH)]_2$, $[(Me_2Al)_2(\mu\text{-}O_2CC_6H_4\text{-}2\text{-}\mu\text{-}NMe)]_2$ and $[(^{i}Bu_2Al)_2(\mu\text{-}O_2CC_6H_4\text{-}2\text{-}\mu\text{-}NMe)]_2$, consisted of a central distorted 12-membered macrocycle, formed by two [Al-O-C-O-Al-X] units (X= O,N) and was found to be dimeric. The reaction between anthranilic acid derivatives and AlR_3 could also take place in a one-to-one ratio. For anthranilic acid and N-methylanthranilic acid the obtained crystals only allowed a qualitative analysis and showed the structure of the products, $[MeAl(\mu\text{-}O_2CC_6H_4\text{-}2\text{-}\mu\text{-}NH)]_4$, $[^{i}BuAl(\mu\text{-}O_2CC_6H_4\text{-}2\text{-}\mu\text{-}NMe)]_4$ to be tetrameric and each consisting of a distorted 16-membered ring formed by four [O-C-O-Al] units. With the reaction of N-phenylanthranilic acid it was possible to isolate a structural analogous product $[^{i}BuAl(\mu\text{-}O_2CC_6H_4\text{-}2\text{-}\mu\text{-}NPh)]_4$ which could be fully characterised by x-ray crystallography and NMR spectroscopy. Where the quantity and quality of the obtained product was sufficient, the solution behaviour of the compounds was elucidated by multinuclear and multidimensional NMR spectroscopic techniques. The ^{27}Al NMR showed that the aforementioned aggregates are maintained in solution, which for the 12-membered [Al-O-C-O-Al-N] macrocycle of $[(^{i}Bu_2Al)_2(\mu\text{-}O_2CC_6H_4\text{-}2\text{-}\mu\text{-}NH)]_2$ was confirmed by a NOESY spectrum.

The second part of this project focused on the preliminary studies towards the application of aluminium compounds in the crosslinking of guar and carboxymethyl hydroxypropyl guar, which are common additives in hydraulic fracturing. Different commercially available aluminium compounds were tested for their general ability to crosslink the aforementioned polysaccharides, yielding promising results for alu-

minium lactate, aluminium acetylacetonate and aluminium isopropoxide. For the system comprising aluminium lactate in combination with CMHPG, rheological studies were carried out to determine the viscosity, the viscoelasticity, the shear recovery and the stability towards high temperatures. These sought to evaluate the crosslinking properties of the aluminium additive and to optimise the required conditions of the different system components. Finally, it was possible to obtain first proof-of-concept data suggesting that synthetically obtained aluminium compounds such as $[Me_2Al(\mu\text{-}O_2CPh)]_2$ and $Al[MeC(CH_2O)_3]_2(AlMe_2)_3$ can be employed for the crosslinking of guar and CMHPG.

Declaration

The work described in this thesis was carried out in the Department of Chemistry, University of Cambridge, under the supervision of Dr. Andrew Wheatley, between January 2014 and December 2017.

This dissertation is the result of my own work and includes nothing which is the outcome of work done in collaboration except as declared in the Preface and specified in the text.

It is not substantially the same as any that I have submitted, or, is being concurrently submitted for a degree or diploma or other qualification at the University of Cambridge or any other University or similar institution except as declared in the Preface and specified in the text or acknowledgments. I further state that no substantial part of my dissertation has already been submitted, or, is being concurrently submitted for any such degree, diploma or other qualification at the University of Cambridge or any other University or similar institution except as declared in the Preface/acknowledgements and specified in the text

This thesis does not exceed 60,000 words.

The views expressed in this thesis are those of the author and not the University.

Acknowledgements

I wish to thank Dr. Andrew Wheatley for giving me the opportunity to work in his group and for the interesting research topic and also Prof. Dominic Wright for the co-supervision of my project and the numerous ideas provided.

Furthermore I wish to thank Schlumberger Gould Research Cambridge for funding the project and Gary Tustin and Seth Hartshorne especially for the support during my first year and Isabelle Atheaux for the help with the rheology experiments.

Thanks to Dr. Nick Bampos and Prof. Janusz Lewiński for examining this dissertation.

Thanks go to Dr. Andrew Peel and Dr. Andrew Bond for the help with the crystallography.

Thanks to everyone at Darwin College for being a great and welcoming community and to the DCSA committees of 2014 and 2016.

A huge thank you to everyone from Darwin College Boat Club who rowed with me or coxed me in the past three years or who I had the pleasure of coaching. Although, as a friend once said, we are only rowing for the social aspects, I have to say in the end I enjoyed the early mornings, the long ergs, the defeats and the victories and most of all the friendships.

Thanks to all the wonderful colleagues on the third floor for making the lab a great place to work in and for countless coffee breaks.

I would like to thank all my wonderful friends who, even when they accompanied me for only a short time during my PhD, made a great difference. There are too many to mention and I will thank each and every one of you in person.

The biggest thanks go to my Family. Thank you for always believing in me and even more important thank you for teaching me to believe in myself.

Contents

List of Schemes

List of Figures

List of Tables

Abbreviations

3c2e	three-center-two-electrons
A	Surface area
A^*	constant related to molecular motion
a, b, c	unit cell lengths
Ac	acetyl
acac	acetylacetonate
Ar	aryl group
BHT	bottom hole temperature
BINOL	1,1′-Bi-2-naphthol
Bu	butyl
CMHPG	carboxymethyl hydroxypropyl guar
COSHH	Care of Substances Hazardous to Health
Cp	cyclopentadienyl
CVD	chemical vapour deposition
Cy	cyclohexyl
d	doublet
DABA	3,5-diaminobenzoic acid
DCM	dichloromethane
DiBAl-H	diisobutylaluminium hydride
Dipp	2,6-diisopropylphenyl
DMF	N,N-dimethyl formamide
dpt	1,3-triphenyltriazene
E^0	standard electronic potential
E_a	Activation energy
Et	ethyl
F	Force
f	Frequency
FLP	Frustrated Lewis Pair
G	Shear module
G′	Elastic module
G″	Viscous module
GoF	goodness of fite

Hal	halogen
hacet	2'-hydroxyacetophenone
Hz	Hertz
HPG	hydroxypropyl guar
iPP	isotactic polypropylene
lac	lactate
m	mass
LVER	Linear viscoelastic regime
MAO	methylaluminoxane
Me	methyl
Mes	mesityl
mu	multiplet
M_W	molecular weight
NMR	Nuclear Magnetic Resonance
OLED	organic light-emitting diode
PE	polyethylene
Ph	phenyl
ppm	parts per million
Pr	propyl
Py	pyridine
R	general organic group
R_1	R-factor (unweighted)
REACH	registration, evaluation, authorisation and restriction of chemicals
R_{int}	merging R factor
RT	product of gas constant and temperature T
S	goodness of fit
singlet	Singlet
T	temperature
t	triplet
^{t}Bu	*tert*-butyl
TEA	triethylalumnium
THF	tetrahydrofurane
TiBA	triisobutylaluminium
TMA	trimethylaluminium

TMEDA	N,N,N′,N′-tetramethyldiethylenediamine
TMS	tetramethylsilane ($Si(CH_3)_4$)
V	Volume
XRD	x-ray diffraction
Z	number of formula units per unit cell
α, β, γ	unit cell angles
δ	chemical shift
γ	Shear rate
$\dot{\gamma}$	shear strain
λ	wavelength
η	Shear viscosity
τ	shear stress
τ_1	mixing time
ωR_2	R-factor (weighted)

1 Aim of Project

The aim of this project is the investigation of aluminium compounds and complexes for their use in biopolymer crosslinking. The crosslinking process is important for a range of oil field applications, especially hydraulic fracturing. In this process, also known as fracking, a special liquid is injected in to a wellbore to crack rock and obtain natural gas or petroleum. The fracturing liquid needs to have a certain viscosity to ensure an effective process. Currently this is achieved by the addition of guar or synthetic derivatives like CMHPG to the fracking fluid. Supplementary crosslinkers are added to increase the viscosity of the gel as required. The most common crosslinkers currently in use are based on borate, however, borates are known to have negative effects on the ecological system and environment. Furthermore animal studies have shown that these crosslinkers can be harmful to human health, interfering with reproductive processes.[1]

This project aims to investigate aluminium compounds as a more sustainable alternative for the crosslinking process by using the well known amphoteric behaviour of aluminium and the switching from Al-OH_2 $\longrightarrow$ Al-OH $\longrightarrow$ Al-O-Al bonding that occurs as a function of increasing pH values. The synthesis of suitable aluminium compounds which can be tuned to varying requirements of different hydraulic fracturing problems can provide new opportunities for crosslinking.

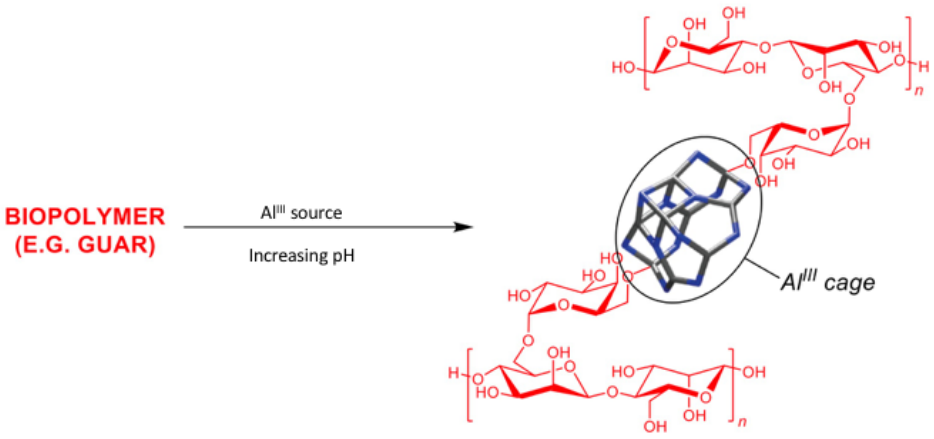

Figure 1: The aim of the project is to establish aluminium compounds as crosslinking agents for polymers like guar or CMHPG.

2 Theoretical Background

2.1 Aluminium Chemistry

2.1.1 Aluminium Organic Chemistry

2.1.1.1 Bonding motifs in Aluminium Organic Compounds

Organometallic compounds are an indispensable part of our world. Many modern-day processes in material science depend on organometallic reagents[2], either as building blocks (for example in metal organic vapour deposition[3]) or as catalysts in the production of modern materials (such as polyethene)[4]. Furthermore, metal catalysed reactions such as the Suzuki coupling are an important tool in synthetic pharmaceutical and agricultural chemistry.[5]

In the narrowest definition, organometallic compounds contain at least one metal-carbon bond and the most obvious way to categorise these compounds is the nature of the metal, as shown in Figure 2. Transition metals and actinides can bind to the carbon via multiple bonds which consist of σ- and π-bonds. Their chemistry is influenced by the π-back donation through the metal or the π-accepting abilities of the ligand. Main group and d^{10}-metals, on the other hand, reveal a range of different bonding schemes, such as ionogenic bonding, electron deficiency and covalent σ-M-C bonds.[6] Other methods to distinguish between different organometallic compounds are their structural motifs, (*e.g.* sandwich complexes, carbenes) or the electronic configuration.[7]

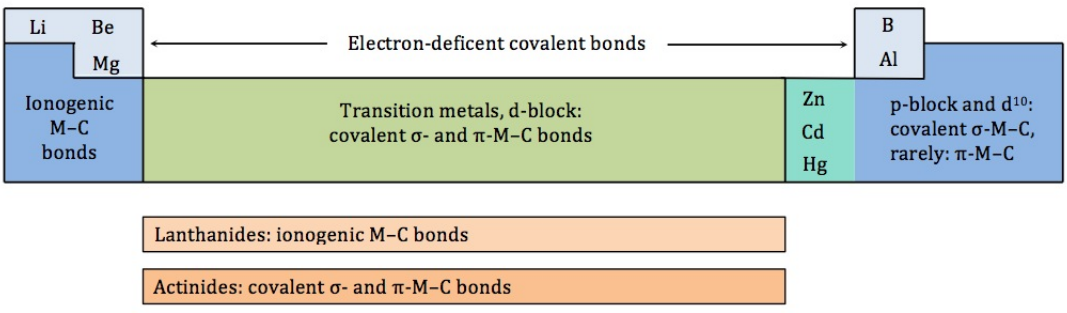

Figure 2: Character of M—C bonds for different metals.

Scheme 1 shows different aluminium organyls. The most common species are alanes (c), derived from the trivalent aluminium.[8][9] These will be the main focus of this thesis. However, other lower valent aluminium organyls have been studied. The best example for such a low valent organyl in the +1 oxidation state is $AlCp^*$, which forms a tetramer $Al_4Cp^*_4$ in the solid state, but is a monomer in the gas phase.[10][11] The alanyl radical (b) is not very well studied thus far but can be generated by stabilisation with electron donors such as NMe_3. The resulting radical $(Me_3N)_2\dot{A}lH_2$ is isoelectronic with the phosphoranyl radical $(Me_3C)_2\dot{P}H_2$ and adopts a quasi-trigonal bipyramidal structure.[12] The alanyl cation (d) is equally rare. One of the few examples in the literature was reported by Young *et al.* with the synthesis and characterisation of $[(2,6-Mes_2C_6H_3)_2Al]^+[B(C_6F_5)_4]^-$.[13][14] One example of a higher valence in aluminium compounds is the aluminate (e), which is formed as an alane adduct with organic donors or are inorganic compounds such as lithium aluminium hydride $LiAlH_4$ and its derivatives.[15][16][17]

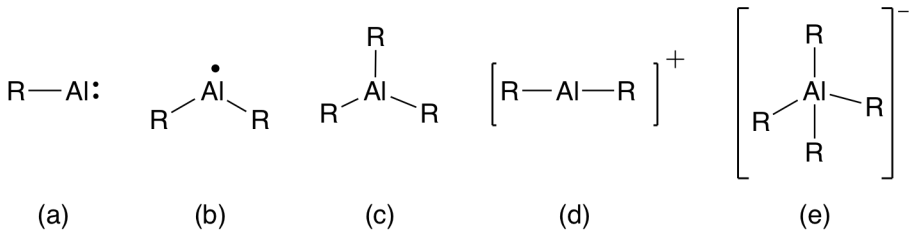

Scheme 1: Aluminium organyls of different valencies (R=organic or inorganic residue or donor).

Aluminium compounds with monovalent groups of the formula AlX_3 consist of an electron sextet and show a relatively low tendency to form π-bonds. Therefore, many of these compounds undergo oligomerisation to gain intermolecular valence stabilisation by the formation of three-centre-two-electron bonds (3c2e). The degree of oligomerisation is dependent on the size and nature of X. Since aluminium prefers octahedral coordination, $AlCl_3$ is polymeric, with each Al atom participating in six halogen bridges. However, for the larger halogenides $AlBr_3$ and AlI_3, this is not possible due to steric reasons, resulting in the formation of dimers.[18][19][20] Corresponding effects are observed for aluminium organyls AlR_3. The most simple one, $AlMe_3$, forms a dimer in

both the solid state and in hydrocarbon solution and dissociates only in the gas phase at high temperatures (Equation 1).[21][22]

$$(AlMe_3)_2 \rightleftharpoons 2\,AlMe_3 \quad \Delta H = 82.9\text{kJ} \tag{1}$$

Equally, for steric reasons, the tendency to form dimers varies with the steric demand of the organic residue: $AlPh_3$ is dimeric in the solid phase, monomeric in the gas phase, and shows a mixture of monomers and dimers in solution[23] whereas Al^iBu_3 is dimeric in the solid state but mostly monomeric in solution.[24] Furthermore, alane derivatives with the formula R_2AlX and $RAlX_2$ form dimers or trimers with Al-X-Al bridges depending on the sizes of R and X (with X= H, R, Hal, OR or NR_2). The tendency to form the respective Al-X-Al bridges decreases along the series NR_2 > OR > Cl > Br > Ph > Me > Et > ^{i}Bu > ^{i}Pr > ^{t}Bu.[6][21] The bonding mechanism of these bridges can be described as the interaction between one sp^3 orbital of each participating Al atom and one or two orbitals of the bridging ligand to form the 3c2e-bond. Scheme 2 shows the corresponding MO scheme for the example of $AlMe_3$. Due to the formation of two anti-bonding, two non-bonding, and two filled bonding orbitals the dimeric species is no longer an electron deficient compound.

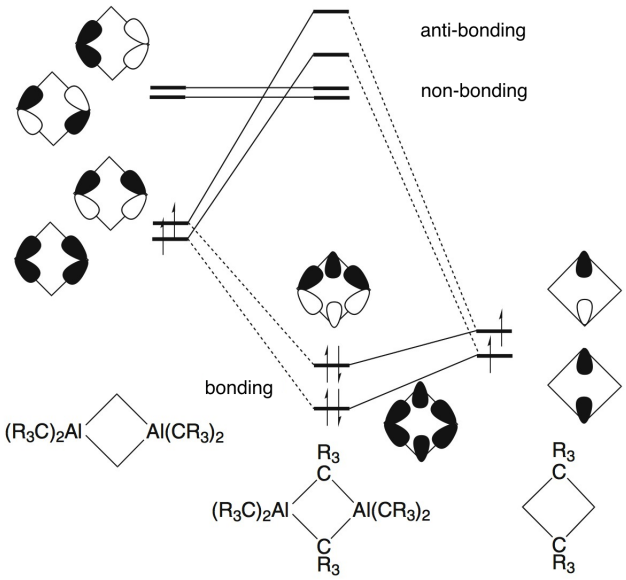

Scheme 2: MO scheme for the formation of $(AlR_3)_2$.[6]

The steric demands of the aluminium substituents also influence the bonding angles in the dimer. Scheme 3 compares the structures of $(AlMe_3)_2$ and $(AlPh_3)_2$. In

$(AlPh_3)_2$, the Ph plane is perpendicular to the aluminium axis and in comparison to $(AlMe_3)_2$ which is bridged by a sp^3 orbital of the methyl group, here the phenyl group contributes two σ-orbitals to the Al-C-Al bridge.

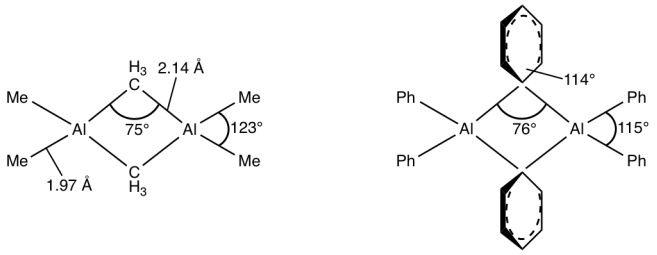

Scheme 3: Comparison of the bridged species $(AlMe_3)_2$ and $(AlPh_3)_2$.[21]

Trivalent aluminium organyls readily form adducts with Lewis bases by donation of an electron pair into the empty 2p orbital of the metal, leading to a four-coordinated Al centre of the type R_3AlL. One known exemption is the reaction of $AlMe_3$ with an excess of the sulfur crown ether [12]aneS_4, which yields a five-coordinated adduct of the type Me_3AlL_2 and trigonal bipyramidal metal centre.[25][26]

In contrast to the aforementioned electron deficient bonding, penta-coordinated aluminium complexes show electron rich hypervalent bonding from the interaction of the vacant 2p orbital of the aluminium with two lone pair electrons from the apical ligands. This leads to a linear three-centre-four-electron bonding (3c4e).[25][27][28]

2.1.1.2 Ziegler-Natta Chemistry

The interest in aluminium organic compounds increased significantly when it was discovered by Ziegler *et al.* that unlike magnesium or lithium organyls the reactivity of alanes increases in ether[29][30] and that aluminium organyls are able to donate hydroaluminium, dehydroaluminium and carbaluminium groups to other molecules. This is used in the polymerisation of olefins[31], which resulted in the awarding of the 1963 Nobel Prize in chemistry to Karl Ziegler and Giulio Natta. To date, this is still one of the most important processes in polymer chemistry.[4][32][33]

Ziegler extensively studied the chemistry of aluminium organyls as well as the polymerisation of olefins. The outcomes of these studies are now known as *Ziegler Chemistry*.[34] Ethylene and TEA react in the absence of any transition metals, exhibiting

a chain growth mechanism that yields alkyl chains with even numbers of carbon and medium molecular weights. Under the right conditions, approx. 70°C and 35 bar, β-elimination occurs, leading to the formation of α-olefins (see Scheme 4).[31][35] The resulting aluminium hydride species can undergo further insertion reactions. If the

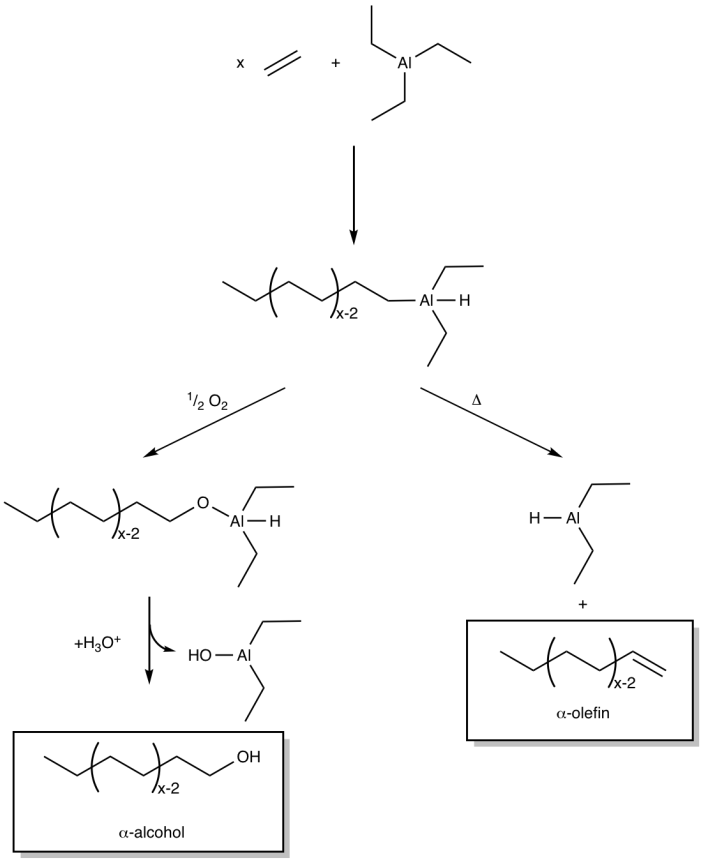

Scheme 4: Two possible reaction pathways for the reaction of $x\,H_2C{=}CH_2$ and $Al(C_2H_5)_3$, which can lead to different products, depending on the conditions. After the first step of the growth process the product can react with oxygen to form α-alcohols or under increased pressure release α-olefines.[4]

aluminium-alkyl adduct is oxidised and hydrolysed, the products are α-alcohols (or *fatty alcohols*) which are important for a number of applications in polymers, surfactants, oil additives, and cosmetics.[36][34] The 2005 production capacity of fatty alcohols was estimated to be $2.5{\cdot}10^6$ tons. Moreover, the byproducts of this process are aluminium hydroxides and oxides, which are valuable resources for the chemical industry as starting materials for hydrogels and composites or as pigments for paints.[36][37]

For his experiments, Ziegler used nickel autoclaves. These were cleaned with sulfuric acid, which leads to the desolvation and deposition of nickel cations on the surface

of the autoclave. The presence of nickel during the experiments resulted not in polymerisation but dimerisation of ethylene, yielding 1-butene.[38][39] Today this effect is known as the *nickel effect*. It prompted Ziegler to further investigate the influence of transition metals on the growth mechanism, leading to the development of the Ziegler-Natta catalyst. In the broadest definition, this catalyst is the combination of a transition metal from groups 3-12 with an organometallic co-catalyst from groups 1, 2 or 13. Ziegler's studies showed that titanium tetrachloride ($TiCl_4$) and TEA give rise to polymers with high molecular weights. In the past decades the conditions have been varied and optimised, but the basic principle is still in use. Although the mechanism has been intensively studied for years it is not fully understood. That said, a now widely accepted mechanism based on molecular calculations was published in 1964 by Cossee and Arlman.[40][41][42] The Ziegler-Natta catalysts can be divided into two classes:[4] On the one hand, there are heterogeneous catalysts, e.g. $TiCl_4$ with TEA as a cocatalyst, with both reagents supported on solid $MgCl_2$. The mechanism for this process is shown in Scheme 5. It is used for the polymerisation of propylene and most higher 1-alkenes. The homogeneous catalysts, on the other hand, typically consists

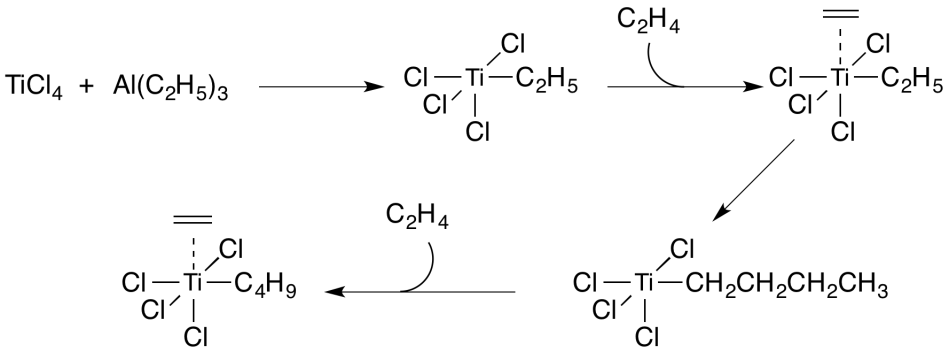

Scheme 5: The role of TEA within heterogeneous Ziegler-Natta catalysis.

of metallocenes with a composition such as Cp_2MCl_2. These metallocenes also need to be activated by a cocatalyst, e.g. methylalumoxane (MAO) to give $Cp_2M^+–CH_3$.[43] In the following step, a 1-alkene can insert into the M-C bond to grow the polymer, with a mechanism similar to that of the heterogeneous reaction. Furthermore, within the class of homogeneous catalytic systems, there is a class of non-metallocene catalysts. These also use MAO as an activator, but the actual catalyst can be from a broad variety of metal complexes based on, e.g. actinides or lanthanides.[44][45]

2.1.1.3 Methylalumoxanes

In the classic Ziegler-Natta process, aluminium triorganyls were used to activate the catalyst. However, in 1976 Kaminsky *et al.* reported that TMA which had been treated with water caused a significant increase in yield and activity for polymerisation reactions when used with Cp_2TiCl_2. They studied various aluminium to water ratios and found that maximal activity was reached for aluminium:H_2O 2:1-5:1. Conversely, inactivity was found for the ratio 1:3, at which point all methyl groups had been hydrolysed. The then newly discovered MAO was also able to activate Cp_2ZrCl_2, which even when fully dehalogenated and treated with TMA or TiBA, did not show any catalytic activity towards olefin polymerisation.[46] Catalysts consisting of metallocenes from group 4 (Ti, Zr, Hf) and MAO are now known as *Kaminsky catalysts*.[47][48]

Since Kaminsky's discovery, the chemical industry adopted MAO and its derivatives as a useful resource.[49] However, its structure has never been fully characterised. MAO has the general formula $(Al(CH_3)O)_n$ and is synthesised by the controlled hydrolysis of TMA in apolar solvents, using a hydrated salt as the H_2O-source, e.g. $CuSO_4 \cdot 5\,H_2O$, $Al_2(SO_4)_3 \cdot 15\,H_2O$. Depending on the reaction conditions and starting materials the composition and structure will vary. Furthermore, there are equilibria between free and associated TMA present within the MAO structure (Equation 2).[43]

$$-[\mathrm{Al(Me)O}]_{\mathrm{n}}- \cdot \mathrm{xAlMe_3} \rightleftharpoons -[\mathrm{Al(Me)O}]_{\mathrm{n}}- \cdot \mathrm{(x\text{-}y)AlMe_3} + \mathrm{yAlMe_3} \qquad (2)$$

Many publications suggest structures for MAO.[50][51][52][53][54] NMR-studies have shown the presence of three- and four-coordinated aluminium centres.[51][55][53] Some of the proposed structures for MAO are shown in Scheme 6. The structures include linear chains (**a**), cyclic one-dimensional arrangements (**b**), two-dimensional structures (**c**), or three-dimensional clusters (**d**), as reported by Sinn *et al.* Structure (**e**) is based on a *tert*-butylalumoxane, which, due to the sterically more demanding *tert*-butyl groups, could be crystallised and analysed crystallographically using x-ray diffraction.[56][45][57] $[Al_4O_3(CH_3)_6]_4$ (**d**) shows a methyl:aluminium ratio of approximately 3:2. This corresponds with the general formula $[AlO_{0.8-0.75}(CH_3)_{1.4-1.5}]_n$ reported by researchers from Albemarle *Corp.* based on ^{1}H-NMR measurements.[58]

Due to the aforementioned equilibria between free and associated TMA (Equation 2) different structures of MAO, such as the types represented by **(a)**, **(b)** and **(c)** can also be interconverted, making it more complex to gain structural insights about the system.[45] [43] [59] [52] [46]

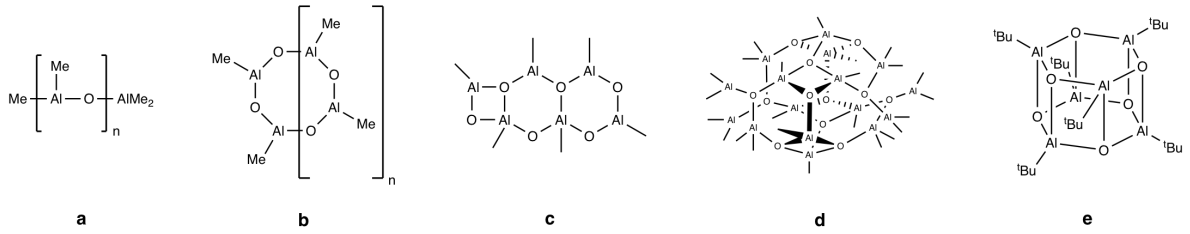

Scheme 6: Proposed structural motifs for alumoxanes, based on spectroscopic data and calculations .[45] [53] [54]

Studies by Zijlstra *et al.* showed that MAO oligomers can undergo ageing processes. If exposed to oxygen free $AlMe_3$ reacts with O_2 to form Me_2AlOMe which is slowly incorporated into the oligomeric structure.[60] Furthermore MAO of low average M_W is over time slowly converted to higher oligomers through an ageing process. MAO is ionised by the loss of $[Me_2Al]^+$ and the remaining anions react with MAO oligomers to yield high M_W clusters. The same ionisation is observed for oxidised MAO and the abstraction of $[Me_2Al]^+$ is favoured by the presence of weak donor molecules.[60] [61]

2.1.1.4 Further Applications of Aluminium Organic Compounds

Apart from polymer chemistry, homoleptic aluminium organyls are, for example, used in materials chemistry for the production of III/V semiconductors (consisting of group 13 and 15 elements).[62] [63] Many of these materials are generated by the CVD of organometallic precursors, such as TMA or TiBA[64], resulting e.g. in aluminium nitride (AlN) and aluminium gallium nitride (AlGaN) films.[65] The band gaps of these compounds at room temperature are wider than those of typical silicon semiconductors (1.1 eV)[66]: AlN has a band gap of 6.2 eV[67] and the band gap of AlGaN can be tuned between 3.4-6.1 eV depending on the composition.[68] These ultra-wide band gap semiconductors are commonly used in optoelectronic devices.[69]

In synthetic chemistry aluminium organyls are used, e.g. in the methylenation of carbonyls with Tebbe's reagent[70] [71] [72] and in the preparation of designer Lewis

acids, such as aluminum tris(2,6-diphenylphenoxide) and methylaluminum bis(2,6-di-tert-butyl-4methylphenoxide), which can be applied in stereoselective synthesis, e.g. in Diels-Alder reactions.[73][74][75]

Furthermore, trimethylaluminium is used as a tracer molecule in geophysics to study wind patterns. To do this, TMA is released by sounding rockets into the atmosphere. Upon reacting with oxygen it creates a chemoluminescence event which can be tracked photographically for 5-10 minutes. Using a stellar background and photographs from at least two different sites the location and movement of winds can be studied.[76]

2.1.1.5 Synthesis and Production of Aluminium Organic Compounds

The industrial production of aluminium starts from pure aluminium oxide, Al_2O_3, which is extracted from bauxite. The Al_2O_3 is subjected to a melt electrolysis to produce the metal. Aluminium chloride is not suitable for electrolysis (it does not conduct electricity) and neither are aqueous aluminium salts due to the strongly negative deposition potential of aluminium (ε_0 = -1.662 V).[21]

The first aluminium organic compound was synthesised by Hallwachs and Schafarite in 1859 (Equation 3)[77] and the first aluminium triorganyl by Buckton and Odling in 1865 (Equation 4).[78]

$$2\,\mathrm{Al} + 3\,\mathrm{EtI} \longrightarrow \mathrm{Et_3Al_2I_3} \tag{3}$$

$$2\,\mathrm{Al} + 3\,\mathrm{HgR_2} \longrightarrow 2\,\mathrm{AlR_3} + \mathrm{Hg} \tag{4}$$

Given the high commercial availability of aluminium organyls, the preparation of homoleptic aluminium compounds at a laboratory scale is seldom required but can be achieved either by transmetallation, for example with diphenyl mercury (Reaction 5), or by metathesis of aluminium trichloride with lithium organyls or Grignard reagents (Reaction 6).[21][79]

$$2\,\mathrm{Al} + 3\,\mathrm{HgPh_2} \longrightarrow 2\,\mathrm{AlPh_3} + 3\,\mathrm{Hg} \tag{5}$$

$$\mathrm{AlCl_3} + 3\,\mathrm{RLi} \longrightarrow \mathrm{AlR_3} + 3\,\mathrm{LiCl} \tag{6}$$

On an industrial scale, trialkylaluminium compounds are produced in the two-step Ziegler direct process. In the first step (Reaction 7) aluminium is reacted with hy-

drogen yielding the dialkylaluminium hydride. In the second part of this process (Reaction 8), the hydride is reacted with a terminal alkene in a hydroalumination and the final aluminium compound can be obtained. Reaction 9 summarises these two reactions.[80][81] The reactivity of aluminium can be improved by adding 0.01-2 wt% titanium as an alloy.[79]

$$3\,\mathrm{Al} + \frac{3}{2}\,\mathrm{H_2} + 2\,\mathrm{AlR_3} \longrightarrow 3\,\mathrm{R_2AlH} \tag{7}$$

$$3\,\mathrm{R_2AlH} + 3\,\mathrm{H_2C{=}CHR} \longrightarrow 3\,\mathrm{Al(CH_2CH_2R)_3} \tag{8}$$

$$3\,\mathrm{Al} + \frac{3}{2}\,\mathrm{H_2} + 3\,\mathrm{H_2C{=}CHR} \longrightarrow \mathrm{AlR_3} \tag{9}$$

Due to the reversibility of the hydroalumination reaction several organoaluminium compounds can be obtained from, e.g. TiBA. The affinity of the aluminium hydride bond for terminal alkenes increases $H_2C{=}CR_2 < H_2C{=}CHR < H_2C{=}CH_2$. Hence, TiBA can be converted to TEA via Al^nPr_3 (Scheme 7).[79]

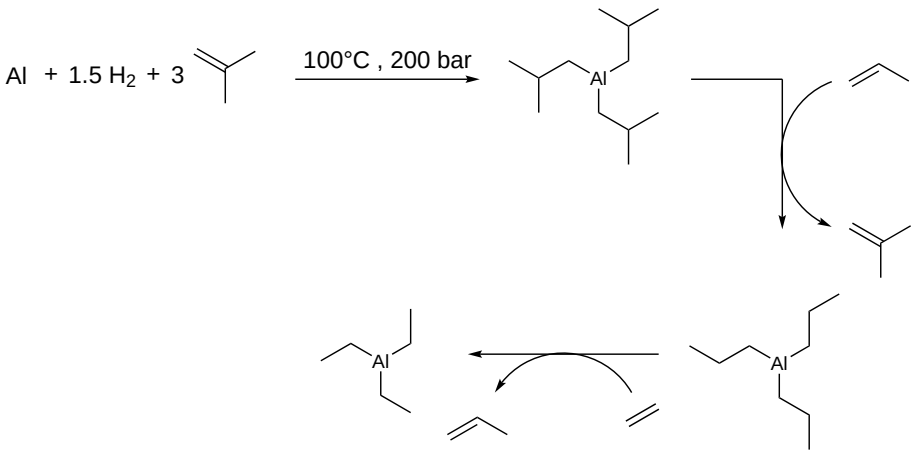

Scheme 7: Converting Al^iBu_3 to Al^nPr_3 and $AlEt_3$.

2.1.2 Aqueous and Coordination Chemistry of Aluminium

The understanding of coordination chemistry was one of the major achievements of the latter half of the 19th century. At this time, Alfred Werner showed that $Co^{(3+)}$ and ammonia form an octahedral complex. Even though such complexes had been known for some time, e.g. Prussian Blue[82][83], it was now possible to understand this new type of chemical bonding.[84]

The bond fundamental to this type of chemistry is formed between a species with a filled orbital, which is referred to as the donor or ligand and an atom or ion which is usually metallic and which has an empty orbital which is considered the acceptor or the coordination centre.[85]

The coordination chemistry of transition metals has been the centre of academic interest for many years. They show countless applications in catalysis and synthesis, e.g. Pd and Pt are used for cross-coupling reactions.[86][87][88] However, the coordination chemistry of main group metals has significant applications as well. Hence, lithium is used in the production of OLEDs[89] or to provide chiral carbanions in asymmetric synthesis.[90] Antimony and lead halogenides show a versatile photochemistry and are used for optical devices.[91][92] Aluminium coordination compounds are, apart from the applications outlined in Section 2.1.1, being investigated, e.g. for the selective reduction of CH_4 to CO_2.[93][94]

The aqueous chemistry of aluminium has long been considered as "difficult", although it is the most abundant metal in the Earth's crust and is typically found in the form of oxides, e.g. Al_2O_3, hydroxides, e.g. $Al(OH)_3$ or species in between and combinations thereof.[21] The standard reduction potential of E^0 = -1.67 V shows that Al^{3+} is the only possible oxidation state in water, and with an ionic radius of 0.53 Å, Al^{3+} is a small and highly charged cation, forming strong bonds with oxygen. In the absence of any competing ligands, Al^{3+} ions are easily hydrolysed in water. Intermolecular and ligand exchange reactions in water are slow and according to Langford and Gray follow the dissociative interchange (I_D) mechanism[95][96], as with the small ionic radius it is necessary for the outgoing ligand to dissociate before another molecule can coordinate.

Anation reactions occur significantly faster for compounds such as $[Al(OH)(H_2O)_5]^{2+}$ compared to $[Al(H_2O)_6]^{3+}$.[96][97]

Due to its amphoteric character, $Al(OH)_3$ can be dissolved in acids (Equation 10) as well as in bases (Equation 11).

$$Al(OH)_3 + 3\,H^+ \rightleftharpoons Al^{3+} + 3\,H_2O \tag{10}$$

$$Al(OH)_3 + OH^- \rightleftharpoons Al(OH)_4^- \tag{11}$$

In aqueous solutions with a low pH, as shown in Equation 10, Al^{3+} remains unhydrolysed and $[Al(H_2O)_6]^{3+}$ is the main mononuclear species to form, with an octahedral coordination of H_2O molecules. With an increase in pH, the water molecules are successively replaced by hydroxide anions.[21][98]

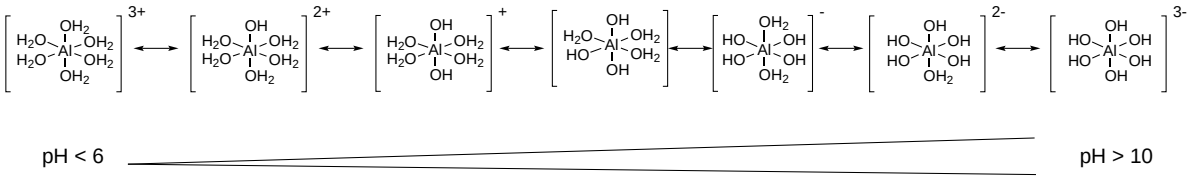

Scheme 8: Amphoteric behaviour of aluminium under aequous conditions.

For high aluminium concentrations, it is possible to form more complex and polynuclear species. $[Al_2(OH)_2(H_2O)_8]^{4+}$, $[Al_3OH)_4(H_2O)_{10}]^{5+}$ and $[Al_{13}O_4(OH)_{24}(H_2O)_{12}]^{7+}$ are three examples of these compounds that have been isolated and spectroscopically and crystallographically characterised in the past.[99][100][101]

AlX_3 compounds are good electron pair acceptors and can form coordinative bonds with one or more donor molecules, which is shown in the polymeric structures of $([AlF_4]^-)_x$ and $([AlF_5]^{2-})_x$ and the monomeric $[AlF_6]^{3-}$. Compared to fluoroborate, $[BF_4]^-$, where the boron forms the centre of a tetrahedron, all aluminium fluorates maintain an octahedral coordination of the metal centre.[21] As seen above, dissolving AlX_3 leads to the formation of a hexaaqua complex with the water molecules replacing the anions to yield the octahedral complex (Equation 12). The high oxygen affinity of aluminium strengthens the Al-O bond and weakens the O-H bond within the water molecule, resulting in the deprotonation of the water ligand to form an aluminium aqua hydroxo complex. Consequently, dissolving AlX_3 compounds in water will (de-

pending on the nature of X) yield acidic solutions by emitting a proton, which changes the pH and leads to a more acidic solution. The pH has a significant impact on the species that is formed when an aluminium salt is dissolved in water, as Scheme 8 shows.[21]

$$AlCl_3 \xrightarrow{H_2O} [Al(H_2O)_6]^{3+} + 3\,Cl^- \xrightarrow{H_2O} [Al(H_2O)_5(OH)]^{2+} + H_3O^+ + 3\,Cl^- \qquad (12)$$

The coordination chemistry of aluminium, especially in aqueous conditions is of great significance when it comes to public health. Crumbliss and Garrison thoroughly compare the similarities of Al^{3+} and Fe^{3+} and how these similarities affect the human body. Although if ingested most aluminium will be eliminated from the body as insoluble hydroxides and phosphates[102], the citrate which is present in blood plasma with a concentration of approx. 0.1 mmol·l^{-1} is able to complex Al^{3+} effectively.[102] It forms a neutral complex, which is suspected of being able to pass through membranes.[103] Other, even stronger complexing agents are the glycoproteins transferrin and ferritin. One of the roles these proteins have is the complexation and transportation of iron in the body. Aluminium utilises the iron transport system, causing the development of plaques in the brain. These plaques are suspected to give rise to neurodegenerative diseases, such as Alzheimer's.[104] The average intake of aluminium per person has increased over the past years[105][106], as it is used more and more for applications, e.g. in cosmetics, as an anti-transpirant, but also because there is an enrichment of aluminium in the food chain.[107] Increasing emissions of sulfur and nitrogen oxides by industrial plants result in the precipitation of acidic rain. This acidic rain is able to release aluminium from minerals into the aquatic environment from where it eventually enters into the food chain.[108][109]

2.2 Polymers

2.2.1 Crosslinking of Polymers

Polymers affect many aspects of our day-to-day life. Coatings[110], rubber[111], adhesives[112], fibres[113], cellulose[114], proteins[115] are just a few examples we encounter every day. Polymer products show a broad range of properties according to their application. As discussed in Chapter 2.1.1.2 aluminium compounds are used as co-catalysts for the production of polyolefins. In 2015 more than 178 million tons of polyolefins were produced.[116] Polyethylene (PE) and isotactic polypropylene (iPP) are important materials for a large variety of applications. The versatile use of polymers can also be seen in the use of polymers for textile fibres which can be divided into two classes: Polymers such as carbohydrates (cotton)[117] or proteins (silk, wool)[118][119] originated from natural sources. The cotton fibre consists almost purely of cellulose[120], whereas, e.g. silk consists of fibroin, a protein-based polymer with a high molecular weight.[118][119] On the other hand, synthetic polymers such as polyesters and polyamides (e.g. nylon), are of great significance. Polyester is the most widely used polycondensation polymer.[121] Modern textiles with synthetic polymers can show very interesting properties, such as shape changing or shape memory. These materials consist of actively moving polymers and adapt their shape depending on factors such as temperature, light or pH. If they show shape memory they can be deformed and fixed in a temporary shape, but then reverted to their original shape.[122] On the other hand, phenolic resins are used for the production of protective equipment, e.g. helmets, or in the aerospace industry due to their rigidity and their tolerance to temperature differences.[123][124] These examples show that for every application, there is a polymer that either due to its unique properties or for economical considerations is more suitable than other materials. These properties are based on different parameters, such as chain lengths, functionalities, branchings and links between the different chains.

Apart from grafting and blending, crosslinking is one of the most important techniques by which polymers are tuned for specific requirements. Crosslinking prevents the polymer chains from sliding past each other and thereby influences chemical and physical properties such as viscosity[125], crystallinity[126], melting point[127],

flexibility[128] and hardness[129]. There are two different types of crosslinking: intramolecular crosslinks influence the folding of a polymer, which is of importance for, e.g. proteins.[130] Intermolecular crosslinking, on the other hand, links separate chains together. This has a profound influence on, e.g. the mechanical properties of materials (Figure 3).[131] Depending on the crosslinking density the polymer can become elastic - when the crosslink density is low - and therefore any deformation will to some extent be reversible, or if the crosslink density is very high the polymer will become rigid and potentially brittle.[132][133]

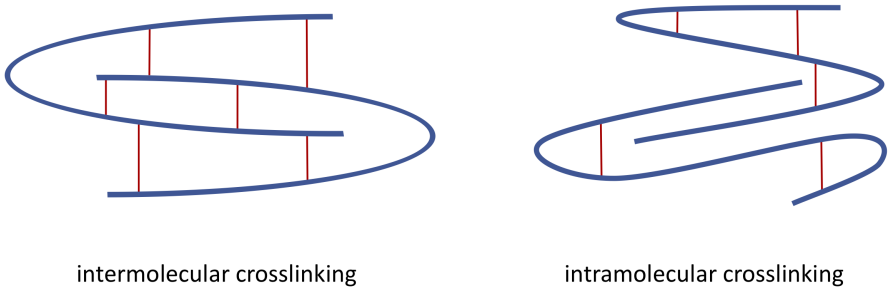

Figure 3: Comparison of intermolecular crosslinking and intramolecular crosslinking.

Crosslinking can occur during the polymerisation process if multifunctional monomers are used instead of bifunctional ones or as a separate process after the linear or branched polymer is already formed.[134] Independent of whether the crosslinking takes place during the polymerisation or afterwards, two different types of crosslinking can be distinguished: Chemical crosslinking via covalent or ionic bonds and physical crosslinking which is achieved, e.g. via hydrogen bonds or Van-der-Waals interactions (Figure 4).

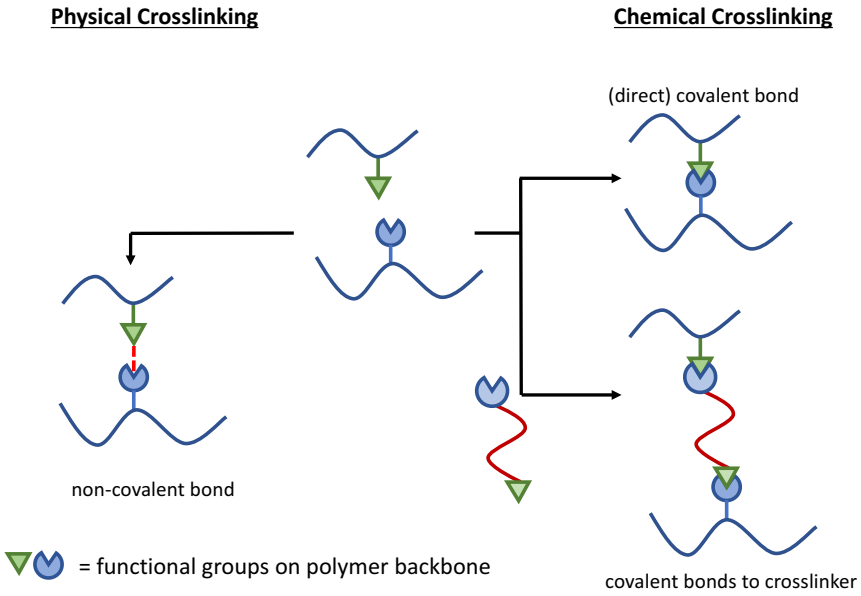

Figure 4: Comparison of physical crosslinking via non covalent bonds, e.g. hydrogen bonds, with chemical crosslinking either via direct covalent bonds or through a covalently binding crosslinker.

Covalently crosslinked polymers are hard to recycle or reuse once they are fixed in their form.[135] This has encouraged scientists to develop techniques that either use thermally labile crosslinks which break upon heating or radiation, or links via secondary bonding interactions.[135][136] A well-known example of a material based on physical crosslinks is the aramid fibre Kevlar®, which was developed by Stephanie Kwollek (Scheme 9).[137][138]

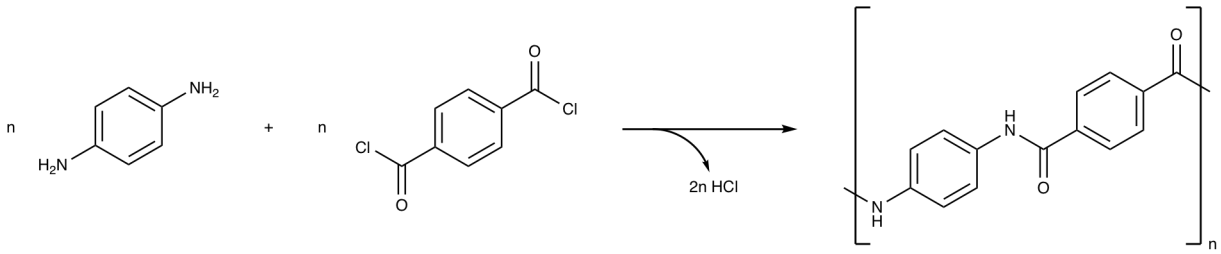

Scheme 9: Synthesis of Kevlar®.[137]

The Kevlar®-polymer has very strong intermolecular interactions through hydrogen bonds between the amide groups (Scheme 10) and aromatic stacking interactions. The fibre is rigid, but still spinnable and has a sheet-like structure, similar to silk. Additionally, it has unique mechanical properties and is stable over a wide temperature range, making it a useful material for protective equipment.[134][139]

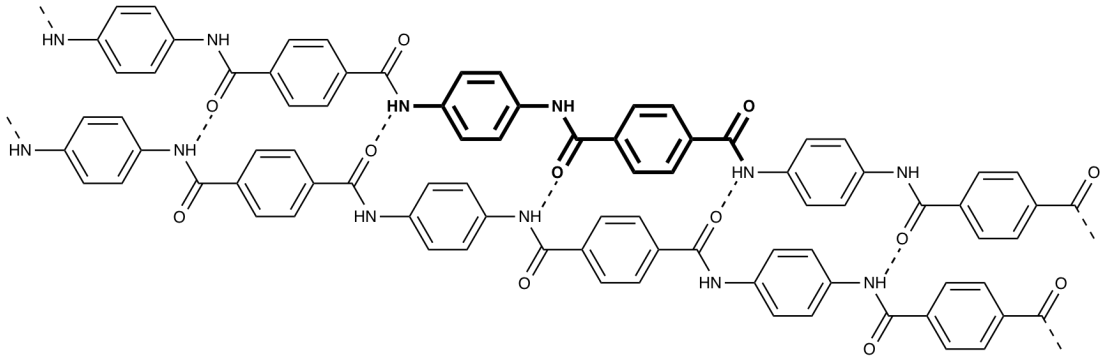

Scheme 10: Physical interactions in Kevlar®-polymers.[137]

The chemical crosslinking of polymers can be achieved in various ways, e.g. by radical polymerization of small monomers with suitable reagents.[140] One of today's most common crosslinking reactions used is the vulcanization during rubber production. It was invented by Charles Goodyear in 1839 and was used for a broad range of applications, the most important of which is debatably the production of tyres.[111][141] During this process natural rubber or related polymers are converted into more durable materials through the addition of sulfur. The polymer chains are crosslinked by sulfur-bridges and so prevented from sliding past each other (Scheme 11). For the finished product, the level of vulcanisation determines its properties: the more sulfur crosslinks are formed, the harder the finished product is, and the less elastic it becomes.[142][143]

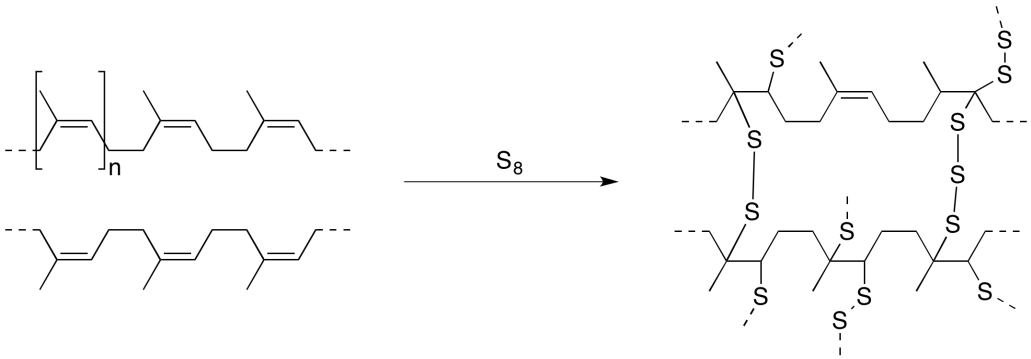

Scheme 11: Vulcanization of rubber with sulfur according to Goodyear.[141][143]

2.2.2 Rheology and Viscosity

The morphology of a polymer, the structure, arrangement of molecules and the physical form of the polymer are important factors that influence the characteristic features of a potential material. Two morphologies can be distinguished: The crystalline state and the amorphous state. For the first of these physical states, the polymer molecules are oriented or aligned in a regular lattice, analogous to those present in crystals. However, polymers never achieve 100% crystallinity, so they are often referred to as *semi*crystalline.[134][144][145]

The amorphous state describes polymers that are in a solid state but do not show any tendency towards crystallinity. Whereas in the solid state the molecular motion is restricted to short range vibrations and rotations, the liquid state allows conformational and segmental freedom by the rotation of chemical bonds. In the amorphous state, the system shows a certain degree of rotational freedom and can be deformed and even flow if the molecules begin to move past each other, but not to the extent found in liquids.[146][147][148]

The study of deformation and flow of matter is called rheology.[149] From the variety of forces that can be applied to a polymer, the shear (or tangential) stress is one of the most important forces for rheological study. The shear force is applied to one side of a surface in a parallel direction. Figure 5 illustrates the shear stress on a rectangle which is turned into a parallelogram. The shear stress τ (Equation 13) is defined as

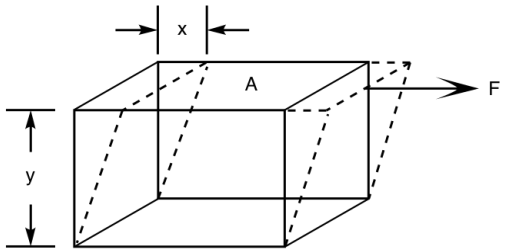

Figure 5: Representation of shear forces on a polymeric system.

the force F (in newtons) per unit of surface area A (in square meters).

$$\tau = \frac{F}{A} \tag{13}$$

The shear strain γ (Equation 14) describes the amount of deformation of the two planes with respect to each other.

$$\gamma = \frac{x}{y} \tag{14}$$

The ability of a polymeric system to resist shear is expressed by the shear module G, the ratio of shear stress and shear strain (Equation 15).

$$G = \frac{\tau}{\gamma} \tag{15}$$

Apart from the shear strain γ, which describes the relative distance of the shear, it is also important to look at the shear rate $\dot{\gamma}$, the rate at which the planes flow relative to each other (Equation 16) and which is given by the derivation of γ over time t.

$$\dot{\gamma} = \frac{d\gamma}{dt} \tag{16}$$

If the shear stress τ of a liquid increases in proportion to the shear rate $\dot{\gamma}$ it is a Newtonian liquid (as it follows Newton's law of viscosity, Equation 17). The proportionality constant η is the viscosity, it is given in Pascal-seconds (Pa s = Newton s m^{-2}).

$$\tau = \eta\dot{\gamma} \tag{17}$$

However, most liquids do not obey Newton's law and show either a thinning (pseudoplastic) or thickening (dilatant) behaviour upon shearing (Figure 6).

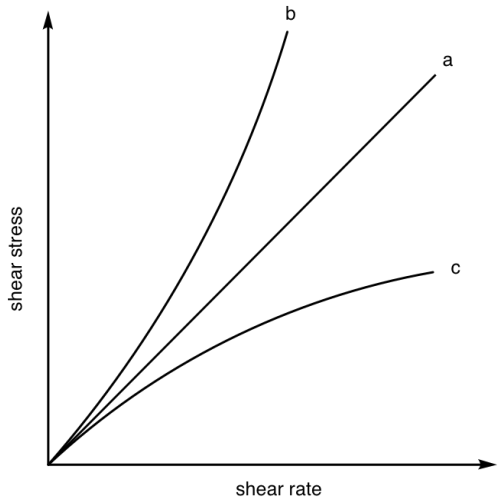

Figure 6: Shear thickening **(b)**, Newtonian **(a)**, and shear thinning fluids **(c)**.

Most polymers show shear thinning with increasing shear rates. In the amorphous state the polymer chains are entangled, which might be disrupted to a certain degree at low shear rates, but essentially persists as the chains re-entangle. As the shear rate increases, this disruption occurs faster and more severely so that the chains cannot resume their entanglement. As a result, the molecules flow with less resistance and the viscosity decreases. If the shear rate increases accordingly, chain rupture can be observed, which will result in a drop in the molecular weight.

The viscosity η is also related to the temperature via the Arrhenius equation (Equation 18). Here A^* is a constant related to molecular motion and E_a is the activation energy for viscous flow, which is determined by the segmental motion of polymer chains. The bulkier a chain branch is, the higher the activation energy is, and the more sensitive the viscosity towards changes in temperature.

$$\eta = A^* e^{-\frac{E_a}{RT}} \tag{18}$$

2.3 Hydraulic Fracturing

Crosslinking, as outlined in the previous section, has numerous applications. In addition to those mentioned in Section 2.2.1, it is also applied in different oil-field processes, e.g. hydraulic fracturing.[150]

In this process, also known as "fracking", rock is fractured by a special liquid consisting of water, a proppant - usually sand - and several additives (Table 1). This fracturing fluid is injected into the wellbore with high pressure.[151] When the pressure generated from the fluid exceeds the pressure of the surrounding rock it will crack and fractures are formed, in which the fracturing fluid is injected (Figure 7).[152] The first fracking experiments were conducted in 1947 in Kansas and used gasoline-based napalm.[153] By 1950 the process was commercially applied and during the 1980's water-based fracking fluids, crosslinked with guar were established.[154][155] Hydraulic Fracturing is currently one of the most controversial oil-field processes.[156] In the USA, hydraulic fracturing is an established process and is used in many states. Supporters argue that it has boosted the economy, while critics raise concerns about the impact on environmental and public health. Based on these arguments several countries in Europe and some states within the US, e.g. New York, Colorado and Texas, issued a moratorium against hydraulic fracturing.[157][158][159]

The fracking process comprises several different stages:[160][161]

- In the initial acid stage, diluted acids (usually hydrochloric acid, although hydrofluoric acid is used occasionally as well[162]) are pumped into the drilling well to clear cement debris and provide an open conduit for the other fracturing fluids. This mixture also assists in opening fractures around the wellbore.

- In the following pad stage, slick water is used to fill the wellbore. This helps to open the formation and facilitate the flow of proppant material.

- The third stage is called the prop sequence stage. At this point, the actual fracturing fluid is injected. The fracturing fluid consists of 98-99.5% water and sand (the proppant). Furthermore, different additives, which serve to extend

fractures and modify the flowing properties of the extract, are added. Table 1 provides an overview of the additives and their effects and gives examples of which chemicals are used.

- The final stage of the fracking process is the flushing stage at which point fresh water is used to flush any excess of fracturing fluid from the wellbore.

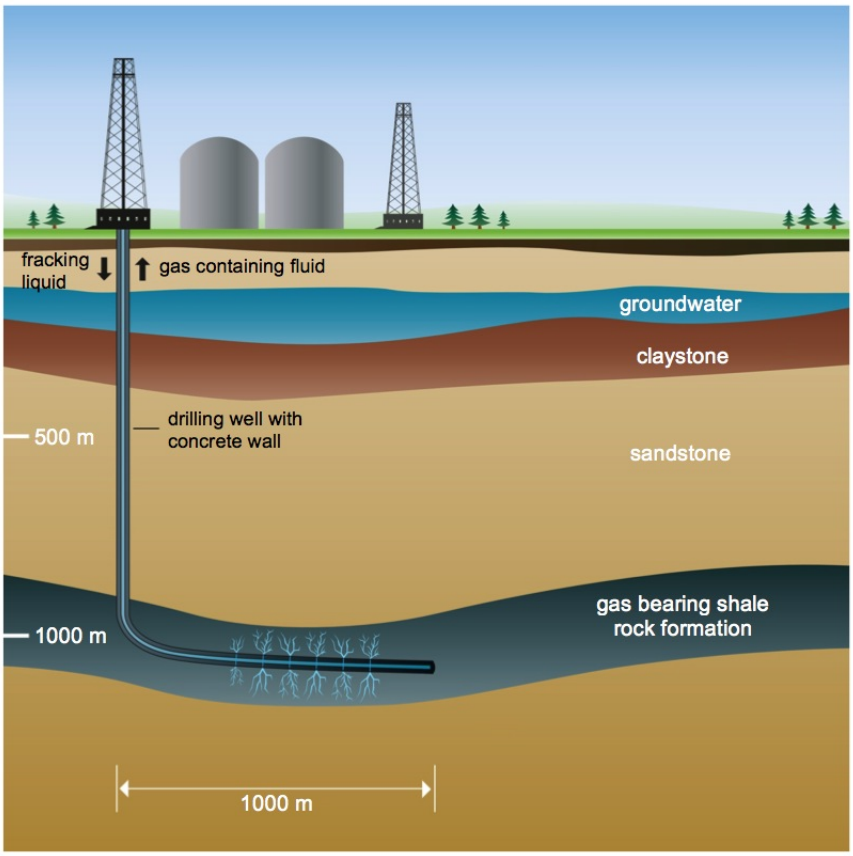

Figure 7: Hydraulic fracturing process.[163]

Between 2011 and 2014 more than 300 different chemicals have been used in fracturing operations. These chemicals are not used at the same time but have to be adjusted to the specific fracking situation. On average around 23 different chemicals are added to a fracturing fluid.[162] [164]

The most common additives used in fracturing fluids are gelling agents such as guar gum, crosslinkers, and breakers, that are used to modify the viscosity of the fluid.[162] The viscosity of the fracturing fluid has to be adjusted according to the specific requirements of the drilling well. Fluids with a high viscosity are used for more ductile rock since it promotes short, wide fractures. However, if the rock is brittle a lower viscos-

Table 1: Fracturing fluid additives and purposes.[165] [166]

Additive	Example	Purpose
Diluted acid	Hydrochloric acid	Dissolves minerals and cracks rocks
Biocides	Glutaraldehyde	Eliminates bacteria that produce corrosive byproducts
Breaker	Ammonium persulfate	Allows a delayed breakdown of gel polymer chains
Corrosion inhibitor	DMF	Prevents pipe corrosion
Crosslinker	Borate salts	Maintain fluid viscosity as temperature increases
Fricton reducer	Polyacrylamide, mineral oil	reduce friction between fluid and pipe
Gel	Guar gum, hydroxyethyl cellulose	Thickens water to suspend sand
Iron control	Citric acid	Prevents precipitation of metal oxides
KCl	Potassium chloride	Creates a brine carrier fluid
Oxygen scavenger	Ammonium bisulfate	Removes oxygen from the water to promote the stability of the gel
pH adjusting agent	Sodium or potassium carbonate	Maintains the effectiveness of other components (e.g. crosslinkers)
Proppant	Silica and quartz sand	Allows the fractures to remain open, so gas can escape
Scale inhibitor	Ethylene glycol	Prevents scale deposit in the pipe
Surfactant	2-Propanol	Is used to reduce interfacial surface tension

ity leads to finer fractures.[167] Breakers are used to reduce the viscosity after the fracturing process to facilitate an easier transport of the fluid.[161] Crosslinkers that are currently used include titanium compounds with α-hydroxy carboxylic acids[168], zirconium chelates[169], and borates - all of which are currently used by Schlumberger. However, the combination of guar gum or CMHPG as polymers and borates as crosslinkers is the most established system for hydraulic fracturing. Borate undergoes a condensation reaction with the hydroxy groups of a biopolymer, such as guar, building crosslinking bridges between different polymer chains (Scheme 12).[170][171]

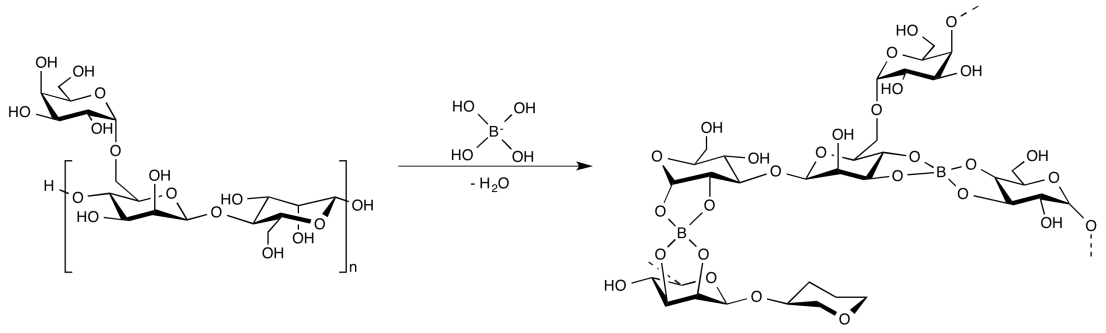

Scheme 12: Crosslinking of guar by borate.

Many of the additives used in hydraulic fracturing are known to have massive effects on the environment and ecosystems, although scientific data regarding long-term effects remains scarce.[157] Furthermore, a number of the additives are known to be carcinogenic, mutagenic or toxic to reproduction or toxic in general. Although boron is part of many naturally occurring minerals and is used in large quantities for the production of glass, and some of its derivatives (borax) are used in skin care products, there have been recent animal studies showing that it can be harmful to reproductive processes and to foetuses.[1] In 2010 borates were included in the REACH "candidate list of substances of very high concern".[172]

Other points of criticism are the amounts of fresh water used in the process, especially in areas that struggle with droughts, and the question of whether the flushing stage of the fracking process is able to remove all chemicals from the ground - or if some of the chemicals or their degradation products remain. Furthermore, in several cases operators of fracturing wells refused to disclose all chemicals used in the process, supporting concerns of anti-fracking activists.[173][174][175][176]

3 State-of-the-Art

3.1 Examples for the Synthetic Application of Aluminium Organic Compounds

Although aluminium organic compounds are not as well known as other main group organometallics, their study has been a constant topic in research publications for years.[16][177][178] Homoleptic alkyl aluminium compounds are some of the most commonly used reagents in organic and organometallic chemistry and valuable catalysts for large-scale processes.[29][70][179] As seen in Chapter 2.1.1 organoaluminium compounds show a strong tendency to maximise their coordination number through the formation of aggregates, by self-association, or by forming adducts with donor ligands.[25]

The chemistry of aluminium organic compounds is determined by the polarity of the aluminium carbon bond on the one hand, and the Lewis acidity of the metal centre on the other. The Lewis acidity makes aluminium a valuable building block in so-called *Frustrated Lewis Pairs* (FLPs). These novel and highly interesting compounds are consist of a Lewis acid and a Lewis base, however, due to steric hindrance they cannot form a classical acid-base adduct as seen for the addition of R_2AlH to **1** yielding the FLP **2** (Scheme 13). The development of FLPs was further propelled when Stephan *et al.* showed that FLPs can be used as a metal-free method for activating hydrogen and other small molecules.[180][181][182][183][184][185]

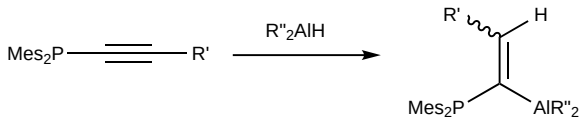

1 **2**

Scheme 13: Generation of a FLP, based on aluminium, which can be used for the activation of small molecules. R'= ^{t}Bu or Ph, R"=$_{t}$Bu or $CH_2{}^{t}$Bu.[186]

The reaction between an alkyl aluminium compound and a Brønsted acid leads to an elimination-condensation sequence (Reaction 19). This reaction forms the basis for large areas of organoaluminium chemistry.

$$AlR_3 + nHL \longrightarrow R_{3-n}Al(L)_n + nHR \tag{19}$$

The reaction is proposed to occur *via* a Lewis acid-base intermediate of the nature $AlR_3(HL)$. However, if the Brønsted acid is oxygen-based this intermediate is very unstable and difficult to isolate. Scheme 14 shows the structure of $^tBu_3Al[O(H)CH_2CH_2CH_2NMe_2]$ **3**, which stands as an example for the aforementioned acid-base intermediate. The bridging hydrogen atom between oxygen and nitrogen enhances the stability of the compound, which enabled Barron *et al.* to isolate and characterise this intermediate. When coordinating to aluminium the strength of the hydrogen bond between nitrogen and oxygen increases, as the proton of the alcohol becomes more acidic. Above 45°C elimination of *tert*-butane takes place from **3** yielding the dimeric alumoxane $[^tBu_2Al(\mu\text{-})OCH_2CH_2CH_2NMe_2]_2$ **4** (Scheme 14).[187]

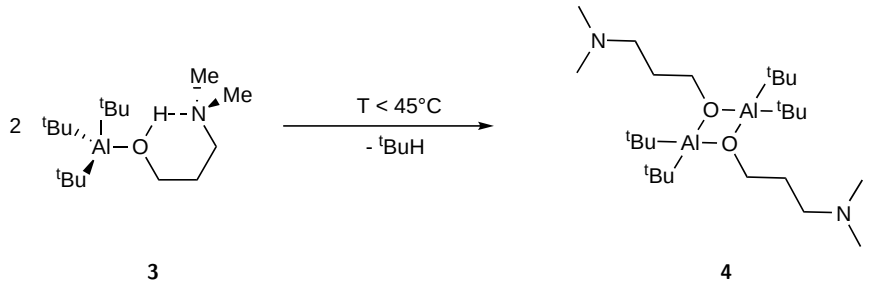

Scheme 14: An example for an isolated Lewis acid-base adduct of AlR_3.[187]

Aluminium has a high affinity towards oxygen and therefore reacts readily with ligands that incorporate hydroxy groups. The addition of one equivalent of an alcohol ROH to a trivalent alkyl aluminium, e.g. TMA, will result in the formation of an aluminium alkoxide with the formula $[Me_2Al(\mu\text{-}OR)]_n$. In the absence of steric bulk and depending on, e.g. the temperature, these alkoxides form dimers (**5**) or trimers (**6**) through bridging oxygen centres in order to raise the coordination number of aluminium. However, if R has a high steric demand as, for example, in the case of 2,6-di-tertbutyl-4-methylphenolate, the resulting alkoxide **7** can be monomeric.

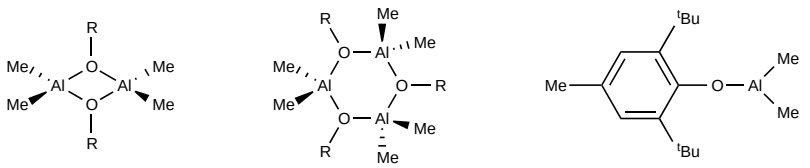

5 **6** **7**

Scheme 15: Examples of dimeric[188], trimeric[189] [190] and monomeric[191] [192] organoaluminium alkoxides.

Another type of aluminium organic compounds uses bidentate ligands with a delocalised bond system. These compounds have proved useful for application as catalysts in polymerisation processes and as precursors for cationic aluminium organic reagents.[193] Lewiński *et al.* showed in extensive studies of the reactions between AlR_3 and O,O′-chelating ligands that the obtained complexes have a tendency to form a dimer **8** in the solid state with two five-coordinated aluminium centres of the general formula $[C_2AlO_3]$ linked through bridging oxygen centres. However, in solution the structure can rearrange to incorporate a four-coordinated aluminium centre via different pathways: Following Path A in aliphatic hydroxy-ethers, where the oxygen centres are separated by long chains the chelation can be revoked and coordination only occurs via the bridging oxygen, yielding a dimer **9**. On the other hand, for an unsaturated O,O′ bidentate ligand the rearrangement follows Path B: π-interaction between the alkoxide oxygen lone pair and the unsaturated system lowers the Lewis basicity of the bridging oxygen, while at the same time increasing the Lewis basicity of the chelating oxygen. This leads to a dissociation of the dimer in solution resulting in the monomer **10**, which can be observed via ^{27}Al-NMR spectroscopy, as the five- and four-coordinated aluminium centres show different shifts.[188] [194]

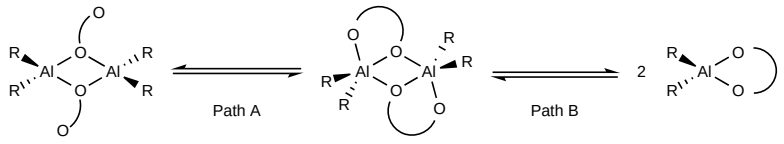

9 **8** **10**

Scheme 16: Possible structural rearrangements for chelated aluminium compounds.[188] [194]

Lewiński *et al.* also studied the reactions of AlR_3 with (O,S)-bidentate ligands and observed the formation of intermolecular S · · · C(π) interactions between the Al-S unit and the π-surface of the ester **12**. This gives rise to a new bonding motif which com-

petes with the usually observed putative hyperconjugated S-Al bond that corresponds with the respective bonding motif found in (O,O′) derivatives.[195]

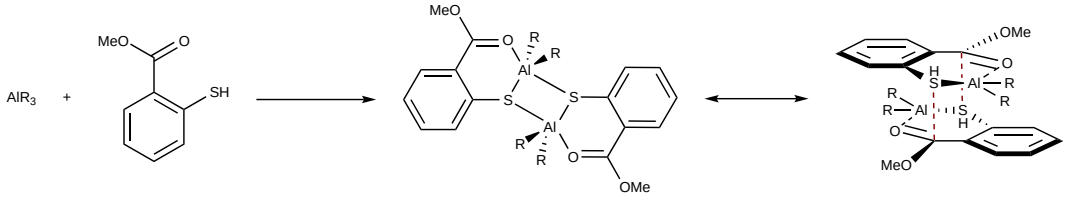

11 **12**

Scheme 17: Different bonding motifs observed in $[Me_2Al(SC_6H_4-2\text{-}CO_2Me)]_2$.[195]

So far all discussed examples for penta-coordinated aluminium compounds consist of two or more Al centres as part of an oligomer. Simple, monomeric five-coordinated aluminium compounds can be obtained by reacting a four-coordinated compound, e.g. $R_2Al(\mu\text{-}O,X)$ with an additional ligand L. However, L needs to be a sufficiently strong Lewis base. The reaction of $Me_2Al(hacet)$ (hacet = deprotonated 2′-hydroxyacetophenone) with γ-picoline yielded compound **13**, in which the aluminium cation adopts a distorted trigonal bipyramidal coordination sphere. The intramolecular C-H···O hydrogen bond and the *trans*-influence of the axial substituents stabilise the complex. Corresponding complexes of the reaction of $Me_2Al(hacet)$ with Et_2O or THF could not be isolated, which was attributed to an insufficient Lewis basicity to stabilise the metal centre.[196]

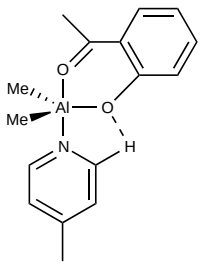

13

Scheme 18: Pentacoordinated complex $Me_2Al(hacet)(py\text{-}Me)$.[196]

Hexa-coordinated aluminium compounds are common for inorganic complexes, such as $Al(H_2O)_6^{3+}$ or $Al(acac)_3$. However, the first simple, monomeric hexacoordinated organic aluminium compound $MeAl(dpt)_2(3,5\text{-}Me_2py)$ **14** was published in 1989 by Barron *et al.* It was obtained by reacting $AlMe_3$ with 1,3-diphenyltriazene in the presence of 3,5-dimethylpyridine (L). The triazene acts as a chelating ligand

around a distorted octahedral aluminium centre (Scheme 19). The distortion is in parts caused by a long aluminium-nitrogen bond *trans* to the Al-bonded methyl group, due to the strong *trans*-influence of the latter.[197]

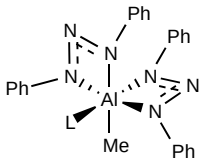

14

Scheme 19: Hexacoordinated complex $Me_2Al(hacet)(3,5\text{-}Me_2py)$.[197]

Another class of aluminium organic compounds are complexes formed with Schiff base ligands. Schiff bases, named after Hugo Schiff, have a general structure $R_2C{=}NR^*$ with $R^*{\neq}H$ and can be regarded as a subtype of imines.[198] An interesting Schiff base ligand is the salen ligand **15**, which is obtained by the reaction of a diamine with two equivalents of salicylaldehyde, as seen in Scheme 20.[199]

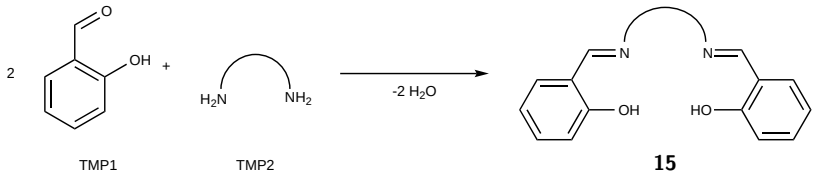

TMP1 TMP2 **15**

Scheme 20: Synthetic route to salen-type Schiff base ligands.[199]

For coordination chemistry, these ligands provide two covalent and two coordinating sites in a planar array, making it ideal for the equatorial coordination of metals. Despite the extensive use of Schiff bases with transition metals, e.g. in catalysis with the Jacobsen catalyst[200], their application in main group metal chemistry, especially within group 13 remains scarce in comparison to the *d*-elements. Scheme 21 shows two different Schiff base complexes of aluminium. In **16** the square based pyramidal coordination with the Al atom above the N_2O_2 plane the hydrogen atoms of the methyl group are eclipsed in relation to the substituents on the Al centre. For longer and less rigid N-N backbones a trigonal bipyramidal coordination is preferred, with the hydrogen atoms of the methyl group being staggered. Other than the nature of the N-N backbone in the salen ligand the size of the additional substituent on the metal also influences the geometry of the complex. Hence, **17**, [salen(^{t}Bu)AlMe] shows a distorted trigonal bipyramidal coordination, due to the sterically demanding

^{t}Bu ligand. A third factor is the size of the metal: For Ga and In complexes with the salen ligand that adopt the square based pyramidal geometry of **16**, the distance between the metal centre and the N_2O_2 plane increases as the size of the metal ion increases.[201] [202] [203] [204]

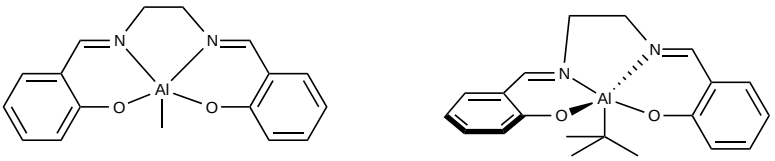

16 AlMe(salen)

17 Al^{t}Bu(salen)

Scheme 21: Representative Schiff base complexes of aluminium. **16** is in a square pyramidal coordination sphere and eclipsed hydrogen atoms on the methyl group. **17** adopts a trigonal bipyramidal coordination sphere.[203]

Coates and co-workers investigated chiral aluminium alkoxide complexes as catalysts for the stereocontrolled polymerisation of lactide. In order to add the stereochemical information they used the chiral Schiff base derivative [2,2'-[(1,1'-binaphthalene)-2,2'-diylbis(nitrilo- methylidyne)]bisphenol] **18**. If reacted with $AlEt_3$ and MeOH the chiral catalyst **19** is formed. From the same reaction mixture Coates and co-workersÂ also isolated the bimetallic compound **20**, which did not display any catalytic activity.

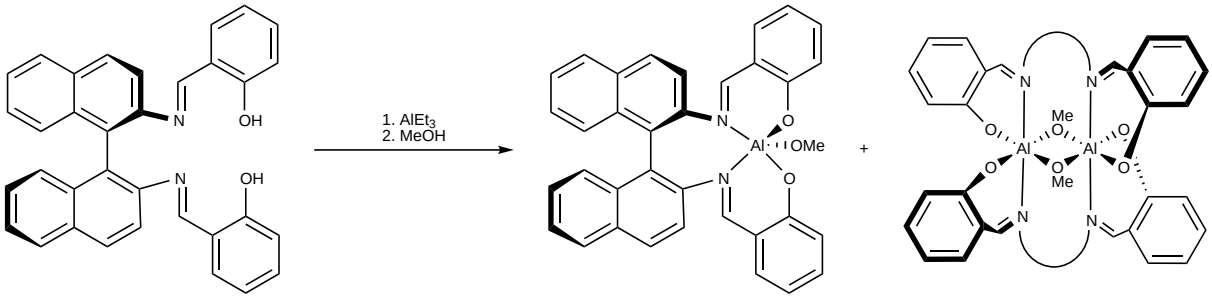

18 **19** **20**

Scheme 22: Formation of a chiral and bimetallic aluminium Schiff base complex.[205]

Under aqueous conditions or in the presence of oxo-donors (salen)AlR compounds can be hydrolysed or reacted with alcohols to give the respective hydroxide (salen)AlOH (or alkoxide (salen)AlOR for the reaction with the corresponding alcohol ROH). If unreacted (salen)AlR is present after the hydrolysis this can react with the newly formed hydroxide to yield a dimeric species $(Al(salen))_2(\mu\text{-}O)$ with a bridging oxygen (Scheme 23).[201] [206]

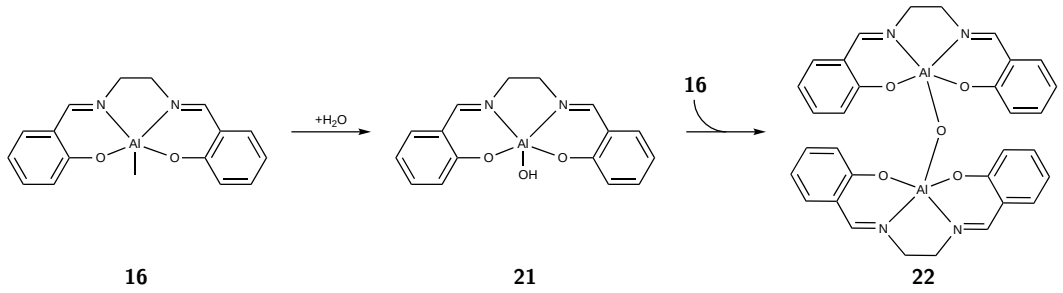

Scheme 23: Hydrolysis of (salen)AlMe.

The hydrolysis of (salen)AlR under acidic conditions by protonating the R group should be straightforward and thermodynamically favourable. However, with no strongly coordinating anions present (especially oxo-donors) this would leave a square planar coordinated Al centre. The ionic radius of Al^{3+} is comparable to those of high-valent 1st-row transition metals, and the d-orbitals in Al^{3+} are too high in energy so that no suitable hybridisation scheme is available. The Al^{3+} ion would correspond with a d^0 system, which prefers a trigonal bipyramid over the square pyramidal coordination.[202]

The first crystallographic evidence for square planar coordinated aluminium **25** was published in 2014. Berben *et al.* reacted $AlCl_3$ with a phenylsubstituted bis-(imino)-pyridine **23**, followed by lyophilisation with toluene (Scheme 24). Although the origin of the energetic driving force for the formation of this - for Al unusual - coordination remains unknown and is subject to theoretical studies, the compound provides an interesting possibility for the application as a Lewis acid with two vacant and accessible coordination sites.[207]

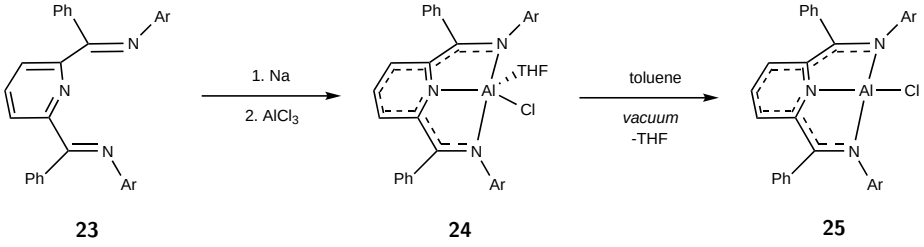

Scheme 24: The first crystallographically characterised square planar aluminium compound.[207].

Organoaluminium carboxylates are useful precursors for Al-based mixed-metal oxide clusters, Al fibres and alumoxanes.[208] [209] [210] The bonding between the aluminium

and the carboxylate can follow different modes (Scheme 25). It can either act as a monodentate ligand (I), where the coordination can be *syn* (Ia) or *anti* (Ib). Furthermore, the carboxylate can act as a bidentate ligand and either form a dimeric complex (II) where the carboxylate bridges two Al centres, or it could act as a chelating ligand, following mode (III). All three modes are difficult to distinguish by spectroscopic methods such as infra-red spectroscopy.[211][212]

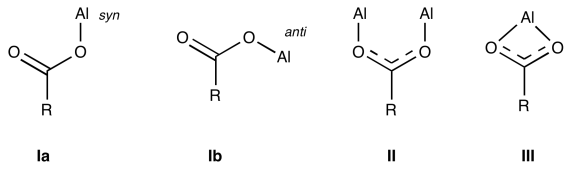

Scheme 25: Possible bonding modes in aluminium carboxylates.[211]

The equimolar reaction of an aluminium alkyl, AlR_3, and benzoic acid yielded a dimeric structure **27** (Scheme 26) in the solid state. The central eight-membered $Al_2O_4C_2$ ring can adopt different shapes depending on the nature of R. For R=Me the ring is almost flat, whereas the use of bulkier ligands like R=^{t}butyl results in a chair-like conformation in order to minimize strain and bond pair repulsion.[212]

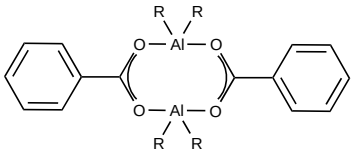

27

Scheme 26: Reaction product for the equimolar reaction of AlR_3 and benzoic acid.[212]

Barron *et al.* showed in calculations that if dimerisation could be precluded, the chelating bonding mode III in Scheme 25, which results in a tetrahedral coordination of the Al, would be preferred over a three-coordinated aluminium centre. One possibility to prevent dimerisation could be the use of sterically demanding acids. This has been attempted by Dickie *et al.*, but even the use of 2,4,6-triphenylbenzoic acid still yielded a dimer.[212][213] Lewiński and co-workers, however, succeeded in synthesising compound **28**, which shows the chelating binding mode III in an octahedral coordination of the aluminium centre (Scheme 27).

The aforementioned influence of hydrogen bonding on the coordination of aluminium (Scheme 14) sparked interest in the influence of an *ortho* substituent on the aromatic

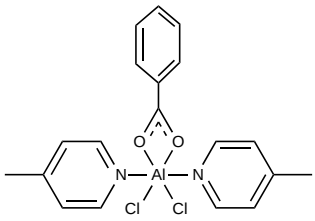

TMP1

Scheme 27: Chelating binding mode in an aluminium carboxylate.[211]

ring. Barron *et al.* studied the geometry of the products for the reaction between salicylic acid and Ga^tBu_3 (Scheme 28). The intramolecular hydrogen bond in carboxylate **29** between the proton of the *ortho* functionality and the carboxylate oxygen causes a nearly planar geometry between the arene and the carboxylate moiety, with the torsional angle between O1-C1-C2-C3 being 2.9°. To prove that this planarity results from the intramolecular hydrogen bond Barron *et al.* conducted a control experiment with *o*-toluic acid. This yielded the carboxylate **30**, with a more twisted geometry in solid state and a torsional angle between O1-C1-C2-C3 of 42.6°.[214] Lewiński *et al.* succeeded at synthesising a analogus compound with $AlEt_3$ and salicylic acid.[216]

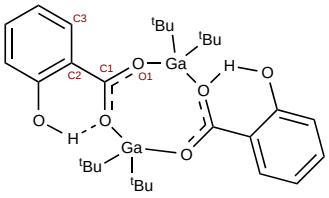

29

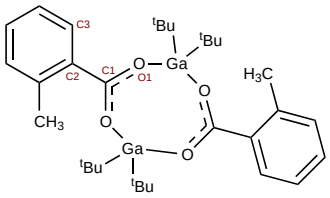

30

Scheme 28: $[(^tBu)_2Ga(\mu\text{-}O_2CC_6H_4\text{-}2\text{-}OH)]_2$ (**29**) and $[(^tBu)_2Ga(\mu\text{-}O_2CC_6H_4\text{-}2\text{-}Me)]_2$ (**30**), which in solid state differ in the planarity between O1-C1-C2-C3 by 39.7°.[214]

Lewiński *et al.* also studied the reactions between *ortho* functionalised derivatives of benzoic acid aluminium alkyls. The reaction of anthranilic acid with one equivalent of $AlEt_3$ yields a dimeric compound $[Et_2(O_2CC_6H_4\text{-}2\text{-}NH_2)]_2$ that is unstable at ambient temperature. Scheme 29 shows the reaction between two equivalents of TEA and anthranilic acid, which leads to the formation of a tetranuclear species $[Et_2Al]_4[\mu\text{-}O_2CC_6H_4\text{-}2\text{-}\mu\text{-}NH]_2$ **31** in which, according to x-ray crystallography, both protic environments are involved in the coordination of the aluminium. ^{27}Al-NMR showed that the tetranuclear species is retained in solution. The solid state structure consists of three fused, distorted heterocyclic rings: two six-membered rings

and one twelve-membered ring in which one aluminium is coordinated *anti* and one *syn* by the carboxylate. Two of the diethylaluminium units bridge between the arylamino group and the carboxylate oxygen of the second ligand and the other two $AlEt_2$ units are chelated between the carboxylate oxygen and the NH-group. In either case, Al is in a distorted tetrahedral coordination environment. The product of the reaction between two equivalents of TEA and one equivalent of salicylic acid, $[Et_2Al]_4[\mu\text{-}O_2CC_6H_4\text{-}2\text{-}\mu\text{-}O]_2$ has a corresponding structure to **31**.[215] [216]

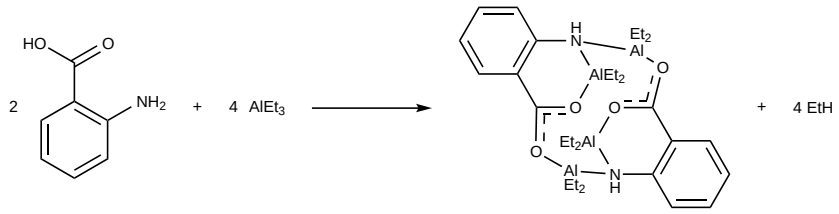

31

Scheme 29: Synthesis of the tetranuclear species $[Et_2Al]_4[\mu\text{-}O_2CC_6H_4\text{-}2\text{-}\mu\text{-}NH]_2$ (**31**).[215]

Another interesting aromatic carboxylate for use as a ligand in aluminium organic chemistry is phthalic acid. This dicarboxylate reacts with $AlMe_3$ in a 1:2 ratio, yielding a tetranuclear adduct $[(AlMe_2)_2(\mu\text{-}O_2C)_2\text{-}1,2\text{-}C_6H_4]_2$ **32**. The centrosymmetric compound consists of three fused heterocyclic rings: two seven-membered rings and one distorted 16-membered $Al_4(OCO)_4$ ring. The bridging $AlMe_2$ unit is *syn* bonded and the chelating unit *anti*. The Al-O distances to the chelating oxygen atoms are shorter than those to the bridging one, suggesting that the *anti*-bond is stronger.[217]

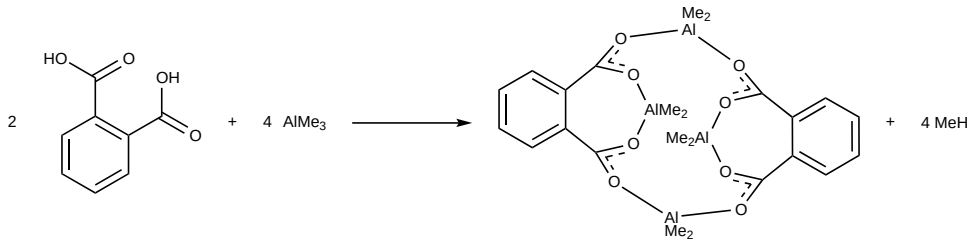

32

Scheme 30: Synthesis of $[(AlMe_2)_2(\mu\text{-}O_2C)_2\text{-}1,2\text{-}C_6H_4]_2$ (**32**).[217]

Redshaw *et al.* used a more complex benzoic acid derivative **33** that can act as a tridentate Schiff base. The adduct **34**, that results from the reaction with two equivalents of $AlMe_3$ contains tetra-coordinated aluminium in $AlMe_2$ units as well as hexa-coordinated aluminium in a 16-membered macrocycle (Scheme 31).[218]

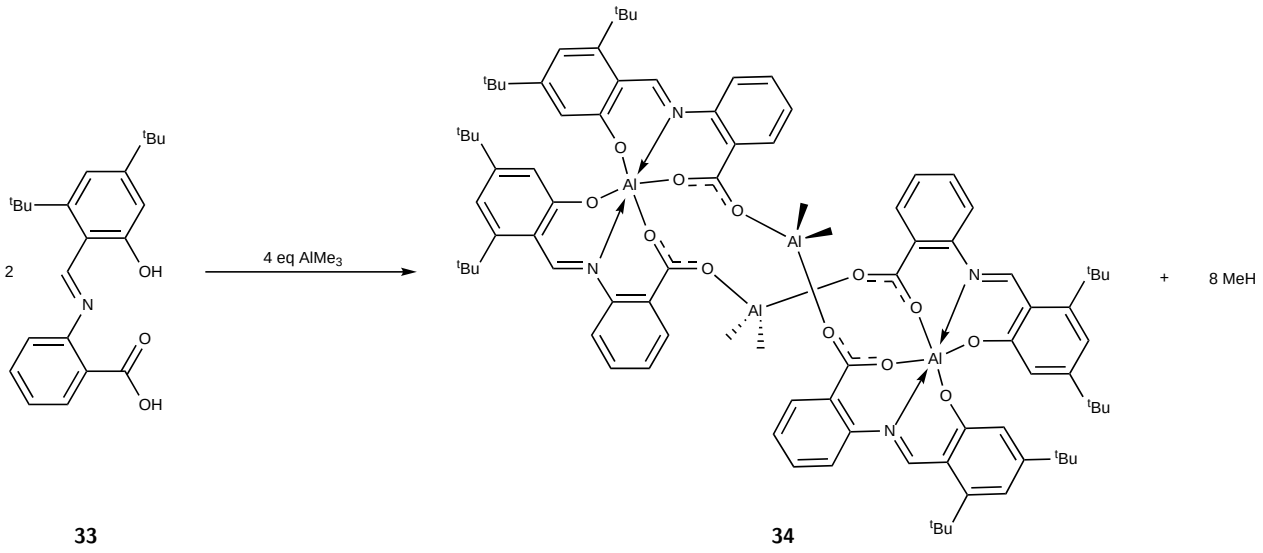

Scheme 31: Macrocyclic aluminiumorganic adduct with hexa- and tetracoordinated aluminium centres.[218]

3.2 Hydrolysis and Oxidation of Aluminium Compounds

As seen in Section 2.1.1, the reaction between organoaluminium compounds such as $AlMe_3$ and water is critical for various applications. The classic way to synthesise aluminium oxides and hydroxides is via alumina gels, a two-phase system consisting of colloidal aluminium oxides or hydroxides and water, which is obtained by the neutralisation of concentrated aluminium salt solutions.[228] A second way to obtain aluminium hydroxides and oxides is the hydrolysis of aluminium alkoxides, $AlOR_3$.[229]

Barron *et al.* studied the hydrolysis of Al^tBu_3 (Equation 20) and thermolysis of the obtained $[^tBu_2Al(\mu\text{-}OH)]_3$ (Equation 21), which yielded a mixture of products. $(^tBuAlO)_6$ and $(^tBuAlO)_9$ have been characterised by X-ray crystallography. The structures are shown in Scheme 32. The hexamer **35** consists of a hexagonal prism with two parallel and almost planar Al_3O_3 units. The nonamer **36** likewise consists of two parallel Al_3O_3 rings which are connected by three bridging oxygen and aluminium centres.[229]

$$Al^tBu_3 \xrightarrow[-{}^tBuH]{H_2O} {}^tBu_2Al(\mu\text{-}OH)]_3 \tag{20}$$

$${}^tBu_2Al(\mu\text{-}OH)]_3 \xrightarrow{\Delta} [{}^tBuAlO]_6 + [{}^tBuAlO]_9 + [{}^tBuAlO]_n \tag{21}$$

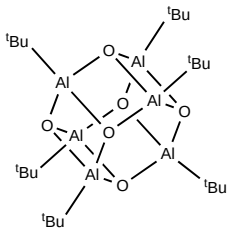

35

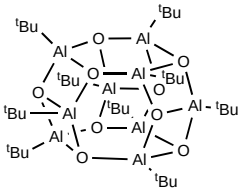

36

Scheme 32: Thermolysis products of $[^tBu_2Al(\mu\text{-}OH)]_3$.[229]

Another way to obtain alumoxanes is direct oxidation, e.g. with potassium superoxide. Atwood *et al.* reacted KO_2 and $AlMe_3$ by refluxing them in benzene. The resulting

product, $K[Al_7O_6Me_{16}]\,C_6H_6$, has been crystallographically characterised: the structure of the anion **37** consists of μ_3-O in an open $(AlO)_6$ ring capped by an additional AlMe unit, which binds to three alternate oxygens (Scheme 33).[230] [231] [283]

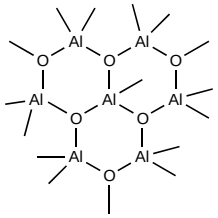

37

Scheme 33: Structure of $[Al_7O_6Me_{16}]^-$.[230] [231]

Bethley *et al.* found a new approach to the synthesis of alumoxanes through the reaction of carboxylic acids with the mineral boehmite (Equation 22). It was based on the observation that the aluminium-oxygen core of stable alumoxanes shows a similar structure to the mineral (Scheme 34). The reaction of the carboxylic acid with boehmite can be seen as an intercalation/exchange process in which the acid replaces hydroxy groups in the oxide double layer.[212] [232]

$$[Al(O)(OH)]_n \xrightarrow{+RCOOH} [Al(O)_x(OH)_y(O_2CR)_z]_n \qquad (22)$$

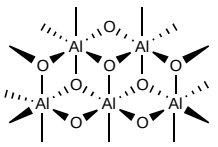

38

Scheme 34: Structure of boehmite.[212]

The reaction of dichloroaluminium carboxylates with water leads to the formation of different hydroxo- and oxoaluminium clusters with bridging carboxylates, depending on the nature of the carboxylate, solvent and ligands. In the presence of THF an oxoaluminium carboxylate $[(Al_3O)(O_2CR)_6(THF)_3][AlCl_4]$ is formed. The structure of the cation consists of distorted octahedral aluminium centres in a planar trigonal arrangement (Scheme 35).[211]

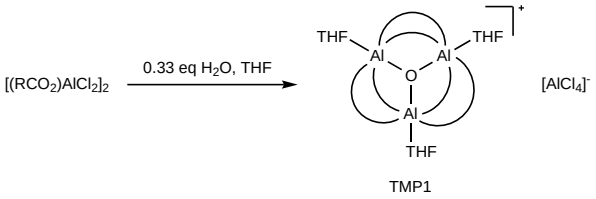

Scheme 35: Reaction of dichloroaluminium carboxylate with water.[211]

Lewiński and co-workers studied the interaction of molecular oxygen with tetrahedral alkylaluminium complexes, as shown in Scheme 36. For the reaction of [($^{t}Bu_3Al$) OEt_2], the product is the expected bridged species **39**. However, when using $^{t}Bu_2Al$(mesal) the product **40** showed that both aluminium-carbon bonds were oxidised. However, it is noteworthy that the dioxygen inserted into one of the aluminium carbon bonds. The resulting alkylperoxo moiety is an important factor in helping to understand the oxygenation of organoaluminium compounds and supports the proposed mechanism of a polar coordination of O_2 to the metal rather than a radical chain mechanism.[233]

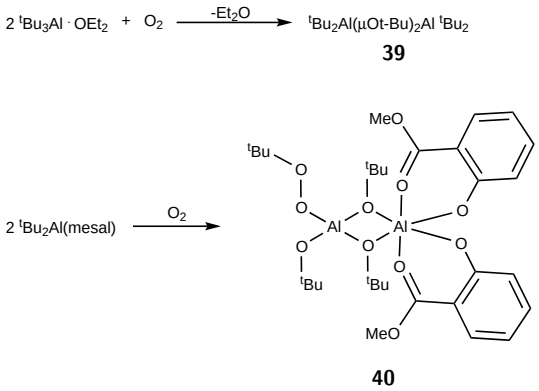

Scheme 36: Oxygenation of tetrahedral alkylaluminium complexes with O_2.[233]

3.3 ^{27}Al-NMR spectroscopy

Aluminium has 24 known isotopes, ranging from ^{19}Al to ^{42}Al. Of these isotopes ^{27}Al occurs naturally and with an abundance of more than 99.9%.[219] It does not absorb neutrons, therefore aluminium is often used to build nuclear reactors.[220] All other isotopes are unstable, with most of them having half-lives of seconds or a few minutes. Only ^{26}Al has a more extended half-life of $7.2 \cdot 10^5$ years. However, it only exists in small traces of less than 0.1% abundance and does not need to be taken into consideration for NMR experiments.[221]

^{27}Al has a high receptivity (D =1170 rel. to ^{13}C) with a spin of $\mathrm{I} = \frac{5}{2}$ and a quadrupole moment of $\mathrm{Q} = 0.14 \cdot 10^{-28}\mathrm{m}^2$.[222] This often leads to very broad and overlapping NMR resonances, though these effects are symmetry dependent. Signals are frequently poorly resolved, though good sensitivity is usual, giving good signal-to-noise ratios.[98] [223] [224]

The Zeeman effect gives rise to six energy levels, according to $(2\mathrm{I}+1)$. These are affected by the first order interaction of the nuclear quadrupole moment eQ (Equation23) with the EFG eq, and this results in five transition frequencies, which are characterised by the quadrupole coupling constant $\mathrm{C_q}$ (Equation 23).[221] [222]

$$\mathrm{C_q} = \frac{\mathrm{e^2qQ}}{\mathrm{h}} \tag{23}$$

Quadrupolar interactions are significantly faster than dipolar or scalar interactions and the fast relaxation leads to a broadening of NMR lines. The line broadening is proportional to Equation 24, in which ν_L is the Larmor frequency of ^{27}Al.

$$\mathrm{L} = \frac{\mathrm{e^2qQ}}{\mathrm{h}\nu_\mathrm{L}} \tag{24}$$

This gives two accessible parameters - the chemical shift and the line-broadening - that allow the extraction of information from a ^{27}Al-spectrum.[222]

The chemical shift of the ^{27}Al nucleus ranges from δ -100 to + 300 ppm. It is measured in reference to $Al(H_2O)_6^{3+}$ at δ 0 ppm and is not noticeably influenced by the solvent. The main piece of structural information that can be obtained is the coordination

number and, to a limited extent, the character of the ligand. Hexa-coordinated aluminium gives rise to signals at higher field resonances, tetra-coordinated to lower field resonances and penta-coordinated aluminium are in an intermediate range. The few available examples of three-coordinated aluminium that are known have displayed the lowest field resonances recorded in ^{27}Al NMR spectroscopy. These have been between δ 220-280 ppm. Figure 8 shows the chemical shift ranges as a function of the coordination and the ligand type.[222] The screening strength increases with the number of bonding ligands. The more an aluminium atom is coordinated by donor ligands the stronger is the shielding. It can be deduced that the shift also depends on the electronegativity of the ligand, which changes the electronic density in the p-bonding orbitals of the aluminium and the shielding.[225] [226]

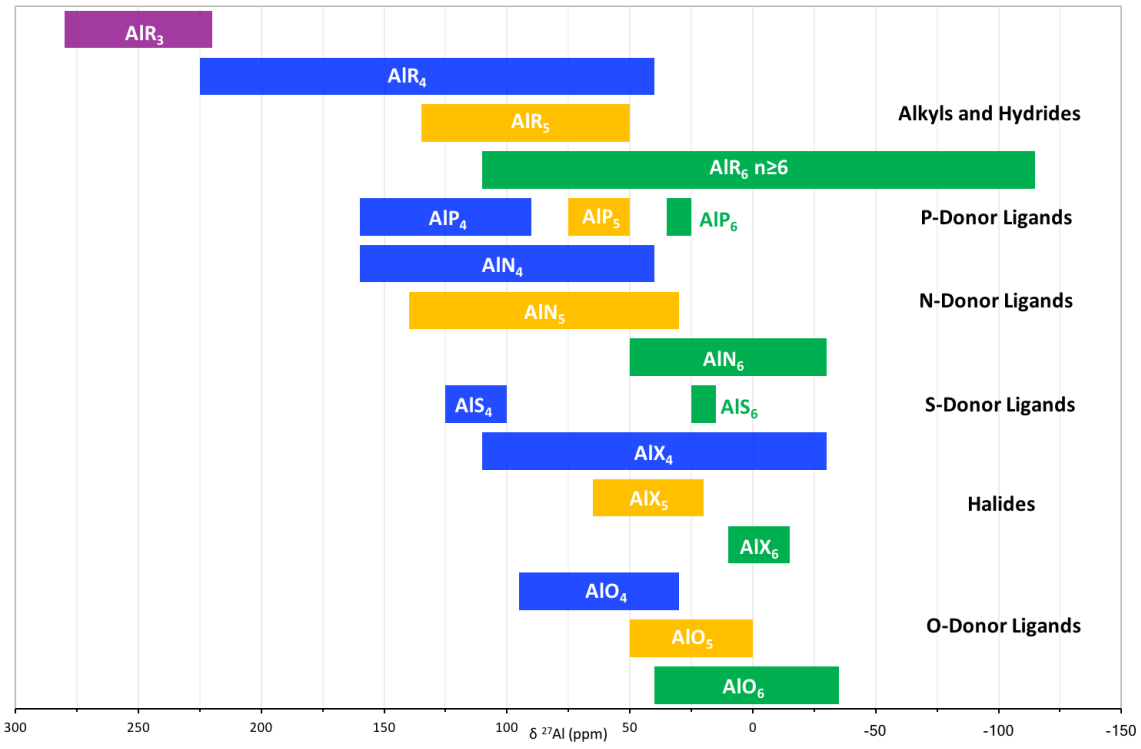

Figure 8: Chemical shift ranges for ^{27}Al NMR as a function of the coordination number and the ligand type. Coordination number of three is given in purple, four in blue, five in yellow and six or higher in green.[222]

Due to the line broadening ^{27}Al-spectroscopy is mainly suitable for highly symmetric or moderately distorted aluminium compounds, where the quadrupolar interactions are small enough to prevent significant signal overlap. More symmetrical environments of the aluminium result in sharper and narrower lines.[222] Tian *et al.* inves-

tigated the use of Al salen complexes as catalysts in carbon dioxide and epoxide coupling reactions. Although they observed very strong but broad signals they utilise ^{27}Al NMR spectroscopy to distinguish four and five coordinated Al species.[227]. Aramini and co-workers study the binding of the protein transferrin from different organisms (human, bovine and chicken transferrin) to aluminium in the presence of carboxylates and oxalates. They observe sharp signals in the ^{27}Al NMR and can distinguish whether the protein binds to the aluminium with the O or N terminal site.[223] Andre and Maecke reviewed the use of group 13 metal NMR spectroscopy as a non-invasive analytical technique for biological systems and emphasise that especially ^{27}Al NMR spectroscopy is of significance to monitor the increased intake of aluminium by organisms and the possible relation to neurological problems.[224]

3.4 Crosslinking of Natural Polymers and Synthetic Alternatives

The most used gelling agents in fracturing fluids is guar. The biopolymer consists of a polymannose backbone with galactose branches. The ratio of mannose to galactose varies between 1.6:1 to 1.8:1 with units of six or more succeeding unbranched mannose forming helix structures.[234]

Guar is susceptible to degradation through the hydrolysis of the acetal linkages in the backbone of the polymer. At high temperatures and low pH values, the degradation creates a sudden loss in viscosity. This can be avoided by using higher pH values or using stabilisers such as methanol, sodium thiosulfate or radical scavengers.[235]

Alternatives to guar are its synthetic derivatives HPG (**41**) and CMHPG (**42**, Scheme 37). These are synthesised by exposing guar powder to high temperatures and high pHs in order to swell the powder and break up the helices of the mannose backbone to allow access for the derivatising agents. HPG and CMHPG show a better stability at higher temperatures, compared to guar.[236] Other substances used as polymers in fracturing fluids include cellulose or synthetic acrylamide-based polymers.[166][234][237]

3.4.1 Crosslinking with Borates

To date, there are no examples of aluminium oxide or hydroxide clusters used for the crosslinking of guar and its derivatives. So far the most used crosslinker is based on borate, which is able to instantaneously increase the viscosity of a guar-based fracking fluid and also improves the rehealing of the polymer. Rehealing is the ability to regain a certain viscosity after being exposed to high shear rates, e.g. after exiting a pipeline or entering the fracture in a wellbore. Borate-based crosslinkers are typically used for bottom-hole temperatures (BHTs) of up to 165°C and when the crosslinks are required to be stable for more than one hour.[239]

Independent of the borate source, the crosslink always consists of a monoborate, as seen in Scheme 12.[234][240] The crosslinking of guar takes place on the cis OH pairs

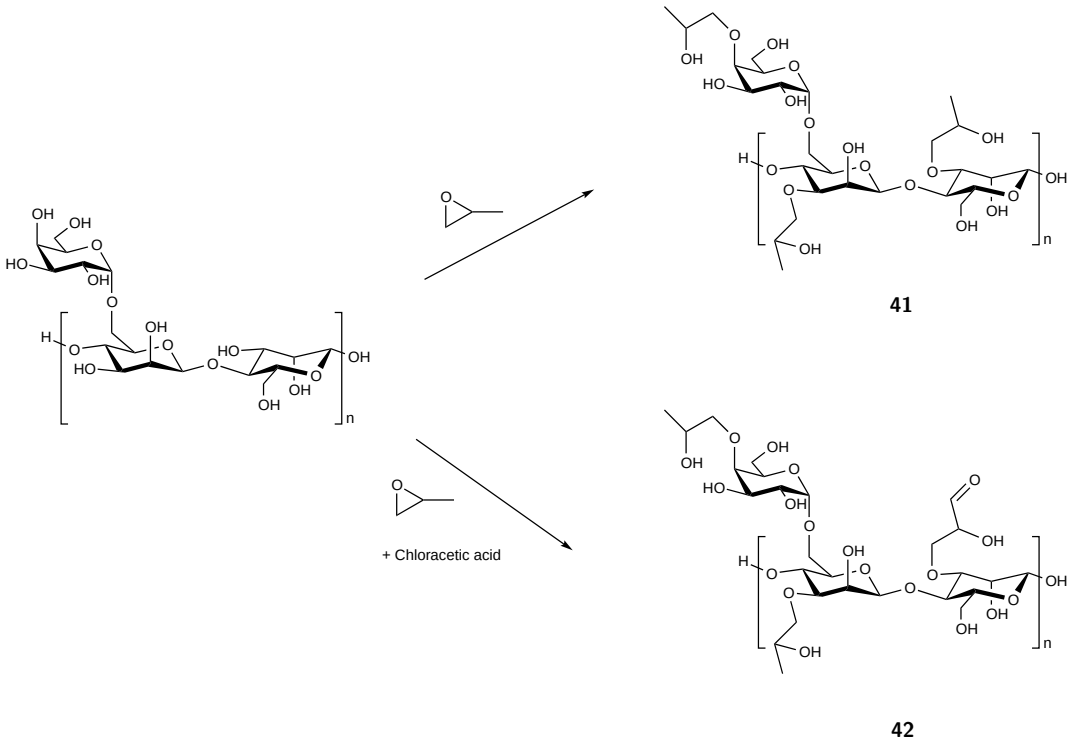

Scheme 37: Commercially applied derivatives of guar.[238]

of the galactose branches and can form an inter or intramolecular link. The borate ion can bind as a 1:1 complex, or as a 2:1 complex, in the latter form the crosslinks between two galactose units have one borate ion binding them. At higher temperatures the number of crosslinks declines as the equilibrium between boronic acid and borate ions (Equation 25), with a pK_A of 9.0-9.2 at room temperature, shifts towards the left-hand side. For higher temperatures, a higher pH is required to achieve similar crosslinking results.[234]

$$B(OH)_3 + H_2O \rightleftharpoons B(OH)_4^- + H^+ \tag{25}$$

The equilibrium also accounts for the quick healing properties of a borate crosslinked gel. At high shear stress, it does not suffer permanent degradation but instead broken crosslinks reform.[234].

Parrish *et al.* showed that the viscosity of borate crosslinked guar decreases reversibly at high pressure. ^{11}B NMR spectroscopy showed that at high pressure the B-O-C bonds break and that 2:1 guar:borate complexes are converted to 1:1 complexes. This behaviour was not observed with other crosslinking agents.[241]

3.4.2 Crosslinking with Transition Metals

As highlighted above, borate is not suitable as a crosslinker at higher temperatures.[234] For BHTs over 165°C transition metal ions such as Cr^{3+}, Zr^{4+} or Ti^{4+} are used as alternative crosslinking agents. These show the best results with synthetic derivatives of guar (Scheme 37) or synthetic polymers such as polyacrylamides. Organometallic crosslinked polymers show a higher thermal stability and are typically used for BHTs up to 200°C. However, for long-term stability they require additional stabilizers or higher pH values of the fracturing fluid.[238] [239] [242]

Although the range of applications for transition metal crosslinked polymers is not as wide as for borate crosslinked systems, due to costs, limits in long-term stability, longer or delayed crosslinking time and poorer shear recovery, it can be adjusted to specific requirements by altering the metal source, the metal to ligand ratio, counter ions, and the pH.[243] For Zr^{4+} the crosslinking reaction requires more time, which is utilised when the viscosity of the fluid needs to change further down in the wellbore.[244]

4 Results and Discussion

4.1 Synthesis

4.1.1 Reactions of Benzoic Acid and its Derivatives with AlR_3

4.1.1.1 Reaction of Benzoic Acid with $AlMe_3$

In the synthetic part of the project, the reactions of benzoic acid derivatives with trivalent aluminium organyls were studied. The equimolar reaction of trimethylaluminium with benzoic acid yielded the alane $[Me_2Al(\mu\text{-}O_2CPh)]_2$ **43**, shown in Scheme 38.

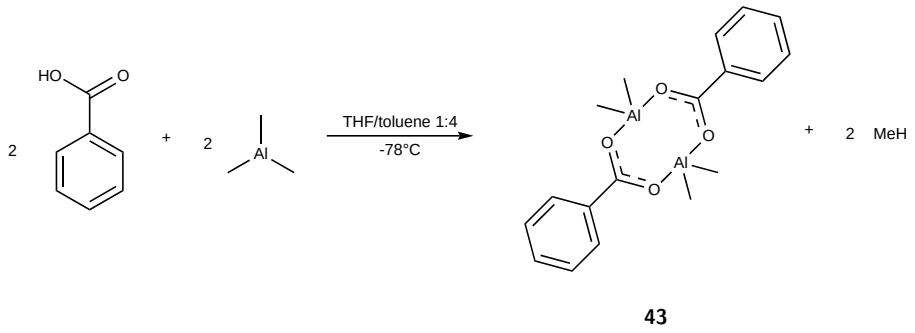

43

Scheme 38: Equimolar reaction of benzoic acid and $AlMe_3$.

Different solvents were tested to crystalise the product and the combination of THF and toluene afforded a white crystalline product. The ^{1}H-NMR spectrum (Figure 9) showed a pure compound with all peaks expected for the product, and the absence of the carboxylic proton, indicating that the benzoate had been formed. The peak attributable to the methyl-groups binding to the aluminium is seen at δ = -0.17 ppm.

The ^{27}Al-NMR spectrum of **43** (Figure 10) shows a peak at δ = 143.7 ppm, which indicates a fourfold coordination of the aluminium.[222] The NMR spectrum was taken in benzene and does not show the presence of THF, which could have remained from the synthesis and would be able to bind to the metal as a Lewis base. Therefore, in the absence of any coordinating solvents, this suggests that the compound probably forms an aggregated species in solution.

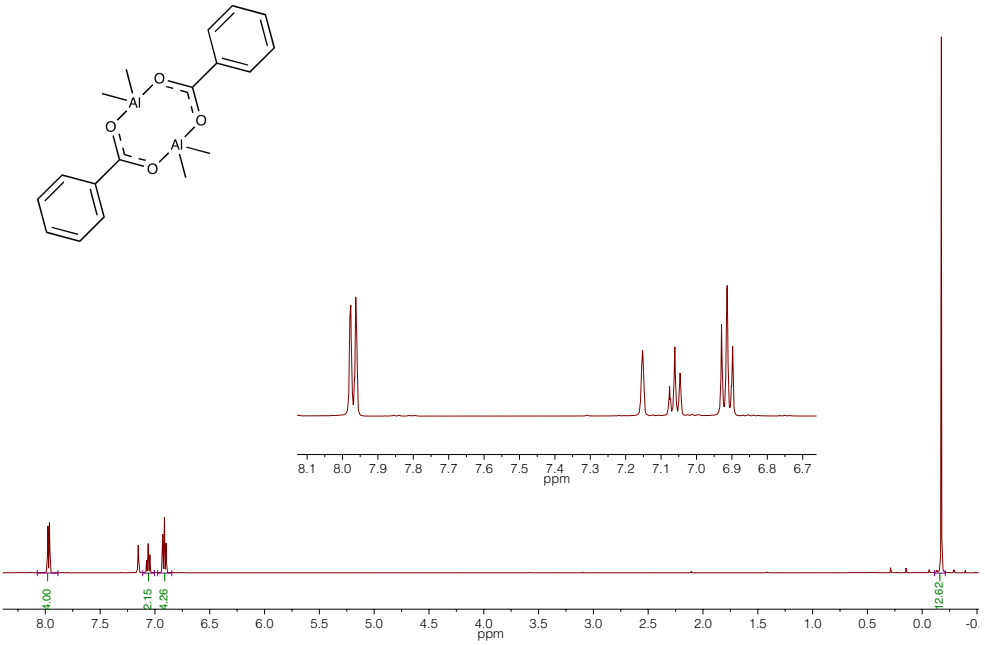

Figure 9: ^{1}H-NMR spectrum of **43** in C_6D_6, with solvent residual peak at $\delta = 7.15$ ppm. The inset shows the expansion of the aromatic region between $\delta = 8.1$-6.7 ppm.

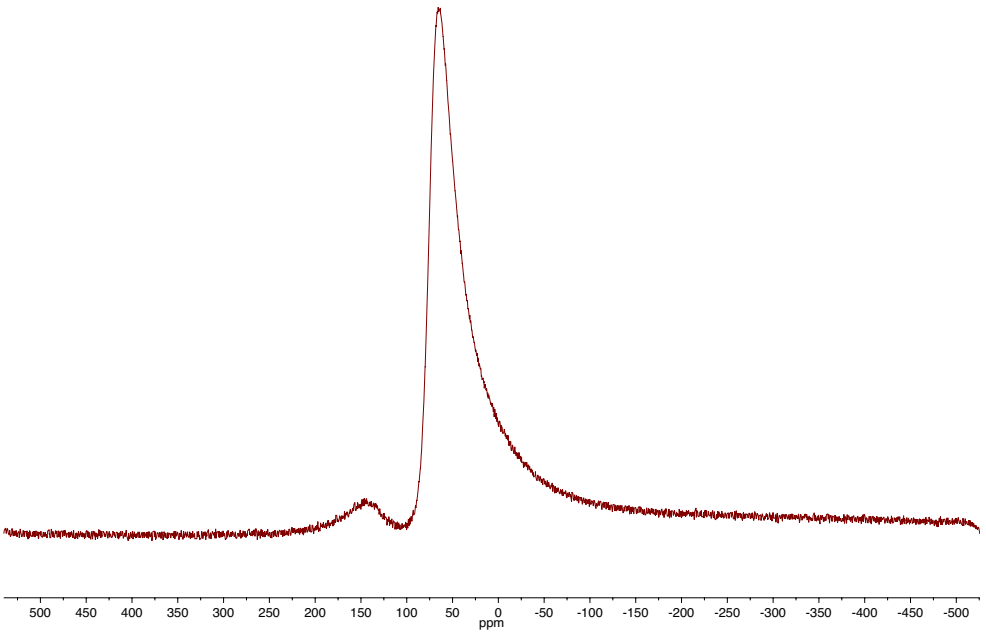

Figure 10: ^{27}Al-NMR spectrum of **43** in C_6D_6. The large artefact at $\delta = 64.7$ ppm results from the background probe signal and is visible in all ^{27}Al NMR spectra. [225] [247] [248]

The crystal structure of $[Me_2Al(\mu\text{-}O_2CPh)]_2$ **43** (Figure 11) confirms the formation of a dimer, with two bridging $AlMe_2$ units. The crystals were obtained from the reaction solution and it is therefore noteworthy that the formation of a Lewis acid/base adduct between the THF and the aluminium is not observed. When originally synthesised in the course of this project this structure had not been reported and the results correspond with the findings of Lewiński *et al.* for the structure of $[Cl_2Al(\mu\text{-}O_2CPh)]_2$ [211] [249] and of Barron *et al.* who reported the structure of $[^tBu_2Al(\mu\text{-}O_2CPh)]_2$. [212]. In 2017 Lewiński *et al.* reported structure **43**. [250]

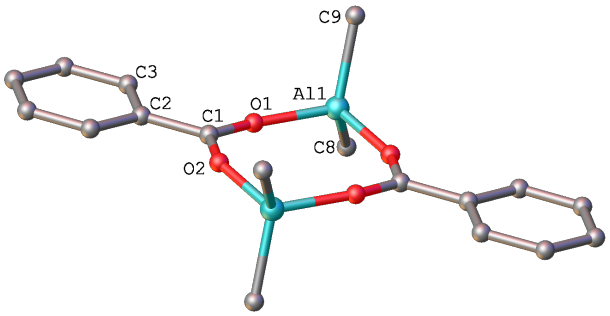

Figure 11: Molecular structure of $[Me_2Al(\mu\text{-}O_2CPh)]_2$ **44**. H-atoms are omitted for clarity. For selected bond lengths and angles see Table 2.

Table 2 compares the bond angles and lengths of these three different structures. **43**, which bond lengths and angles correspond with those reported by Lewiński *et al.* [250], and the structure of $[Cl_2Al(\mu\text{-}O_2CPh)]_2$ reported by Lewiński and co-workers show a planar $Al_2O_4C_2$ ring. The use of the bulkier *tert*-butyl ligand, on the other hand, forces the ring into a more chair-like formation, with the phenyl rings as equatorial substituents and the *tert*-butyl groups being axial and equatorial. This is reflected in the torsion angle between C(7)-O(1)-Al(1)-O(2), which is smallest for $Cl_2Al(\mu\text{-}O_2CPh)]_2$ and largest for $[^tBu_2Al(\mu\text{-}O_2CPh)]_2$. The bond lengths from Al to O are consistent between the different structures, but it should be noted that Al(1)-O(1) bond is always slightly longer than Al(1)-O(2), suggesting that the aluminium is binding more strongly to O(1), which is also reflected in the bond of O(1)-C(7) being 1.253(3) Å compared to 1.251(3) Å for O(2)-C(7). In all three structures, the angle of the carboxylate O(1)-C(7)-O(2) is slightly bigger than for free benzoic acid (120.96°) [251] as a result of the coordination to the aluminium. However, it is smaller than the bond angle in comparable sodium and potassium benzoate dimers, where the corresponding angles are 124.44° and 124.47°, respectively (which are mean values measured manually using Mercury CSD 3.9.). [252]

Table 2: Selected bond lengths and angles for **43** and comparison to related structures. Lengths are given in Å, angles in deg. Torsion angles were measured manually with Mercury CSD 3.9.

	Lewinski [211] [249] $[Cl_2Al(\mu\text{-}O_2CPh)]_2$	**43** $[Me_2Al(\mu\text{-}O_2CPh)]_2$	Barron [212] $[^tBu_2Al(\mu\text{-}O_2CPh)]_2$
C(1)-O(1)-Al(1)-O(2)	14.73	32.37	46.14
O(1)-Al(1)-(O2)	109.16(3)	108.28(10)	107.8(1)
O(1)-C(1)-O(2)	121.4(4)	122.8(2)	122.7(3)
C(8)-Al(1)-C(9)	-	122.05(14)	124.2(2)
Cl-Al-Cl	115.6(6)	-	-
Al(1)-C(8)	-	1.939(3)	1.965(5)
Al-Cl	2.095(1)	-	-
Al(1)-O(1)	1.755(3)	1.7932(19)	1.809(3)
Al(1)-O(2)	1.777(3)	1.802(2)	1.811(3)

Attempts to react $AlMe_3$ with two or three equivalents benzoic acid in attempts to make higher substitutes of **43** were unsuccessful and resulted in the formation of a white solid, irrespective of the reaction conditions in terms of concentration, stoichiometry or solvents. The addition of Lewis bases or heating the suspension had no effect. The elemental analysis of the solid formed after the reaction of $AlMe_3$ with two equivalents of benzoic acid showed C=58.26 % and H=4.76 % [the calculated composition for a successful and complete reaction of one equivalent $AlMe_3$ with two equivalents of benzoic acid would be C=63.38 %, H=4.61 %]. The addition of an additional equivalent of benzoic acid to **43**, the reaction product of the one-to-one reaction of benzoic acid and $AlMe_3$, lead to the same results, with the white solid being formed as soon as the second equivalent of PhCOOH dissolved in the reaction solution. The white solid could be a polymeric alumoxane or a higher aggregate. It was not soluble in hexane, DCM, ether, THF, acetonitrile, DMSO, acetone, ethanol or water. It dissolved poorly in hydrochloric acid, with very little effervescence.

4.1.1.2 Reactions of Salicylic Acid and its Derivatives with AlR_3

After successfully isolating $[Me_2Al(\mu\text{-}O_2CPh)]_2$ the next step was the introduction of an electron-donating functionality in the *ortho*-position. The additional Lewis-base function after expected deprotonation of the hydroxy function should offer additional coordination modes and stabilisation for the metal and give access to different prod-

uct stoichiometries. The reaction of salicylic acid with an equimolar amount of AlR_3 showed some effervescence, but no products or by-products could be isolated or identified. The reaction of salicylic acid with two equivalents of Al^iBu_3 (Scheme 39) led to the formation of the dimeric alane **45**. The carboxylic acid and the phenol group have been deprotonated.

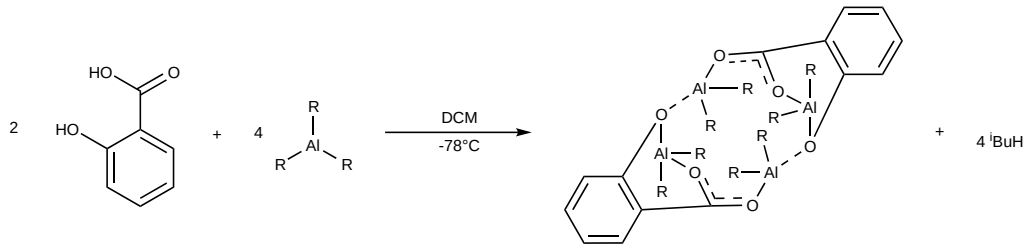

45

Scheme 39: Reaction of salicylic acid and Al^iBu_3(R=^{i}Bu).

The crystal structure of **45** is shown in Figure 12. Selected bond lengths and angles are given in Table 3. The dimeric structure consists of two individual units of [^{i}Bu$_4$Al$_2$(μ-O$_2$CC$_6$H$_4$-2-μ-O)] with an inversion centre. Each molecule has two different Al^iBu_2 units. One Al^iBu_2 unit is chelated between the carboxylate oxygen and the aryloxide oxygen of one salicylic acid molecule respectively, and one Al^iBu_2 unit is bridging between the carboxylate of one ligand and the aryloxide oxygen of the other. The resulting framework consists of three fused heterocyclic rings: one distorted 12-membered ring formed by two [Al-O-C-O-Al-O] fragments, which incorporate the intermolecular- and intramolecular bonded Al, and two distorted six-membered rings formed by the salicylate and the chelated aluminium Al(1). The coordination mode of the carboxylate groups follows a syn-anti conformation (compare to Scheme 25). Both aluminium atoms deviate from the plane of the carboxylate groups by 9.17° for O(3)-C(7)-O(2)-Al(2) and 17.18° for O(2)-C(7)-O(3)-Al(1), which in turn are twisted by 21.97° (C(2)-C(1)-C(7)-O(1)) against the planar phenyl ring. The aluminium atoms are in very distorted tetrahedral environments, with the C-Al-C angles 123.68(16)° and 122.31(19)° respectively, for Al(1) and Al(2). The O-Al-O angles are significantly smaller and close to being right-angled at 94.42(10)° for Al(1) and 90.26(10)° for Al(2). An equivalent compound, using $AlEt_3$ was published by Lewiński *et al.*, using the same solvent, reaction time and stoichiometry of the reagents.[216]

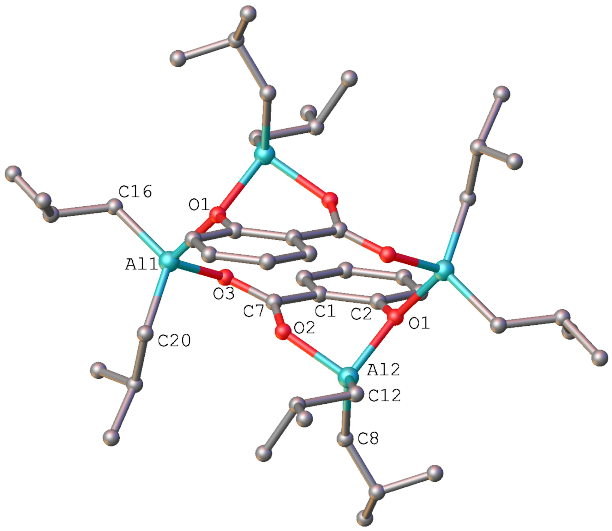

Figure 12: Molecular structure of **45**, $[^{i}Bu_4Al_2(\mu\text{-}O_2CC_6H_4\text{-}2\text{-}\mu\text{-}O)]_2$. H-atoms are omitted for clarity. For selected bond lengths and angles see Table 3.

Table 3: Selected bond lengths and angles for **45**. Lengths are given in Å, angles in deg. Torsion angles were measured manually with Mercury CSD 3.9.

	45 $[^{i}Bu_4Al_2(\mu\text{-}O_2CC_6H_4\text{-}2\text{-}\mu\text{-}O)]_2$
Al(1)-O(1)	1.891(2)
Al(1)-O(3)	1.853(2)
Al(2)-O(1)	1.891(2)
Al(2)-O(2)	1.852(2)
O(3)-Al(1)-O(2)	94.92(10)
O(2)-Al(2)-O(1)	90.26(10)
C(20)-Al(1)-C(16)	123.68(16)
C(8)-Al(2)-C(12)	122.31(19)
O(2)-C(1)-O(1)	121.2(3)
C(2)-C(1)-C(7)-O(3)	21.97
O(3)-C(7)-O(2)-Al(2)	9.17
C(7)-O(2)-Al(2)-O(1)	44.67
O(2)-C(7)-O(3)-Al(1)	17.18

The ^{1}H NMR spectrum of **45** shows no evidence for acidic protons, indicating that no starting material remained. All expected peaks are present. The isobutyl groups of the Al^{i}Bu$_2$ units are inequivalent and bear diastereotopic protons, giving rise to separate peaks.

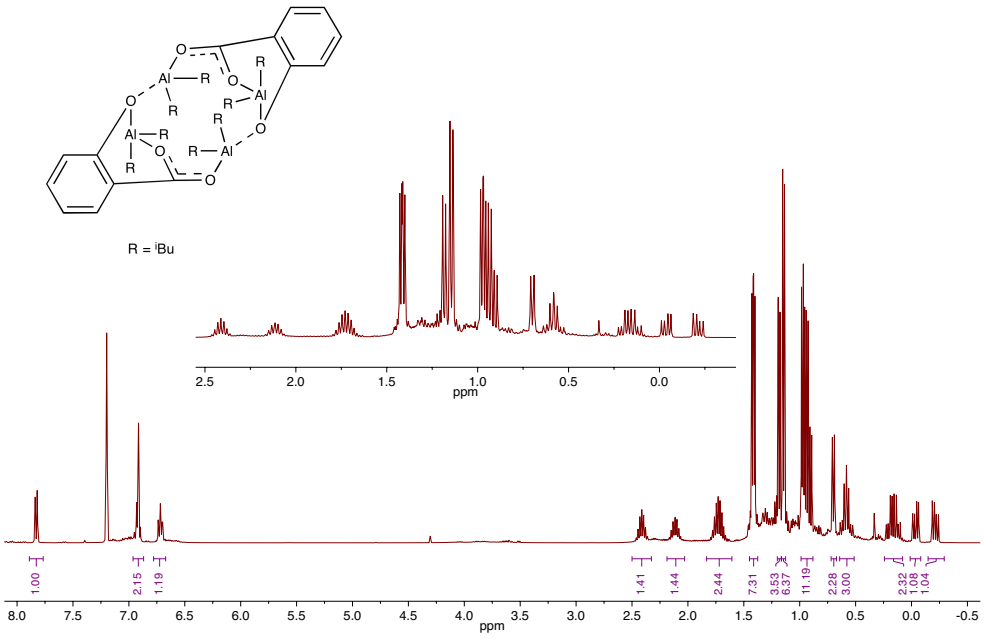

Figure 13: ^{1}H-NMR spectrum of **45** in C_6D_6, with solvent residual peak at δ = 7.15 ppm. The inset shows the expansion of region between δ = 2.5 - -0.7 ppm, with the signals resulting from the hydrogen atoms in the Al^{i}Bu$_2$ groups.

The derivatisation of salicylic acid with $AlMe_3$ resulted in the formation of a white suspension, irrespective of the equivalents of $AlMe_3$ used, the concentration of reactants, the solvent (DCM, THF, hexane, toluene and mixtures thereof) and the reaction time (the suspension formed as soon as the $AlMe_3$ was added and effervescence started). Similar to the white powder obtained for the unsuccessful reaction between $AlMe_3$ and two or three equivalents of benzoic acid, it was not possible to identify the products.

Salicylic acid has two acidic hydrogens which can react with an aluminium organyl, and could theoretically lead to different coordination modes for the metal in the resulting product and/or reactions of different stoichiometry affording single or double metallated species. This was further investigated by substituting the hydrogen atom of the phenolic group by a methyl group to give an ether. Having done this, the reaction of one equivalent of 2-methoxybenzoic acid, also known as *ortho*-anisic acid, and

one equivalent of $AlMe_3$ (Scheme 40) was investigated. The resulting powder did not suffice for investigation by for X-ray diffraction.

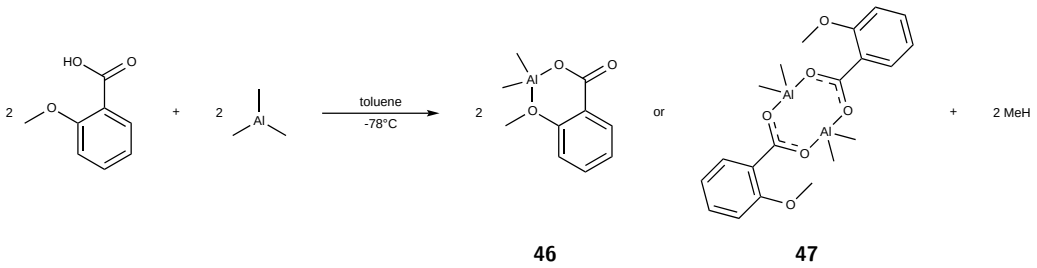

46 **47**

Scheme 40: Reaction of *o*-anisic acid and $AlMe_3$.

The ^1H NMR spectrum of the isolated product suggests that a complete reaction has occurred since no signal for the carboxyl hydrogen is observed at δ = 10.3 ppm. The integrals imply that one equivalent of $AlMe_3$ reacted with one equivalent of acid, as there are six hydrogens binding to aluminium (δ =-0.14 ppm) for one aromatic system (δ = 6.30-8.14 ppm). The ^{27}Al NMR spectrum of **46** shows one peak at δ =143.9 ppm, indicating a tetra-coordinated aluminium centre.[222] This could be explained by the formation of a dimeric species **46** similar to **43**, the reaction product of benzoic acid and $AlMe_3$, which is very common for this class of compounds.[188][214][216]. Another possibility would be the formation of a chelate complex **47** by intramolecular chelation of the $AlMe_2$ unit. This is known for aluminium complexes with O,O′-chelating ligands, such as 2-methoxyphenol or 2-(hydroxymethyl)phenol. These complexes form dimers in the solid state with penta-coordinated aluminium.[188][253][254] Other examples for ligands in aluminium complexes with chelated Al centres are various Schiff base derivatives.[204]

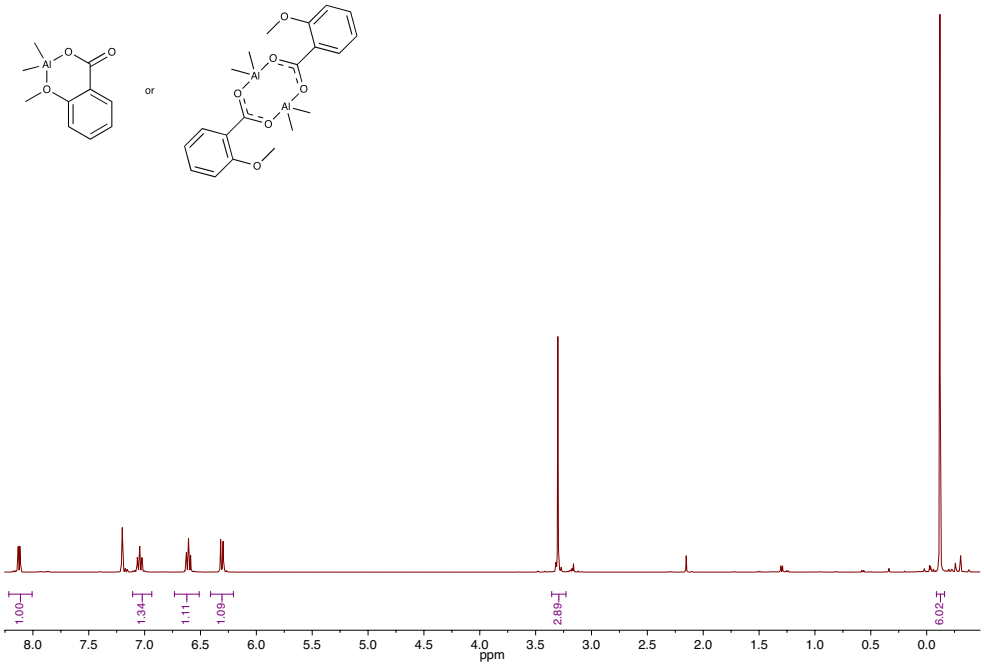

Figure 14: ^{1}H-NMR spectrum of **46** in C_6D_6, with solvent residual peak at $\delta = 7.15$ ppm.

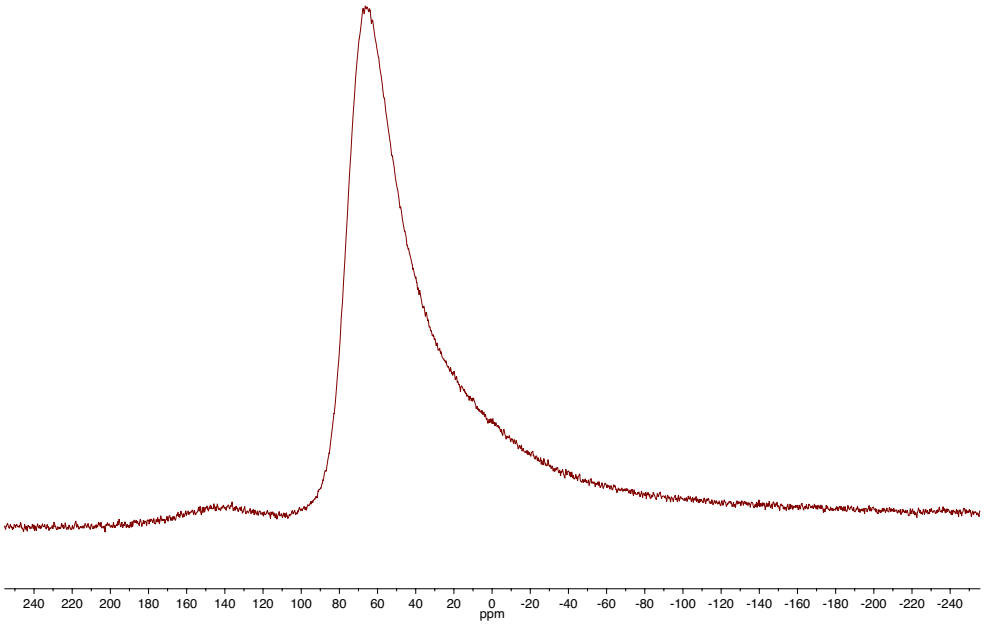

Figure 15: ^{27}Al-NMR spectrum of **46** in C_6D_6. The large artefact at $\delta = 65.9$ ppm results from the background probe signal and is visible in all ^{27}Al NMR spectra.[225] [247] [248]

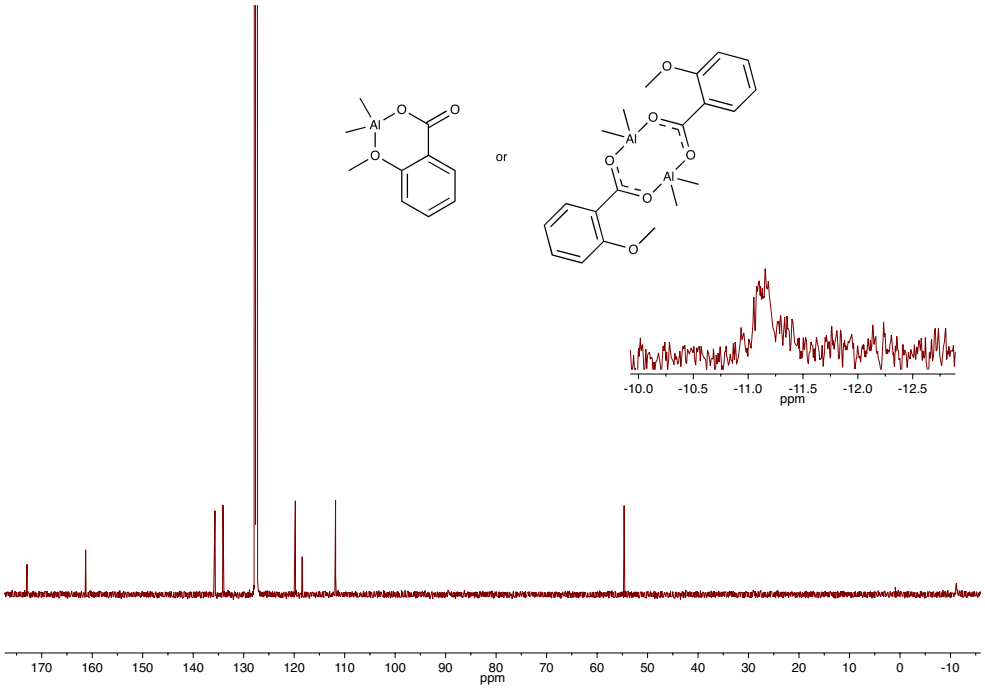

Figure 16: ^{13}C-NMR spectrum of **46** in benzene, with the solvent residual peak at δ = 127.36 ppm. The inset shows the peak resulting from the Al*C*H3 carbon.

For the completeness of this investigation, the reaction of methyl salicylate with $AlMe_3$ was carried out in toluene. By using the ester of salicylic acid the number of available acidic hydrogen atoms is reduced to one, that of the phenolic OH group. The reaction was tried in a one-to-one stoichiometry (Scheme 41) and lead to the formation of the dimeric compound **48** which was analysed by x-ray crystallography.

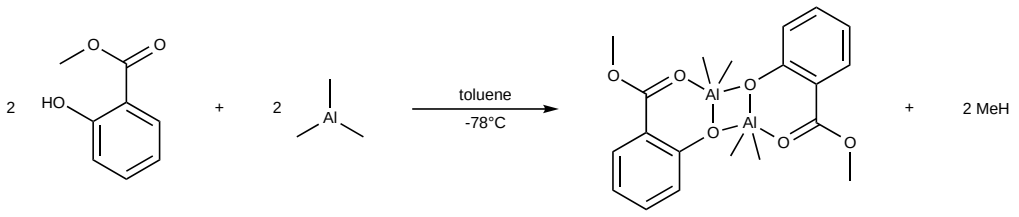

48

Scheme 41: Reaction of methyl salicylate and $AlMe_3$.

The molecular structure of **48** is identical with the one reported by Lewiński *et al.* in 1997.[194] It consists of a four-membered ring, as well as two distorted six-membered rings. The system is almost planar and centrosymmetric. The monomeric molecules are bridged by oxygen atoms from the aryloxide of the methyl salicylate ion. The aluminium centres are penta-coordinated with a distorted trigonal bipyramidal geom-

etry. The distortion results from the strained Al_2O_2-ring. Compared to [^{i}Bu$_4$Al$_2$(μ-O$_2$CC$_6$H$_4$-2-μ-O)]$_2$ **45** the second oxygen O(2) is not involved in bonding to the aluminium. The bond between Al(1) and O(3') is the longest with 2.0702(15) Å and can be assumed to be the bridging bond between the two parts of the dimer. The bond length and angles (Table 4) correspond with the data reported by Lewiński and co-workers, who used identical reaction conditions.

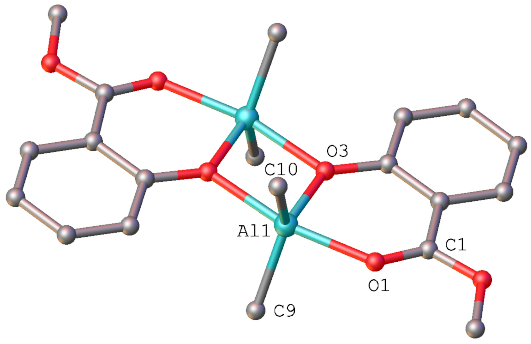

Figure 17: Molecular structure of **48**, [Me$_2$Al(mesal)]$_2$. H-atoms are omitted for clarity. For selected bond lengths and angles see Table 4.

Table 4: Selected bond lengths and angles for **48**. Lengths are given in Å, angles in deg.

	48 [Me$_2$Al(mesal)]$_2$
Al(1)-O(3)	1.8432(16)
Al(1)-O(1)	1.9902(16)
Al(1)-O(3')	2.0702(15)
O(3)-Al(1)-O(3')	76.05(7)
O(1)-Al(1)-O(3)	88.73(7)
Al(1)-O(3)-Al(1')	103.95(7)
O(1)-Al(1)-O(3')	164.78(7)
O(1)-C(1)-O(2)	120.74(19)
O(1)-Al(1)-C(9)	91.27(9)
O(3)-Al(1)-C(9)	115.60(11)
C(9)-Al(1)-C(10)	129.29(13)

The proton NMR spectrum of **48** shows singlets for the Al*Me* and COO*Me* protons as well as well defined multiplets for the aromatic system, confirming the successful synthesis of [Me$_2$Al(mesal)]$_2$.

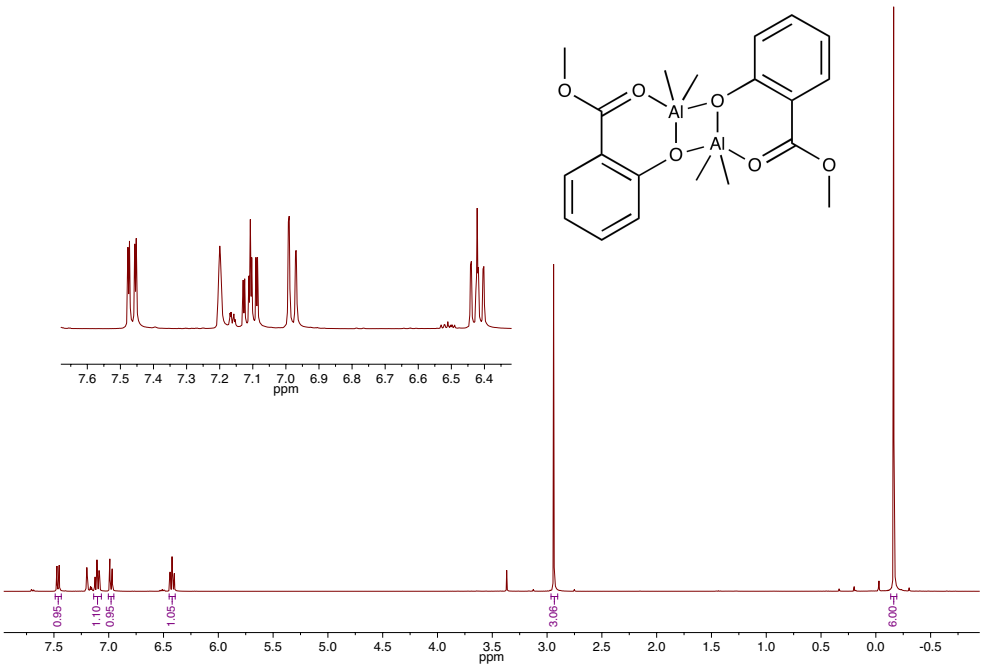

Figure 18: ^{1}H-NMR spectrum of **49** in C_6D_6, with solvent residual peak at $\delta = 7.15$ ppm. The inset shows the expansion of the aromatic region between $\delta = 7.6$ - 6.4 ppm.

4.1.1.3 Reactions of Anthranilic Acid and its Derivatives with AlR_3

4.1.1.3.1 Reactions of Anthranilic Acid and AlR_3

The reactions of salicylic acid and its derivatives with trivalent aluminium organyls yielded interesting structures. In the next step of the project, the focus was shifted to the *ortho*-amino derivatives of benzoic acid. In anthranilic acid, the nitrogen could be deprotonated twice, so it could potentially lead to different bonding motifs with three acidic hydrogen atoms in total. Furthermore, the amino group can be considered softer and more polarisable than the hydroxy group by the rather hard aluminium.

The equimolar reaction of anthranilic acid (2-$NH_2C_6H_4COOH$) itself, and $AlMe_3$ (Scheme 42) yielded a yellow suspension when it warmed up to room temperature, of which the solid was filtered off and analysed by NMR spectroscopy. A small amount of insoluble material remained in the NMR sample and is assumed to be potential by-products, formed during the reaction.

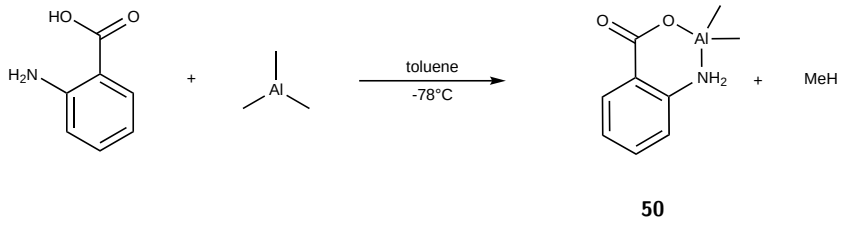

50

Scheme 42: Equimolar reaction of anthranilic acid and $AlMe_3$ with a proposed reaction product based on the ^{1}H-NMR spectrum.

The ^{1}H-NMR spectrum of **50** (Figure 19) showed no signal for the carboxylic acid at δ > 8 ppm, where it would be expected. The signal at δ = 4.92 ppm with an integral of approx. 2 (1.90) corresponds with the amino group hydrogens (NH_2), suggesting that only the more acidic carboxyl group was deprotonated and that no starting material remained. However, the integrals for the aromatic hydrogens (δ = 5.95-7.97 ppm), the amino group hydrogens (δ = 4.92 ppm) and the aluminium methyl protons (δ = -0.24 ppm) showed a ratio of 4:2:6, suggesting that for each $^-OOC–C_6H_4–2\text{-}NH_2$ there must be two methyl groups binding to aluminium. This could be explained by the simple 1:1 reaction, leading to the formation of an alane with a possible structure with the connectivity proposed in Scheme 42 for **50** [$Me_2Al(\mu\text{-}O_2CC_6H_4NH_2\text{-}2)$].

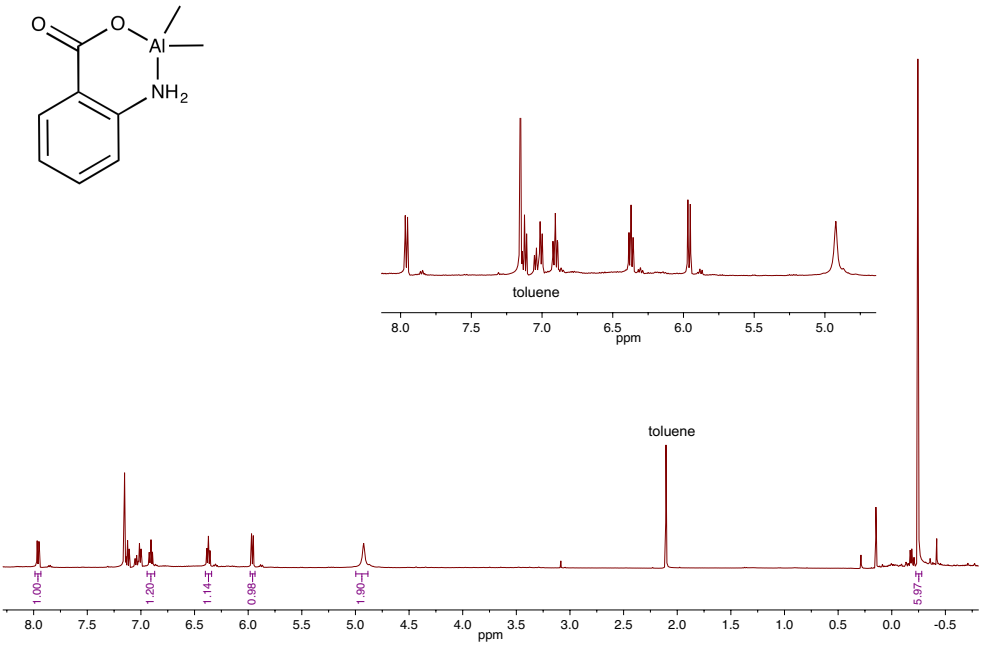

Figure 19: ^{1}H-NMR spectrum of **50** in C_6D_6, with the solvent residual peak at $\delta = 7.18$ ppm. The inset shows the aromatic region and the amino group hydrogens between δ = 8-4.6 ppm.

The ^{27}Al-NMR (Figure 20) shows two product peaks, one at δ = 11.9 ppm, which is consistent with an octahedrally coordinated Al centre.[222] This results most likely from small dissolved amounts of the insoluble compound present in the spectroscopic sample. The second, broad peak at δ = 142 ppm, is in the characteristic area for tetra-coordinated aluminium atoms.[222] This would not agree with the presence of two $AlCH_3$ groups unless the compound would form aggregates. Entropy favours chelation over aggregation, and the shift of δ = 142 ppm supports the assumption that the structure could be similar to the chelate **50** shown in Scheme 42.

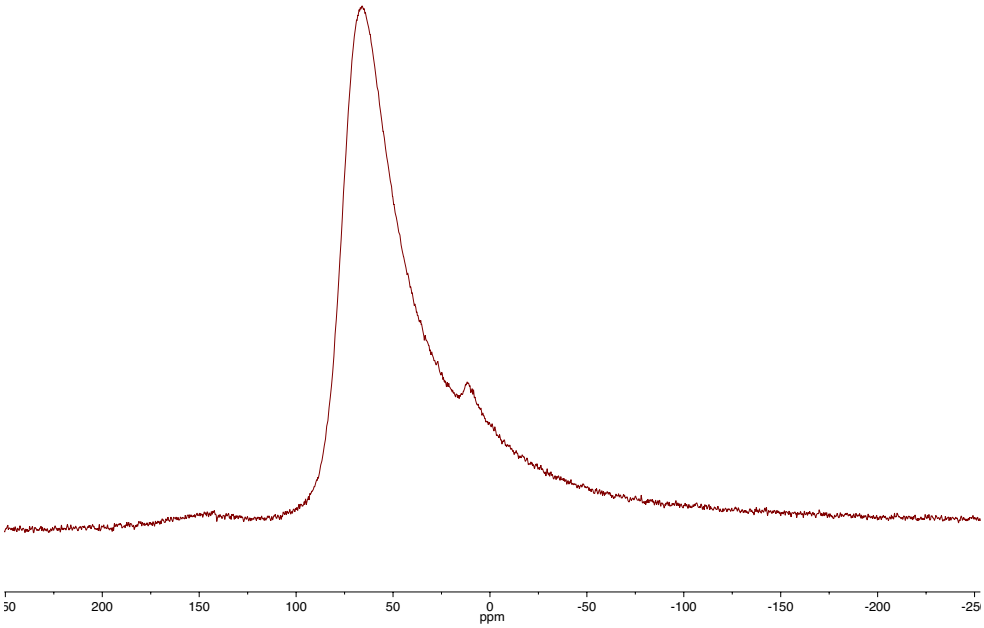

Figure 20: ^{27}Al-NMR spectrum of **50** in C_6D_6. The large artefact at δ = 65.6 ppm results from the background probe signal and is visible in all ^{27}Al NMR spectra.[225] [247] [248].

In order to attempt to obtain a crystal structure of what appeared to be the major product in the NMR, the sample was heated briefly to reflux in order to dissolve the solid material and afterwards placed in the freezer. Colourless, block-shaped crystals were obtained after 72h at -30°C. X-ray diffraction of these crystals revealed a structure (Figure 21) which is inconsistent with the ^{1}H-NMR spectrum. Instead of the expected chelate **50** [$Me_2Al(\mu\text{-}O_2CC_6H_4NH_2\text{-}2)$] it shows a dimeric structure in which the carboxylate is deprotonated but the amino group has been deprotonated once as well, with a NH group remaining. This results in two anthranilates binding to four $AlMe_2$ groups (Scheme 43).

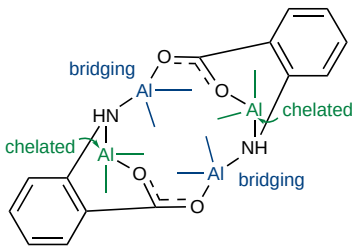

51

Scheme 43: Structure of **51**, $[(Me_2Al)_2(\mu\text{-}O_2CC_6H_4\text{-}2\text{-}\mu\text{-}NH)]_2$, based on the crystal structure Figure 21 with bridging and chelated $AlMe_2$ groups.

Two $AlMe_2$ units are bridging the two anthranilates. Two more dimethylaluminium moieties are being chelated between the amide and carboxylate functionality of the respective anthranilates. Both types of aluminium centre are in distorted tetrahedral coordination environments, which is consistent with the ^{27}Al-NMR spectrum. The angles at the bridging dimethylaluminium fragment are 100.53(10)° (O(2)-Al(2)-N(1)) and 119.83(17)° (C(11)-Al(2)-C(10)). For the chelated $AlMe_2$ O(1)-Al(1)-N(1) is 92.24(10)° and differs more strongly from the ideal tetrahedral angle of 109.5°, C(9)-Al(1)-C(8), on the other hand, with 119.81(17)° is almost identical with the angle at the bridging $AlMe_2$ unit. The dimer consists of a central distorted twelve-membered ring formed of two [O-C-O-Al-N-Al]-units and two very distorted six-membered rings formed by the chelated dimethylaluminium. The carboxylate group is binding to the chelated $AlMe_2$ unit in the *anti*-mode and to the bridging $AlMe_2$ in the *syn*-mode. The *syn*-bond is slightly shorter (1.8294(19) Å) than the *anti*-bond (1.841(2) Å), which suggests that the *syn*-bond is stronger, although the C(7)-O(1) and C(7)-O(2) bonds are very close with 1.266(3) Å and 1.268(3) Å, respectively. The structure of $[(Me_2Al)_2(\mu\text{-}O_2CC_6H_4\text{-}2\text{-}\mu\text{-}NH)]_2$ corresponds with the analogous salicylic acid adduct $[^{i}Bu_4Al_2(\mu\text{-}O_2CC_6H_4\text{-}2\text{-}\mu\text{-}O)]_2$ **45** and with $[Et_4Al_2(\mu\text{-}O_2CC_6H_4\text{-}2\text{-}\mu\text{-}NH)]_2$ which has been reported by Lewiński and co-workers.[215] They also succeeded to synthesise **50**, $[Me_2Al(\mu\text{-}O_2CC_6H_4NH_2\text{-}2)]$, and the $AlEt_3$ equivalent and found that those compounds are unstable at room temperature. Their reaction conditions restricted the temperature during warm up to 10°C and they used DCM as a solvent. For the synthesis of **50** in this project, toluene was used and the reaction was stirred at room temperature during the summer months. The structure also compares to the $Al^{t}Bu_3$ equivalent. Selected bond lengths and angles for **51** are given in Table 5.

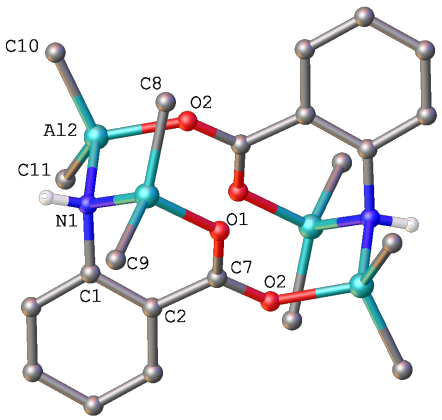

Figure 21: Molecular structure of **51**, $[(Me_2Al)_2(\mu\text{-}O_2CC_6H_4\text{-}2\text{-}\mu\text{-}NH)]_2$. H-atoms are omitted for clarity. For selected bond lengths and angles see Table 5.

Table 5: Selected bond lengths and angles for **51**. Lengths are given in Å, angles in deg.

	51 $[(Me_2Al)_2(\mu\text{-}O_2CC_6H_4\text{-}2\text{-}\mu\text{-}NH)]_2$
Al(2)-O(2)	1.8294(19)
Al(2)-N(1)	1.989(2)
Al(2)-C(10)	1.949(3)
Al(1)-O(1)	1.841(2)
Al(1)-N(1)	1.961(2)
N(1) - H(N)	0.876(18)
O(2)-Al(2)-N(1)	100.53(10)
O(2)-Al(2)-C(10)	104.88(13)
O(2)-Al(2)-C(11)	113.80(13)
C(10)-Al(2)-N(1)	108.16(14)
C(11)-Al(2)-C(10)	119.83(17)
O(1)-Al(1)-N(1)	92.24(10)
O(1)-Al(1)-C(8)	109.56(14)
C(9)-Al(1)-C(8)	119.81(17)

The solid-state structure is also confirmed by NMR spectroscopy although at this point it is not possible to confirm if the aggregation state is retained as well. The ^{1}H-spectrum shows that the ratio between the aromatic, the amide group and dimethylaluminium hydrogens is 4:1:12 (Figure 22), compared to 4:2:6 in Figure 19, where it indicated a one to one reaction (Scheme 42). Figure 22 also shows four distinguishable dimethylaluminium groups, similar to what was seen for the diisobutylaluminium groups in **45** ($[^iBu_4Al_2(\mu\text{-}O_2CC_6H_4\text{-}2\text{-}\mu\text{-}O)]_2$). The ^{27}Al-NMR spectrum shows one very broad signal at δ = 157.0 ppm, confirming a tetrahedral coordination of the aluminium atoms and suggesting that in the absence of coordinating solvents (benzene) the dimeric structure appears to be retained in solution.[222]

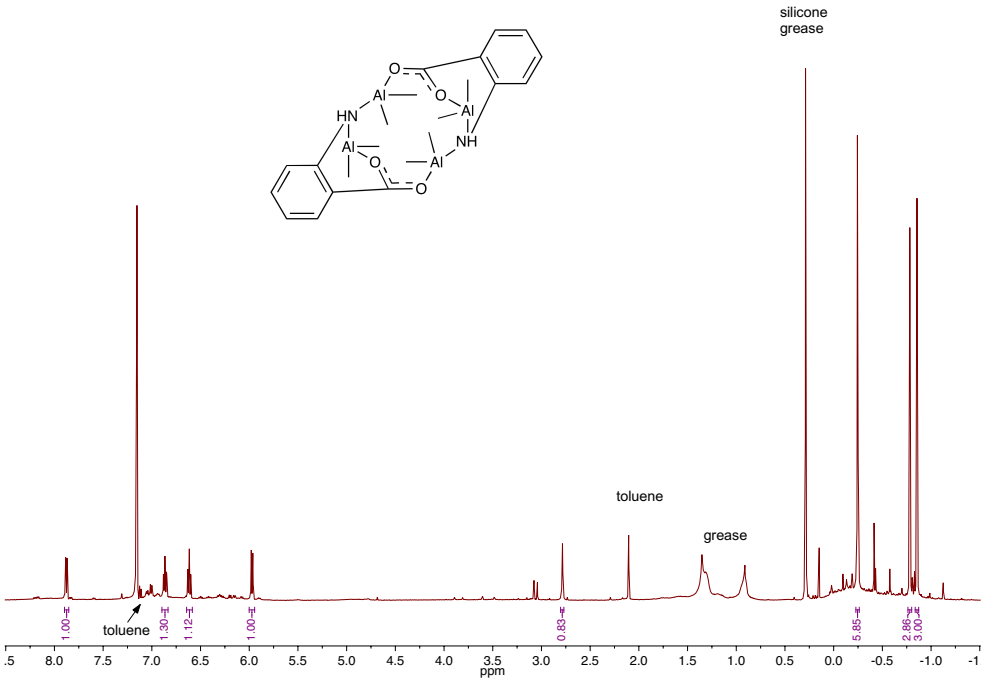

Figure 22: ^{1}H-NMR spectrum of **51** in C_6D_6, with the solvent residual peak at $\delta = 7.18$ ppm. The inset shows the aromatic region and the amino group hydrogens between $\delta = 8$-4.6 ppm.

Taken together, these findings for **51** suggest that upon heating monodeprotonated **50** ([$Me_2Al(\mu$-$O_2CC_6H_4NH_2$-2)]) undergoes further reaction. This could happen by reforming starting material alongside doubly deprotonated **51**, which is supported by the very low yield (30%) that was obtained after the heating of **50**. Although such a form of dismutation has, to the best of my knowledge, not been reported in the literature, there are examples for dismutations during the reaction of R_2AlCl with bis(trimethylsilyl)hydrazine, where the expected chlorosilane does not form, but the starting material dismutates to tris(trimethylsilyl) hydrazine and trimethylsilyl hydrazine.[255] [256] Furthermore, in the synthesis of ionic liquids with Tf_2N^- anions it was found that the adduct $AlCl_3$ can dismutate to $[AlCl_4]^-$ and $AlCl_2Tf_2N$.[257] Another explanation could be a product inhibition: After a certain percentage of anthranilic acid has reacted with one equivalent of $AlMe_3$ the formed intermediate **50** prevents further reaction of unreacted acid. Instead any remaining aluminium reagent reacts with **50**, although the NMR spectrum Figure 19 does not indicate the presence of unreacted starting material.

It was possible to reproduce the synthesis of **51**, $[(Me_2Al)_2(\mu$-$O_2CC_6H_4$-2-μ-$NH)]_2$, directly by setting up the reaction of anthranilic acid with two equivalents of $AlMe_3$ in

toluene and letting the reaction warm to room temperature. In order to get a solution, 20 mL of toluene were required for 1 mmol of anthranilic acid, whereas for the synthesis of **50**, [$Me_2Al(\mu\text{-}O_2CC_6H_4NH_2\text{-}2)$] only 5 mL were used. The yield for the direct synthesis of **51** was 90 %. The reaction between one equivalent of anthranilic acid and one equivalent of Al^iBu_3 did not produce an analogous compound to **50**, instead yielded reaction products that could not be identified by NMR spectroscopy. From the reaction of two equivalents of Al^iBu_3 with antranilic acid a product corresponding to **51** was obtained (Scheme 44) and characterised by x-ray crystallography and NMR spectroscopy.

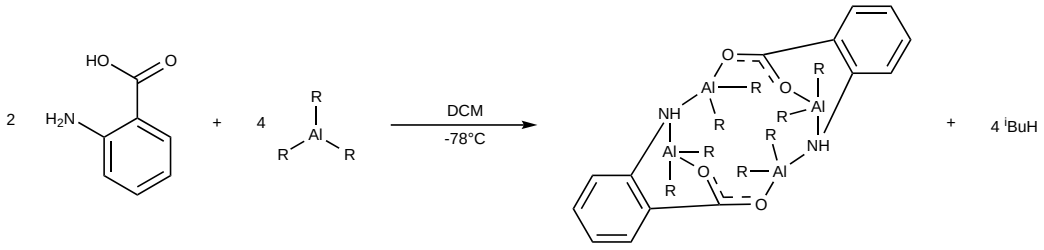

52

Scheme 44: Reaction of anthranilic acid with Al^iBu_3(R=^{i}Bu).

The crystal structure of compound **52** is shown in Figure 23. The tetranuclear structure is formed of two dimers, bridged by diisobutylaluminium units. The isobutyl groups of the chelated Al^iBu_2 moiety are disordered. The structure is centrosymmetric and the bond lengths and angles are similar to those observed for **51**. Values for selected lengths and angles are given in Table 6.

Compound **52** was analysed by NMR spectroscopy. The ^{1}H-NMR spectrum (Figure 24) shows all peaks that are expected based on the spectroscopic data of **45**, $[^iBu_4Al_2(\mu\text{-}O_2CC_6H_4\text{-}2\text{-}\mu\text{-}O)]_2$, and **51**, $[(Me_2Al)_2(\mu\text{-}O_2CC_6H_4\text{-}2\text{-}\mu\text{-}NH)]_2$. The singlet at δ = 3.05 ppm is the signal for the remaining hydrogen of the amido group. The area below δ = 2.5 ppm shows, apart from some impurities, signals for the protons of the aluminiumdiisobutyl groups, which, similar to those of **45**, are diastereotopic.

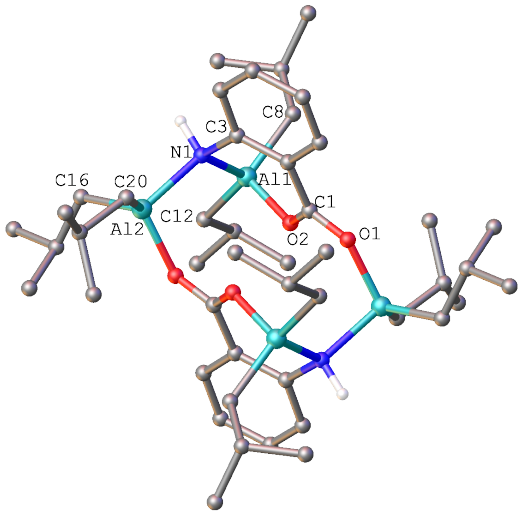

Figure 23: Molecular structure of **52**, $[(^{i}Bu_2Al)_2(\mu\text{-}O_2CC_6H_4\text{-}2\text{-}\mu\text{-}NH)]_2$. A disorder in the alkyl chains has been removed. CH-atoms are omitted for clarity. For selected bond lengths and angles see Table 6.

Table 6: Selected bond lengths and angles for **52**. Lengths are given in Å, angles in deg.

	52 $[(^{i}Bu_2Al)_2(\mu\text{-}O_2CC_6H_4\text{-}2\text{-}\mu\text{-}NH)]_2$
Al(2)-O(2)	1.8294(19)
Al(2)-N(1)	2.000(3)
Al(2)-C(16)	1.960(3)
Al(1)-O(1)	1.849(2)
Al(1)-N(1)	1.964(2)
N(1) - H(N)	1.000
O(2)-Al(1)-N(1)	91.00(10)
O(2)-Al(1)-C(12)	111.60(14)
O(2)-Al(1)-C(8)	107.09(13)
C(12)-Al(1)-N(1)	112.72(13)
C(8)-Al(1)-C(12)	121.25(16)
O(1)-Al(2)-N(1)	100.60(11)
O(1)-Al(2)-C(16)	107.48(14)
C(16)-Al(2)-C(20)	118.55(15)

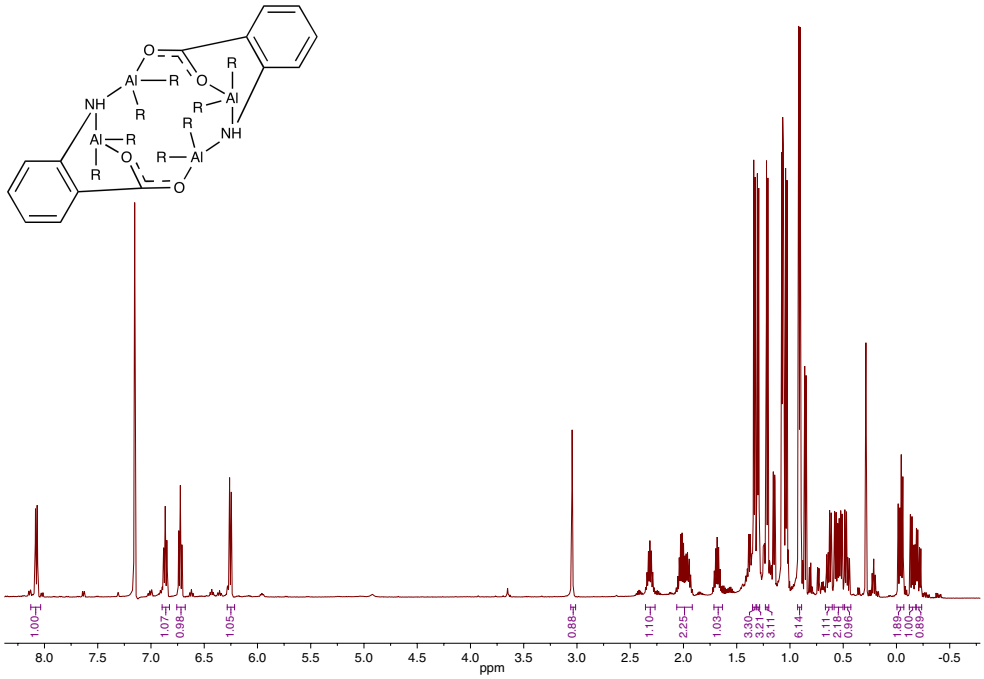

Figure 24: ^{1}H-NMR spectrum of **52** in C_6D_6, with the solvent residual peak at δ = 7.18 ppm.

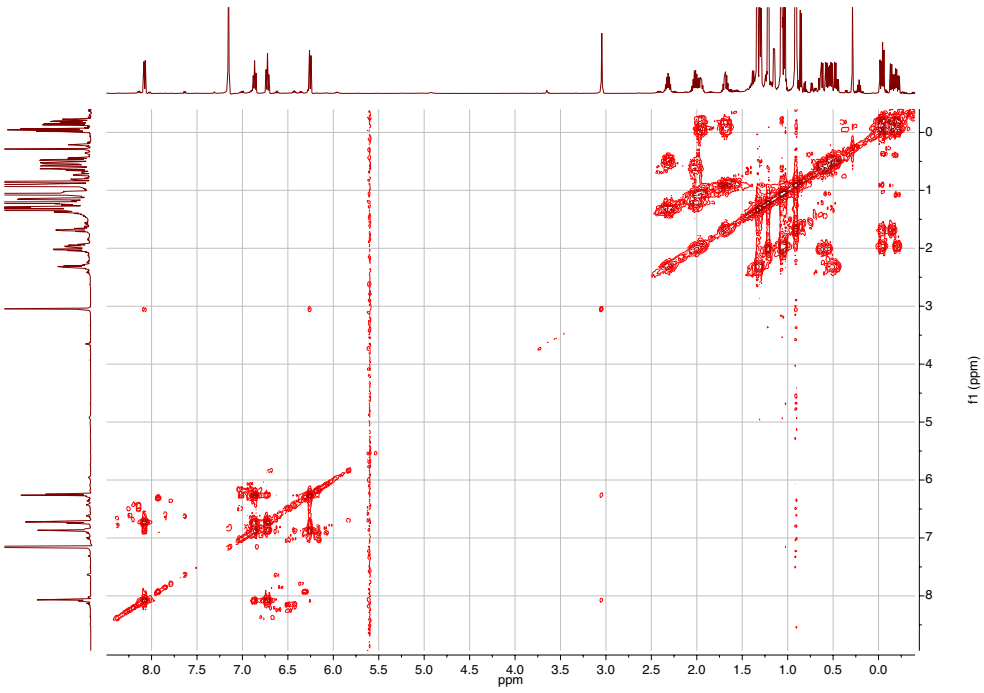

Figure 25: ^{1}H,^{1}H-COSY-NMR spectrum of **52** in C_6D_6.

The ^{1}H,^{1}H-COSY-NMR spectrum of compound **52**, Figure 25 shows cross peaks between the amido proton and the aromatic region. The information obtained from the HSQC spectrum (Figure 26) allowed the identification of most of the relevant ^{13}C-NMR signals (Figure 27). For better understanding, Scheme 45 shows the monomeric unit of **52** with numbered atoms.

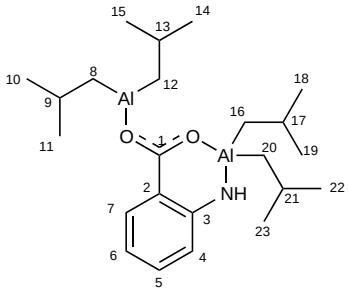

52

Scheme 45: Monomeric unit of **52**, with numbered carbon atoms, based on the crystal structure.

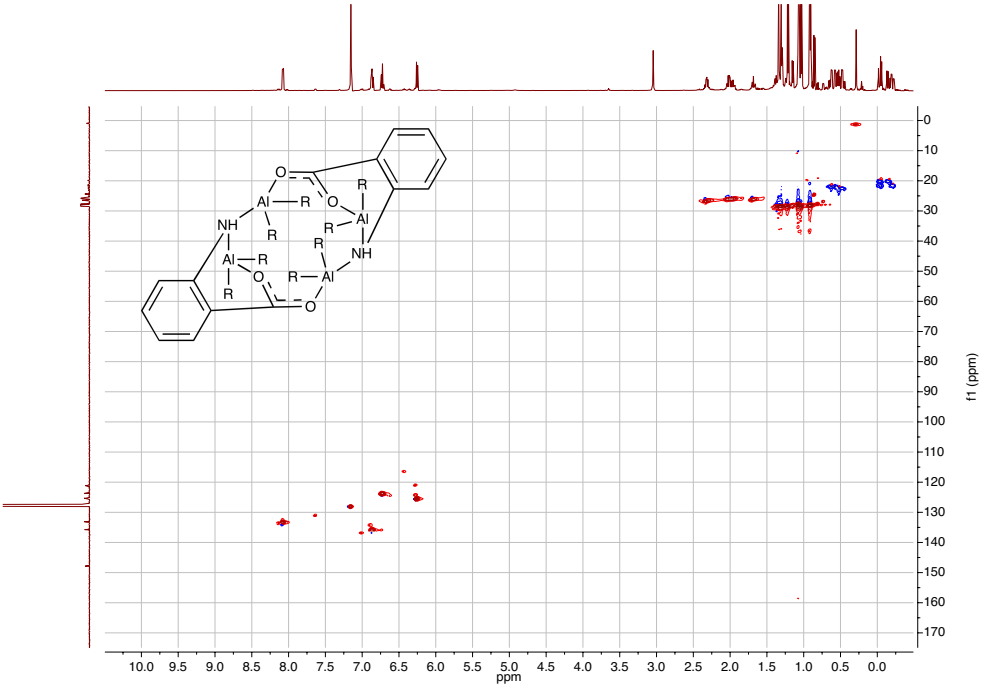

Figure 26: ^{1}H,^{13}C-HSQC-NMR spectrum of **52** in C_6D_6.

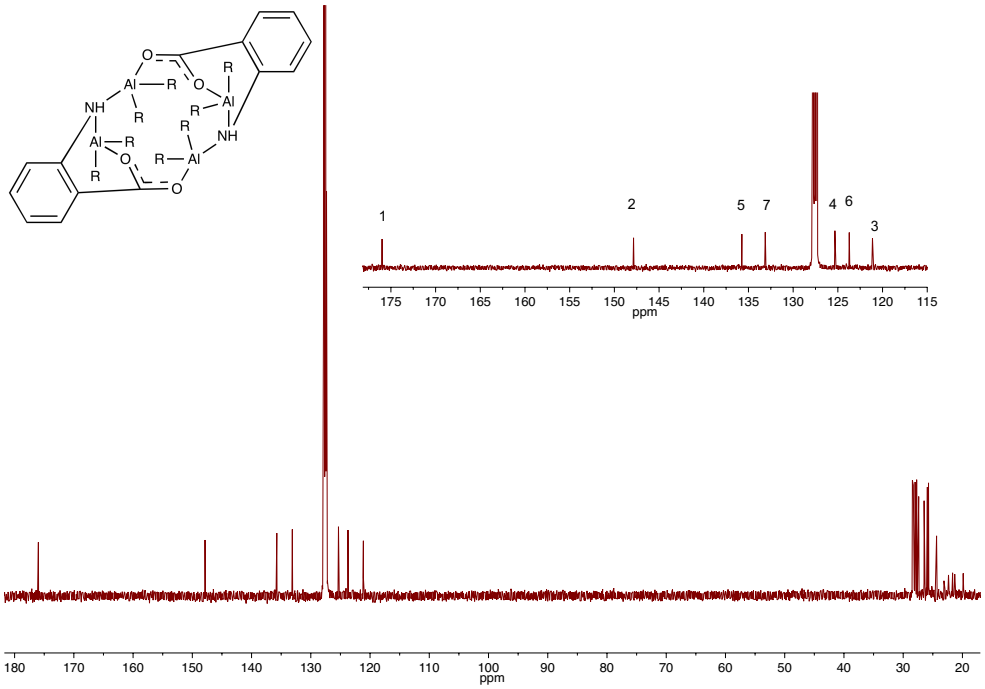

Figure 27: ^{13}C-NMR spectrum of **52** in C_6D_6, with the solvent residual peak at δ = 124.8 ppm. The inset shows the region for the aromatic system and the signal for the carboxylate carbon.

The HMBC spectrum (Figure 28) made it possible to distinguish between hydrogens 4 and 7: The ^{1}H-NMR signal at δ = 8.07 ppm shows a cross signal to the ^{13}C-NMR signal resulting from the quaternary carbon 2 at δ = 147.86 ppm, suggesting that both atoms must be in close proximity. Additionally, the ^{1}H-NMR signal at δ = 6.25 ppm shows a cross signal to the ^{13}C-NMR signal resulting from the quaternary carbon 3 at δ = 121.13 ppm.

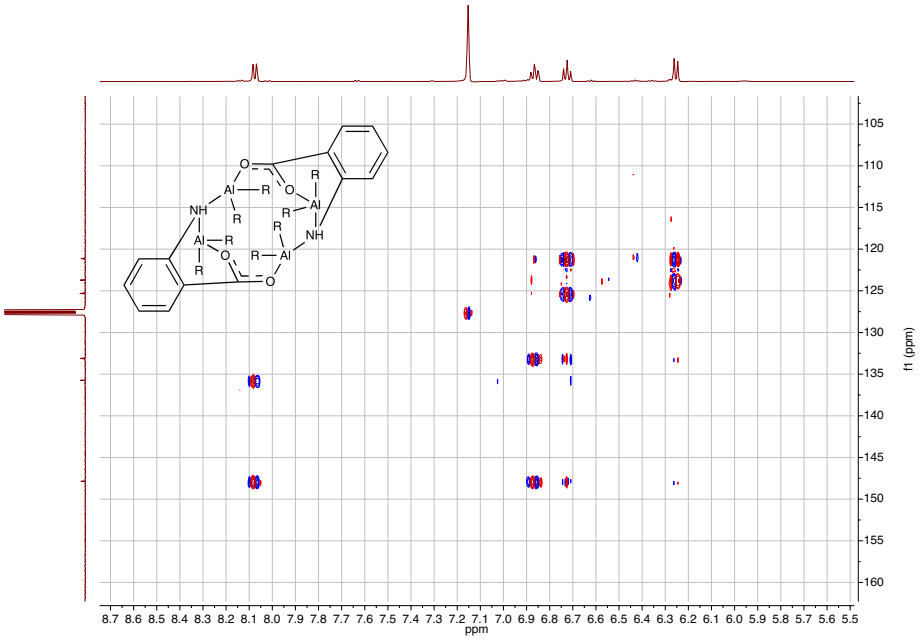

Figure 28: ^{1}H,^{13}C-HMBC-NMR spectrum of **52** in C_6D_6.

With this information the ^{1}H-NMR spectrum the signals for the aromatic system can be assigned as shown in Figure 29.

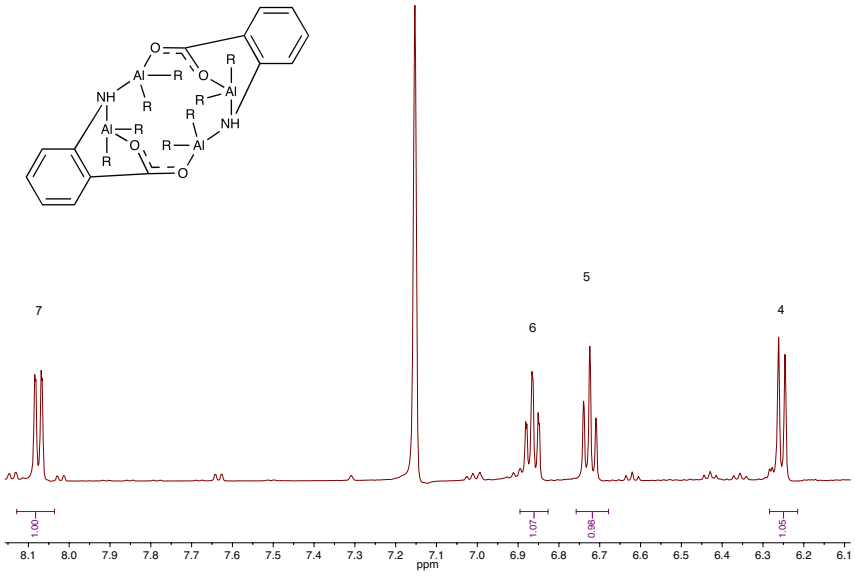

Figure 29: ^{1}H-NMR spectrum of **52** with assigned aromatic peaks, solvent: C_6D_6.

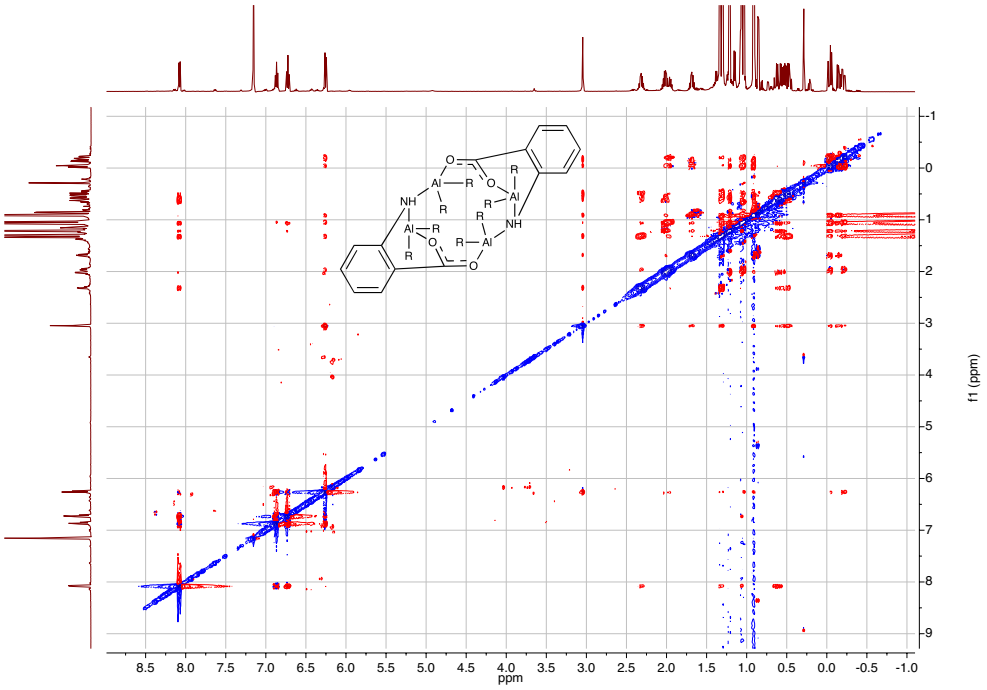

Figure 30: ^{1}H,^{1}H-NOESY-NMR spectrum of **52** in C_6D_6, mixing time $\tau_1 = 1.2$ s.

A NOESY spectrum was recorded (Figure 30) for **52**. The NOESY spectrum is obtained similar to a COSY spectrum, resulting in the appearance of diagonal peaks and cross peaks, based on the nuclear Overhouser effect (NOE).[258] In the COSY spectrum, the cross peaks show hydrogen atoms coupling with each other through chemical bonds, indicating that they are structurally close to each other. In the NOESY the cross signals show spatial closeness, that is not necessarily reflected in the two-dimensional structure.[259] The intensity of the NOE is proportional to the distance between the hydrogens ($1r^{-6}$), and the maximum distance for the observation of NOE cross signals is 4-5 Å.[260] For **52** the NOESY spectrum shows cross peaks between the diisobutylaluminium peaks and the aromatic system. Figure 31 provides a close-up of this area. Together with the crystal structure, the signals in the NOESY allow the assignment of the isobutyl group signals in the ^{1}H spectrum (Figure 32).

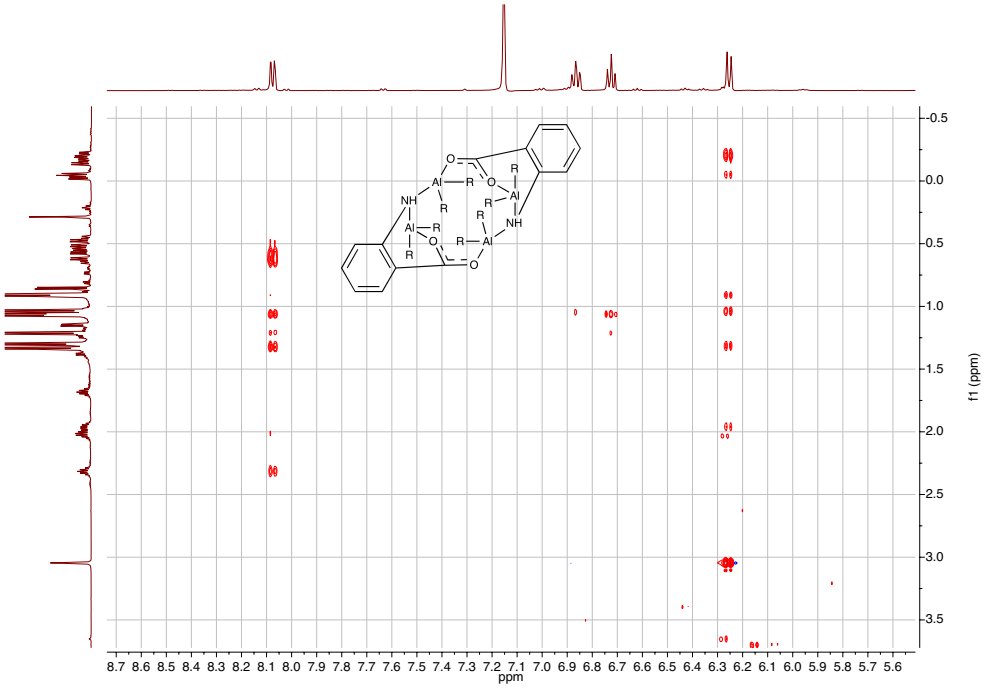

Figure 31: Expansion of the ^{1}H,^{1}H-NOESY NMR spectrum of **52** in C_6D_6, mixing time τ_1 = 1.2 s.

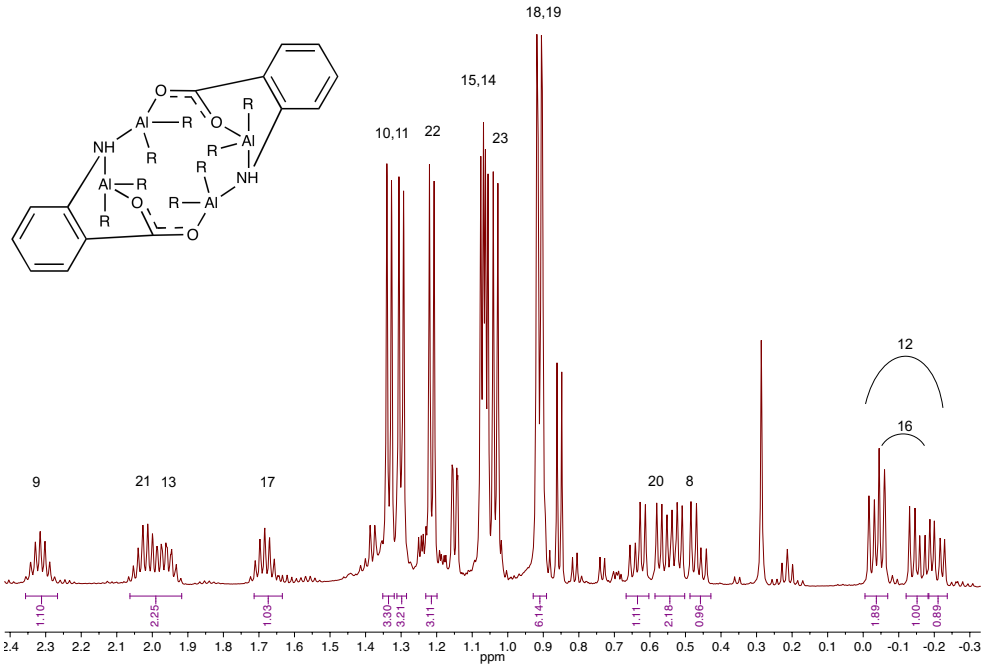

Figure 32: ^{1}H-NMR spectrum of **52** in C_6D_6 with assigned peaks below δ = 2.5 ppm. Unassigned peaks are from minor impurities. The ^{1}H,^{1}H-COSY and ^{1}H,^{13}C-HMBC allowed to distinguish between the hydrogen atoms of the product and those of different systems.

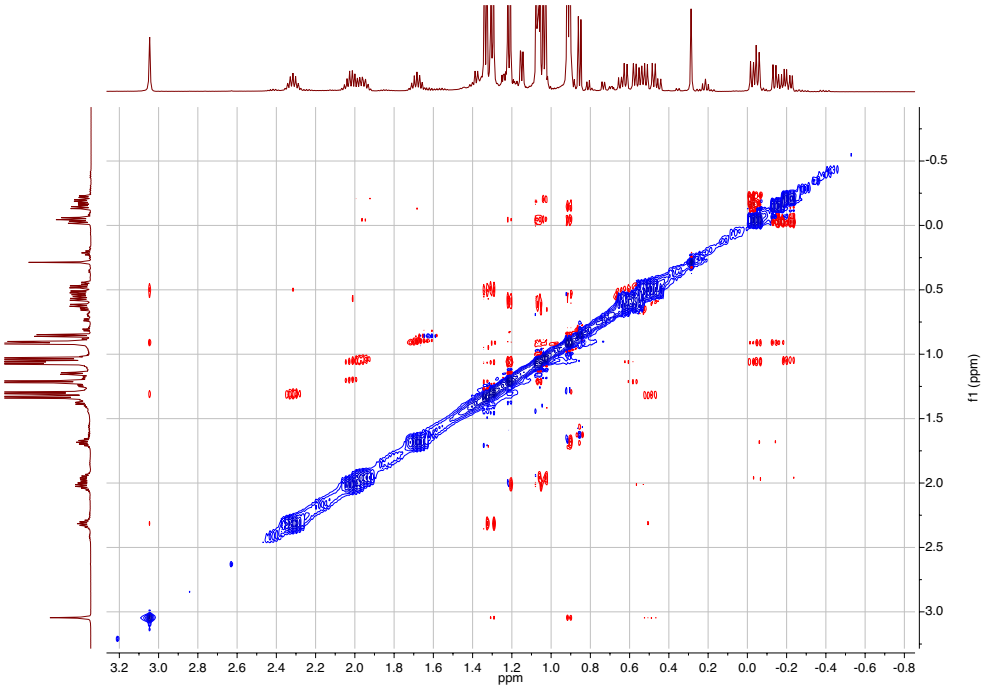

Figure 33: Expansion of the organometallic region in the ^{1}H,^{1}H-NOESY NMR spectrum of **52** in C_6D_6, mixing time $\tau_1 = 1.2$ s.

Cross peaks between H(7) and the terminal isobutyl CH_3 and CH groups of the bridging $AlMe_2$ moiety, as well as with the CH_2 groups of the chelated $AlMe_2$ moiety show the spatial closeness between these groups. Table 7 shows the values for the distances in the crystal structure measured between the hydrogen atoms of the given cross peaks. Some cross signals between H(5) and the isobutyl groups were not assignable due to the distortion of the isobutyl groups, however, this does not affect the assignment of the isobutyl groups, as there are sufficient data points within the ^{1}H,^{1}H-COSY, HSQC and HMBC to identify the different signals.

Table 7: Cross signals of the NOESY spectrum and spatial distances in the crystal structure of **52**. The distances were measured manually in Mercury CSD 3.9.

Hydrogen cross signal	Distance (Å)
H(7)-H(20)	2.681
H(7)-H(15,14)	3.686
H(7)-H(10,11)	3.304
H(7)-H(9)	2.942
H(5)-H(18,19)	3.843
H(4)-H(12)	2.817
H(4)-H(21)	3.825
H(13)-H(23)	3.873
H(4)-H(N)	2.265
H(N)-H(8)	2.614
H(N)-H(18,19)	2.545

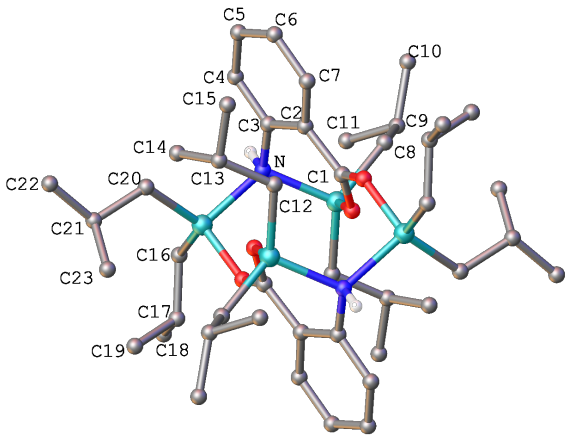

Figure 34: Molecular structure of **52** for NOESY interpretation. Disorder in the alkyl chains has been removed. CH-atoms are omitted for clarity, but the hydrogen number corresponds with the number of the carbon atom it is attached to.

The data from Table 7 suggests that the dimeric structure of **52** seen crystallographically might be retained in solution. Cross peaks are observed from the aromatic H(7) to H(15,14), which are the CH_3 groups of a chelated Al^iBu_2 group, and H(13), which is the CH group of the same chelated Al^iBu_2 group to H(23), a CH_3 group of the bridging Al^iBu_2 moiety. This indicates that the correlating hydrogen atoms were in close proximity to each other and therefore most likely part of the same compound. Figure 34 shows that this, at least in the solid state, would not be the case for the monomeric form of **52**. However, it might be possible that the structure rearranges in solution and the distances in the molecule change, which at this stage was not further investigated.

In order to understand the aforementioned conversion of compound **50** ([$Me_2Al(\mu$-$O_2CC_6H_4NH_2$-2)]) to compound **51** ([$(Me_2Al)_2(\mu$-$O_2CC_6H_4$-2-μ-NH)]$_2$) the reaction for the synthesis of **50** was repeated several times. However, it was not possible to produce a structure that matched the NMR seen in Figure 19, where the amino group is retained (visible as 2 NH hydrogens in the ^{1}H-NMR spectrum) and two methyl groups binding to aluminium are present. Repeated attempts to achieve a reaction between one equivalent of anthranilic acid and one equivalent of $AlMe_3$ showed that the reproducibility of the synthesis of **50** was a challenge. The synthesis of **50** was carried out in toluene (4 ml for 1 mmol of anthranilic acid) and yielded a white precipitate which analysed by NMR spectroscopy yielded the NMR spectrum in Figure 19. To dissolve this precipitate a brief heating of the solution was required and it is assumed that this lead to the discussed dismutation. In order to avoid heating the sample in some attempts of the reaction of anthranilic acid and $AlMe_3$, more solvent was used initially (10 ml toluene for 1 mmol of anthranilic acid). When the reaction was stirred for 60 min and warmed to room temperature during this time a solution had formed. The reaction volume was carefully reduced to approximately one-third of the original volume and the vessel containing the pale yellow solution was placed in the freezer. After three weeks colourless crystals were obtained and characterised by x-ray crystallography. The crystal structure is shown in Figure 35. The dataset was of low quality but suffices to demonstrate the general bonding pattern.

This tetranuclear structure in Figure 35 reveals another, as yet unseen mode of reactivity in these evidently highly complex systems. The structure does not correspond with the previous observations by NMR spectroscopy, as there is still only one hydro-

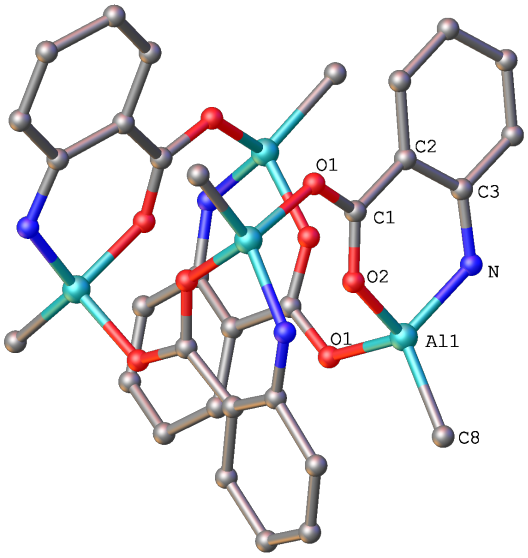

Figure 35: Molecular structure of **53**, $[MeAl(\mu\text{-}O_2CC_6H_4\text{-}2\text{-}\mu\text{-}NH)]_4$. H-atoms are omitted for clarity. The quality of the data set was insufficient for a detailed discussion of bondlengths and angles.

gen remaining at the amido group but the $AlMe_3$ has reacted twice with each amido group in spite of the fact that each $AlMe_3$ molecule consumed has, in fact, reacted twice, losing two CH_3 groups, resulting in four AlMe units bridging four anthranilate moieties. The aluminium centres in this tetramer are each tetra-coordinated, with two coordinative bonds from one carboxylate oxygen and the amino nitrogen of one anthranilate anion, one coordinative bond from the carboxylate oxygen of the adjacent anthranilate and one covalent bond from the remaining methyl group. The resulting tetramer's central bent 16-membered ring consists of four [O-C-O-N] units, which is fused with four six-membered rings formed by the anthranilate chelating the AlMe unit. In contrast to **51** and **52** here the aluminium is bridging and being chelated at once. As it can be seen from the crystal structure in Figure 35 the six-membered rings are relatively flat, although the low quality of the crystal data prevents a further discussion of the structural details.

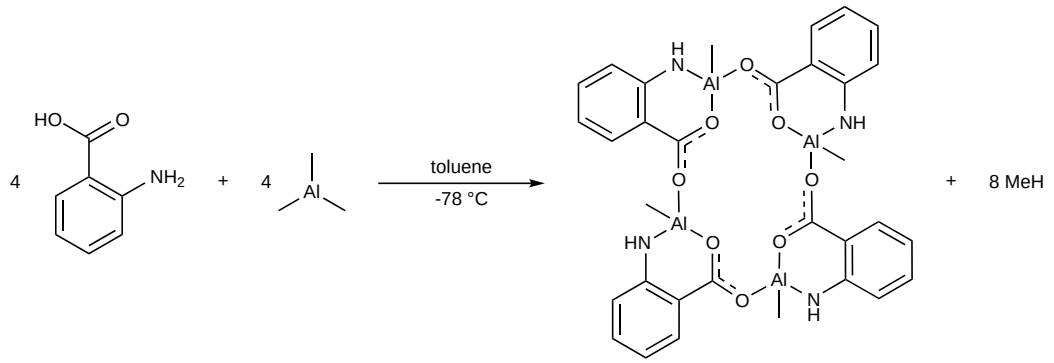

53

Scheme 46: Reaction of anthranilic acid with $AlMe_3$, in an attempt to reproduce the synthesis of **50** ($[Me_2Al(\mu\text{-}O_2CC_6H_4NH_2\text{-}2)]$). To avoid the formation of the white precipitate that yielded **50** the concentration of the reaction was reduced by using 10 ml of toluene for 1 mmol of anthranilic acid and after completion of the reaction reducing the reaction volume to approximately one third of the original volume.

The sample decomposed during the crystallographic analysis and it was not possible to obtain an NMR spectrum. Numerous attempts to repeat this result failed, leading either to inconclusive NMR spectra with broad and undistinguishable signals or to the formation of insoluble white solid. Again, the reproducibility of the results proved challenging and is assumed to result from the number of acidic protons in this structure.

4.1.1.3.2 Reactions of Secondary Amine derivatives of Anthranilic Acid with AlR_3

As a consequence of the findings for the reaction of anthranilic acid and aluminium organyls, in the next step, the number of acidic hydrogens available for the reaction was reduced. To do this, N-methylanthranilitc acid was used. It was reacted with two equivalent of $AlMe_3$ (Scheme 47), producing a tetranuclear, dimeric structure **54**, which, after crystallographic analysis was found to have the formula $[(Me_2Al)_2(\mu\text{-}O_2CC_6H_4\text{-}2\text{-}\mu\text{-}NMe)]_2$.

This corresponds with bonding motifs seen in **51** ($[(Me_2Al)_2(\mu\text{-}O_2CC_6H_4\text{-}2\text{-}\mu\text{-}NH)]_2$) and **52** ($[(^iBu_2Al)_2(\mu\text{-}O_2CC_6H_4\text{-}2\text{-}\mu\text{-}NH)]_2$): A distorted twelve-membered ring consisting of two [O-C-O-Al-N-Al] units, that is fused with two distorted six-membered rings

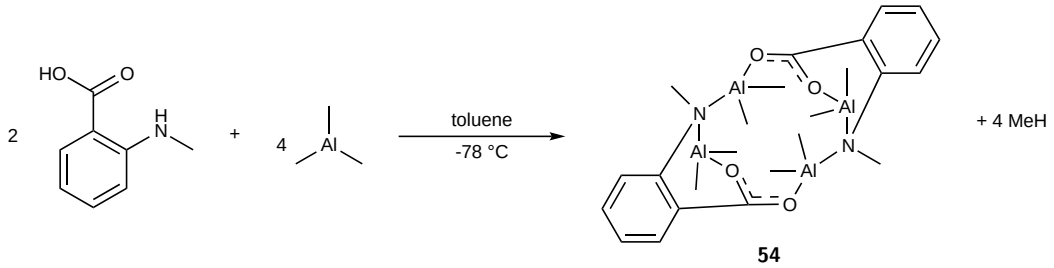

54

Scheme 47: Reaction of N-methylanthranilic acid with two equivalents of $AlMe_3$ in toluene.

formed by the chelated $AlMe_2$ moiety. The angle O(1)-Al(2)-N(1) is 94.25(8)˚ and shows the extent of the distortion. Figure 36 shows that Al(2) is significantly raised above the plane of an ideal six-membered ring. Both, the bridging and the chelated $AlMe_2$ unit are tetrahedrally coordinated. The angles at the bridging dimethylaluminium are 101.26(9)° for O(2)-Al(1)-N(1) and 119.52(13)° for C(10)-Al(1)-C(11). For the chelated dimethyl aluminium the angles are 94.25(8)° for O(1)-Al(2)-N(1) and 119.26(13)° for C(8)-Al(2)-C(9). These values are corresponding with the observations for **51**. The angle for the chelated aluminium centre is significantly smaller than for the bridging aluminium centre. Again, the carboxylate group is binding to the chelated dimethylaluminium group in the *anti*-mode and to the bridging $AlMe_2$ unit in the *syn* mode. The *syn*-bond Al(1)-O(2) is slightly shorter with 1.8225(18) Å compared to the *anti*-bond Al(2)-O(1) with 1.8355(18) Å. The bonds in the carboxylate group C(1)-O(1) and C(1)-O(2) are almost identical with 1.265(3) Å and 1.268 Å, respectively.

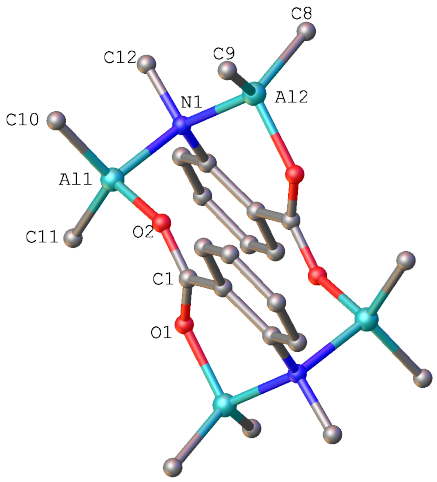

Figure 36: Molecular structure of **54**, $[(Me_2Al)_2(\mu\text{-}O_2CC_6H_4\text{-}2\text{-}\mu\text{-}NMe)]_2$. H atoms are omitted for clarity. For selected bond lengths and angles see Table 8.

Table 8: Selected bond lengths and angles for **54**. Lengths are given in Å, angles in deg.

	54 $[(Me_2Al)_2(\mu\text{-}O_2CC_6H_4\text{-}2\text{-}\mu\text{-}NMe)]_2$
Al(2)-O(1)	1.8355(18)
Al(2)-N(1)	1.968(2)
Al(2)-C(9)	1.946(3)
Al(2)-C(8)	1.951(3)
Al(1)-O(2)	1.8225(18)
Al(1)-N(1)	2.014(2)
Al(1)-C(11)	1.947(3)
Al(1)-C(10)	1.954(3)
C(1)-O(1)	1.265(3)
C(1)-O(2)	1.268(3)
O(1)-Al(2)-N(1)	94.25(8)
O(1)-Al(2)-C(9)	107.33(11)
O(1)-Al(2)-C(8)	111.28(11)
C(9)-Al(2)-N(1)	113.87(11)
C(9)-Al(2)-C(8)	119.26(13)
C(8)-Al(2)-N(1)	108.03(11)
O(2)-Al(1)-N(1)	101.26(9)
C(10)-Al(1)-C(11)	119.52(13)

Moving to the equimolar reaction between N-methylanthranilic acid and Al^iBu_3 (Scheme 48), it was possible to reproduce the tetrameric structure seen for **53**, $[MeAl(\mu\text{-}O_2CC_6H_4\text{-}2\text{-}\mu\text{-}NH)]_4$, in Figure 35. Compound **53** was synthesised using $AlMe_3$ and anthranilic acid. With changing to Al^iBu_3 it was hoped to improve the crystallinity of the product and see if the altered steric demand of the organometallic reagent influences the bonding motifs observed. The reaction yielded colourless crystals, which were analysed by x-ray crystallography. The obtained solid-state structure of the product $[^i BuAl(\mu\text{-}O_2CC_6H_4\text{-}2\text{-}\mu\text{-}NMe)]_4$ shows that after the first reaction of Al^iBu_3 the resulting Al^iBu_2 moieties reacted again to yield four Al^iBu units between bridging between four deprotonated methylanthranilates (Figure 37).

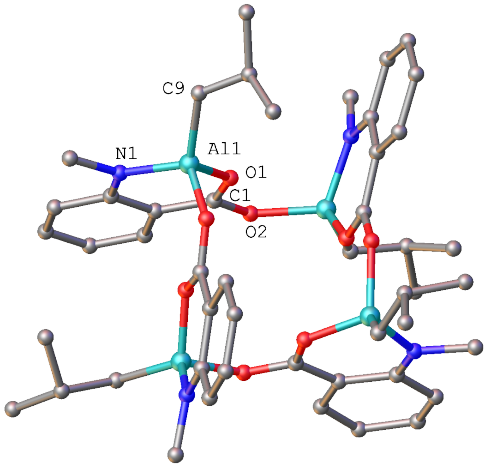

Figure 37: Molecular structure of **55**. Due to low quality data-set no bond lengths and angles are given.

The crystallographic data was of low quality (R_1 = 9.1496, R_{int} = 0.0427, max GoF = 1.959) so it was attempted to repeat the reaction to obtain better crystals. However, several attempts to repeat the equimolar reaction yielded products which were unsuitable for crystallographic analysis. For three of the reactions it was possible to obtain NMR spectra from small crystals formed, but in all three experiments, the resulting NMR spectra indicated a reaction of two equivalents of Al^iBu_3, following the reaction in Scheme 49. This suggests a product with the structural motif seen before for **54**, $[(Me_2Al)_2(\mu\text{-}O_2CC_6H_4\text{-}2\text{-}\mu\text{-}NMe)]_2$.

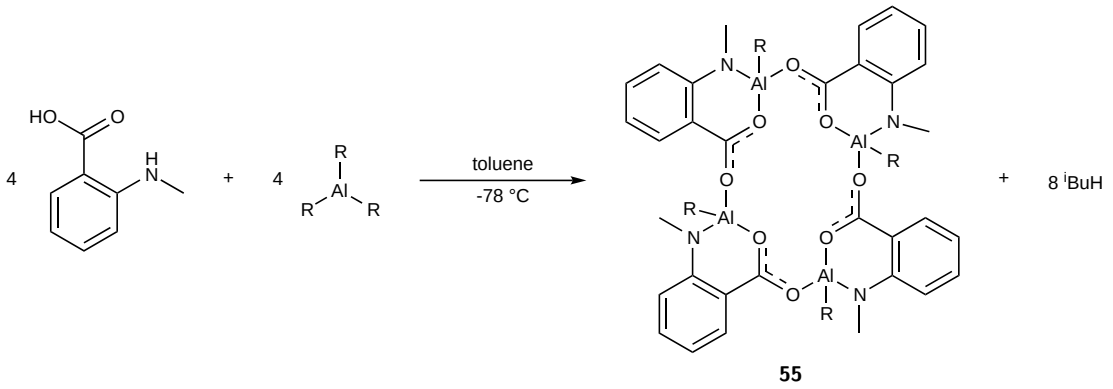

55

Scheme 48: Reaction of N-methylanthranilic acid with $Al^{i}Bu_3$(R = ^{i}Bu) in toluene. Colourless crystals were obtained from the reaction solution after being stored one month at -27°C. X-ray crystallography showed the crystals to be **55**.

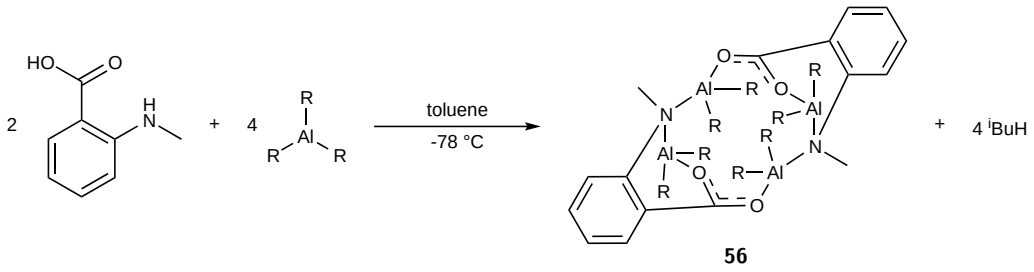

56

Scheme 49: Reaction of N-methylanthranilic acid with $Al^{i}Bu_3$ (R = ^{i}Bu), based on NMR spectra obtained from small crystals formed.

The integration of the ^{1}H-NMR spectrum shows that for each N-methylanthranilate ion there are two isobutyl groups. This representative result was obtained from one of several reactions that were set up as formally equimolar reactions. The ^{27}Al-NMR shows a peak at δ = 151.0 ppm, consistent with a tetra-coordinated aluminium.[222]

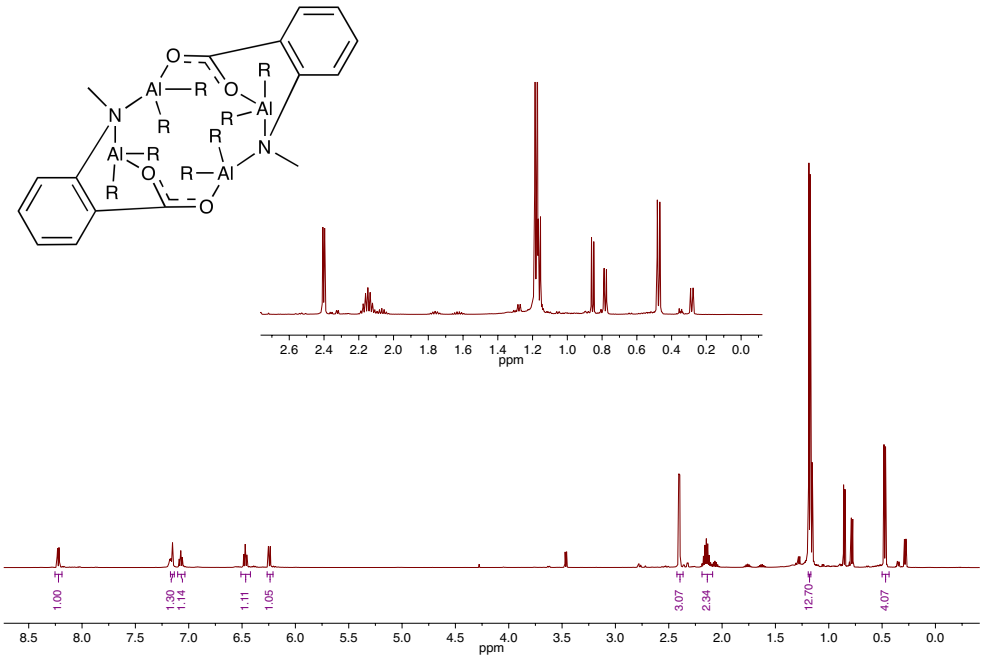

Figure 38: ^{1}H-NMR spectrum of **56** in C_6D_6, with the solvent residual peak at δ = 7.15 ppm. The inset shows the integrals for the Al^{i}Bu$_2$ groups, indicating that the reaction between N-methylanthranilic acid and Al^{i}Bu$_3$ took place in a one to two ratio, yielding [(^{i}Bu$_2$Al)$_2$(μ-O$_2$CC$_6$H$_4$-2-μ-NMe)]$_2$.

As it can be seen from **51** ([(Me$_2$Al)$_2$(μ-O$_2$CC$_6$H$_4$-2-μ-NH)]$_2$), **54** [(Me$_2$Al)$_2$(μ-O$_2$CC$_6$H$_4$-2-μ-NMe)]$_2$, and **56** ([(^{i}Bu$_2$Al)$_2$(μ-O$_2$CC$_6$H$_4$-2-μ-NMe)]$_2$) for the dimeric species and from **53** ([MeAl(μ-O$_2$CC$_6$H$_4$-2-μ-NH)]$_4$) and **55** ([^{i}BuAl(μ-O$_2$CC$_6$H$_4$-2-μ-NMe)]$_4$) it appears that the steric demands of the aluminiumalkyl do not influence the structural outcome of the reaction between (methyl)anthranilic acid and AlR$_3$.

In order to make the chemistry more reproducible and attempting to get a fully characterised example for the 16-membered macrocycle seen in **53** and **55**, or even find a new bonding motif, the steric demand of the anthranilic acid was increased by the use of N-phenylanthranilic acid in an equimolar reaction with Al^{i}Bu$_3$ (Scheme 50). The reaction yielded reproducibly the tetrameric reaction product **57**, [^{i}BuAl(μ-O$_2$CC$_6$H$_4$-2-μ-NPh)]$_4$. Each Al^{i}Bu$_3$ molecule had reacted twice to form bridging Al^{i}Bu moieties. The crystallographic data for [^{i}BuAl(μ-O$_2$CC$_6$H$_4$-2-μ-NPh)]$_4$ was of sufficient quality

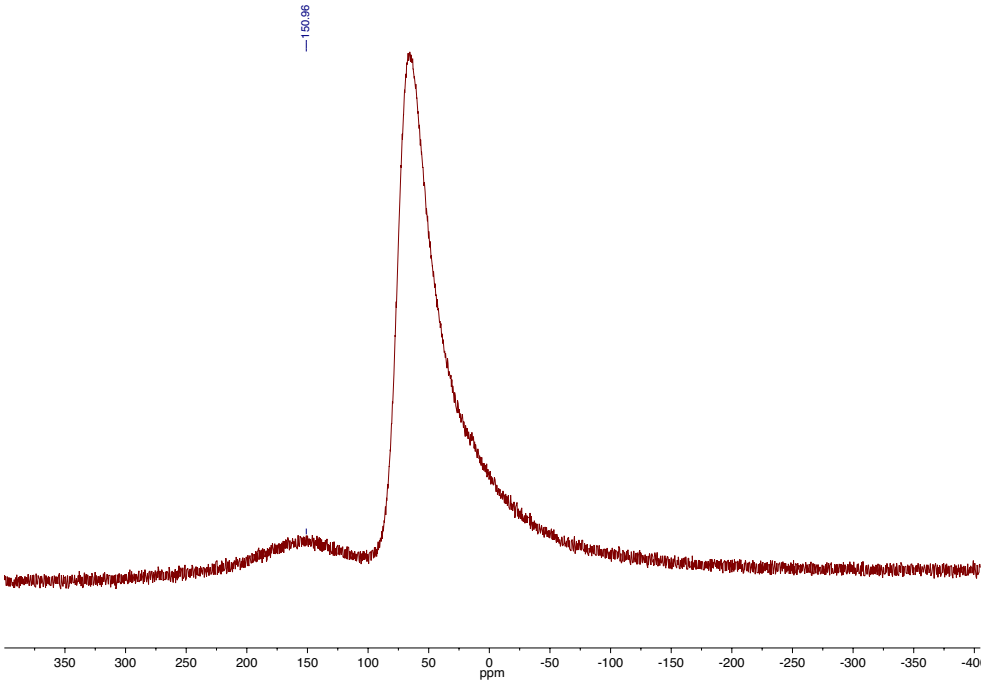

Figure 39: ^{27}Al-NMR spectrum of **56** in C_6D_6. The large artefact at $\delta = 64.2$ ppm results from the background probe signal and is visible in all ^{27}Al NMR spectra.[225] [247] [248].

to enable an exact discussion of structural parameters, and selected bond lengths and angles are given in Table 9. The crystals belong to the tetragonal crystal system with the $P\bar{4}2_1c$ space group. The structure consists of a central 16-membered ring based on four [O-C-O-Al] units. There are four distorted six-membered rings fused to the macrocycle. The aluminium centres are coordinated in a distorted tetrahedral geometry, which is reflected in the uneven bond angles around the aluminium. The smallest bite angle is O(1)-Al(1)-N(1) with 97.59° and the largest bite angle N(1)-Al(1)-C(14) with 120.64°. The torsion angles between the units of the tetramer are 102.14° for O(2)-Al(1)-N(1)-C(3) and 107.38° for O(2)-Al(1)-O(1)-C(1). The carboxylate oxygens bind to the aluminium in the *syn*-mode for Al(1)-O(2) and the *anti*-mode for Al(1)-O(1). The *syn*-bond is longer (1.808 Å) and therefore weaker than the *anti*-bond (1.795 Å). This differs from the structures of the dimeric tetranuclear species found for **45**, **51** and **54**, where the *syn*-bond was stronger.

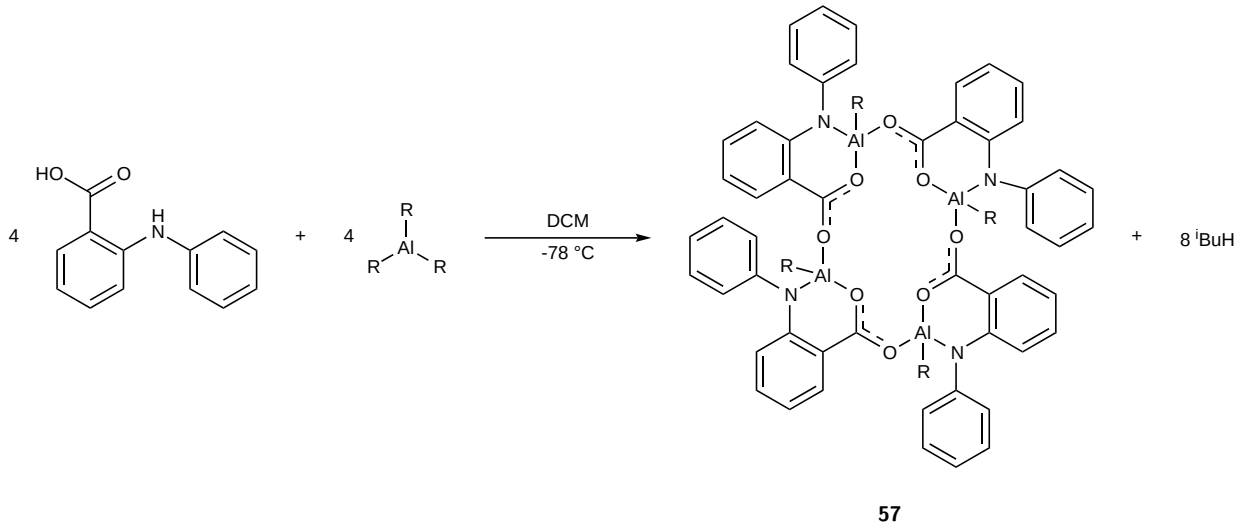

Scheme 50: The reaction of N-phenylanthranilic acid with $Al^{i}Bu_3$ ($R = {}^{i}Bu$) in DCM yielded large colourless crystals, which were studied, using x-ray crystallography. The structure obtained proved to be the tetrameric product **57**.

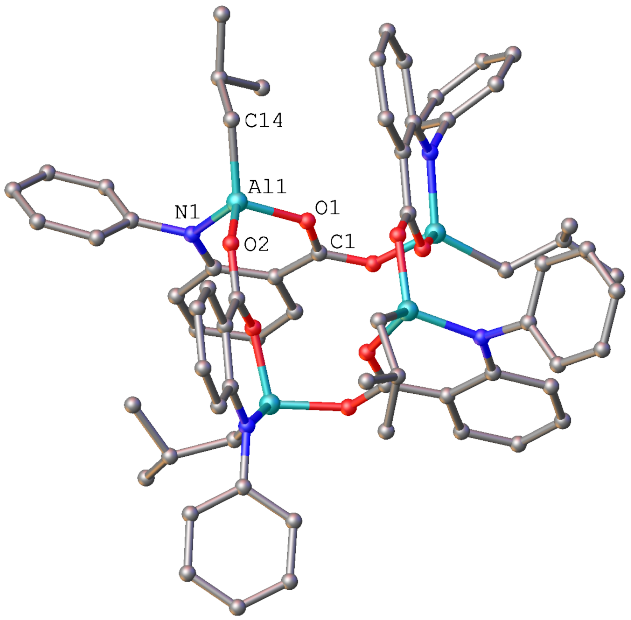

Figure 40: Molecular structure of **57**. Hydrogen atoms and a disordered DCM molecule are omitted for clarity. For selected bond lengths and angles see Table 9.

Table 9: Selected bond lengths and angles for **57**. Lengths are given in Å, angles in deg. Torsion angles were measured manually using Mercury CSD 3.9.

	57 $[^{i}BuAl(\mu\text{-}O_2CC_6H_4\text{-}2\text{-}\mu\text{-}NPh)]_4$
Al(1)-O(1)	1.795(2)
Al(1)-O(2)	1.808(2)
Al(1)-N(1)	1.847(3)
Al(1)-C(14)	1.938(3)
O(1)-Al(1)-O(2)	104.99(11)
O(1)-Al(1)-N(1)	97.59(11)
O(2)-Al(1)-N(1)	111.15(12)
O(1)-Al(1)-C(14)	112.34(13)
O(2)-Al(1)-C(14)	108.74(12)
N(1)-Al(1)-C(14)	120.64(13)
O(2)-Al(1)-N(1)-C(3)	102.14
O(2)-Al(1)-O(1)-C(1)	107.38

The ^{1}H-spectrum of **57** (Figure 41) shows all the expected peaks based on the crystal structure. The CH_3 groups of the isobutyl moiety give two separate doublets at δ = 0.89 ppm and δ = 0.81 ppm which both couple to the CH group, as seen in the ^{1}H,^{1}H-COSY spectrum (Figure 42). The splitting of the signals attributed to the isobutyl groups, especially the doublet of doublet peak resulting from the CH_2 group, show the presence of a chiral aluminium centre. The overall integration of the aromatic region shows the presence of nine hydrogen atoms. The COSY allows the distinction between the two aromatic systems, one from the aminophenyl group and one from the anthranilate, where the latter shows defined multiplets with a broad range of shifts, whereas the aminophenyl aromatic system gives rise to one triplet and one broad singlet, which could be caused by rotation of the phenyl group along the C-N bond. The ^{27}Al-spectrum did not show any peaks, but any potential peak might be covered by the probe signal or too broad to be distinguished from the baseline.

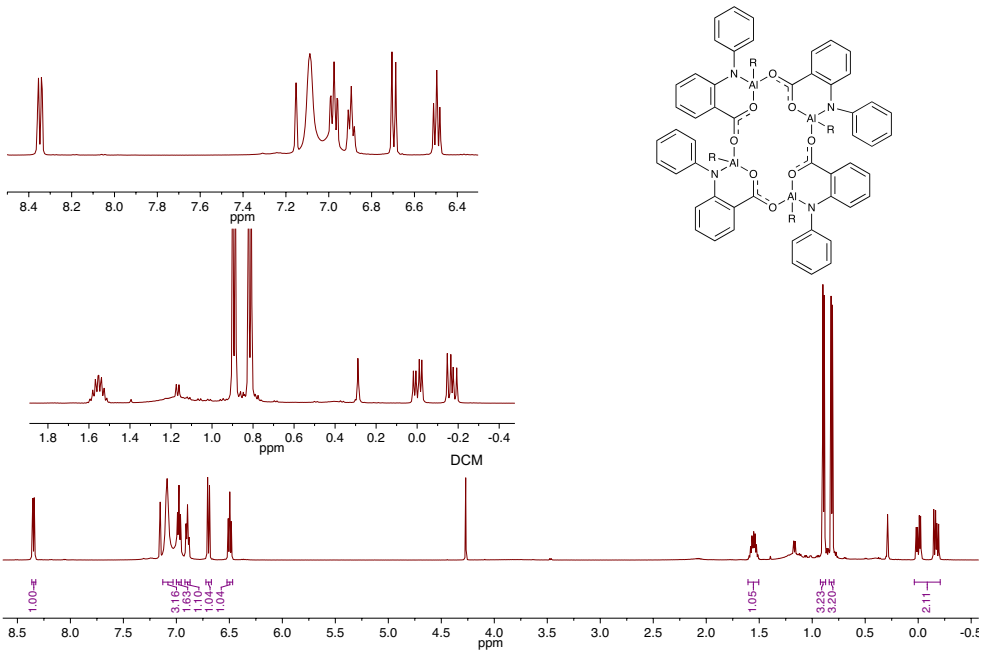

Figure 41: ^{1}H-NMR spectrum of **57** in C_6D_6, with the solvent residual peak at $\delta = 7.16$ ppm. The inset shows the peaks originating from the two aromatic systems between $\delta = 8.4$-6.4 ppm.

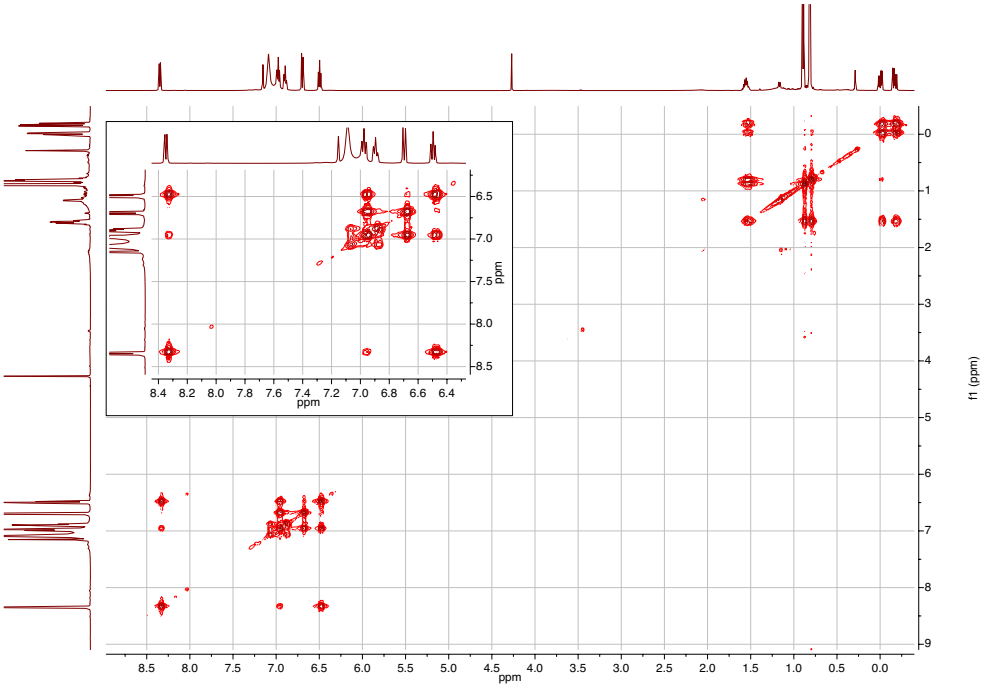

Figure 42: ^{1}H,^{1}H-COSY spectrum of **57** in benzene. The inset shows the cross peaks for the aromatic systems.

Following up on the reaction of N-phenylanthranilic acid with Al^iBu_3 (Scheme 50), which led to the formation of $[^iBuAl(\mu\text{-}O_2CC_6H_4\text{-}2\text{-}\mu\text{-}NPh)]_4$ (**57**), attempts were made to increase the steric bulk of the substituent on the nitrogen in order to investigate the influence of the steric demands of the amine substituent in secondary amine derivatives of anthranilic acid. The results discussed so far in this section show that with the smaller methyl substituent the formation of the dimeric product **54**, $[(Me_2Al)_2(\mu\text{-}O_2CC_6H_4\text{-}2\text{-}\mu\text{-}NMe)]_2$, is preferred, even for a formally equimolar reaction. The use of TMA versus the use of TiBA did not lead to different outcomes, so it was assumed that the steric demand of the aluminium organyl is of secondary importance for the formation of the dimeric or tetrameric product. The use of N-phenylanthranilic acid, on the other hand, yielded the tetrameric structure **57**, $[^iBuAl(\mu\text{-}O_2CC_6H_4\text{-}2\text{-}\mu\text{-}NPh)]_4$ reproducibly and in good yields. Consequently, it was investigated whether an increased steric bulk on the amine, by using 2,6-disubstituted phenyl residues on the nitrogen, would also lead to a preference for the formation of the tetrameric species, during which each AlR_3 reacts twice, as seen for **57**, if it would yield a dimeric species similar to **58**, or maybe give rise to new bonding motifs. For this investigation, 2-chlorobenzoic acid was reacted with different 2,6-substituted anilines, following a procedure for amination reactions developed by Mei and co-workers to obtain N-(2,6-alkylphenyl)anthranilic acid derivatives.[261] The reaction of 2-chlorobenzoic acid with 2,6-diisopropylaniline was not successful, as the ^{1}H-NMR showed only unreacted starting material even after heating the reaction to reflux for several days. Assuming that the steric load was too high it was reduced by using the less bulky 2,6-dimethylaniline (Scheme 51) and reacting it with 2-chlorobenzoic acid. The reaction product was obtained as an off-white solid and characterised by NMR spectroscopy to ensure complete reaction. The ^{1}H-NMR spectrum of **59** shows a complete reaction with the COO*H* proton appearing as a very broad singlet at δ = 11.91 ppm.

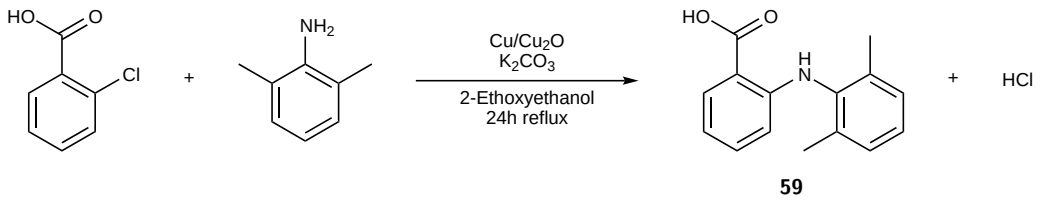

59

Scheme 51: Synthesis of 2-((2,6-dimethylphenyl)amino)benzoic acid **59**.

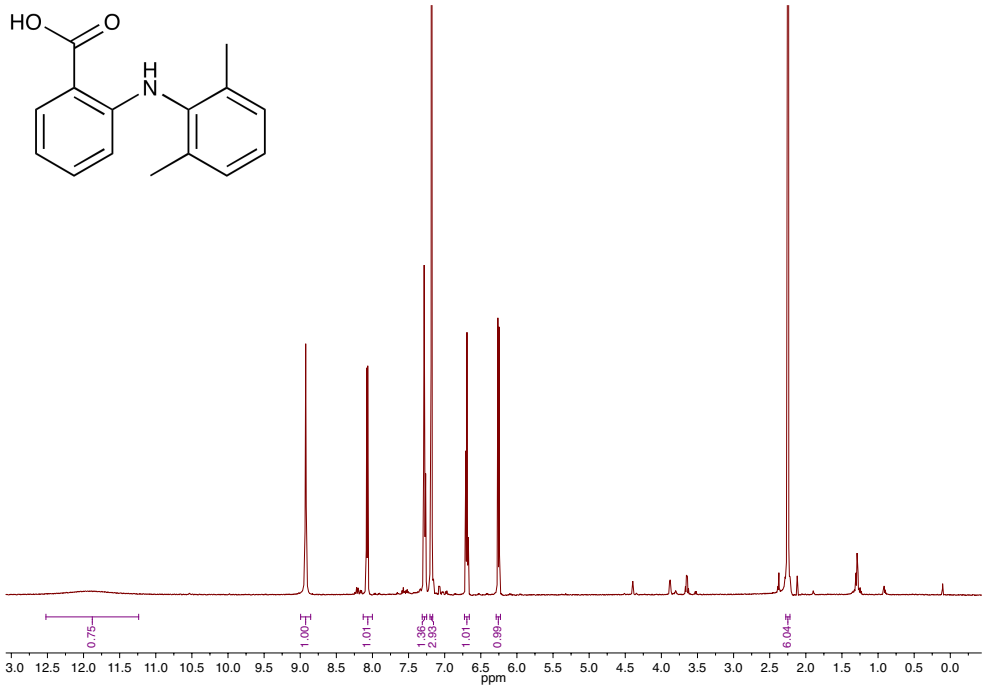

Figure 43: ^{1}H-NMR spectra of **59** in C_6D_6 with the solvent residual peak at $\delta = 7.17$ ppm..

Compound **59** was used as a starting material for the next reaction step without further purification. **59** was reacted with one equivalent of $AlMe_3$ in DCM to yield a white powder which was soluble in benzene and investigated by NMR spectroscopy (Scheme 52).

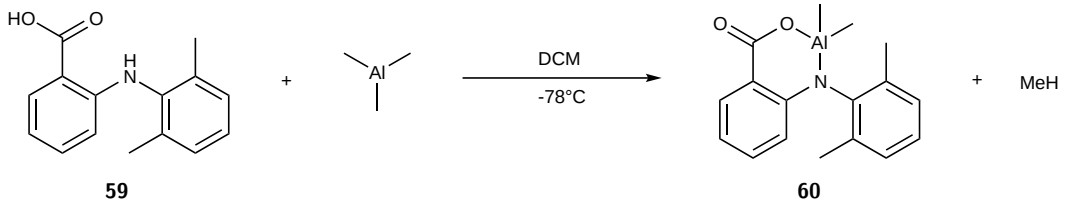

Scheme 52: Synthesis of $[Me_2Al(\mu\text{-}O_2CC_6H_4\text{-}2\text{-}\mu\text{-}N\text{-}(C_6H_4\text{-}2,6\text{-}CH_3))]$ **60** in DCM yielded an off white powder which was soluble in C_6D_6. Based on the NMR spectroscopic results, structure **60** is proposed as a possible outcome.

The ^{1}H-NMR spectrum of **60** (Figure 44) shows six hydrogens pointing to two methyl groups on the aluminium at δ = -0.24 ppm, suggesting that, unlike the reaction for $[^{i}BuAl(\mu\text{-}O_2CC_6H_4\text{-}2\text{-}\mu\text{-}NPh)]_4$, the 2-((2,6-dimethylphenyl)amino)- benzoic acid **59**, has reacted once with one equivalent of $AlMe_3$. This suggests that a different bonding motif is present, compared to those discussed in this section so far. Before, the bonding motifs were either based on a dimeric structure with two AlR_2 units for each anthranilate or else based on a tetrameric structure with one AlR unit for every anthranilate. The ^{1}H-NMR spectroscopic data for **60** suggests the presence of either one

$AlMe_2$ group or two AlMe groups for each ligand. For the second possibility to take place, however, it would have been necessary to protonate four CH_3 groups (i.e. generate four equivalents CH_4) when there are only two acidic hydrogen atoms available in **59**, those of the carboxylic acid and of the amine. The ^{1}H,^{1}H-COSYspectrum was used to distinguish between the two aromatic systems in **60**. Based on these considerations, the suggested structure for **60** is shown in Scheme 52. The additional peak at δ = 0.29 ppm in the ^{1}H-NMR spectrum, with an integral of two hydrogens cannot be explained. However, in the 2D spectra (COSY, HSQC, HMBC) it does not show any cross peaks to the product, so it is currently assumed that it is an impurity, e.g. silicon grease.

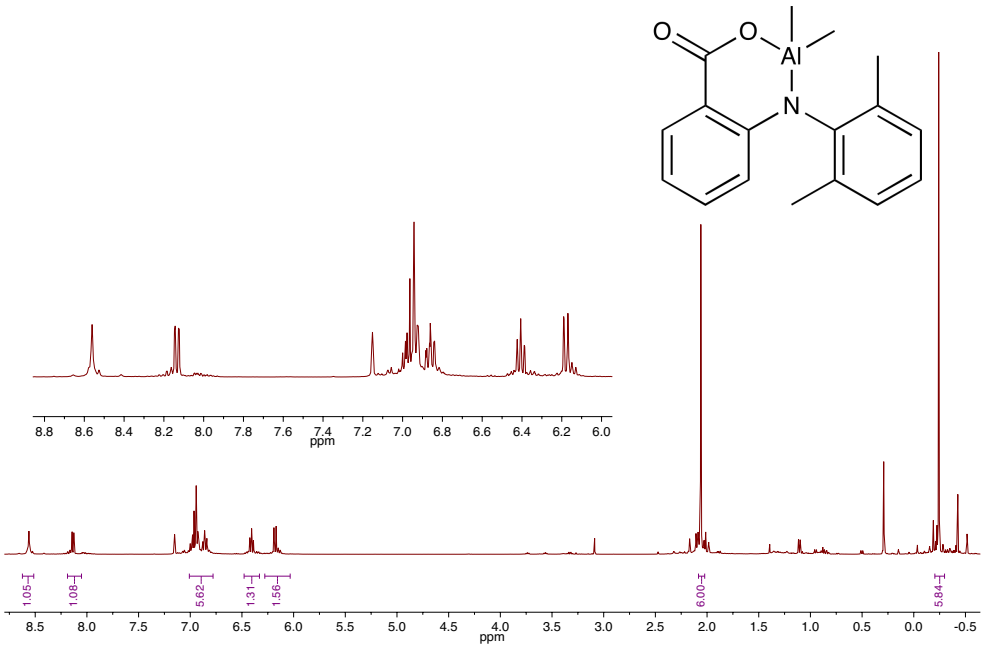

Figure 44: ^{1}H-NMR spectra of **60** in C_6D_6 with the solvent residual peak at δ = 7.15 ppm. The two insets show the signals corresponding with the two aromatic systems in **60**.

The product was obtained as a white powder. Various attempts were undertaken in order to crystallise the product (redissolving in different solvents, different concentrations at different temperatures and layering different solvents) but proved to be unsuccessful. Obtaining crystals suitable for x-ray analysis and purification of **60** for elemental analysis and melting point are subject to future work on this product.

4.1.1.3.3 Reactions of Tertiary Amine Derivatives of Anthranilic Acid with $AlMe_3$

The use of anthranilic acid and its secondary amine derivatives yielded structurally very interesting compounds, but also showed that the presence of three acidic hydrogen atoms gives rise to the complexity of this system. This is seen in the two major bonding motifs observed. On the one hand, the acid can react with two equivalents of AlR_3, yielding a dimeric structure with a central 12-membered ring, on the other hand, the acid can react twice with one equivalent, resulting in the formation of a tetrameric structure with a central 16-membered ring. Following up from these results, the next step was reducing the number of available acidic hydrogens by using the tertiary amine derivative, N,N-dimethylanthranilic acid with aluminium organyls. Reactions between those compounds gave, in almost every case, a yellow, oil-like or highly-viscous resin-like substance upon removal of the solvent and even if the solvent was not completely evaporated an oily phase would form, independent of the use of toluene, DCM, hexane or THF or combinations thereof. However, in one case, the reaction between two equivalents of $AlMe_3$ and one equivalent of N,N-dimethylanthranilic acid the solution remained homogeneous and after three months colourless crystals were obtained. The following crystallographic analysis showed the most interesting product **61**, $MeAl(AlMe_3\text{-}\mu\text{-}O_2CC_6H_4\text{-}2\text{-}\mu\text{-}NMe_2)_2$ (Scheme 53).

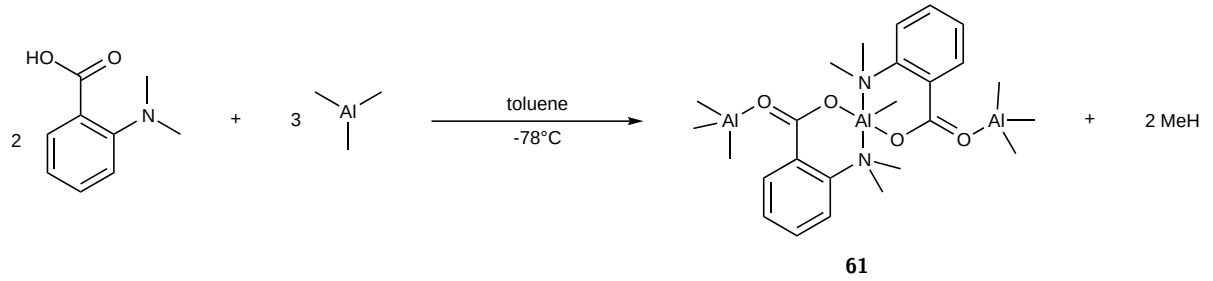

61

Scheme 53: The reaction of N,N-dimethylanthranilic acid with $AlMe_3$in toluene yielded pale yellow crystals after being stored at -27°C for four months. The crystals were analysed using x-ray crystallography and the solid-state structure of compound **61** was obtained.

The structure of **61**, $MeAl(AlMe_3\text{-}\mu\text{-}O_2CC_6H_4\text{-}2\text{-}\mu\text{-}NMe_2)_2$, in Figure 45 shows a very symmetric structure in the C2/c space group. It consists of a central AlMe unit which is binding to two anthranilate moieties, in each case via one carboxylate oxygen and the nitrogen of the amino group, resulting in a distorted trigonal-bipyramidal coordination of the aluminium. Additionally, and highly unusual, one $AlMe_3$ unit each is binding to the remaining carboxylate oxygens.

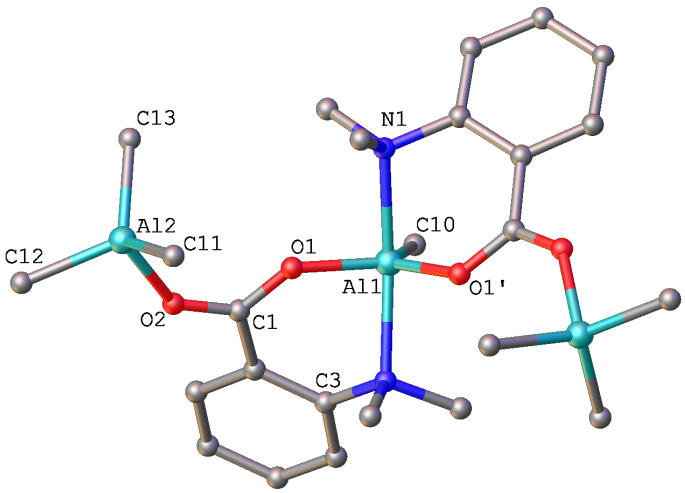

Figure 45: Molecular structure of **61**. Hydrogen atoms are omitted for clarity. For selected bond lengths and angles see Table 10.

The aforementioned trigonal-bipyramidal geometry at the central aluminium Al(1) (Figure 45) can be seen in the bond angles. The distortion, although not very extensive, is reflected in the angle between the apices of the bipyramid: The N(1)-Al(1)-N(1') angle is 165.43(11)° and differs from the ideal 180° by approximately 8.1%. The angles between the long axis and the base are also close to the ideal 90° with 86.18(7)° (O(1)-Al(1)-N(1)), 86.13(7)° (O(1)-Al(1)-N(1')) and 97.29(6)° (C(10)-Al(1)-N(1)). The latter results from the distortion from the ideal trigonal bipyramid, since $\frac{360°-165.43°}{2} = 97.29°$, and also has a difference of 8.1% to 90°. The bond between Al(1) and O(1) is in the *anti*-mode and 1.841(15) Å long. The bond to nitrogen, Al(1)-N(1=1') is significantly longer with 2.1210(16) Å. This shows the aluminium oxygen bond is stronger, which can be explained by the greater difference in electronegativity. Since the nitrogen did not lose any of its substituents the binding occurs presumably via the nitrogen lone pair.

The bond between the second carboxylate oxygen and the $AlMe_3$ unit Al(2)-O(2) is in the *syn*-mode and is longer (1.962(3) Å) than the Al(1)-O(1) bond. The weaker bond corresponds with the formation of an adduct between the $AlMe_3$ and the carboxylate. This aluminium is in a distorted tetrahedral coordination, with all angles differing from the ideal 109.5° by 5.6-9.6%.

Table 10: Selected bond lengths and angles for **61**. Lengths are given in Å, angles in deg.

	61 $MeAl(AlMe_3$-μ-$O_2CC_6H_4$-2-μ-$NMe_2)_2$
Al(1)-C(10)	1.963(3)
Al(1)-O(1)	1.841(15)
Al(1)-O(1')	1.841(15)
Al(1)-N(1)	2.1210(16)
Al(1)-N(1')	2.1210(16)
Al(2)-O(2)	1.9163(18)
Al(2)-C(11)	1.962(3)
C(1)-O(1)	1.287(2)
C(1)-O(2)	1.246(2)
N(1)-Al(1)-N(1')	165.43(11)
O(1)-Al(1)-O(1')	116.16(11)
O(1)-Al(1)-C(10)	121.92(5)
O(1)-Al(1)-N(1)	86.18(7)
O(1)-Al(1)-N(1')	86.13(7)
C(10)-Al(1)-N(1)	97.29(6)
O(2)-Al(2)-C(11)	105.44(13)
O(2)-Al(2)-C(12)	98.98(11)
C(11)-Al(2)-C(12)	115.68(15)
C(12)-Al(2)-C(13)	115.71(13)

Lewiński and co-workers encountered a similar bonding pattern when investigating the reactions of salicylic and anthranilic acids with Al^tBu_3. They were able to isolate the monomeric compound **62** in which Al^tBu_3 added to the carbonyl oxygen of the carboxylate.[214]

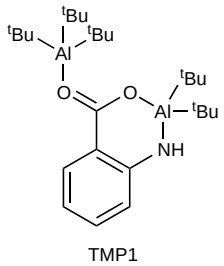

TMP1

Scheme 54: A literature example for a $AlMe_3$-O adduct, published by Lewiński and co-workers when studying the reaction of Al^tBu_3 and anthranilic acid.[214]

Similar adducts have also been reported in the search for FLP, for example between sterically congested NHC adducts with $AlMe_3$, where the $AlMe_3$ binds to the nitrogen.[262] Wang *et al.* synthesised a nitrogen-aluminium adduct of $AlMe_3$ and benzoquinoline.[263] Examples for adducts between $AlMe_3$ and oxygen are also known.

Hogerheide and co-workers synthesised monomeric aluminium phenolate complexes and observed adducts of $AlMe_3$ as shown in Scheme 55. Corresponding with the distances measured for **61**, in **63** the distance between O and the Al of the $AlMe_3$ group is longer (1.989(2) Å) than the bond between O and the chelated Al centre (1.855(2) Å).[264] The crystal structures of adducts CH_3COO^- and two $AlMe_3$ showed an O-Al bond length of 1.868(9) Å and a C-O bond length in the acetate of 1.95(2) Å, which is significantly longer than the bond lengths in **61**.[265]

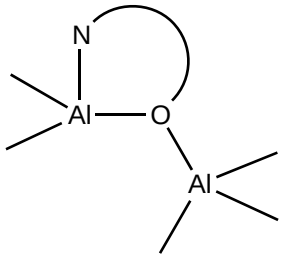

63

Scheme 55: A literature example for a $AlMe_3$-O adduct, published by Hogerheide and co-workers when studying monomeric aluminium phenolate complexes.[264]

After the crystallographic analysis, the sample showed signs of decomposition: the colour darkened from pale yellow to a deep yellow and the solution started turning slightly cloudy. The recorded ^{1}H-spectrum (Figure 46, lower spectrum) shows the expected peaks in the aromatic region and the peak for the NMe_2 groups. For better understanding, the spectrum of the starting material (N,N-dimethylanthranilic acid) was added (Figure 46, upper spectrum, the peak of the acid proton at δ = 18.08 ppm is omitted for clarity). The original peak for the NMe_2 group is slightly lowered to δ = 2.4 ppm and shows an integral of 11.54. An additional peak is found at δ = 3.13 ppm with an integral of 5.48. For δ < 0.5 ppm two peaks can be seen, which could correspond with the methyl groups on the AlMe (δ = 0.29 ppm, 3 H) and $AlMe_3$ units (δ = 0.40 ppm, 24 H). The integral for the latter is slightly too high, as the two $AlMe_3$ adducts would be 18 hydrogens.

The ^{27}Al-spectrum of **61** (Figure 47) shows two very distinct peaks, confirming that there are two different aluminium environments. The large peak at δ = 144.5 ppm is consistent with a tetra-coordinated aluminium centre. The peak at δ = 2.7 ppm, however, is not typical for penta-coordinated aluminium, which is usually expected between δ = 50-100 ppm.[222] If such a peak is present, it may be obscured by the

probe signal. It is possible that the peak at δ = 2.7 ppm, which seems to show several sharper spikes on top of the peak, as well as the sharp peak visible at δ = 4.9 ppm, could be caused by decomposition or rearrangement products with an octahedral coordination.

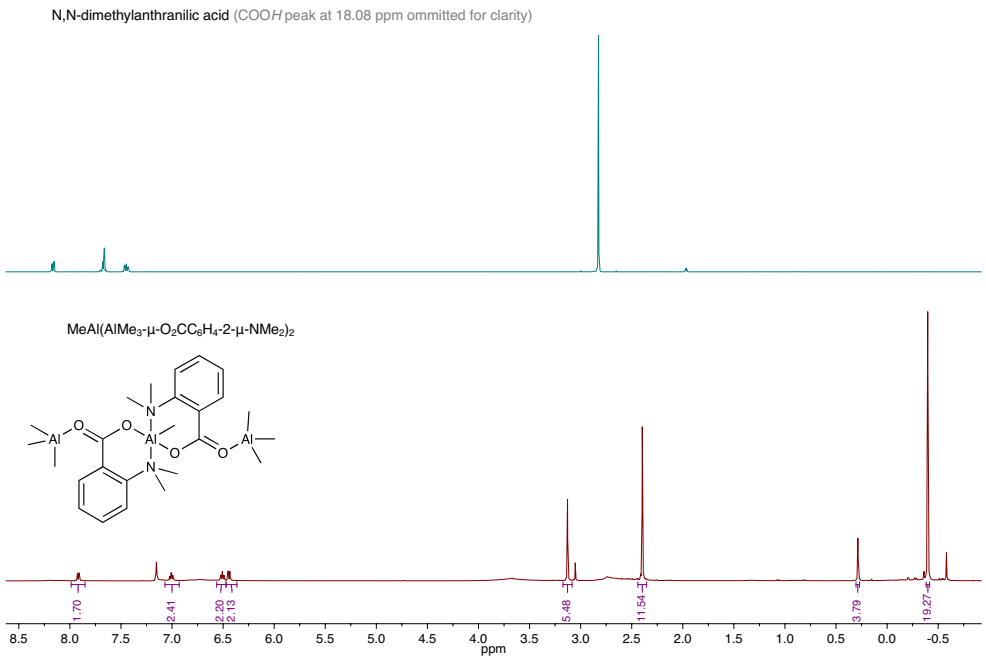

Figure 46: ^{1}H-NMR spectra of **61** in C_6D_6 with the solvent residual peak at δ = 7.17 ppm, and the starting material N,N-dimethylanthranilic acid in CD_3CN with the solvent residual peak at δ = 1.94 ppm.

More than 30 attempts were made to reproduce the result of this reaction. Variations to reaction stoichiometry included using the same starting conditions with two equivalents of $AlMe_3$ and one equivalent of N,N-dimethylanthranilic acid (2:1), different equivalents of starting material, e.g. three equivalents of $AlMe_3$ with two equivalents N,N-dimethylanthranilic acid (3:2), as this is the ratio found in **61**, a ratio of one equivalent of $AlMe_3$ with two equivalents of acid (1:2), assuming that the product would be similar to **61** but not have the $AlMe_3$ units binding. Other parameters that were varied were the concentration (higher dilution in order to avoid the formation of an oil or resin), different solvents or solvent combinations, attempting to crystalise the oil, reaction time and temperature and storage time in the freezer, since the crystals leading to structure **61** were formed over the course of four months. None of these reactions produced new conclusive results or confirmed the results of Scheme 53.

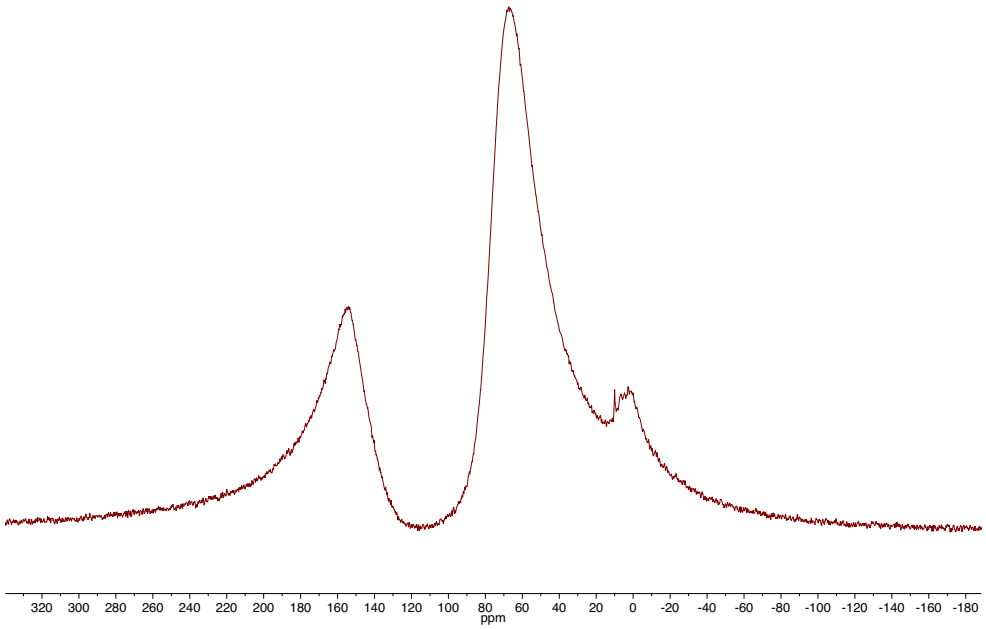

Figure 47: ^{27}Al-NMR spectra of **61**. The large artefact at $\delta = 51.0$ ppm results from the background probe signal and is visible in all ^{27}Al NMR spectra.[225] [247] [248].

4.1.2 Reactions of $[Me_2Al(\mu\text{-}O_2CPh)]_2$

Based on the synthetic work presented in Section 4.1.1 several strategies were pursued in order to further diversify the chemistry. This includes the functionalisation of **43** ($[Me_2Al(\mu\text{-}O_2CPh)]_2$), variations in the sterical demands of the amino substituent in the secondary amine derivatives of anthranilic acid and the use of new ligands. Although several of these projects lead to interesting results, future work is needed to clarify the data from the initial experiments.

In order to test the functionalisation of compound **43** ($[Me_2Al(\mu\text{-}O_2CPh)]_2$) it was tested as a starting material for further reactions. As mentioned in section 4.1.1.1 above, the reaction between $AlMe_3$and two equivalents of benzoic acid failed. Therefore, in order to attempt the synthesis of a species of the nature of $[MeAl(\mu\text{-}O_2CPh)_2]_x$, **43** was reacted with an additional equivalent of benzoic acid (Scheme 56). Regardless of the reaction conditions, this led to the formation of an insoluble white powder. The same result was seen for the reaction of three equivalents benzoic acid. Attempts to characterise the sample via NMR spectroscopy or mass spec failed due to the insolubility of the white solid in all feasible solvents.

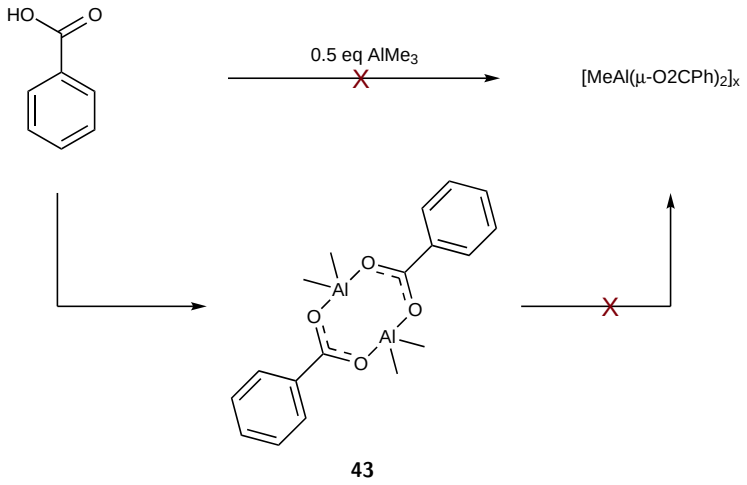

Scheme 56: Attempts for the synthesis of $[MeAl(\mu\text{-}O_2CPh)_2]_x$.

In order to functionalise **43**, $[Me_2Al(\mu\text{-}O_2CPh)]_2$ was also reacted with one equivalent of 8-hydroxyquinoline (Scheme 57), attempting to synthesise a compound **64**, with one benzoate and the hydroxyquinolate as ligands (or any oligomer thereof). Upon the addition of 8-hydroxyquinoline to a solution of **43** in DCM, gas evolution was observed. The reaction mixture was placed in the freezer and after one week crystals

were obtained. The crystal structure showed one aluminium centre with a distorted octahedral coordination by three hydroxyquinolates. The crystal system is triclinic and the space group P-1 (Figure 48, Table 11). The yield was very low (16%), which suggests that other products were present in the reaction mixture, but $Al(C_9H_6NO)_3$ was the only one to crystallise.

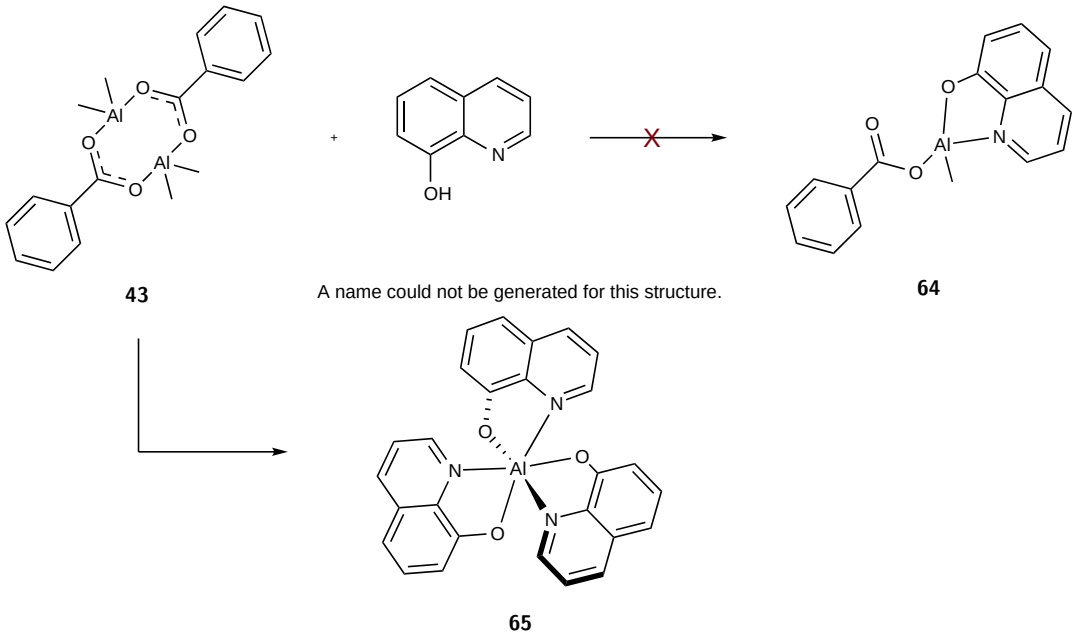

Scheme 57: Attempted synthesis of **65** and isolation of **64**.

Table 11: Selected bond lengths and angles for **65**. Lengths are given in Å, angles in deg.

	65 $Al(C_9H_{6N\text{-}8\text{-}O})_3$
Al(1)-O(1)	1.8713(16)
Al(1)-O(2)	1.8456(18)
Al(1)-O(3)	1.8679(16)
Al(1)-N(1)	2.0256(19)
Al(1)-N(2)	2.0445(19)
Al(1)-N(3)	2.056(2)
O(1)-Al(1)-O(2)	96.86(8)
O(1)-Al(1)-O(3)	170.35(8)
O(2)-Al(1)-O(3)	91.84(8)
O(1)-Al(1)-N(1)	83.15(8)
N(1)-Al(1)-N(2)	171.60(8)

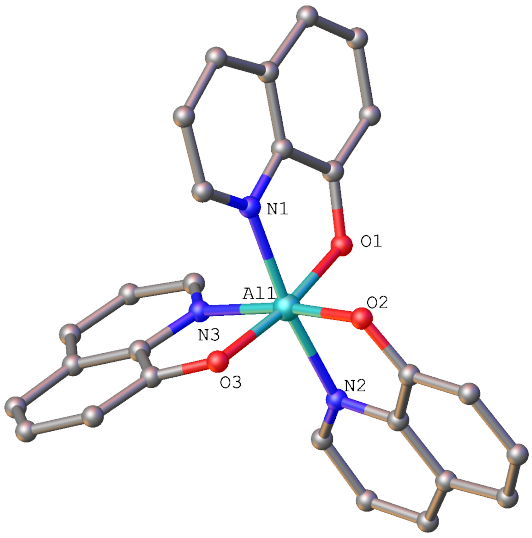

Figure 48: Crystal structure of **65**. Hydrogen atoms and two DCM molecules are omitted for clarity. For selected bond lengths and angles see Table 11.

The sample used for crystallography decomposed during analysis. In order to obtain spectroscopic data, the reaction was repeated with the exact same conditions. The ^{1}H-NMR spectrum obtained for **65** in pyridine-d_5 shows two or more compounds to be present, with similar aromatic systems. It was not possible to isolate or purify any of the products, although attempts were undertaken to recrystallise the sample. The ^{27}Al-spectrum shows a broad signal at δ = 34.70 ppm, which appears to have sharper signals underneath at δ = 35.32 ppm and 33.17 ppm. Two broader signals are visible on the highfield side of the probe artefact with δ = 43.45 ppm and 47.49 ppm, confirming that multiple Al species are present in the sample. Attempts to repeat the reaction in Scheme 57 and synthesise **64** were not successful. It was tried to keep the temperature below 0°C to slow the reaction down to avoid multiple substitutions and to vary the concentration of the reaction mixture. However, it was not possible to isolate and identify any reaction products, other than compound **65**.

Since aluminium has a high affinity towards oxygen, and because the aluminium centres are relatively hard it was attempted to functionalise **66** ($[Me_2Al(\mu\text{-}O_2CPh)]_2$) with alcohols, to protonate the CH_3 group and substitute it by the alkoxide RO^- (Scheme 58), dependent on the equivalents of alcohol used.[266] The alcohols tested were methanol and ^{t}butanol. Methanol is relatively small and was thought to replace the methyl group in the dimeric solid-state structure of **43**, as suggested for **67** in

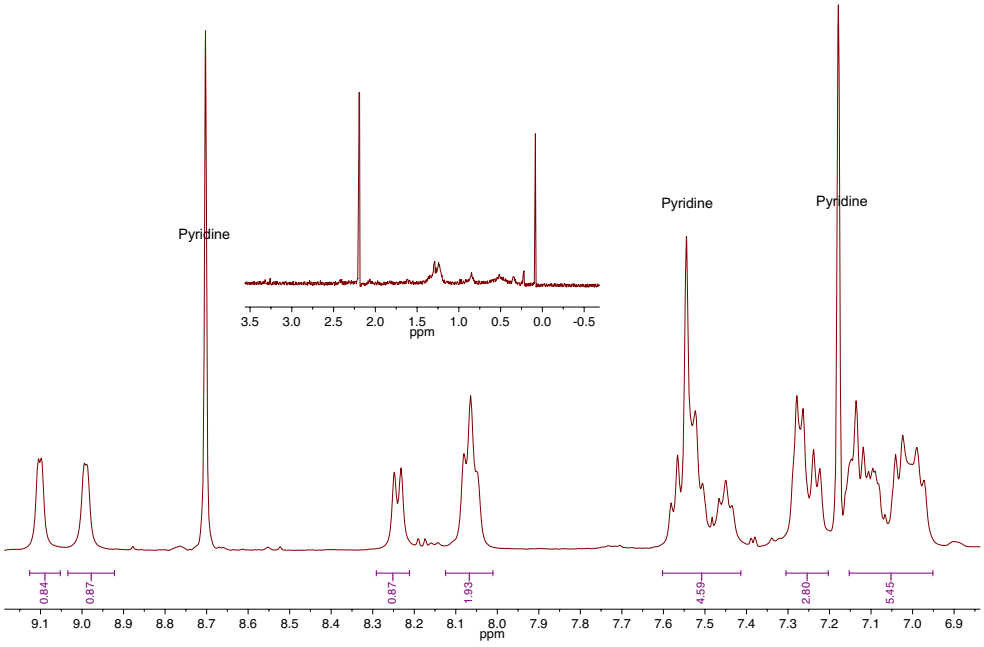

Figure 49: ^{1}H-NMR spectrum for **65** in pyridine with the solvent residual peaks at δ = 8.70, 7.51 and 7.17 ppm. The inset shows the absence of significant product peaks between 4 to -0.05 ppm.

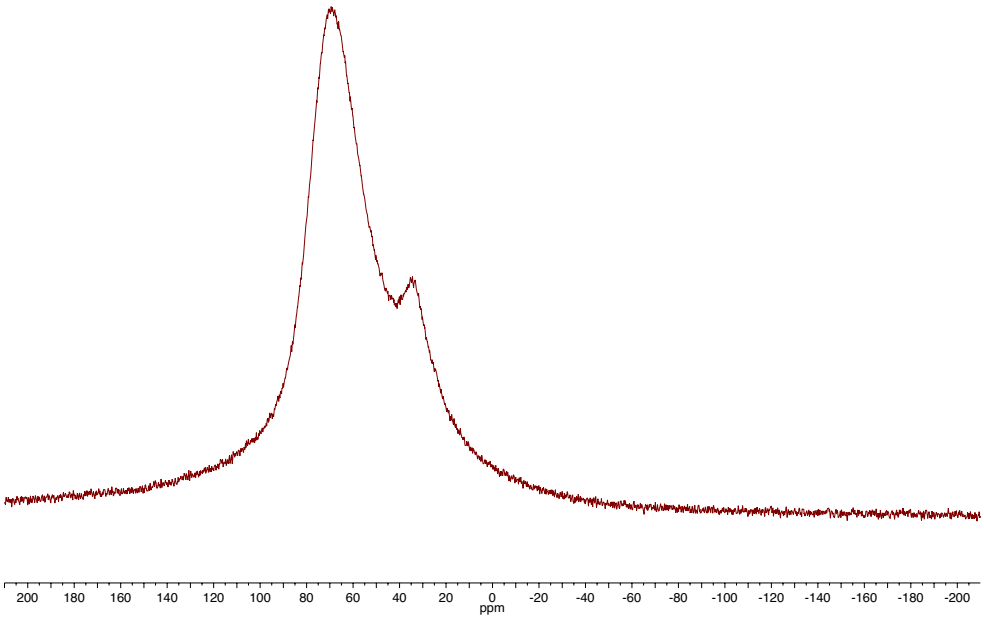

Figure 50: ^{27}Al-NMR spectrum for **65**. The large artefact at δ = 67.2 ppm results from the background probe signal and is visible in all ^{27}Al NMR spectra.[225] [247] [248].

Scheme 58. ^{t}BuOH on the other hand, has a very large steric demand, so it could maybe help to either create new bonding motifs, or act as a bulky enough ligand to create a monomeric, tris-coordinated aluminium centre (**68**, Scheme 58).

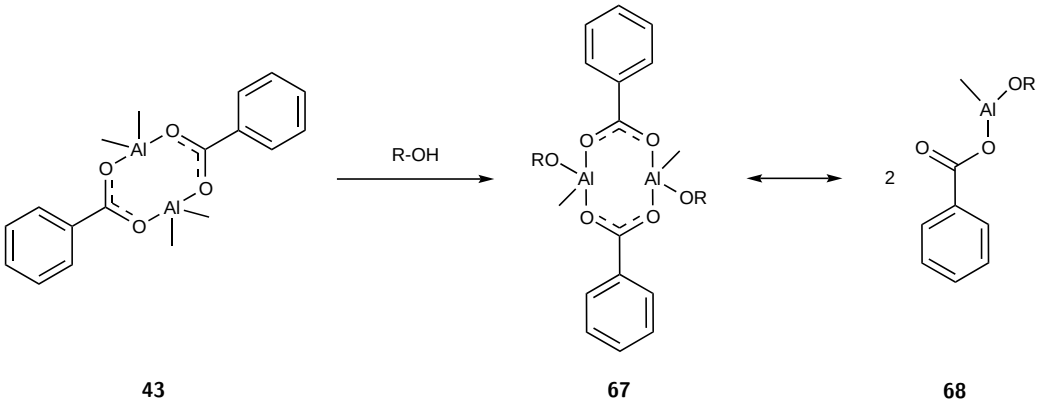

Scheme 58: Proposed reaction between **43** and 1 eq of R-OH (R = Me, ^{t}Bu).

The addition of methanol led to immediate gas evolution, indicating that protonation of the methyl group is taking place. The reaction yielded a white insoluble powder, which could be due to the formation of oligomeric or polymeric aggregates of AlR'OR (R' = $PhCOO^{-}$) since aluminium can form μ^2 and μ^3-bridges with oxygen atoms. Furthermore, the methyl group does not have a large steric demand to prevent the formation of higher aggregates. The reaction of ^{t}BuOH and $AlMe_3$ yielded a white powder as well, however, unlike the powder obtained for the same reaction with methanol, it was soluble in benzene and analysed by NMR spectroscopy. The ^{1}H-spectrum (Figure 51) shows undefined peaks in the aromatic region, and two sharp singlets at δ = 1.36 ppm and δ = 1.26 ppm. Furthermore, there is a smaller multiplet at δ = -0.36 ppm, which could be the AlMe group. The expected peaks for *tert*-butanol are at δ = 1.05 ppm and δ = 1.55 ppm. This indicates that some form of reaction has taken place, although it is difficult to make a statement on what the possible reaction product is. The ^{27}Al-spectrum in Figure 52 shows the starting material (green), which has one broad signal at δ = 146.9 ppm and a flat broad peak at δ = -6.2 ppm. The reaction product (red), on the other hand, shows an additional broad peak at δ = 97.29 ppm, indicative of an AlO_4-species[222], as well as four relatively sharp peaks at δ = 21.80 ppm, 6.72 ppm, -5.76 ppm and -14.50 ppm, which indicate the presence of several octahedrally coordinated aluminium species.[222] This contradicts the suggested structure **68** in Scheme 58. However, it could be possible that a dimeric species (**67**) is formed, and that the tendency to form aggregates and maximise the coordination number is stronger than avoiding steric clash between the ^{t}Bu and the Me group.

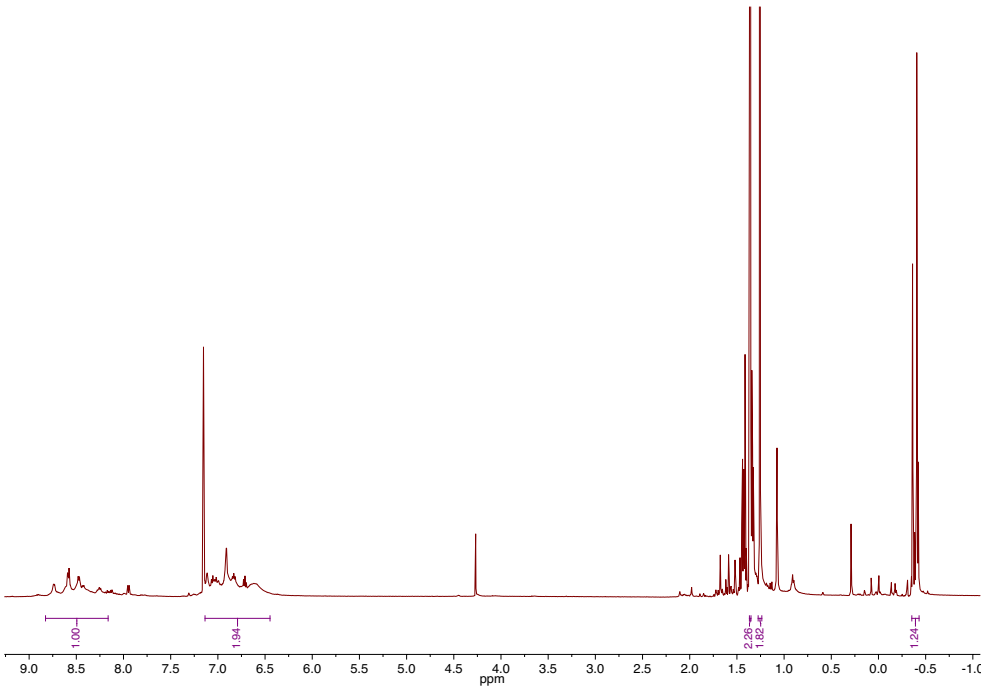

Figure 51: ^{1}H-NMR spectrum for the isolated reaction products of the equimolar reaction between **43** ($[Me_2Al(\mu\text{-}O_2CPh)]_2$) and ^{t}BuOH. Measured in C_6D_6, with the solvent residual peak at $\delta = 7.18$ ppm. Peak labeling has been omitted for clarity.

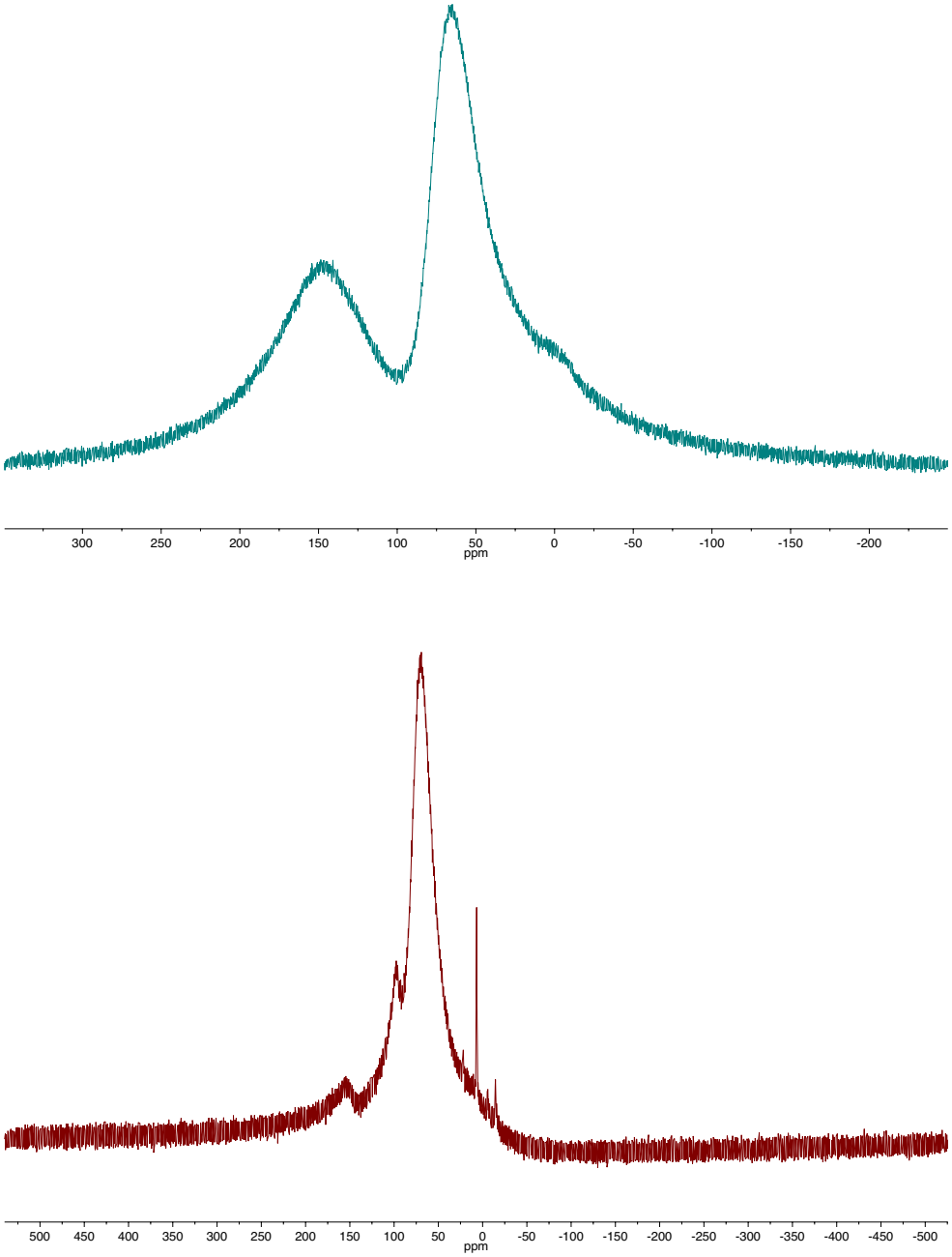

Figure 52: ^{27}Al-NMR spectrum for the isolated reaction products of the reaction between **43** and ^{t}BuOH (red) and in comparison that of the starting material [$Me_2Al(\mu$-$O_2CPh)]_2$ (green). The spectrum was measured in C_6D_6. The large artefact at δ = 65.4 ppm (green) and 69.9 ppm (red) result from the background probe signal.[225] [247] [248].

For the potential use of the synthesised compounds in alkali-activated polymer cross-linking many attempts were undertaken to prepare, isolate and characterise hydrolysis and oxidation products of **43**, $[Me_2Al(\mu\text{-}O_2CPh)]_2$. For this systematic hydrolysis study, **43** was dissolved in toluene and/or THF under a nitrogen atmosphere and a 1 M solution of H_2O in THF was added to introduce a defined amount of water between 0.02 and 1 eq in relation to **43** ($[Me_2Al(\mu\text{-}O_2CPh)]_2$). Figure 53 shows one representative example, obtained for the reaction of **43** with 0.2 eq of H_2O. It can be seen that the peaks arising from the starting material, **43** are still present and additionally underlying broader signals in the aromatic region that are less distinguishable, due to the multitude and the broadening of the signals. Furthermore, the signal that can be assigned to organometallic bonding around δ = 0 ppm multiplied into multiple smaller signals, suggesting that not one uniform product was formed, but a complex mixture of slightly different structures, that still incorporate the phenyl ring from the starting material, as well as organometallic bonds.

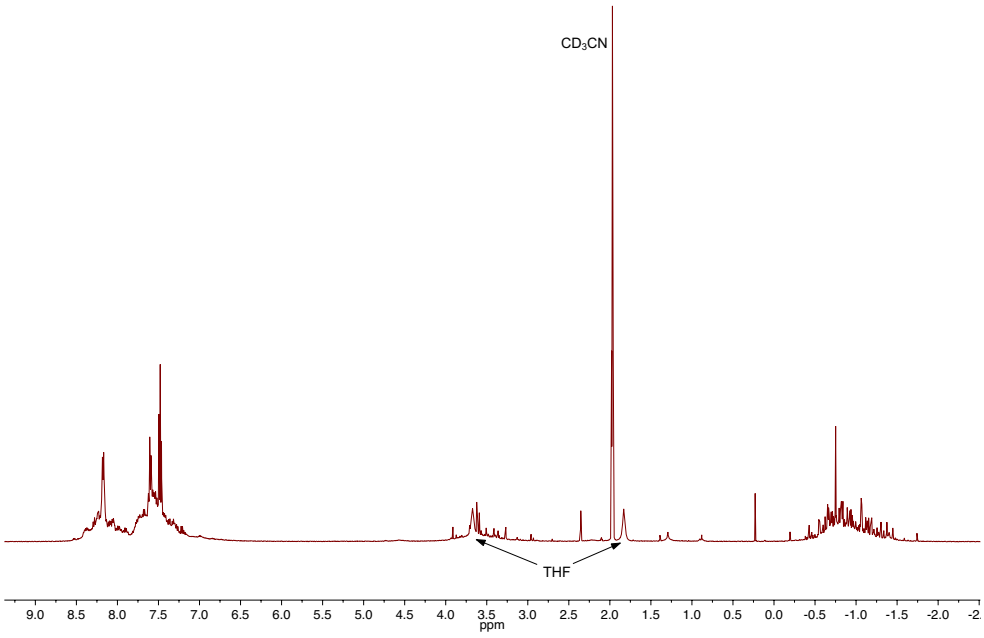

Figure 53: ^{1}H-NMR spectrum for the hydrolysis of **43** with 0.2 eq H_2O measured in CD_3N, with the solvent residual peak at δ = 1,97 ppm. Peak labeling has been omitted for clarity.

The corresponding ^{27}Al- spectrum still shows a peak at δ = 145.9 ppm, which corresponds with the tetrahedrally coordinated aluminium in **43**. Additionally, two major new product peaks appeared at δ = 2.19 and 2.33 ppm, showing that the multiple new species present are AlO6-type systems.[222]

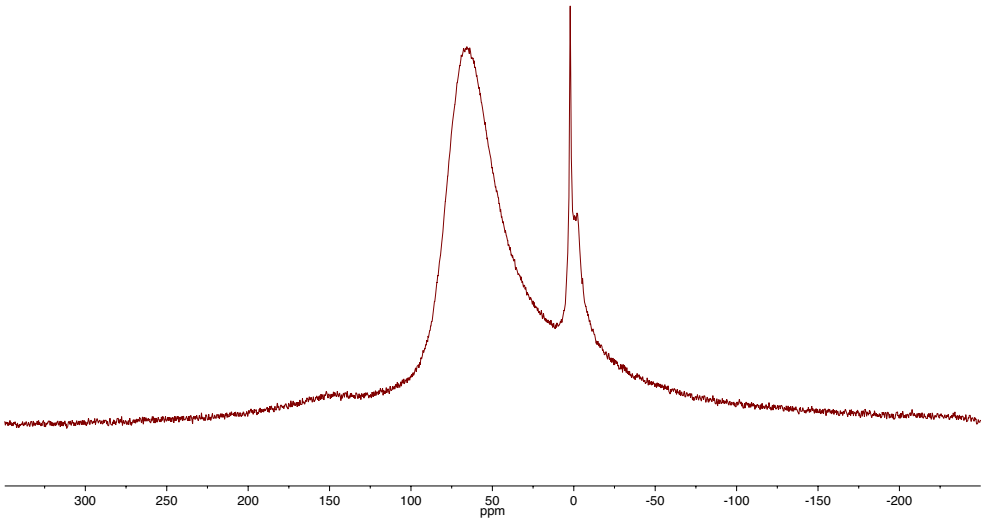

Figure 54: ^{27}Al-NMR spectrum for the reaction product obtained from the hydrolysis of **43** with 0.2 eq H_2O. Measured in benzene. The large artefact at $\delta = 69.5$ ppm results from the background probe signal.[225] [247] [248]

It was not possible to isolate any crystals suitable for x-ray analysis from any of the reactions or to purify any of the compounds for a more detailed NMR analysis.

4.2 Crosslinking and Rheology

4.2.1 Crosslinking of Guar and CMHPG with Different Aluminium Compounds

The second part of this research project looks at the crosslinking of guar and CMHPG. At the beginning, several commercially available and accessible aluminium compounds were tested for their qualitative ability to crosslink the aforementioned polymers. For this, a defined amount of aluminium was mixed with the polymer and the pH increased. The pH was recorded as a function of V(NaOH) and the viscosity was gauged by haptic behaviour and vision. The pH of guar gum without any crosslinking agent present was pH = 6.82.

Guar was crosslinked with $Al(O^iPr)_3$ and $Al(acac)_3$. Figure 55 shows the titration curve for the system of guar and $Al(O^iPr)_3$. The initial pH of all titration experiments was between 8.60 and 8.92. Upon addition of NaOH the pH increased, following the titration curve of a weak acid. An increase in $m(Al(O^iPr)_3)$ caused a decrease in the gradient of the curve. For $Al(O^iPr)_3$, gelling of approximately 20 g polymer was observed for $m(Al(O^iPr)_3)$ = 510 mg between pH = 12.97 and 13.10, and for $m(Al(O^iPr)_3)$ = 620 mg between pH = 12.99 and 13.10. This corresponds with a m(Al) in the polymer of 67.5 mg and 82.1 mg respectively. For lower concentrations of aluminium, a thickening of the polymer was observed, but the gelling point not was reached. Table 27 and Table 28 in Chapter 7.4.2 give an overview of the exact values. Following up on these results it can be determined that at least 0.34 % aluminium in relation to the hydrated polymer is needed for sufficient crosslinking to occur, in order to reach the gelling point.

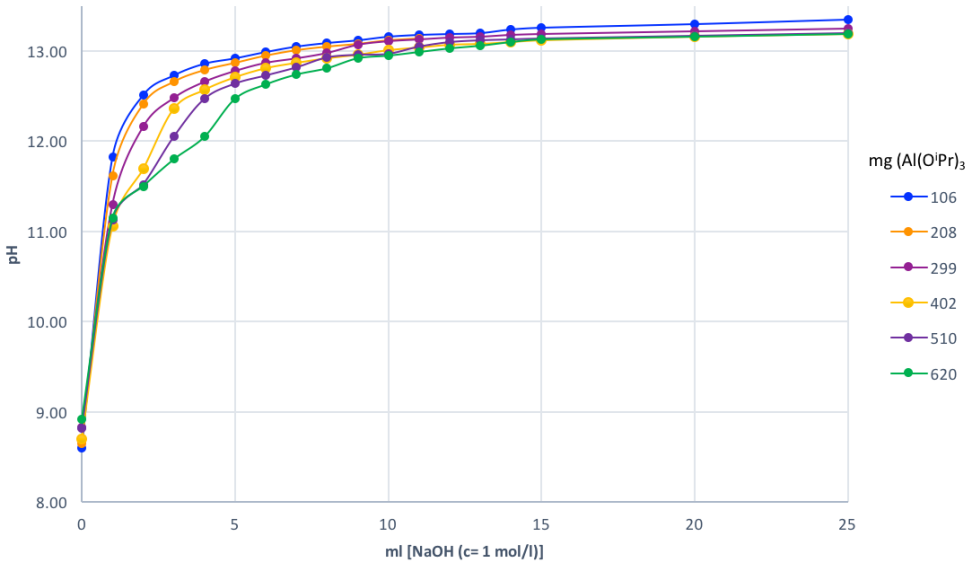

Figure 55: Titration curve for the crosslinking of guar with $Al(O^iPr)_3$.

For the crosslinking of approximately 20 g polymer (guar) with $Al(acac)_3$the titration curve looks similar (Figure 56) to that for $Al(O^iPr)_3$, but the concentration of $Al(acac)_3$ has a more severe impact. When m($Al(acac)_3$) increases, the system shows the behaviour of a diprotic acid with a second equivalent point at approx. pH = 11.8, since the acac ligand can be deprotonated by strong bases. When using $Al(acac)_3$ for crosslinking no gelling point was observed. Although the mixture showed an increase and sequential decrease of thickening when the pH was raised, it was not as well defined as for $Al(O^iPr)_3$ and it was not possible to point out the point of maximum viscosity. Table 29 and then Table 30 in Chapter 7.4.2 give an overview of the exact values.

CMHPG was crosslinked with $Al(lac)_3$ due to the fact that CMHPG requires generally lower pH ranges for crosslinking to occur.[240] The initial pH without crosslinking agent present was pH = 6.08. The amounts of $Al(lac)_3$ required to reach the gelling point are significantly lower (m($Al(lac)_3$) = 10 mg), which equals 0.01 % Al in respect to the used CMHPG. The pH was raised to pH = 6.18 at which point the gelling point was reached. For m($Al(lac)_3$) = 27 mg (0.03 % Al) it was pH = 6.10. The strongest gelling was observed for m($Al(lac)_3$) = 150 mg at pH = 6.20 (0.17 % Al). The volumes of NaOH required to raise the pH were smaller compared to the experiments with $Al(O^iPr)_3$ and $Al(acac)_3$, as the acidic system reacted more sensitively to the introduction of a base (volumes of 0.05 and 0.1 ml were added). Details on the values can be found in

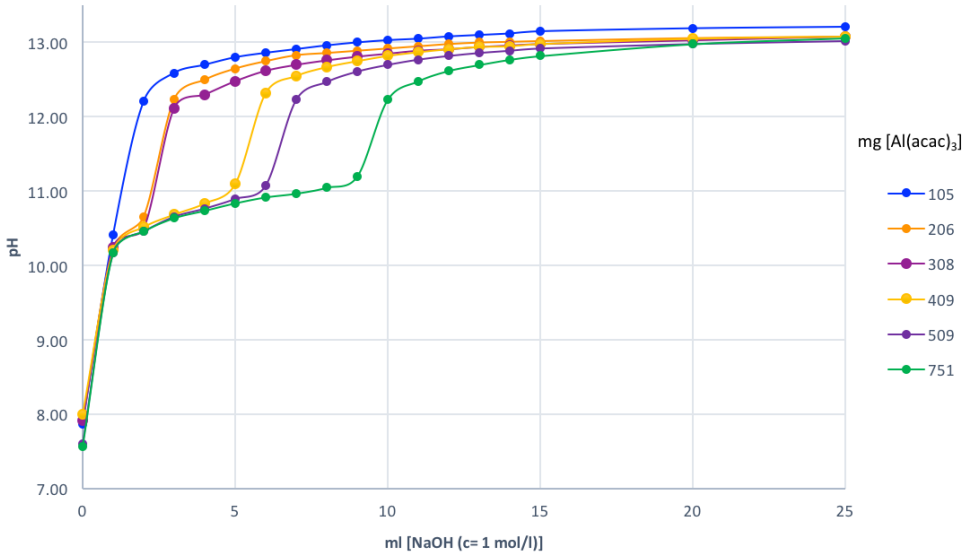

Figure 56: Titration curve for the crosslinking of guar with $Al(acac)_3$.

Table 31 and Table 32.

The aforementioned gelling point was noticeable as a thickening coincident with the polymer solution remaining in a spatula when this was removed from the solution. Figure 57 shows this behaviour for CMHPG crosslinked with $Al(lac)_3$.

Figure 57: Physical behaviour of the polymer when the gelling point was reached (crosslinking of CMHPG with $Al(lac)_3$ on the left and Guar with $Al(O^iPr)_3$ on the right).

4.2.2 Rheoligcal Studies of CMHPG Crosslinked with $Al(lac)_3$

Based on the results from the preliminary studies into the crosslinking of guar and CMHPG, it was decided to take the system of aluminium lactate and CMHPG as a model for rheological experiments. A concentration of 0.17 % aluminium with respect to the CMHPG was chosen and the viscosity was measured for different pH values at shear rates of $\dot{\gamma}$ = 1, 10 and 100 s^{-1} and back to 10 and 1 s^{-1}. This was to see how the crosslinked systems can recover from the shear stress applied. The shear rates were maintained for 125 s before moving to the next stage of the experiment and the viscosity η was recorded, in each case, all 5 s. For the calculation of the average viscosity, only the last five data points of each series were considered, in accordance with established procedures at Schlumberger Gould Research, as it is assumed that the viscosity is at a stable level after an initial deviance when the rate was changed. Figure 58 shows a typical shear profile, here as an example for pH = 6.00. As expected η decreases when the shear rate is raised. For a shear rate of 1 s^{-1} the viscosity stabilises itself at 12.08 Pa s. When the shear rate is increased to 10 s^{-1} it decreases to 2.90 Pa s which is a loss of approximately 75 % in shear viscosity. When further increased to 100 s^{-1} the viscosity is 0.38 Pa s, a drop of 88 %. When the shear rate is increased again the values for 10 and 1 s^{-1} are lower than before. It seems that the crosslinked system does not recover fully from the introduced shear stress. For 10 s^{-1} and 1 s^{-1} it only reaches approximately 62 % of the initial shear viscosity. This can be due to multiple reasons. It is possible that the polymer shows a very slow shear recovery or thixotropic effects. It could also be the case that the crosslinking is incomplete at first and that further crosslinking happens during the recovery, which has different effects on the intact and the sheared gel.

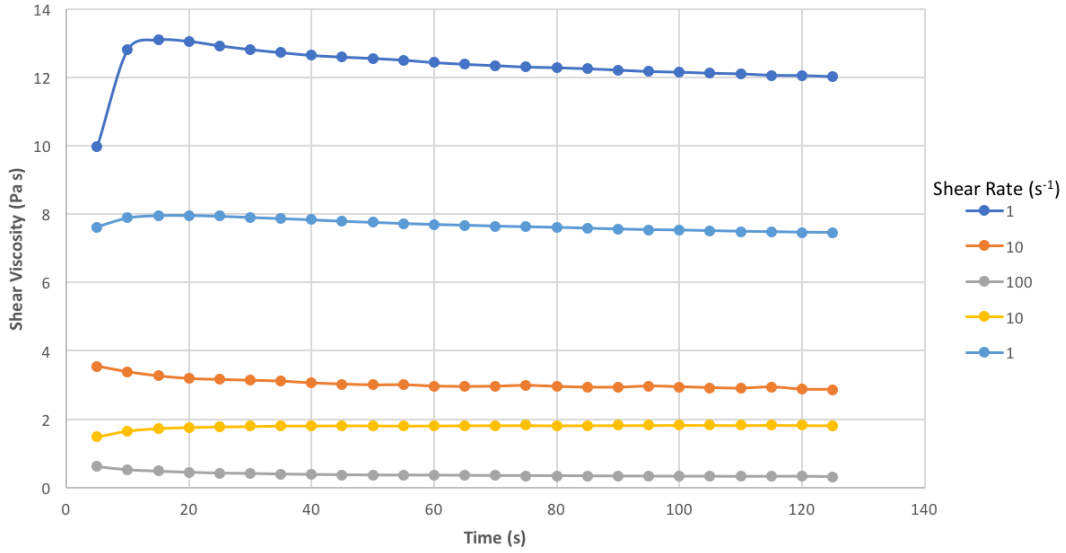

Figure 58: Shear viscosity η at $\dot{\gamma}$= 1, 10, 100, 10 and 1 s^{-1} for pH = 6.00 and 0.17 % Al ($Al(lac)_3$) in CMHPG.

Table 12 shows the shear viscosity η of CMHPG crosslinked with aluminium lactate as a function of the shear rate $\dot{\gamma}$ and the pH value. The results are displayed in Figure 59. It can be seen that the maximum viscosity is reached at pH = 6.29.

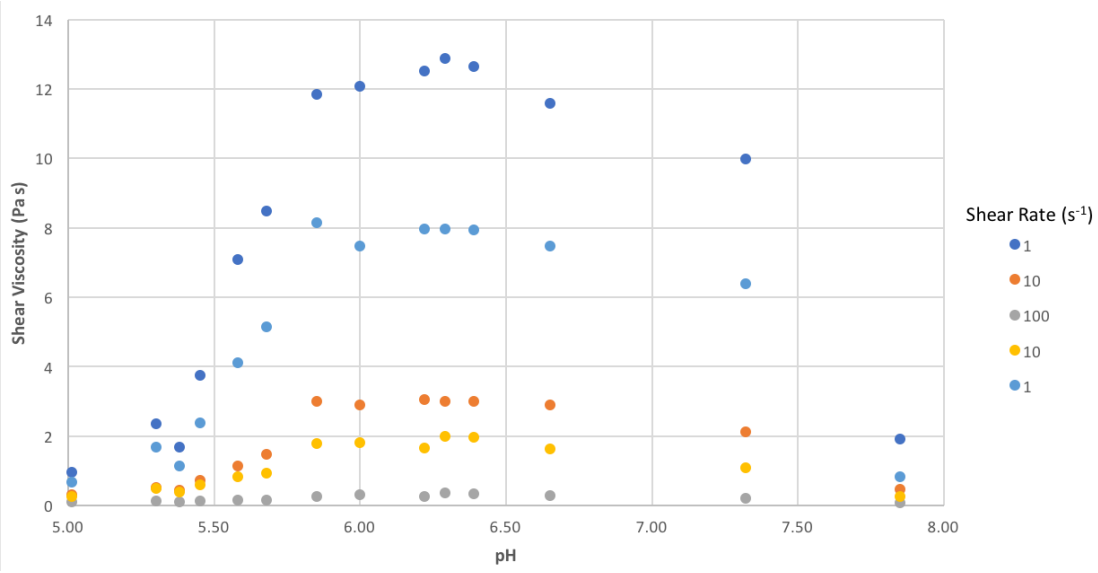

Figure 59: Shear viscosity (in Pa s) of CMHPG crosslinked with $Al(lac)_3$ (0.17 % Al) at different shear rates.

Table 12: Shear viscosity (in Pa s) of CMHPG crosslinked with $Al(lac)_3$ (0.17 % Al) at different shear rates.

	Shear Viscosity η (Pa s)				
pH	1 s^{-1}	10 s^{-1}	100 s^{-1}	10 s^{-1}	1 s^{-1}
5.01	0.9718	0.3189	0.0995	0.2752	0.6895
5.30	2.3594	0.5318	0.1312	0.5088	1.6854
5.38	1.6894	0.4573	0.1171	0.3827	1.1428
5.45	3.7514	0.7388	0.1437	0.6048	2.3872
5.58	7.0772	1.1398	0.1713	0.8297	4.1132
5.68	8.4930	1.4796	0.1725	0.9378	5.1488
5.85	11.8560	3.0164	0.2724	1.7774	8.1520
6.00	12.0800	2.9010	0.3187	1.8206	7.4822
6.22	10.7640	2.7996	0.2674	1.6960	7.8134
6.29	12.8720	3.0156	0.3593	2.0058	7.9812
6.39	12.6480	3.0146	0.3532	1.9734	7.9382
6.65	11.5920	2.9048	0.2861	1.6276	7.4668
7.32	9.9752	2.1292	0.2017	1.0948	6.3904
7.85	1.9074	0.4595	0.0859	0.2583	0.8393

The graph also shows the aforementioned difference in viscosity ($\Delta\eta$), when the shear rate is decreased again. For shear rates 1 s^{-1} and 10 s^{-1} respectively, the absolute value of $\Delta\eta$ increases at higher viscosities. However, for $\dot{\gamma}$= 1s^{-1} the difference is mostly between 30-40 %, whereas for $\dot{\gamma}$ = 10s^{-1} $\Delta\eta$ is more widespread between 10-20 % for pH > 5.5 and $\Delta\eta$= 40-50 % for pH < 6.5. The difference in viscosity between the initial shear rate and the same rate after an increase in $\dot{\gamma}$ shows that the applied force causes ruptures in the crosslinked polymer, but also that the pH has an effect, as especially for $\dot{\gamma}$= 10s^{-1}, $\Delta\eta$ increases with the pH.

Table 13: $\Delta\eta$ for $\dot{\gamma} = 1$, 10 s^{-1} before and after an increase of $\dot{\gamma}$.

	$\Delta\eta$ (%)	
pH	1 s^{-1}	10 s^{-1}
5.01	29.1	13.7
5.30	28.6	4.3
5.38	32.4	16.3
5.45	36.4	18.1
5.58	41.9	27.2
5.68	39.4	36.6
5.85	31.2	41.1
6.00	38.1	37.2
6.22	27.4	39.4
6.29	38.0	33.5
6.39	37.2	34.5
6.65	35.6	44.0
7.32	35.9	48.6
7.85	56.0	43.8

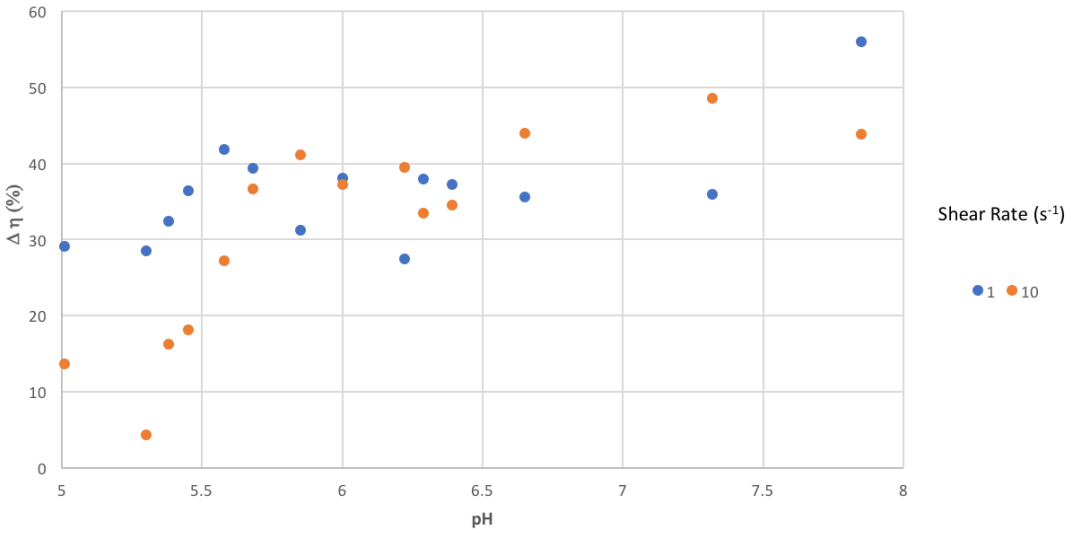

Figure 60: $\Delta\eta$ for $\dot{\gamma} = 1$, 10 s^{-1} before and after an increase of $\dot{\gamma}$.

In comparison to Figure 58, Figure 61 shows how CMHPG behaves at pH = 6 when no crosslinker is present. The viscosity is significantly lower with 0.133 Pa s for 1 s^{-1} and 0.094, 0.043, 0.091 and 0.126 Pa s for the remaining shear rates. $\Delta\eta$ is $\leq$ 5% and therefore significantly lower than the non-crosslinked polymer at pH = 6, confirming that the loss in viscosity after the increased shear stress is related to the crosslinker.

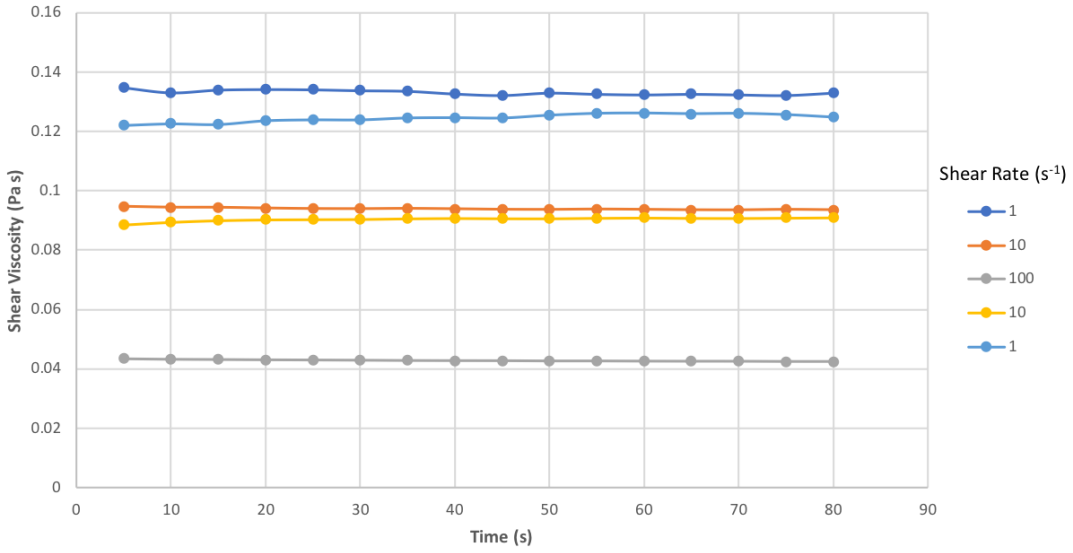

Figure 61: Shear viscosity of CMHPG at 1, 10, 100, 10 and 1 s^{-1} for pH=6.00 without a crosslinker.

For the sample at pH = 5.85 the viscosity was measured again after a rest time of 5 h, to see if the viscosity recovers. However, Table 14 shows that the viscosity actually decreased further.

Table 14: η of CMHPG crosslinked with $Al(lac)_3$ at pH = 5.85 measured at the beginning of the experiment (initially) and after a rest time of 5 h.

	η (Pa s)				
	1 s^{-1}	10 s^{-1}	100 s^{-1}	10 s^{-1}	1 s^{-1}
pH 5.85 initially:	11.856	3.016	0.272	1.774	8.152
pH 5.85 after rest:	6.888	1.017	0.149	0.649	2.975

Following from these first preliminary studies on the correlation between the pH and the viscosity of the gel, two samples with promising viscous properties were further studied to determine more insights about the polymeric characteristics of the aluminium crosslinked CMHPG. The samples were gels at pH = 6.29 which showed the maximum viscosity in the preliminary studies discussed above, and pH = 6.22 as a

sample close to the maximum viscosity but with lower viscosity. Here the aim was to study the importance of the correct pH for the rheological properties of the gel.

In the experiments discussed so far, $\dot{\gamma}$ was set to fixed rotation speeds of 1, 10, and 100 s^{-1} and kept at the respective speed for 125 s. To further determine the viscous behaviour of the polymer in a new experiment the rotation was increased continuously from 0.1 s^{-1} to 200 s^{-1} (ramp up) and then decreased back to 0.1 s^{-1} (ramp down). This process was carried out at 25°C, 80°C and again at 25°C. The data in Figure 62 shows a reversible shear thinning behaviour for pH = 6.29 at low and high temperatures. At higher shear rates the viscosity drops but returns to its original magnitude, when the shear rate is lowered again. The ramp down curve at 80°C is lowered compared to the other runs, but in the following run at 25°C the polymer shows the same behaviour as it did before being heated. The crosslinked polymer is therefore stable at higher temperatures. In Figure 58 and Figure 59 a loss in viscosity was observed after the samples were exposed to higher set shear rates. However, this behaviour is not seen for the steady increase and decrease experiment. It can, therefore, be concluded, that possible damage to the polymer seem only to occur after longer times at high shear rates.

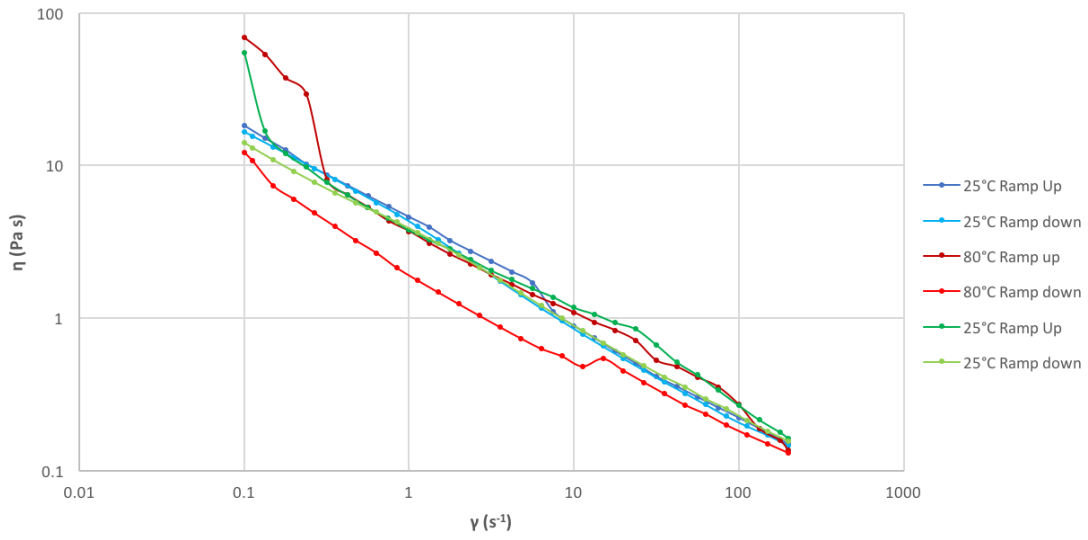

Figure 62: Viscometric studies of CMHPG crosslinked with $Al(lac)_3$ at pH = 6.29, Shear rate $\dot{\gamma}$ 0.1 to 200 s^{-1} (ramp up) and 200 to 0.1 $^{-1}$ (ramp down), Temperature was varied in the order 25°C, 80°C, 25°C.

For the sample with pH = 6.22, the behaviour differs to a small extent. As seen in Figure 63 the differences between the ramp up and the ramp down are more pronounced for the initial 25°C and for 80°C. The second run at 25°C fails to reach the

same viscosity than the one observed in the first sequence, but for both the ramp up and the ramp down process the values correspond to the lower viscosity of the initial ramp down at 25°C.

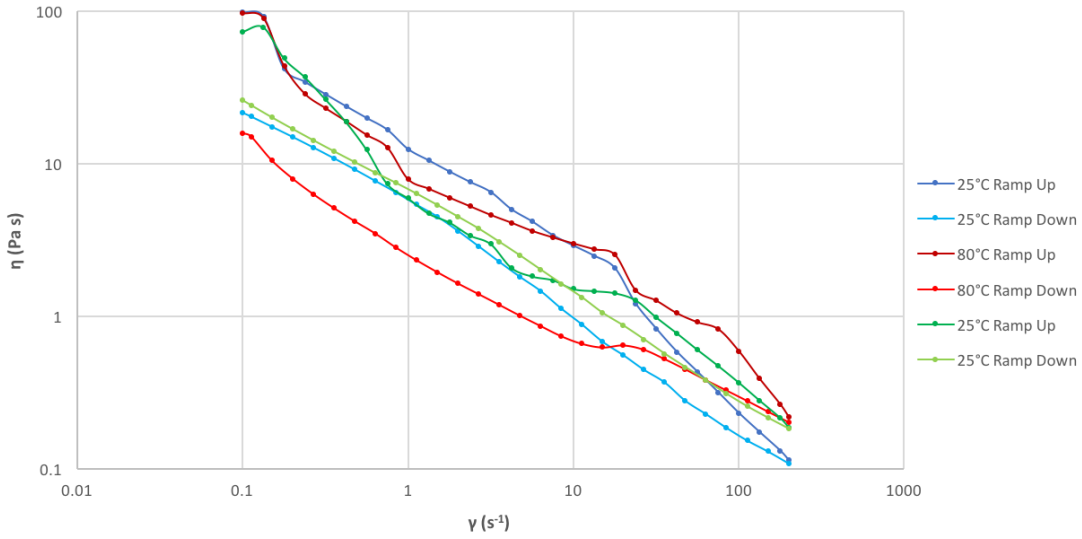

Figure 63: Viscometric studies of CMHPG crosslinked with $Al(lac)_3$ at pH = 6.22. Shear rate $\dot{\gamma}$ 0.1 to 200 s^{-1} (ramp up) and 200 to 0.1 $^{-1}$ (ramp down), temperature 25°C, 80°C, 25°C.

Materials that exhibit both elastic and viscous behaviour when experiencing shear stress are referred to as viscoelastic. They show a time-depending relationship between shear and strain. The shear module G consists of two components, the elastic module G′ and the viscous module G″. In a so-called linear viscoelastic system, this time-dependent relationship is linear. In order to determine the limits of the linear viscoelastic regime (LVER) for the CMHPG/Al system the polymer was exposed to an oscillating shear stress, with γ given in % of the shear strain. As it can be seen in Figure 64 for pH = 6.29 the polymer shows a wide linear range for low temperatures (25°C), higher temperature (80°C) and a lower temperature after being exposed to heat (25°C), although for 80°C there is more deviation from the linear range at high and low shear stress.

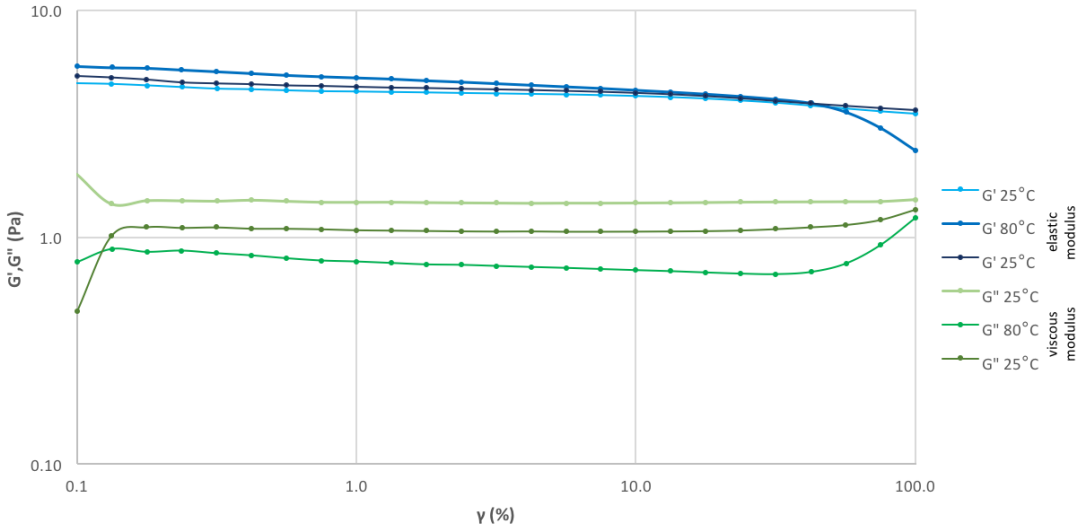

Figure 64: Determination of the linear viscoelastic regime by oscillation amplitude studies for pH = 6.29 of CMHPG crosslinked with $Al(lac)_3$. G′ shows the elastic module, G″ the viscous module. Shear strain γ = 0.1-100%, frequency f= 1Hz, temperature 25°C, 80°C, 25°C.

For pH = 6.22 the behaviour is similar (Figure 65), here the polymer also exhibits a wide linear region, but there is a stronger deviation between the temperatures within the elastic module. The elastic modulus for the initial sweep at 25°C is lower than that at 80°C and the final sweep at 25°C after being heated. It seems that upon heating a change occurs in the polymer, that was not observed at pH = 6.29. This can be attributed to an incomplete crosslinking at 25°C, which was completed at 80°C. The now crosslinked gel has a stable elastic module, of the same magnitude as it is at 80°C.

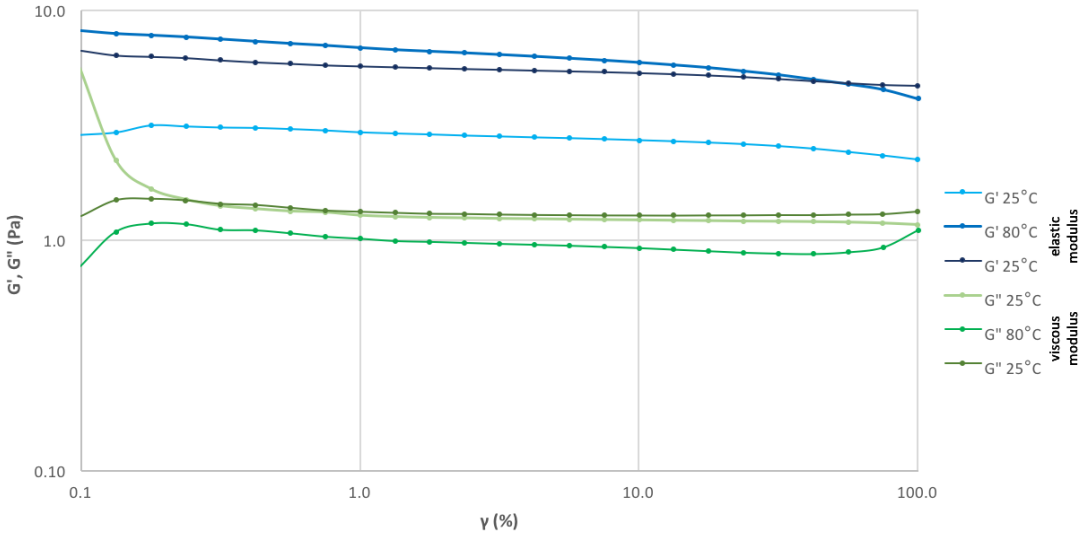

Figure 65: Determination of the linear viscoelastic regime by oscillation amplitude studies for pH = 6.22 of CMHPG crosslinked with $Al(lac)_3$. G′ shows the elastic module, G″ the viscous module. Shear strain γ = 0.1-100%, frequency f= 1Hz, temperature 25°C, 80°C, 25°C.

Figure 66 shows the data of the oscillation frequency sweep of CMHPG crosslinked with $Al(lac)_3$ at pH = 6.29, where the shear strain γ was kept within the linear viscoelastic region at 3% and the frequency decreased gradually from 100 Hz to 0.1 Hz. The blue curves represent the elastic module of the polymer (G′), which is larger than the viscous module (G″) for the frequency f < 100 Hz. G′ > G″ is characteristic for the three-dimensional network of a crosslinked gel. The observed behaviour is the same for 25°C, 80°C and 25°C after heating, confirming the stability of the crosslinking at higher temperatures.

For pH = 6.22 the observations from the frequency sweep (Figure 67) correspond mostly with the behaviour of the polymer for pH = 6.29. At a frequency of 56 Hz, the value seems to differ, with G″ > G′, which is not taken into account, as these values are outside the limits of reliable measurements.[267] Apart from these values, the elastic and viscous module follow the trend of G′ > G″. Above a frequency of 20 Hz the results can deviate from the expected trends, due to limitations of the measurement.

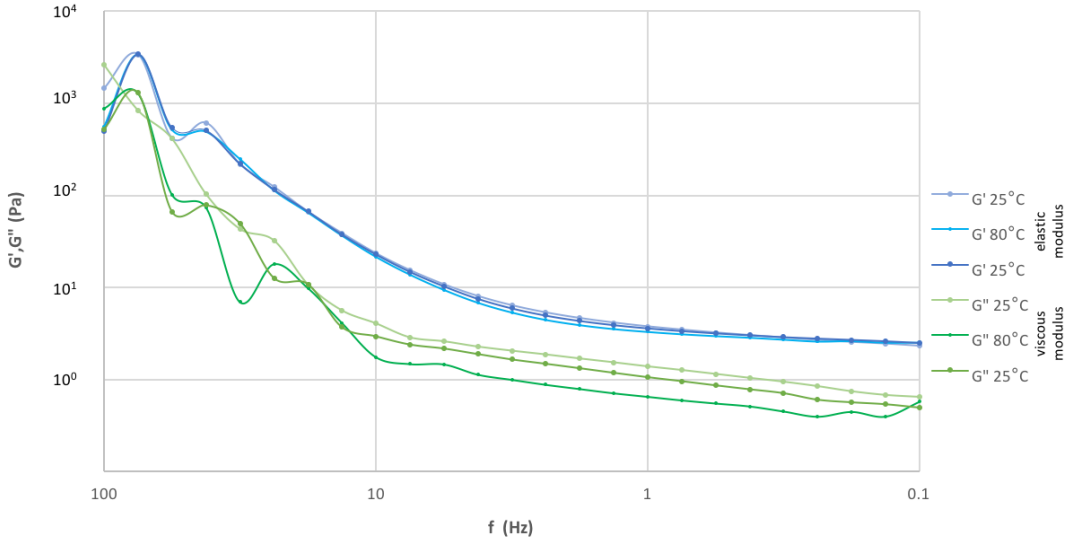

Figure 66: Frequency sweep at strain amplitude within linear regime for pH = 6.29 of CMHPG crosslinked with $Al(lac)_3$. G′ shows the elastic module, G″ the viscous module.. Frequency 100-0.1 Hz, shear strain $\gamma = 3\%$, temperature 25°C, 80°C, 25°C.

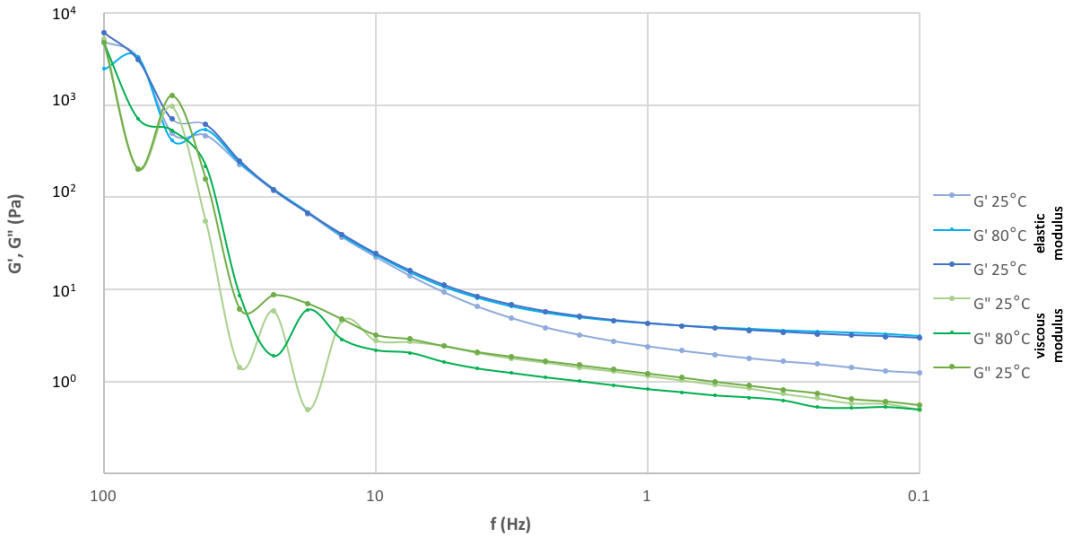

Figure 67: Frequency sweep at strain amplitude within linear regime for pH = 6.22 of CMHPG crosslinked with $Al(lac)_3$. G′ shows the elastic module, G″ the viscous module.. Frequency 100-0.1 Hz, shear strain $\gamma = 3\%$, temperature 25°C, 80°C, 25°C.

Due to the many variables to be considered for rheological measurements of systems such as those discussed above it was not possible to obtain values for a quantitative comparison and discussion. However, the overall qualitative results, such as the stability towards higher temperatures and the reversible shear thinning correspond with characteristics observed for both, borate- and organometallic crosslinked gels. [238] [268]

4.2.3 Use of Novel Aluminium Organic Compounds as Crosslinking Agents for Guar and CMHPG

The concentration of aluminium is of the utmost importance for the aforementioned crosslinking processes, as it determines the concentration of crosslinks in the polymer and the viscosity. It would be desirable to use compounds that have a high aluminium content in their composition, in order to minimise the amounts of crosslinker required. As seen in Table 15, $Al(acac)_3$ has the lowest aluminium content of the tested commercially available compounds with 8.3 %, $Al(O^iPr)_3$ has the highest with 13.2 %. Compound **43** ($[Me_2Al(\mu\text{-}O_2CPh)]_2$), which is one of the compounds synthesised at the beginning of this project, has an Al content of 15.1 %.

Table 15: Chemical formula, molar mass and aluminium content for commercially available aluminium compounds and **43** ($[Me_2Al(\mu\text{-}O_2CPh)]_2$).

Compound	Empirical formula	M ($g \cdot mol^{-1}$)	Al (%)
$Al(O^iPr)_3$	$C_9H_{21}O_3Al$	204.25	13.2
$Al(acac)_3$	$C_{15}H_{21}O_6Al$	324.31	8.3
$Al(lac)_3$	$C_9H_{15}O_9Al$	294.19	9.2
$[Me_2Al(\mu\text{-}O_2CPh)]_2$	$C_9H_{11}O_2Al$	178.17	15.1

In the course of work going on in the Wheatley group, $AlMe_3$ was reacted with trimethyloethane and $Al[MeC(CH_2O)_3]_2(AlMe_2)_3$ **69** (Scheme 59) obtained. Compound **69** has the empirical formula $C_{16}H_{36}O_6Al_4$ and an aluminium content of 25.0 %, so a quarter of its mass.

Because of their high Al content, the compounds **43** and **69** were also tested for crosslinking. However, the strong reactivity of the remaining aluminium carbon bonds towards water resulted in difficulties with the control of the reaction, since

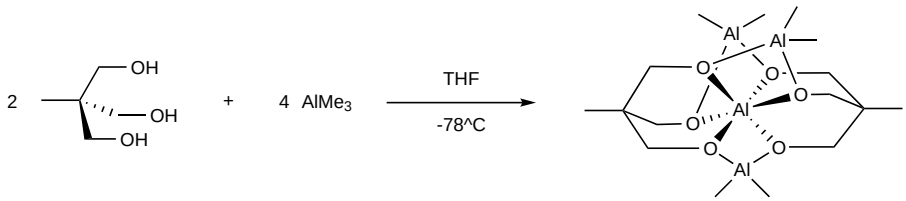

69

Scheme 59: Reaction of trimethyloethane and $AlMe_3$.

the polymer is an aqueous system. There are examples in the literature, whereupon reaction of lithium aluminates with oxygen templation reactions occurred, in which the templated core of the aluminate made it possible to retain aluminium carbon bonds.[269] [270] This could potentially also be applicable to the system used for these preliminary proof-of-concept reactions of **43** and **69** with CMHPG and Guar. Another challenge was the choice of a suitable solvent for the crosslinker since the gel had to be in an aqueous system, but the compounds were too reactive to dissolve them in water before the reaction. Attempts were therefore undertaken to dissolve 13 mg of **69** in 2 ml dry THF before adding it to 5g of aqueous guar solution. Some effervescence was observed and while stirring it was noticed that the gel thickened before suddenly forming a clod, surrounded by a thinner liquid. Considering the smell of the surrounding liquid it appeared to be water and THF, although at this stage confirmation by GC/MS or NMR was omitted. It was assumed that the THF caused a dehydration of the gel due to diffusion (Figure 68).

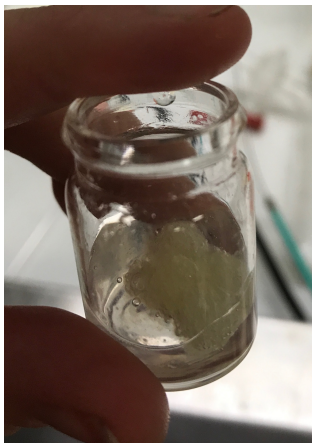

Figure 68: Attempted crosslinking of guar with **69** in water and THF.

Consequently, for these preliminary experiments, it was attempted to add the crosslinker **69** directly to the polymer, without using a solvent. To do this **69** was weight out under an N_2 atmosphere in a sealed container and added under ambient conditions while trying to minimise the exposure to air and moisture in the process. After adding

15 mg of **69** to 5 g CMHPG intense effervescence started, as seen in Figure 69, and persisted for several minutes. After the reaction had ceased a very highly viscous gel had formed, as shown in Figure 70. The formation of a surrounding liquid as in Figure 68 was not observed, confirming that in the reaction discussed above the THF interfered either with the crosslinking reaction or with the formed polymer.

Figure 69: Attempted crosslinking of CMHPG with **69** in water.

Figure 70: Attempted crosslinking of CMHPG with **69** in water after the visible signs of a reaction had stopped.

As a proof-of-principle, this shows that synthesised organoaluminium compounds such as **69** are capable of crosslinking guar and CMHPG. However, the presence of aluminium-carbon bonds gives rise to quite violent reactions with water and significant gas evolution, making it difficult to control the crosslinking process and optimising the conditions. Strategies to control this reactivity are discussed in Section 6, as the effervescence is not insurmountable on a laboratory scale, but will prove very problematic for the intended application.

5 Conclusion

The project presented in this dissertation consists of two parts: On the one hand, the reactions of aluminium triorganyls with benzoic acid and derivatives thereof were studied. In the second part, the employability of commercially available and synthetic compounds in crosslinking of polysaccharides was tested to show that aluminium compounds, similar to those made in this project, are suitable for this application.

In the synthetic project, it was possible to repeat successful results, e.g. the synthesis of $[Me_2Al(\mu\text{-}O_2CPh)]_2$ **43**, which, during the course of this project, has been reported by Lewiński *et al.* (Scheme 60).

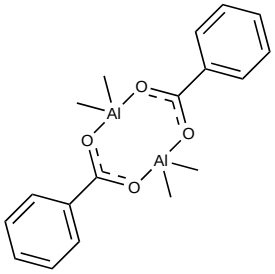

43

Scheme 60: The structure of Compound **43**, $[Me_2Al(\mu\text{-}O_2CPh)]_2$, based on data obtained by x-ray crystallography.

The chemistry was then extended by using *ortho* oxygen functionalised derivatives of benzoic acid, such as salicylic acid, *ortho*-anisic acid, and methyl salicylate. $[^iBu_4Al_2(\mu\text{-}O_2CC_6H_4\text{-}2\text{-}\mu\text{-}O)]_2$, **45**, was shown in the solid-state to be a dimeric compound with a 12-membered macrocycle containing two [O-Al-O-C-O-Al] units, where salicylic acid had reacted with two equivalents of Al^iBu_3. The reaction of *ortho*-anisic acid and TMA yielded the product $[Me_2Al(\mu\text{-}O_2CC_6H_4OMe\text{-}2)]$, **46**, which was characterised in solution by NMR spectroscopy and was found to consist of one $AlMe_2$ unit for each ligand. The solid-state structure of $[Me_2Al(mesal)]_2$, **48**, the reaction product of methyl salicylate and TMA, showed a dimeric compound with a central four-membered $[Al\text{-}O]_2$ ring and two fused six-membered rings originating from the chelation of $AlMe_2$ between the carboxyl and the phenol oxygen. All three structures demonstrated the versatility of bonding motifs originating from the additional functionality in *ortho* position to the carboxylic acid or carboxylate.

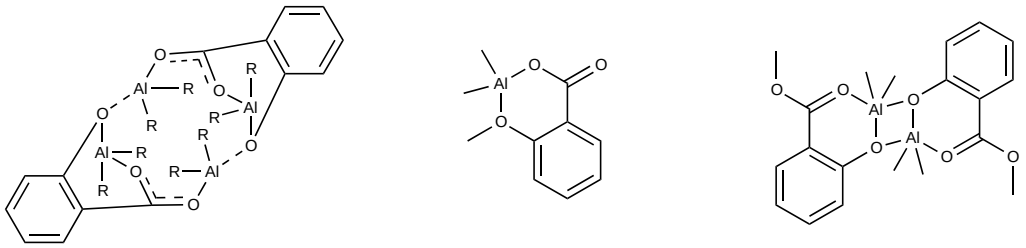

Scheme 61: Structures of the compounds **45** ($[^{i}Bu_4Al_2(\mu\text{-}O_2CC_6H_4\text{-}2\text{-}\mu\text{-}O)]_2$), **46** ($[Me_2Al(\mu\text{-}O_2CC_6H_4OMe\text{-}2)]$) and **48**. The structures for **45** and **48** are based on obtained crystal structures. The structure of **46** is proposed based on the evidence from solution NMR spectroscopy.

The use of *ortho* nitrogen functionalised derivatives of benzoic acid showed a further diversity of products and bonding motifs. In the reaction with aluminium organyls the amino group, with two acidic hydrogen atoms, yielded products of similar and also different stoichiometries, compared to salicylic acid. At first the reaction of anthranilic acid with $AlMe_3$ at -78°C to room temperature seemed to have proceeded in a simple one-to-one reaction, forming $[Me_2Al(\mu\text{-}O_2CC_6H_4NH_2\text{-}2)]$ **50**. However, after recrystallising the compound from boiling toluene the crystallographic analysis revealed the formation of a dimeric species $[(Me_2Al)_2(\mu\text{-}O_2CC_6H_4\text{-}2\text{-}\mu\text{-}NH)]_2$ **51**, in which anthranilic acid had reacted with two equivalents of $AlMe_3$. During attempts to reproduce this dismutation process, the tetrameric species $[MeAl(\mu\text{-}O_2CC_6H_4\text{-}2\text{-}\mu\text{-}NH)]_4$ **53** was isolated. It consisted of a 16-membered macrocycle, formed by four [Al-O-C-O] units. Fused with the macrocycle are six distorted six-membered rings formed by the additional coordination of the amido nitrogen to the aluminium centre. Although the crystal data for this species was of insufficient quality for a detailed discussion of bonding parameters, it gave an unambiguous idea about the composition of and bonding motifs present in this compound. Scheme 62 shows the different structures obtained during the study of the reactions of anthranilic acid with AlR_3. In compound **50** anthranilic acid and TMA had reacted one to one. In compounds **51**, **52** and **53** the reaction had occurred one to two, whereby for **53** this was achieved through anthranilic acid reacting twice with one equivalent of $AlMe_3$ and in **51** and **52** the acid reacted once with two equivalents of AlR_3.

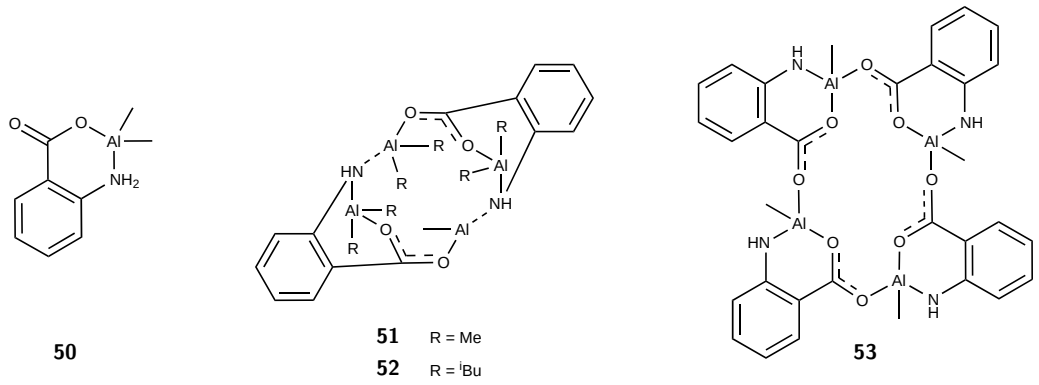

Scheme 62: Structures of the compounds **50** ($[Me_2Al(\mu\text{-}O_2CC_6H_4NH_2\text{-}2)]$), **51** ($[(Me_2Al)_2(\mu\text{-}O_2CC_6H_4\text{-}2\text{-}\mu\text{-}NH)]_2$), **52** ($[(^iBu_2Al)_2(\mu\text{-}O_2CC_6H_4\text{-}2\text{-}\mu\text{-}NH)]_2$) and **53** ($[MeAl(\mu\text{-}O_2CC_6H_4\text{-}2\text{-}\mu\text{-}NH)]_4$). The structures for **51**, **52** and **53** are based on structures obtained by x-ray crystallography. The structure of **50** is proposed based on the evidence from solution NMR spectroscopy.

In order to further understand the different bonding motifs shown in Scheme 62, derivatives of anthranilic acid were reacted with aluminium reagents. By using N-methylanthranilic acid it was possible to reproduce the bonding motifs seen with anthranilic acid: the formation of a dimeric species $[(Me_2Al)_2(\mu\text{-}O_2CC_6H_4\text{-}2\text{-}\mu\text{-}NMe)]_2$ **54** with the 12-membered central macrocycle and also the tetrameric species $[^iBuAl(\mu\text{-}O_2CC_6H_4\text{-}2\text{-}\mu\text{-}NMe)]_4$ **55** with the larger, 16-membered ring (Scheme 63). The preference for one or the other aggregate was found to be influenced by the chosen reaction stoichiometry, but the formation of the dimeric species appeared to be preferred, as attempts to reproduce the structure of **55** resulted in the isolation of **56**. The reaction of N-phenylanthranilic acid yielded exclusively the tetrameric species $[^iBuAl(\mu\text{-}O_2CC_6H_4\text{-}2\text{-}\mu\text{-}NPh)]_4$ **57**, even when an excess of Al^iBu_3 was used. The crystals obtained from this reaction were of suitable quality for X-ray analysis and support the bonding patterns observed for **53** and **55** (Scheme 63.) One conclusion drawn from these observations is that the steric demand of the amino substituent appears to influence the bonding motif of the obtained compound. In order to further investigate this assumption, the steric demand was increased by using N-(2,6-dimethylphenyl)-anthranilic acid. Although it was not possible to obtain a crystal structure for the isolated product the NMR spectroscopy suggested that the reaction had occurred in a one-to-one ratio, with one equivalent of acid reacting once with one equivalent of $AlMe_3$. The proposed structure for $[Me_2Al(\mu\text{-}O_2CC_6H_4\text{-}2\text{-}\mu\text{-}N\text{-}(C_6H_4\text{-}2,6\text{-}CH_3))]$, **60**, is shown in Scheme 63.

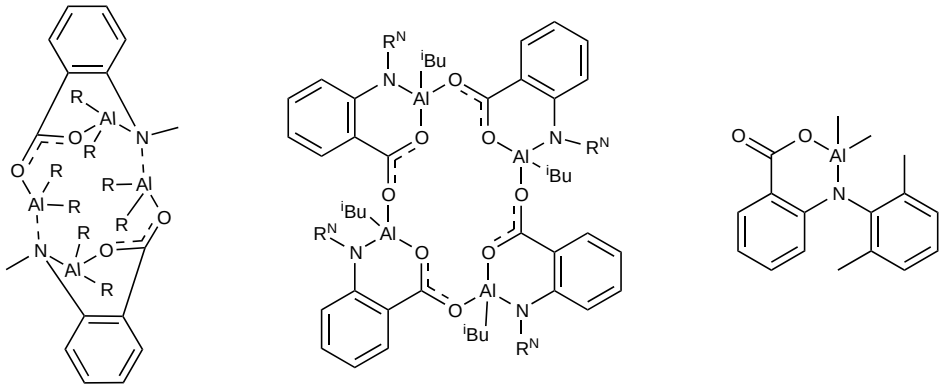

54 R = Me
56 R = ^{i}Bu

55 R^N = Me
57 R^N = Ph

60

Scheme 63: Structures of the compounds **54** ($[(Me_2Al)_2(\mu\text{-}O_2CC_6H_4\text{-}2\text{-}\mu\text{-}NMe)]_2$), **56** ($[(^{i}Bu_2Al)_2(\mu\text{-}O_2CC_6H_4\text{-}2\text{-}\mu\text{-}NMe)]_2$), **55** ($[^{i}BuAl(\mu\text{-}O_2CC_6H_4\text{-}2\text{-}\mu\text{-}NMe)]_4$), **57** ($[^{i}BuAl(\mu\text{-}O_2CC_6H_4\text{-}2\text{-}\mu\text{-}NPh)]_4$) and **60** ($[Me_2Al(\mu\text{-}O_2CC_6H_4\text{-}2\text{-}\mu\text{-}N\text{-}(C_6H_4\text{-}2,6\text{-}CH_3))]$). The structures for **54**, **56**, **55** and **57** are based on structures obtained by x-ray crystallography. The structure of **60** is proposed based on the evidence from solution NMR spectroscopy.

These results confirm that in contrast to the use of the parent acid, the use of benzoic acids with an additional donor functionality in the *ortho* position favours a 1:2 reaction with aluminium reagents of the type AlR_3, but that there are at least two ways by which this can be achieved: either by reacting once with two equivalents AlR_3 to form a dimeric species with a distorted 12-membered macrocycle consisting of two [Al-O-C-O-Al-N] units and with this two fused six-membered rings originating from the chelation of on $AlMe_2$ unit, or by reacting twice with one equivalent AlR_3, forming a tetramer with a 16-membered macrocycle consisting of four [Al-O-C-O] units and four fused six-membered rings.

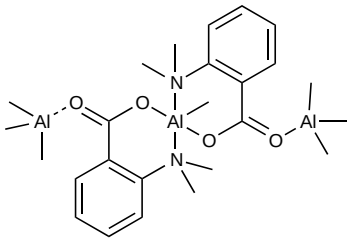

61

Scheme 64: Structure of Compound **61** ($MeAl(AlMe_3\text{-}\mu\text{-}O_2CC_6H_4\text{-}2\text{-}\mu\text{-}NMe_2)_2$) based on data obtained from x-ray crystallography.

The use of N,N-dimethylanthranilic acid resulted in a product $MeAl(AlMe_3\text{-}\mu\text{-}O_2CC_6H_4\text{-}2\text{-}\mu\text{-}NMe_2)_2$ **61** (Scheme 64), which consists of a central AlMe unit, coordinated by two ligands, which in turn are binding to one unreacted $AlMe_3$ unit each. Unfortunately,

so far it was not possible to reproduce this very interesting product, which remains a challenge for future research.

Other synthetic work included attempts to further functionalise the obtained compounds. For example, by reacting $[Me_2Al(\mu\text{-}O_2CPh)]_2$ with alcohols or additional equivalents of benzoic acid. However, despite numerous attempts with different conditions in regards to solvents, stoichiometries, temperature etc, this proved to be unsuccessful. Similarly challenging were the studies on the hydrolysis and oxidation of $[Me_2Al(\mu\text{-}O_2CPh)]_2$. The introduction of water into the system led to the formation of insoluble products that could not be analysed further. The introduction of molecular oxygen showed changes in the ^{1}H- and ^{27}Al-NMR spectrum, but the spectra did not allow a confident characterisation of the formed products.

The second part of this project looked at the application of aluminium compounds as crosslinkers for polysaccharides such as guar and CMHPG. In the beginning commercially available Al sources such as $Al(O^iPr)_3$, $Al(acac)_3$, and $Al(lac)_3$ were used for preliminary studies to gain experience that can later be applied to more complex systems. Data showed that $Al(O^iPr)_3$ can crosslink guar at an approximate pH of 13 and that $Al(lac)_3$ is suitable to crosslink CMHPG at a pH of approximately 6.

In order to determine the pH for the best crosslinking results the system of $Al(lac)_3$ and CMHPG was chosen for further rheological studies. The outcome of these studies showed that the highest viscosity was achieved for pH = 6.29. This sample and one at a lower viscosity, at pH = 6.22, were used for more in-depth studies at different temperatures. These variable temperature studies proved that the crosslinked gels are stable at higher temperatures (80°C) and show a reversible shear thinning at higher shear rates. Both properties are essential for application in hydraulic fracturing, as the temperatures in the drilling well of a hydraulic fracturing facility can easily exceed 150°C.

In oscillation experiments, the viscoelasticity of the $Al(lac)_3$ crosslinked CMHPG gel was studied. The amplitude sweep showed a very broad LVER at 25°C and 80°C and that the elastic modulus was higher than the viscous modulus, which was also seen in the frequency sweep. This is very characteristic for three dimensional crosslinked gels,

as required for hydraulic fracturing. The data further confirmed that the crosslinks within the gel remained stable when the temperature is raised.

By using $[Me_2Al(\mu\text{-}O_2CPh)]_2$ **43** and $Al[MeC(CH_2O)_3]_2(AlMe_2)_3$ **69** in preliminary tests it was possible to employ newly synthesised compounds in Al crosslinking. Although these initial experiments were undertaken without the opportunity for optimisation, the findings obtained nonetheless formed a promising starting point for further research and development of the method. It was possible to form over-crosslinked polymers of guar and CMHPG, which had a very high viscosity. The crosslinked gels degraded quickly due to the use of organic solvents, which may have caused a dehydration of the gel or other unknown side-reactions between the solvent and the functional groups in the polymer, or between the solvent and products or by-products of the crosslinking reaction.

In summary, it can be said that over the course of this project it was possible to synthesise several novel aluminium compounds that showed interesting organometallic macrocyclic motifs, which in the case of **52** was shown to be retained in solution. Furthermore, to the best of our knowledge, it has been shown for the first time that aluminium organic compounds can be employed as alkali activated crosslinkers for guar and CMHPG, opening new possibilities for the application of this Al-based system in hydraulic fracturing.

6 Future Work

Although the projects discussed in this dissertation yielded significant and promising results, both in the synthetic part as well as the rheological experiments, the outcomes also provide a base for significant further research. This can be categorised as short-term (answering specific outstanding questions and establishing the reproducibility of some observed products) and long-term (wider-reaching development and strategic advances, particularly of an applied nature) future work.

6.1 Short-Term Future Work

In the short term, it will be essential to work on the reproducibility of certain reactions as this was one of the main challenges encountered during the course of this project. Despite numerous attempts to repeat the synthesis of [$Me_2Al(\mu\text{-}O_2CC_6H_4NH_2\text{-}2)$] **50** with different solvents (toluene, dichloromethane, THF, hexane or combinations thereof) and variations in reaction time and the time for which the temperature was maintained at -78°C, it was not possible to reproduce the structure for further analysis. Compound **50** seems to be a very unstable product. Therefore, working with low temperatures and quick analysis might be one way to repeat its formation. If the isolation of suitable crystals persists to be unsuccessful another approach could be to carry out the synthesis on a much lower scale in a suitable NMR solvent, such as toluene d-8 and monitor the reaction by variable temperature NMR. However, this must be done very carefully, as there will be an evolution of methane during the reaction which may cause an undesired increase in pressure within the NMR tube. One possible way around this problem could be the use of an aluminium reagent which will release an alkane with a higher boiling point, e.g. Al^iBu_3, which will release isobutane (boiling point of -11.7°C[271]) or even to use $AlPh_3$ which would result in the release of benzene, although it would require studying if the chemistry remains comparable to those reactions of anthranilic acid with $AlMe_3$ and Al^iBu_3. The variable temperature NMR could also provide a method to study the dismutation of [$Me_2Al(\mu\text{-}O_2CC_6H_4NH_2\text{-}2)$] **50** to [$(Me_2Al)_2(\mu\text{-}O_2CC_6H_4\text{-}2\text{-}\mu\text{-}NH)]_2$ **51**.

The structure of $[MeAl(\mu\text{-}O_2CC_6H_4\text{-}2\text{-}\mu\text{-}NH)]_4$ **53**, which was encountered during the attempts to repeat the synthesis of $[Me_2Al(\mu\text{-}O_2CC_6H_4NH_2\text{-}2)]$, and the analogous structure of $[^iBuAl(\mu\text{-}O_2CC_6H_4\text{-}2\text{-}\mu\text{-}NMe)]_4$ **55** need to be confirmed. For both, the crystals were of insufficient quality and the reactions so far not reproducible. Many attempts to reproduce **55** yielded **56** instead or no identifiable products at all. Two main factors to consider are the concentration of the reaction solution and the way the aluminium is added, as it is a competition between one or two equivalents reacting. When the concentration of AlR_3 is kept low, either by working with more diluted solutions of acid and AlR_3 or by adding the aluminium reagent drop-wise, the acid might react more easily twice with one equivalent AlR_3.

One of the interesting structures encountered during the work on this thesis is $MeAl(AlMe_3\text{-}\mu\text{-}O_2CC_6H_4\text{-}2\text{-}\mu\text{-}NMe_2)_2$ **61**, which consists of a central AlMe unit co-ordinated by two ligands, which in turn are binding to one unreacted $AlMe_3$ each. The crystals were isolated from a Schlenk flask which was stored for several weeks at -27°C. Many attempts have been made to reproduce this reaction in different stoichiometries and under different conditions. In most cases, a yellow oil was formed, which up to now proved impossible to crystallise and which did not yield interpretable NMR data, as the spectra showed very broad and undistinguishable peaks. These attempts would need to be repeated with more attention to the variations in temperature and solvent. Applying different crystallisation techniques such as layering with a less polar solvent, could also be employed in order to obtain a crystalline product. Another approach could be the extension of the chemistry to different aluminium reagents, such as $AlPh_3$ or the variation of substitution patterns and introduction of electrophilic substituents on the aromatic ring of the anthranilic acid.

The immediate future work on the rheological side of this project should, on the one hand, include the extension of the rheological studies to the system of guar and $Al(O^iPr)_3$ in order to be able to evaluate and compare the rheological properties of this system with the CMHPG/$Al(lac)_3$ system. For both systems, it is vital to test different conditions for the crosslinking process in terms of concentration, pH, temperature, and pressure to build a systematic understanding of the effects of different conditions and consequently in the future mimic conditions as they would be found in hydraulic fracturing applications.

First experiments with compound **69** showed that synthetic aluminium organic compounds can be utilised as crosslinkers for Guar and CMHPG. However, their use is limited by the strong reaction between the aluminium carbon bonds and the water contained in the gel, which cannot be avoided since the polymer is only soluble in water.

6.2 Long-Term Future Work

The work discussed in Chapter 4.1.2 provides a base for more extensive research work. It would be interesting to see if reaction stoichiometries other than one-to-one are possible for the reaction of benzoic acid with AlR_3. Previous attempts were carried out with two or three equivalents of benzoic acid per equivalent of AlR_3. It was also attempted both to react one equivalent of $AlMe_3$ with one equivalent of benzoic acid in a direct reaction as well as adding one additional equivalent of benzoic acid to $[Me_2Al(\mu\text{-}O_2CPh)]_2$. So in order to determine if other stoichiometries, such as three-to-two equivalents (acid to AlR_3) similar to (**70**) or different aggregates (**71**) are possible for this reaction the conditions have to be varied in terms of concentration, solvent and temperature. Based on the structures encountered during the project and on structures known for other metal acetates, Scheme 65 shows some proposed structures for the products of these reactions.[272] [273] [274] [275] [276]

In the next step, the reactions of $[Me_2Al(\mu\text{-}O_2CPh)]_2$ **43** with other reagents such as alcohols or Lewis bases can be studied further. By reducing the number of Al-C bonds the reactivity of the compounds can be lowered which should make them more suitable for use as crosslinkers in aqueous systems. For oxophilic metals such as aluminium, alkoxide ligands can offer particular scope for stabilising the metal centre.[277] First attempts to functionalise $[Me_2Al(\mu\text{-}O_2CPh)]_2$ with alcohols have been undertaken with MeOH and ^{t}BuOH. The use of MeOH has so far led only to the formation of a white powder, which is possibly due to the formation of polyaggregated aluminium methoxide species.[278] This was not observed for ^{t}BuOH, but it was also not possible to identify reaction products, despite many attempts with variations in the solvents used (hexane, DCM, THF, ether, acetonitrile), concentration of the reactants and reaction temperature (-78°C, 0°C, and heating to reflux). The reaction

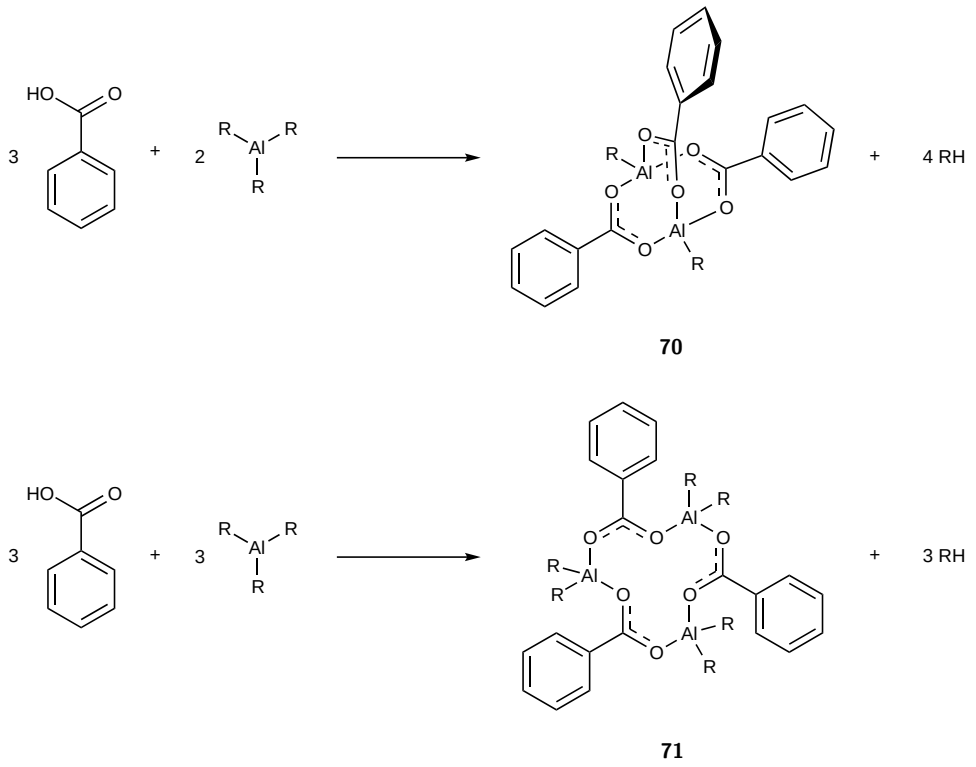

Scheme 65: Possible future work for the reactions of benzoic acid and AlR_3 based on the structures of other metal acetates. [272] [273] [274] [275] [276] [250]

of **43** and alcohols can also be varied in concentration, solvent and temperature, and if necessary followed by *in situ* NMR spectroscopy. Furthermore, a change of the alcohol in terms of steric and electronic properties could be beneficial, e.g. for zinc organooxides the use of phenol derivatives has lead to the formation of mononuclear compounds and for aliphatic alcohols it can be attempted to introduce a CF_3 group in the α-position with respect to the hydroxy group. Due to the strong electron-withdrawing character of the trifluoride group inter- and intramolecular electrostatic repulsion within and between the molecules can aid to prevent polyagggregation of the product. [278]

The functionalisation of **43** could also be achieved by the use of non-protic reagents, such as Lewis bases, e.g. amines of the type NR_3 (Scheme 66) or chelating, bidentate donors. Furthermore, for the reaction with Lewis bases the influence of hard bases, such as ethers, compared to soft bases, e.g. thioethers, on the stability of the products would be of interest for future applications in crosslinking, as the crosslinkers need to be stable in aqueous conditions. The reaction of **43** with Lewis bases would retain

the aluminium carbon bonds, but similar to the templation reaction described by Wheatley *et al.*, the Lewis bases could stabilise the Al-C bonds towards water and oxygen.[270]

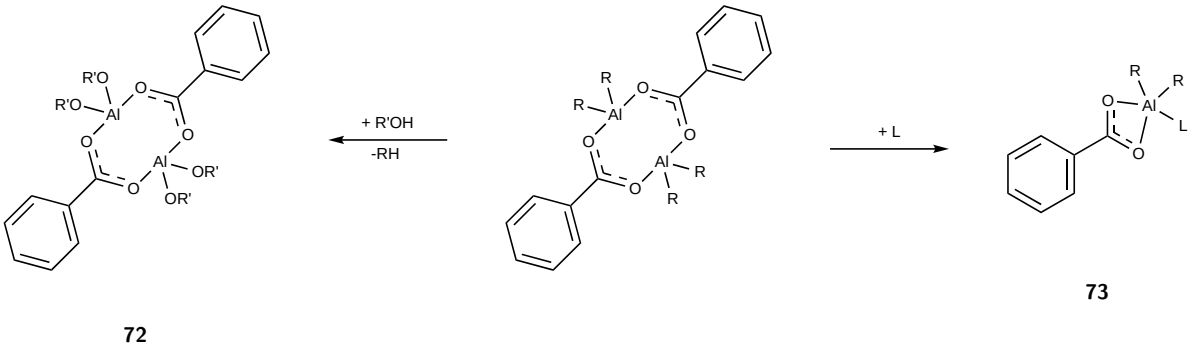

72 73

Scheme 66: Possible future work on the functionalisation of $[Me_2Al(\mu\text{-}O_2CPh)]_2$ **43**. This can either be achieved by using an alcohol R′OH or a Lewis base L. Based on the stoichiometry and structure of R′OH and L, other aggregates and structures will be possible, for example when multidentate, chelating or sterically demanding bases or alcohols are used.[279]

Initial attempts at the controlled hydrolysis and oxygenation of the synthesised aluminium compounds were carried out on **43** but did so far not yield any conclusive results. For the hydrolysis, the water has been introduced to a solution of $[Me_2Al(\mu\text{-}O_2CPh)]_2$ in toluene, with water being used in defined stoichiometries either directly or as a solution in THF, as described by Lewiński *et al.*[211] In the current work this has been unsuccessful, so other approaches should be investigated. One such approach might be the use of water-containing aluminium salts such as $Al_2(SO_4)_3 \cdot 18\ H_2O$, similar to those used in the synthesis of MAO.[43] Lewiński and co-workers also describe the use of other solvents, such as MeCN or 3-picoline for the hydrolysis of $[Cl_2Al(\mu\text{-}O_2CPh)]_2$, although the conditions would have to be adjusted for the present system.[211][280] According to the examples in the literature oxygen is usually introduced as dried molecular O_2, which can be either be bubbled through the reaction solution, as done in several attempts during the course of this project. Or, alternatively, it can be introduced by saturating the atmosphere above the solution with O_2. Both the hydrolysis and the oxygenation processes are expected to lead to the formation of bridging oxygen species, as it is reported for e.g., organozinc compounds.[281] With water, higher aggregates and cage structures can be expected to be formed.[282] The introduction of oxygen, on the other hand, should result in the insertion of oxygen into the M-C bond and the formation of smaller aggregates and possibly μ_3 or μ_4 bridging oxygen centres.[283][281]

In regard to the potential application of the Al compounds as crosslinkers in industrial processes such as hydraulic fracturing, it is of advantage if the crosslinking agents have a high aluminium content. Therefore, the synthesis of poly-aluminium compounds such as $Al[MeC(CH_2O)_3]_2(AlMe_2)_3$ **69** and the subsequent functionalisation for increased stability of the compounds towards water to make the reaction with the polymer more controllable provide the potential for further research work. A further aspect to consider is the solubility of the compounds since it was observed that guar is insoluble in aprotic organic solvents such as acetone or THF and in hydrocarbons. It would be necessary for the crosslinking that the polymer and crosslinking agent are soluble in the same or at least similar systems. It would, therefore, be desirable that future crosslinkers are water soluble, or at least water stable.

The rheological studies of the aluminium crosslinked polymers have only just been initiated, with only very preliminary data reported in this thesis. Although this is very early days, there were some promising results such as the proof that $Al(lac)_3$ can lead to temperature and shear stable crosslinks in CMHPG. Rheology should be extended to other aluminium species, especially with stable poly-aluminium compounds. When the strength of the crosslinking is dependent on the amount of aluminium present, as discussed in Section 4.2.1, it could be beneficial for a sustainable crosslinking process to use compounds that have a higher aluminium content and therefore require the use of less substance overall.

Up to now the rheological studies of crosslinker action have mainly focused on varying pH values and the stability of the crosslinked gel at higher temperatures, so for further optimisation, factors like concentration, significant variations in temperature, pressure and stability over time require investigation. The concentration of the crosslinker and the temperature of the fracturing fluid might not be uniform across the wellbore. Therefore, it is important to test the tolerance of the gel to fluctuations of these parameters. The effect of the pressure on the crosslinked gel has not been investigated at all so far, as all experiments and rheological studies have been carried out at normal pressure, However, during the fracturing process, the fluid is injected at high pressure into deep layers of rock, which might influence the crosslinking process and the behaviour of the crosslinked gel. As the fracturing fluid remains in the wellbore for a certain time, depending on the pressure of injection and the depth and length of the fractures, the stability over time has to be investigated and, depending on the

requirements of the process, adjusted if needed, for example if a delayed crosslinking or an early breaking of crosslinks is required. There might be other parameters and conditions which might be relevant for the final and technical application, which have not been considered so far, such as the effects of large scales and non-laboratory conditions, e.g. the use of waste water. These factors need to be addressed by an interdisciplinary research team that includes chemists as well as chemical and mechanical engineers.

7 Experimental Procedures

7.1 General Procedures

7.1.1 Care of Substances Hazardous to Health (COSHH)

In accordance with the health and safety regulations within the department a risk assessment was carried out for each experiment. For each substance hazards and according control and safety procedures were documented. All synthetic work was carried out using a ventilated fume cupboard. Personal protection equipment in the form of safety glasses, lab coat and gloves were used as required.

7.1.2 Air Sensitive Procedures

Due to their sensitivity towards air and moisture all organometallic reagents were handled using standard Schlenk techniques. Reaction vessels were oven dried and purged with nitrogen prior to use. Solid reagents were added prior to the first purge and were held under vacuum for at least 10 minutes before continuing the procedure. Liquid reagents were added through a dry nitrogen-purged syringe and with a positive pressure of nitrogen inside the reaction vessel. Suba seals^{TM} were used to ensure the smallest possible levels of oxygen or moisture contamination. Solid reaction products were isolated by removal of any supernatant and drying *in vacuo*.

7.1.3 Glove Box Techniques

All air sensitive solid analytical samples were handled in a glove box under a nitrogen atmosphere. To ensure an oxygen- and moisture-free environment the gas was re-circulated through four columns, one with molecular sieves (BDH 3 Å, 16") and three containing an oxygen scavenging Cu catalyst (BASF Cu catalyst R11). Items were

transferred to the glove box via an airtight port which was evacuated (30 minutes the first time, 5 minutes thereafter) and purged with nitrogen three times.

7.1.4 Reagents and Solvents

All reagents were received from Sigma Aldrich Co. Trimethylaluminium (2.0 M in toluene), triethylaluminium (1.0M in hexane), and triisobutylaluminium (1.0M in hexane) stored at 5°C. Solvents were distilled off sodium metal (hexane, toluene) or sodium wire/benzophenone (THF) under a nitrogen atmosphere and collected with a dry, nitrogen flushed syringe. Deuterated benzene was stored over sodium metal or molecular sieves. Deuterated chloroform and deuterated acetonitrile were used without further purification.

7.2 Characterisation Procedures for Synthetic Experiments

7.2.1 Single Crystal X-Ray Diffractometry

Crystals were transferred directly from the mother liquor to a microscope slide with a drop of dried perfluoropolyether oil. A stream of cold nitrogen was applied to the slide to prevent reaction or re-dissolvation of the crystals. Suitable crystals were selected and attached to the goniometer head by a MicroLoop^{TM}, which was then centred on the diffractometer. Data was collected using a Bruker D8 Quest or Nonius Kappa CCD. Data collection took place at 180 K by default, but the temperature was adjusted where it was deemed neccessary. Structures were solved by direct methods and refinement was by full-matrix least squares refinement on F^2.[245] [246] Hydrogen atom positions were calculated geometrically and refined with a riding model.

7.2.2 Nuclear Magnetic Resonance (NMR) Spectroscopy

Approximately 20 mg of sample was dissolved in a suitable deuterated solvent. Air sensitive samples were then transferred to thin walled glass Youngs tap NMR tubes (Wilmad, 528-PP), while normal samples were transferred to standard glass NMR tubes. NMR spectroscopy was carried out observing ^{1}H, ^{13}C and ^{27}Al nuclei. Chemical shifts were calculated relative to TMS for ^{1}H and ^{13}C. Chemical shifts of ^{27}Al were calculated relative to $\mathrm{Al(NO_3)_3}$ in $\mathrm{D_2O}$. Unless otherwise stated measurements were carried out at 25°C on a Bruker 500 MHz AVIII HD Smart Probe spectrometer.
All chemical shifts are given in ppm.

7.2.3 Elemental Analysis

For carbon, hydrogen and nitrogen analysis a small amount (*circa* 1 mg) of sample was weighed into a a pre-weighed alumium boat which then was sealed by using a press. Elemental analysis was carried out on a Perkin-Elmer 240 Elemental Analyser.

7.2.4 Melting Point

Single-sided open capillaries were filled with small amounts of sample. For air sensitive samples the tube was sealed by silicon grease. Melting points were determined using Griffin melting point equipment.

7.3 Synthetic Procedures

7.3.1 (Benzoyloxy)dimethylaluminium - **43** - $[Me_2Al(\mu\text{-}O_2CPh)]_2$

Benzoic acid (366 mg, 3 mmol, 1 eq) was dissolved in toluene (4 ml) and THF (1 ml) and cooled to -78°C. $AlMe_3$ (1.5 ml, 3 mmol, 1 eq) was added dropwise. The mixture was stirred for 30 minutes and was allowed to warm up to room temperature during this time. Afterwards the reaction volume was reduced to about two thirds of the original volume and the vessel was placed in the freezer. Crystals of $[Me_2Al(\mu\text{-}O_2CPh)]_2$ were obtained after 24h.

Yield: 465 mg (87%); Melting Point: 162-163°C; Elemental Analysis (calcd for $C_9H_{11}AlO_2$: C: 60.67, J: 6.29) C: 60.21, H: 6.22; NMR: ^1H (C_6D_6): δ = 7.97 [d, 2H, CH_{Ar}], 7.06 [t, 1H, CH_{Ar}], 6.91 [t, 2H, CH_{Ar}], -0.17 [s, 6H, $AlCH_3$]; ^{13}C (C_6D_6): δ = 173.0 [COO], 134.57 [CH_{Ar}], 131.14 [CH_{Ar}], 129.53 [CH_{Ar}], 128.34 [CH_{Ar}], -11.34 [$AlCH_3$]; ^{27}Al: δ = 146.1.

Table 16: Crystal data for $[Me_2Al(\mu\text{-}O_2CPh)]_2$.

Parameter	$\mathbf{[Me_2Al(\mu\text{-}O_2CPh)]_2}$
molecular formula	$C_{18}H_{22}Al_2O_4$
formula weight	356.33
temperature, K	249.99
crystal size, mm	0.150 x 0.170 x 0.270
wavelength (λ, Å)	1.54184
crystal habit	clear, colourless block
cryt. syst.	triclinic
a, Å	7.4949(3)
b, Å	8.8234(4)
c, Å	9.2974(4)
α	114.9507(16)°
β	113.2479(18)°
γ	93.575(2)°
volume, $Å^3$	492.49(5)
R_{int}	0.0297
R_1	0.0559
wR_2	0.1528
max. GoF	1.187
S	1.187
highest peak, $eÅ^{-3}$	+0.615
deepest hole, $eÅ^{-3}$	-0.268
refl. collected	6917
Absorption Correction	multi-scan

7.3.2 ((2-Hydroxybenzoyl)oxy)bis(triisobutyl)aluminium - **45** - $[^iBu_4Al_2(\mu\text{-}O_2CC_6H_4\text{-}2\text{-}\mu\text{-}O)]_2$

Salicylic acid (0.497 g, 3.6 mmol, 1 eq) was dissolved in DCM (11 ml) and cooled to -78°C. Al^iBu_3 (7.2 mL, 7.2 mmol, 2 eq) was added drop wise. The colourless solution turned to pale yellow. The solution was stirred for 90 minutes and allowed to warm to room temperature during this time. Half of the original solvent volume was removed in vacuo and the remaining solution was placed in the freezer (-27°C). After one week block-like translucent crystals of $[^iBu_4Al_2(\mu\text{-}O_2CC_6H_4\text{-}2\text{-}\mu\text{-}O)]_2$ were obtained.

Yield = 510 mg (34.13%); Melting Point: 144.7 - 146.5°C; Elemental Analysis (calcd for $C_{46}H_{80}Al_4O_6$: C: 66.01, H: 9.63) C: 65.86; H: 9.63; NMR: ^1H (C_6D_6): δ = 7.83 [dd, 1H, C*H*$_{Ar}$], 6.92 [mu, 2H, C*H*$_{Ar}$], 6.72 [dt, 2H, C*H*$_{Ar}$], 2.40 [mu, 1H, CH (^{i}Bu)], 2.12 [mu, 1H, CH (^{i}Bu)], 1.73 [mu, 1H, CH (^{i}Bu)], 1.41 [dd, 6H, CH_3 (^{i}Bu)], 1.16 [dd, 9H,

CH_3 (^{i}Bu)], 1.06 - 0.93 [dd, 9H, CH_3 (^{i}Bu)], 0.70 [d, 2H, CH_2 (^{i}Bu)], 0.65 - 0.45 [dd, 2H, CH_2 (^{i}Bu)], 0.16 [dd, 2H, CH_2 (^{i}Bu)], -0.13 [dd, 2H, CH_2 (^{i}Bu)]

Table 17: Crystal data for $[^i Bu_4Al_2(\mu\text{-}O_2CC_6H_4\text{-}2\text{-}\mu\text{-}O)]_2$.

Crystal Parameter	$\mathbf{[^iBu_4Al_2(\mu\text{-}O_2CC_6H_4\text{-}2\text{-}\mu\text{-}O)]_2}$
Molecular Formula	$C_{46}H_{80}O_6Al_4$
Formula mass (g mol-1)	837.02
Temperature (K)	180
Crystal Size (mm)	0.130 x 0.130 x 0.050
Wavelength, λÅ	1.54184
Crystal Habit	Colourless Block
Crystal System	monoclinic
a (Å)	10.5323(3)
b (Å)	16.8396(5)
c (Å)	14.7258(4)
α	78.278(7)°
β	105.179(1)°
γ	90°
Volume (rA^3)	2520.65(12)
R_{int}	0.0705
R_1	0.0943
wR_2	0.1802(4470)
Max. GoF	1.025
S	1.025
Highest Peak (eÅ^{-3})	0.745
Deepest Hole (eÅ^{-3})	-0.672
Total Reflections Number	4470
Absorption Correction	Multi-Scan

7.3.3 ((2-Methoxybenzoyl)oxy)dimethylaluminium - **46** - $[Me_2Al(\mu\text{-}O_2CC_6H_4OMe\text{-}2)]$

2-Methoxybenzoic acid (152 mg, 1 mmol, 1 eq) was dissolved in toluene (4 ml) and cooled to -78°C. $AlMe_3$ (0.5 ml, 1 mmol, 1 eq) was added dropwise. The mixture was stirred for 30 minutes and was allowed to warm up to room temperature during this time. Afterwards the reaction volume was reduced to about one third of the original volume and the vessel was placed in the freezer. A fine white precipitate of $[Me_2Al(\mu\text{-}O_2CC_6H_4OMe\text{-}2)]$ was obtained after 24h.

Yield: 170 mg (83 %); Melting Point: 109-112°C; Elemental Analysis (calcd for $C_{10}H_{13}AlO_3$: C:57.69, H: 6.29) C: 55.53, H: 6.02; NMR: ^{1}H (C_6D_6): δ = 8.07 [d, 1H,

CH_{Ar}], 7.0 [t, 1H, CH_{Ar}], 6.56 [t, 1H, CH_{Ar}], 6.28 [d, 1H, CH_{Ar}], 3.26 [s, 3H, OCH_3], -0.17 [s, 6H, AlCH_3]; ^{13}C (C_6D_6): δ = 172.91 [*C*OO], 161.29 [*C*H_{Ar}-OCH_3], 135.68 [*C*H_{Ar}], 134.10 [*C*H_{Ar}], 119.77 [*C*H_{Ar}], 118.41 [*C*H_{Ar}], 111.79 [*C*H_{Ar}], 54.64 [O*C*H_3], -11.16 [Al*C*H_3]; ^{27}Al: δ = 142.0.

7.3.4 Methyl 2-Hydroxybenzoate - [MeO-CO-C_6H_4-OH-2]

H_2SO_4 (4.0 ml, 74.63 mmol, 2 eq) was added to a solution of salicylic acid (5.0 g, 36.20 mmol, 1 eq) in MeOH (60 ml). The reaction mixture was refluxed for 20 h and allowed to cool to room temperature afterwards. It was poured into H_2O (100 ml) and extracted with DCM (120 ml). The organic layer was dried over Na_2SO_4 (anhydrous), filtered and concentrated. The crude residue was flash chromatographed on SiO_2 (5% EtOAc in hexane) to furnish 5.44 g of methyl 2-hydroxybenzoate (colourless, fragrant oil).

Yield: 5.39 g (98%); ^{1}H (C_6D_6): δ = 10.75 [s, 1H, O*H*], 7.84 [dt, 1H, CH_{Ar}], 7.45 [mu, 1H, CH_{Ar}], 6.98 [d, 1H, CH_{Ar}], 6.87 [mu, 1H, CH_{Ar}], 3.95 [s, 3H, OCH_3]

7.3.5 ((Methyl 2-hydroxybenzoyl)oxy)dimethylaluminium - **48** - $[Me_2Al(mesal)]_2$

Methyl salicylate (1.522 g, 10 mmol, 1 eq) was dissolved in toluene (10 mL). The resulting solution was cooled to -78°C, then $AlMe_3$ (5 mL, 10 mmol, 1 eq) was added drop wise. The reaction mixture was left to stir for 90 minutes, during which time it was allowed to warm to room temperature. The solvent was completely removed in vacuo to yield a white powdered solid. Hexane (10 mL), toluene (10 mL) and DCM (3 mL) were sequentially added for dissolving the product. The flask was placed in the fridge at 3°C, yielding large, colourless crystals of $[Me_2Al(mesal)]_2$ after two weeks.

Yield = 44.99%; Melting Point: 80-81°C; Elemental Analysis (calcd for $C_{10}H_{14}AlO_3$) C: 57.67, H:6.30) C: 56.93, H: 6.20; NMR ^{1}H (C_6D_6): δ = 7.46 [dd, 1H, CH_{Ar}], 7.11 [dt, 1H, CH_{Ar}], 6.98 [dd, 1H, CH_{Ar}], 6.42 [dt, 1H, CH_{Ar}], 2.94 [s, 3H, OC*3H*], -0.16 [s, 6H, AlCH_3]

Table 18: Crystal Data for $[Me_2Al(mesal)]_2$.

Parameter	$\mathbf{[Me_2Al(mesal)]_2}$
Molecular Formula	$C_{20}H_{26}O_6Al_2$
Formula mass (g mol-1)	416.37
Temperature (K)	199
Crystal Size (mm)	0.50 x 0.40 x 0.20
Wavelength, λÅ	0.71073
Crystal Habit	Colourless Block
Crystal System	Triclinic
a (Å)	7.418(2)
b (Å)	8.863(2)
c (Å)	9.317(2)
α	78.278(7)°
β	66.890(8)°
γ	70.446(8)°
Volume ($Å^3$)	529.1(2)
R_{int}	0.0402
R_1	0.0526
wR_2	0.1192(1858)
Max. GoF	1.046
S	1.046
Highest Peak ($eÅ_{-3}$)	0.290
Deepest Hole ($eÅ^{-3}$)	-0.199
Total Reflections Number	1858
Absorption Correction	Multi-Scan

7.3.6 Synthesis of ((2-aminobenzoyl)oxy)dimethylaluminium - Isolation of **50** $[Me_2Al(\mu\text{-}O_2CC_6H_4NH_2\text{-}2)]$, **51** $[(Me_2Al)_2(\mu\text{-}O_2CC_6H_4\text{-}2\text{-}\mu\text{-}NH)]_2$

2-Aminobenzoic acid (137 mg, 1 mmol, 1 eq) was dissolved in toluene (4 ml) and cooled to -78°C. $AlMe_3$ (0.5 ml, 1 mmol, 1 eq) was added dropwise. The mixture was stirred for 60 minutes and was allowed to warm up to room temperature during this time. Afterwards the reaction volume was reduced to about one third of the original volume and the vessel was placed in the freezer. A fine white precipitate of $[Me_2Al(\mu\text{-}O_2CC_6H_4NH_2\text{-}2)]$ was obtained after 24 h and characterised by NMR spectroscopy.

Yield: 120 mg (62%), Melting Point: Decomposition >180°C, NMR: ^1H (C_6D_6): δ = 7.96 [d, 1H, CH_{Ar}], 6.91 [t, 1H, CH_{Ar}], 6.37 [t, 1H, CH_{Ar}], 5.96 [d, 1H, CH_{Ar}], 4.92 [s, 2H, NH_2], -0.24 [s, 6H, $AlCH_3$]; ^{13}C (C_6D_6): δ = 173.90 [*C*OO], 152.0 [CH_{Ar}-NH_2], 136.18 [CH_{Ar}], 133.43 [CH_{Ar}], 128.84 [CH_{Ar}], 125.20 [CH_{Ar}], -11.08 [$AlCH_3$]; ^{27}Al: δ = 149.0.

The solid of the previous reaction was redissolved under heating in toluene (6 ml). The solution turned yellow. It was placed in the freezer (-27°C). After one week crystals of $[(Me_2Al)_2(\mu\text{-}O_2CC_6H_4\text{-}2\text{-}\mu\text{-}NH)]_2$were obtained.

$[(Me_2Al)_2(\mu\text{-}O_2CC_6H_4\text{-}2\text{-}\mu\text{-}NH)]_2$ was also synthesised directly: 2-aminobenzoic acid (137 mg, 1 mmol, 1 eq) was dissolved in toluene (20 ml) and cooled to -78°C. $AlMe_3$ (1 ml, 2 mmol, 2 eq) was added dropwise. The mixture was stirred for 60 minutes and was allowed to warm up to room temperature during this time. Afterwards the reaction volume was reduced to about one third of the original volume and the vessel was placed in the fridge. After two days an off-white solid was formed.

Yield: 90% (378 mg). Melting Point: Decomposition >220°C. Elemental Analysis (calcd for $C_{32}H_{36}Al_4N_4O_8$: C: 54.24 H:4.55, N: 7.91): C: 53.43, H: 4.17, N: 7.68. NMR: ^1H (C_6D_6): δ = 7.88 [dd, 1H, CH_{Ar}], 6.86 [td,1H, CH_{Ar}], 6.62 [td, 1H, CH_{Ar}], 5.98 [dd, 1H, CH_{Ar}], 2.78 [s, 1H, N*H*], -0.24 [s, 3H, $AlCH_3$], -0.25 [s, 3H, $AlCH_3$], -0.78 [s, 3H, $AlCH_3$], -0.86 [s, 3H, $AlCH_3$]. ^{13}C (C_6D_6): δ = 175.99 [*C*OO], 147.76 [C_{Ar}], 135.52 [CH_{Ar}], 132.97 [CH_{Ar}], 124.97 [CH_{Ar}], 123.55 [CH_{Ar}], 120.77 [C_{Ar}], 0.93 [$AlCH_3$]. ^{27}Al: δ= 157.0.

Table 19: Crystal data for $[(Me_2Al)_2(\mu\text{-}O_2CC_6H_4\text{-}2\text{-}\mu\text{-}NH)]_2$.

Parameter	$\mathbf{[(Me_2Al)_2(\mu\text{-}O_2CC_6H_4\text{-}2\text{-}\mu\text{-}NH)]_2}$
molecular formula	$C_9H_{12}AlNO_2$
formula weight	193.18
temperature, K	180
crystal size, mm	0.06 x 0.150 x 0.360
wavelength (λ, Å)	1.54184
crystal habit	clear, colourless block
cryt. syst.	triclinic
a, Å	8.2370(5)
b, Å	8.8853(5)
c, Å	12.5755(7)
α	102.1299(18)°
β	97.5661(18)°
γ	105.7559(17)°
volume, $Å^3$	848.42(14)
R_{int}	0.0249
R_1	0.0452
wR_2	0.1199
max. GoF	1.130
S	1.131
highest peak, $eÅ^{-3}$	+0.330
deepest hole, $eÅ^{-3}$	-0.252
refl. collected	8465
Absorption Correction	multi-scan

7.3.7 ((2-aminobenzoyl)oxy)bisdiisobutylaluminium - **52** - $[(^iBu_2Al)_2(\mu\text{-}O_2CC_6H_4\text{-}2\text{-}\mu\text{-}NH)]_2$

2-Aminobenzoic acid (0.274 g, 2 mmol, 1 eq) was dissolved in DCM (8 ml). The mixture was cooled to -78°C and Al^iBu_3 (4 ml, 4 mmol, 2 eq) was added dropwise and the resulting solution was stirred for 2h. The reaction volume was reduced to half of the original volume *in vacuo*. The yellow solution was stored at -27°C. After 48 h large colourless crystals of $[(^iBu_2Al)_2(\mu\text{-}O_2CC_6H_4\text{-}2\text{-}\mu\text{-}NH)]_2$ were obtained.

Yield: 41% (170 mg); Melting Point: Decomposition >150°C; Elemental Analysis (calcd for $C_{46}H_{84}Al_4N_2O_2$: C: 66.0, H: 10.11, N: 3.35): C: 66.08, H: 10.24, N: 3.48; NMR: ^1H (C_6D_6): δ = 8.12 [dd, 2H, CH_{Ar}], 6.91 [dt, 2H, CH_{Ar}], 6.77 [t, 2H, CH_{Ar}], 6.30 [d, 2H, CH_{Ar}], 3.09 [s, 1H, NH], 2.36 [mu, 1H, CH (^{i}Bu)], 2.04 [mu, 1H, CH (^{i}Bu)], 1.95 [mu, 1H, CH (^{i}Bu)], 1.68 [mu, 1H, CH (^{i}Bu)], 1.32 [dd, 6H, CH_3 (^{i}Bu)], 1.23 [dd, *J*=

90.14 Hz, 6H, CH_3 (^{i}Bu)], 1.07 [dd, 6H, CH_3 (^{i}Bu)], 0.91 [dd, 6H, CH_3 (^{i}Bu)], 0.60 [dd, 2H, CH_2 (^{i}Bu)], 0.50 [dd, 2H, CH_2 (^{i}Bu)], -0.09 [dd, 2H, CH_2 (^{i}Bu)], -0.11 [dd, 2H, CH_2 (^{i}Bu)]; ^{13}C (C_6D_6): δ = 175.99 [*C*OO], 147.85 [*C*H_{Ar}], 135.74 [C_{Ar}-COO], 133.11 [*C*H_{Ar}], 125.33 [*C*H_{Ar}], 123.72 [C_{Ar}-NH], 121.12 [*C*H_{Ar}], 28.44 -27.38 [*C*H_3 (^{i}Bu), *C* (^{i}Bu)], 26.47 [*C*H (^{i}Bu)], 25.93 [*C*H (^{i}Bu)], 25.69 [*C*H (^{i}Bu)], 28.44-27.38 [*C*H (^{i}Bu)], 22.35 [*C*H_2 (^{i}Bu)], 21.66 [*C*H_2 (^{i}Bu)], 21.29 [*C*H_2 (^{i}Bu)], 19.87 [*C*H_2 (^{i}Bu)]; ^{27}Al: no signal (maybe covered by probe signal).

Table 20: Crystal data for $[(^i Bu_2Al)_2(\mu\text{-}O_2CC_6H_4\text{-}2\text{-}\mu\text{-}NH)]_2$.

Parameter	$\mathbf{[(^iBu_2Al)_2(\mu\text{-}O_2CC_6H_4\text{-}2\text{-}\mu\text{-}NH)]_2}$
molecular formula	$C_{46}H_{82}Al_4N_2O_4$
formula weight	835.05
temperature, K	180
crystal size, mm	0.210 x 0.190 x 0.150
wavelength (λ, Å)	1.54184
crystal habit	clear, colourless block
cryt. syst.	triclinic
a, Å	10.0688(5)
b, Å	11.2456(5)
c, Å	12.2370(6)
α	103.993(2)°
β	100.867(2)°
γ	97.545°
volume, Å^3	1297.42(11)
R_{int}	0.0708
R_1	0.0824
wR_2	0.2086
max. GoF	1.052
S	1.052
highest peak, eÅ^{-3}	+1.632
deepest hole, eÅ^{-3}	-1.135
refl. collected	4586
Absorption Correction	multi-scan

7.3.8 Attempted synthesis of **53** - $[MeAl(\mu\text{-}O_2CC_6H_4\text{-}2\text{-}\mu\text{-}NH)]_4$

2-Aminobenzoic acid (137 mg, 1 mmol, 1 eq) was dissolved in toluene (10 ml) and cooled to -78°C. $AlMe_3$ (0.5 ml, 1 mmol, 1 eq) was added dropwise. The mixture was stirred for 60 minutes and was allowed to warm up to room temperature during this time. Afterwards the reaction volume was reduced to about one third of

the original volume and the vessel was placed in the freezer. Colourless crystals of [$Me_2Al(\mu\text{-}O_2CC_6H_4NH_2\text{-}2)$] were obtained after three weeks and crystallographically characterised. During this the sample decomposed and it was not possible to obtain any other analytical results. Many attempts to repeat this synthesis were unsuccessful. The crystallographic data is of insufficient quality for a thorough discussion of bond lengths and angles, but gives a general idea of the bonding motif.

Table 21: Crystal data for $[MeAl(\mu\text{-}O_2CC_6H_4\text{-}2\text{-}\mu\text{-}NH)]_4$.

Parameter	$\mathbf{[MeAl(\mu\text{-}O_2CC_6H_4\text{-}2\text{-}\mu\text{-}NH)]_4}$
molecular formula	$C_{46}H_{82}Al_4N_2O_4$
formula weight	835.05
temperature, K	180
crystal size, mm	0.110 x 0.086 x 0.064
wavelength (λ, Å)	1.54178
crystal habit	clear, colourless block
cryt. syst.	monoclinic
a, Å	19.392(2)
b, Å	9.7413(8)
c, Å	23.510(2)
α	90°
β	91.923°
γ	90°
volume, $Å^3$	4438.6
R_{int}	0.0495
R_1	0.1584
wR_2	0.4582
max. GoF	4.149
S	4.147
highest peak, $eÅ^{-3}$	+0.97
deepest hole, $eÅ^{-3}$	-0.93
refl. collected	7272
Absorption Correction	multi-scan

7.3.9 ((2-(Methylamino)benzoyl)oxy)bisdimethylaluminium - **54** - $[(Me_2Al)_2(\mu\text{-}O_2CC_6H_4\text{-}2\text{-}\mu\text{-}NMe)]_2$

2-(Aminomethyl)benzoic acid (0.151 g, 1 mmol, 1 eq) was dissolved in toluene (20 ml). The mixture was cooled to -78°C and $AlMe_3$ (1 ml, 2 mmol, 2 eq) was added dropwise and the resulting solution was stirred for 30 min. The batch was stored at -27°C. After 24 h a white precipitate was formed which was isolated and redissolved by brief

reflux in 20 ml toluene. Afterwards the batch was stored at 4°C. After seven days large colourless als of $[(Me_2Al)_2(\mu\text{-}O_2CC_6H_4\text{-}2\text{-}\mu\text{-}NMe)]_2$ were obtained.

Yield: 45% (240 mg). Melting Point: Decomposition >180°C. Elemental Analysis (calcd for $C_{24}H_{40}Al_4N_2O_4$ C: 54.54, H: 7.63, N: 5.30): C: 53.28, H: 7.19 N: 4.80. NMR: ^{1}H (C_6D_6) δ = 8.00 [dd, 1H, CH_{Ar}], 7.04-6.99 [mu, 2H CH_{Ar}], 6.68 [td, 1H, CH_{Ar}], 6.57-6.52 [mu, 2H, CH_{Ar}], 2.42 [s, 3H, NCH_3], -0.21 [s, 3H, AlCH_3], -0.27 [s, 3H, AlCH_3], -0.92 [s, 3H, AlCH_3], -0.97 [s, 3H, AlCH_3]; ^{27}Al δ = 160.36; ^{13}C (C_6D_6) δ = 175.27 [*C*OO], 152.63 [C_{Ar}COO], 135.82 [*C*H$_{Ar}$], 133.45 [*C*H$_{Ar}$], 123.00 [*C*H$_{Ar}$], 121.77 [C_{Ar}NMe], 120.28 [*C*H$_{Ar}$], 33.99 [N*C*H$_3$], signals for Al*C*H$_3$ not visible in noise. ^{27}Al: δ = 160.4.

Table 22: Crystal data for $[(Me_2Al)_2(\mu\text{-}O_2CC_6H_4\text{-}2\text{-}\mu\text{-}NMe)]_2$.

Parameter	$\mathbf{[(Me_2Al)_2(\mu\text{-}O_2CC_6H_4\text{-}2\text{-}\mu\text{-}NMe)]_2}$
molecular formula	$C_{24}H_{38}Al_4N_2O_4$
formula weight	526.22
temperature, K	180
crystal size, mm	0.050 x 0.070 x 0.110
wavelength (λ, Å)	1.54184
crystal habit	clear, colourless block
cryt. syst.	triclinic
space group	P-1
a, Å	7.9659(5)
b, Å	8.8926(6)
c, Å	11.3802(7)
α	104.783(3)°
β	110.349(3)°
γ	98.447(3)°
volume, Å^3	704.90(10)
R_{int}	0.0430
R_1	0.0554
wR_2	0.1254
max. GoF	1.025
S	1.025
highest peak, eÅ^{-3}	+0.504
deepest hole, eÅ^{-3}	-0.211
refl. collected	7022
Absorption Correction	multi-scan

7.3.10 ((2-(Methylamino)benzoyl)oxy)isobutylaluminium - **55** - $[^{i}BuAl(\mu\text{-}O_2CC_6H_4\text{-}2\text{-}\mu\text{-}NMe)]_4$

2-(Aminomethyl)benzoic acid (0.151 g, 1 mmol, 1 eq) was dissolved in DCM (5 ml). The mixture was cooled to -78°C and $Al^{i}Bu_3$ (1 ml, 1 mmol, 1 eq) was added dropwise and the resulting solution was stirred for 30 min while warming up to room temperature. The batch was stored at -27°C. After one month colourless crystals of $[^{i}BuAl(\mu\text{-}O_2CC_6H_4\text{-}2\text{-}\mu\text{-}NMe)]_4$ were obtained and crystallographically characterised. During this, the sample decomposed and it was not possible to obtain any other analytical results. Many attempts to repeat this synthesis were unsuccessful. The crystallographic date is of insufficient quality for a thorough discussion of bond lengths and angles, but gives a general idea of the bonding motif.

Yield: 36% (360 mg)

Table 23: Crystal data for $[^{i}BuAl(\mu\text{-}O_2CC_6H_4\text{-}2\text{-}\mu\text{-}NMe)]_4$.

Parameter	$\mathbf{[^{i}BuAl(\mu\text{-}O_2CC_6H_4\text{-}2\text{-}\mu\text{-}NMe)]_4}$
molecular formula	$C_{48}H_{68}Al_4N_4O_8$
formula weight	936.432
temperature, K	180
crystal size, mm	0.140 x 0.120 x 0.070
wavelength (λ, Å)	0.71073
crystal habit	clear, colourless block
cryt. syst.	triclinic
space group	P-1
a, Å	11.7132(4)
b, Å	12.3597(5)
c, Å	17.9135(9)
α	94.067(2)°
β	95.321(2)°
γ	103.1330(10)°
volume, $Å^3$	2503.31(18)
R_{int}	0.0427
R_1	0.1496
wR_2	0.3130
max. GoF	1.959
S	1.025
highest peak, $eÅ^{-3}$	+0.65
deepest hole, $eÅ^{-3}$	-0.38
refl. collected	16080
Absorption Correction	multi-scan

7.3.11 ((2-(Methylamino)benzoyl)oxy)bisdiisobutylylaluminium - **56** - $[(^{i}Bu_2Al)_2(\mu\text{-}O_2CC_6H_4\text{-}2\text{-}\mu\text{-}NMe)]_2$

2-(Aminomethyl)benzoic acid (0.151 g, 1 mmol, 1 eq) was dissolved in DCM (5 ml). The mixture was cooled to -78°C and $Al^{i}Bu_3$ (1 ml, 1 mmol, 1 eq) was added dropwise and the resulting solution was stirred for 30 min while warming up to room temperature. The batch was stored at -27°C. After one day very small colourless crystals were formed and analysed by NMR spectroscopy. The spectra showed that $[(^{i}Bu_2Al)_2(\mu\text{-}O_2CC_6H_4\text{-}2\text{-}\mu\text{-}NMe)]_2$ was formed.

Yield: 45%; Melting Point: 135°C; NMR: ^{1}H (C_6D_6): δ = 8.22 [dd, 1H, CH_{Ar}], 7.07 [ddd, 1H, CH_{Ar}], 6.47 [ddd, 1H, CH_{Ar}], 6.24 [dd, 1H, CH_{Ar}], 2.40 [bs, 3H, NCH_3], 2.15 [dt, 2H, CH_2], 1.18 [d, 12H, CH_3], 0.47 [d, 1H, CH_2]; ^{13}C (C_6D_6): δ = 174.73 [*C*OO], 153.11[C_{Ar}COO], 137.06 [*C*H_{Ar}], 134.20 [*C*H_{Ar}], 115.34 [*C*H_{Ar}], 111.51[*C*H_{Ar}], 109.38 [*C*H_{Ar}NMe], 70.60 [N*C*H_3], 27.98 [*C*H_3 (^{i}Bu)], 26.06 [*C*H (^{i}Bu)], 21.26 [*C*H_2 (^{i}Bu)]; ^{27}Al: δ = 150.96 ppm.

7.3.12 ((2-(Phenylamino)benzoyl)oxy)bisdimethylaluminium - **57** - $[^{i}BuAl(\mu\text{-}O_2CC_6H_4\text{-}2\text{-}\mu\text{-}NPh)]_4$

2-Aminophenylbenzoic acid (0.426 g, 2 mmol, 1 eq) was dissolved in DCM (10 ml). The mixture was cooled to -78°C and $Al^{i}Bu_3$ (4 ml, 4 mmol, 2 eq) was added dropwise and the resulting solution was stirred for 30 min. The reaction volum was reduced to one third of the original volume. Afterwards the batch was stored at -27°C. After 28 days large colourless crystals of $[^{i}BuAl(\mu\text{-}O_2CC_6H_4\text{-}2\text{-}\mu\text{-}NPh)]_4$ (290 mg, 0.98 mmol, 49%) were obtained.

Yield: 49%; Melting Point: 148°C; Elemental Analysis: (calcd for $C_{68}H_{76}Al_4N_4O_8$: C: 68.91, H: 6.46, N: 4.73) found: C: 68.40, H: 6.33, N: 4.72; NMR: ^{1}H (C_6D_6): δ = 8.35 [dd, 1H, CH_{Ar}], 7.09 [bs, 3H, $CH_{Ar'}$], 6.98 [t, 2H, $CH_{Ar,Ar'}$], 6.89 [t, 1H, $CH_{Ar'}$], 6.70 [d, 1H, $CH_{Ar'}$], 6.50 [t, 1H, CH_{Ar}], 1.55 [m, 1H, CH (^{i}Bu)], 0.89 [d, 3H, CH_3 (^{i}Bu)], 0.82[d, 3H, CH_3 (^{i}Bu)], 0.00 [dd, 1H, CH_2 (^{i}Bu)], -0.17 [dd, 1H, CH_2 (^{i}Bu)]; ^{13}C (C_6D_6): δ= 176.66 [*C*OO], 158.97 [$C_{Ar'}$], 144.93 [*C*H_{Ar}], 137.42 [*C*H_{Ar}], 130.07 [*C*H_{Ar}], 129.79

[$CH_{Ar'}$], 126.90 [$CH_{Ar'}$], 125.28 [CH_{Ar}], 117.64 [CH_{Ar}], 116.08 [CH_{Ar}], 110.01 [C_{Ar}], 27.79 [CH_3 (^{i}Bu)], 27.07 [CH_3 (^{i}Bu)], 24.99 [CH (^{i}Bu)], 16.19 [CH_2 (^{i}Bu)]; ^{27}Al: no signal (may be covered by probe signal or noise).

Table 24: Crystal data for [^{i}BuAl(μ-$O_2CC_6H_4$-2-μ-NPh)]$_4$.

Parameter	**[^{i}BuAl(μ-$O_2CC_6H_4$-2-μ-NPh)]$_4$**
molecular formula	$C_{68}H_{76}Al_4N_4O_8$
formula weight	1184.49
temperature, K	180
crystal size, mm	0.210 x 0.210 x 0.160
wavelength (λ, Å)	0.71073
crystal habit	clear, colourless block
cryt. syst.	tetragonal
space group	P-42_1c
a, Å	13.87630(10)
b, Å	13.87630(10)
c, Å	17.8443(3)
α	90°
β	90°
γ	90°
volume, Å^3	3435.95(8)
R_{int}	0.0525
R_1	0.0592
wR_2	0.1543
max. GoF	1.151
S	1.025
highest peak, eÅ^{-3}	+0.51
deepest hole, eÅ^{-3}	-0.46
refl. collected	27512
Absorption Correction	multi-scan

7.3.13 (2-((2,6-dimethylphenyl)amino)benzoyl)(dimethyl)aluminium - **60** - [Me_2Al(μ-$O_2CC_6H_4$-2-μ-N-(C_6H_4-2,6-CH_3))]

2-chlorobenzoic acid (2 g, 12.8 mmol, 1 eq), K_2CO_3 (1.77 g, 12.8 mmol, 1 eq), Cu_2O (0.07 g, 0.51 mmol, 0.04 eq) and Cu powder (0.07 g, 1.152 mmol, 0.09 eq) are placed under a nitrogen atmosphere. 2-Ethoxyethanol (4.5 ml) and 2,6-dimethylaniline (1.88 ml, 15.3 mmol, 1.2 eq) are added and the mixture is heated at reflux. After 24 h the reaction is cooled to room temperature and 40 ml cold water are added. The resulting suspension is filtered over celite. Upon acidification with hydrochloric acid (3 mol·l^{-1}) the crude product precipitated. It was filtered off and dissolved in

amminium carbonate solution (5%, 50 ml) and filtered over celite again. The purified product was precipitated by acidification (3 mol·l^{-1}). The filtered product was dried at 80°C to yield 2-((2,6-dimethylphenyl)amino)benzoic acid (1.18 g, 4.8 mmol, 38%).

Yield: 38% (1.18 g). NMR: ^{1}H (CD_3Cl): δ= 11.91 [s, 1H, COO*H*], 8.92 [s, 1H, C$H_{Ar'}$], 8.07 [dd, 1H, CH_{Ar}], 7.31-7.25 [s, 1H, N*H*], 7.18 ([m, 3H, C$H_{Ar'}$, underlying solvent peak], 6.69 [ddd, 1H, CH_{Ar}], 6.25 [dd, 1H, CH_{Ar}]), 2.25 [s, 6H, CH_3].

2-((2,6-dimethylphenyl)amino)benzoic acid (241 mg, 1 mmol, 1 eq) was dissolved in DCM (3 ml) and cooled to -78°C. $AlMe_3$ (0.5 ml, 1 mmol, 1 eq) was added dropwise and the resulting mixture stirred for 30 min while warming up to room temperature. The vessel was placed in the freezer. After 48 h a white precipitate was formed which was analysed via NMR spectroscopy.

Yield: 40% (120 mg). NMR: ^{1}H (C_6D_6): δ= 8.56 [s, 1H, C$H_{Ar'}$], 8.13 [dd, 1H, CH_{Ar}], 7.00-6.91 [mu, 3H, C$H_{Ar'}$, underlying solvent peak], 6.86 [s, 1H, CH_{Ar}], 6.41 [ddd, 1H, CH_{Ar}], 6.18 [dd, 1H, CH_{Ar}], 2.06 [s, 6H, CH_3], 0.29 [s, 2H, impurity], -0.24 [s, 6H, AlCH_3]; ^{13}C (C_6D_6): δ = 174.32 [*C*OOH], 151.45 [*C*H$_{Ar}$], 137.18, 136.36, 136.16, 134.33, 128.76, 127.16, 116.82, 113.33, 109.80, 17.81, -10.94. ^{27}Al: δ= 143.11 ppm.

7.3.14 Bis((2-(dimethylamino)benzoyl)oxy)(methyl)aluminum - **61** - $MeAl(AlMe_3\text{-}\mu\text{-}O_2CC_6H_4\text{-}2\text{-}\mu\text{-}NMe_2)_2$

2-(N,N-dimethylamino)benzoic acid (165 mg, 1 mmol, 1 eq) is dissolved in toluene (20 ml) and cooled to -78°C. $AlMe_3$ (1 ml, 2 mmol, 2 eq) was added. The mixture was stirred for 30 min and warmed to room temperature. The reaction volume was reduced to one third of the original volume and the reaction was stored at -27°C. After four months colourless crystals of $MeAl(AlMe_3\text{-}\mu\text{-}O_2CC_6H_4\text{-}2\text{-}\mu\text{-}NMe_2)_2$ were obtained.

Yield: 17% (90 mg)

Table 25: Crystal data for $MeAl(AlMe_3\text{-}\mu\text{-}O_2CC_6H_4\text{-}2\text{-}\mu\text{-}NMe_2)_2$.

Parameter	**$MeAl(AlMe_3\text{-}\mu\text{-}O_2CC_6H_4\text{-}2\text{-}\mu\text{-}NMe_2)_2$**
molecular formula	$C_{25}H_{41}Al_3N_2O_4$
formula weight	514.54
temperature, K	180
crystal size, mm	0.220 x 0.140 x 0.120
wavelength (λ, Å)	0.71073
crystal habit	clear, colourless block
cryt. syst.	monoclinic
space group	C2/c
a, Å	20.0425(6)
b, Å	10.8380(4)
c, Å	15.2949(5)
α	90°
β	113.021(2)°
γ	90°
volume, $Å^3$	3057.78(18)
R_{int}	0.0498
R_1	0.0858
wR_2	0.1295
max. GoF	1.097
S	1.097
highest peak, $eÅ^{-3}$	+0.41
deepest hole, $eÅ^{-3}$	-0.22
refl. collected	11385
Absorption Correction	multi-scan

7.3.15 Attempted sythesis of **64** $MeAl(\mu\text{-}O_2CPh)(C_9H_6N\text{-}8O)]_x$ and isolation of **65** $Al(C_9H_6N\text{-}8O)_3$

$[Me_2Al(\mu\text{-}O_2CPh)]_2$ (177 mg, 1 mmol, 1 eq) was dissolved in DCM (3 ml) and cooled to -78Â°C. 8-Hydroxyquinoline (145 mg, 1 mmol, 1 eq) was dissolved in DCM (2 ml) and added dropwise to the solution of $[Me_2Al(\mu\text{-}O_2CPh)]_2$. A gas evolution was observed. After the effervescence had stopped the reaction volume was reduced to approximately 2.5 ml and the reaction was placed in the freezer. After 1 week yellow crystals were obtained (78 mg). Crystallographic analysis revealed the structure to be $Al(C_9H_6N\text{-}8O)_3 \cdot 2\ CH_2Cl_2$.

Yield: 17% (78 mg). The NMR data showed the presence of more than one compound and is discussed in Chapter 4.1.2. Melting point or elemental analysis were not obtained.

Table 26: Crystal data for $Al(C_9H_6N\text{-}8O)_3 \cdot 2\ CH_2Cl_2$.

Parameter	**$Al(C_9H_6N\text{-}8O)_3 \cdot 2\ CH_2Cl_2$**
molecular formula	$C_{29}H_{22}Al_{N3}O_3Cl_4$
formula weight	629.27
temperature, K	180
crystal size, mm	0.280 x 0.160 x 0.120
wavelength (λ, Å)	0.71073
crystal habit	clear, colourless block
cryt. syst.	triclinic
space group	P-1
a, Å	10.4527(3)
b, Å	10.8894(4)
c, Å	12.7047(6)
α	101.2290(10)°
β	93.3950(10)°
γ	94.819(3)°
volume, $Å^3$	1409.17(9)
R_{int}	0.0475
R_1	0.0820
wR_2	0.1148
max. GoF	1.037
S	1.037
highest peak, $eÅ^{-3}$	+0.49
deepest hole, $eÅ^{-3}$	-0.64
refl. collected	16393
Absorption Correction	multi-scan

7.4 Rheology

7.4.1 Preparation of Polymers

In order to prepare the polymers guar or CMHPG (800 mg) were mixed with H_2O (199.2 g) and hydrated in a blender for 15 min. The obtained polymer solution was stored at room temperature for up to 5 days in a SIMAX® bottle before it showed visible signs of degradation (grey precipitate started to form).

7.4.2 Crosslinking with Aluminium Compounds

For the crosslinking experiments the aluminium compound to be tested was added to the polymer solution obtained from the procedure in Chapter 7.4.1 and the mixture stirred thoroughly.

The initial pH was measured. Afterwards NaOH (c=1 mol$\cdot$ l^{-1}) was added in 1 ml and 5 ml volumes for guar and in 0.05 ml and 1 ml volumes for CMHPG. After each addition the pH was recorded. The viscosity was judged by the haptic feel of the solution. At first an increase in viscosity was observed when the pH was raised followed by a decrease when the pH was too high.

Crosslinking of Guar with $Al(O^iPr)_3$

Gelling point was reached for m($Al(O^iPr)_3$)= 503 mg (pH 12.97-13.10), for a higher pH the polymer lost its gel like characteristics. For m($Al(O^iPr)_3$)= 402 mg a maximum was reached for pH 12.92 and 12.96, but a gelling point was not observed. For the other experiments with m($Al(O^iPr)_3$)$\leq$ 299 mg no clear maximum was observed.

Table 27: Crosslinking of Guar with $Al(O^iPr)_3$ as a function of the pH.

	m($Al(O^iPr)_3$) [mg]					
	106	**208**	**299**	**402**	**510**	**620**
V(NaOH) [ml]	pH					
0	8.60	8.65	8.83	8.70	8.82	8.92
1	11.82	11.62	11.30	11.06	11.13	11.15
2	12.51	12.41	12.16	11.69	11.52	11.50
3	12.73	12.66	12.48	12.36	12.05	11.80
4	12.86	12.79	12.66	12.57	12.47	12.05
5	12.92	12.87	12.78	12.71	12.64	12.47
6	12.99	12.95	12.87	12.81	12.73	12.63
7	13.05	13.01	12.92	12.87	12.82	12.74
8	13.09	13.05	12.98	12.92	12.93	12.81
9	13.12	13.08	13.07	12.96	12.96	12.92
10	13.16	13.12	13.11	13.01	12.97	12.95
11	13.18	13.14	13.13	13.04	13.05	12.99
12	13.19	13.15	13.15	13.07	13.10	13.03
13	13.20	13.17	13.16	13.08	13.12	13.06
14	13.24	13.18	13.18	13.10	13.13	13.10
15	13.25	13.20	13.19	13.12	13.14	13.13
20	13.28	13.26	13.22	13.16	13.17	13.16
25	13.30	13.29	13.25	13.19	13.20	13.19

Table 28: Crosslinking of Guar with $Al(O^iPr)_3$.

	m($Al(O^iPr)_3$) [mg]					
Values	**106**	**208**	**299**	**402**	**510**	**620**
n[$Al(O^iPr)_3$] /mmol	0.520	1.020	1.466	1.971	2.500	3.039
n[Al] /mmol	0.520	1.020	1.466	1.971	2.500	3.039
m[Al] /mg	14.029	27.529	39.574	53.206	67.500	82.059
m[Polymer] /g	20.03	20.52	22.78	20.02	19.96	20.96
m[Guar] /g	0.080	0.082	0.091	0.080	0.080	0.084
m[Al]/m[Guar]	0.17	0.33	0.43	0.66	0.84	0.97
m[Al]/m[Polymer]	0.0007	0.0013	0.0017	0.0027	0.0034	0.0039

Crosslinking of Guar with Al(acac)$_3$

No gelling point was observed for the experiments with Al(acac)$_3$. A slight increase and decrease was noticed when the pH was raised, but no defined maximum.

Table 29: Crosslinking of Guar with Al(acac)$_3$ as a function of the pH.

	m(Al(acac)$_3$) [mg]						
	105	**206**	**308**	**409**	**509**	**751**	**1200**
V(NaOH) [ml]	pH						
0	7.87	7.93	7.92	8.01	7.61	7.57	8.82
1	10.42	10.22	10.25	10.21	10.18	10.17	11.13
2	12.21	10.66	10.50	10.52	10.46	10.46	11.52
3	12.59	12.24	12.12	10.69	10.66	10.64	12.05
4	12.70	12.50	12.30	10.84	10.77	10.74	12.47
5	12.80	12.65	12.48	11.10	10.90	10.84	12.64
6	12.86	12.75	12.62	12.32	11.08	10.92	12.73
7	12.91	12.83	12.70	12.55	12.23	10.97	12.82
8	12.96	12.86	12.76	12.67	12.47	11.05	12.93
9	13.00	12.89	12.81	12.75	12.61	11.20	12.96
10	13.03	12.92	12.85	12.82	12.70	12.23	12.97
11	13.05	12.95	12.89	12.87	12.77	12.48	13.05
12	13.08	12.98	12.91	12.91	12.82	12.62	13.10
13	13.10	13.00	12.94	12.94	12.86	12.70	13.12
14	13.12	13.01	12.96	12.95	12.89	12.77	13.13
15	13.15	13.02	12.98	12.98	12.92	12.82	13.14
20	13.19	13.06	13.03	13.05	12.98	12.98	13.17
25	13.21	13.08	13.08	13.08	13.02	13.06	13.20

Table 30: Values for the crosslinking with Al(acac)$_3$.

	mg Al(acac)3						
Values	**105**	**206**	**308**	**409**	**509**	**751**	**1200**
n[Al(acac)3] /mmol	0.324	0.636	0.951	1.262	1.571	2.318	3.704
n[Al] /mmol	0.324	0.636	0.951	1.262	1.571	2.318	3.704
m[Al] /mg	8.750	17.167	25.667	34.083	42.417	62.583	100.000
m[Polymer] /g	19.95	20.38	20.98	20.75	20.57	20.25	22.57
m[Guar] /g	0.080	0.082	0.084	0.083	0.083	0.081	0.091
m[Al]/m[Guar]	0.11	0.21	0.30	0.41	0.51	0.77	1.10
m[Al]/m[Polymer]	0.0004	0.0008	0.0012	0.0016	0.0021	0.0031	0.0044

Crosslinking of CMHPG with Al(lac)$_3$

CMHPG was crosslinked by using alumium lactate. The initial pH was lower and the amounts of crosslinker needed were significantly lower. A gelling point was reached for m(Al(lac)$_3$)= 10 mg (pH 6.18), m(Al(lac)$_3$)= 27 mg (pH 6.10) and m(Al(lac)$_3$)= 55 mg (pH 6.61). The volumes of NaOH needed were smaller. Additional increase of NaOH after the gelling point was reached lead to a decrease in viscosity.

Table 31: Crosslinking of CMHPG with Al(lac)$_3$ as a function of the pH.

	m(Al(lac)$_3$) [mg]				
	0	**10**	**27**	**55**	**150**
V(NaOH) [ml]			pH		
0	6.08	4.94	4.57	4.41	4.09
0.05	10.24	5.35			
0.1		6.18	5.52	4.70	4.30
0.15			6.10		
0.2		8.81		5.27	4.58
0.25			8.62		
0.3				5.89	4.91
0.35					
0.4				6.61	5.52
0.45					
0.5				8.94	6.20
0.55					
0.6					6.90

Table 32: Add caption

	mg Al(lac)3				
Values:	**0**	**10**	**27**	**55**	**150**
n[Al(lac)3] /mmol	0.000	0.034	0.092	0.187	0.510
n[Al] /mmol	0.000	0.034	0.092	0.187	0.510
m[Al] /mg	0.000	0.918	2.480	5.051	13.776
m[Polymer] /g	20.03	20.46	19.91	19.67	19.96
m[CMHPG] /g	0.080	0.082	0.080	0.079	0.080
m[Al]/m[CMHPG]	0.00	0.01	0.03	0.06	0.17
m[Al]/m[Polymer]	0.00	$4.49 \cdot 10^{-0.5}$	$1.25 \cdot 10^{-0.4}$	$2.57 \cdot 10^{-0.4}$	$6.90 \cdot 10^{-0.4}$

7.4.3 Rheology Measurements

The rheology of the gels was measured with a Kinexus Pro rheometer using cup and bob geometry model C25DIN. The temperature of the sample was maintained at 25 ±0.1°C and a Peltier stage was used for temperature control. The viscosity of each sample was measured at constant shear rates at set value of 1, 10 and 100 s^{-1}. For the long viscosity measurements the shear rate was raised from 0.1 s^{-1} to 200 s^{-1} and lowered to 0.1 s^{-1} again. The temperature was maintained at 25 ±0.1°C and 80 ±0.1°C. For the oscillation sweep the shear strain was increased from 0.1% to 100%, at 25 ±0.1°C and 80 ±0.1°C with an oscillation frequency of 1 Hz. For the amplitude sweep the shear strain was set to 3% and the oscillation frequency lowered gradually from 100 Hz to 0.1 Hz, both at 25 ±0.1°C and 80 ±0.1°C. The gel was prepared according to the procedure in 7.4.1, with 2.02 g CMHPG in 498.90 g water (w= 0.4%). 250.60 g of this gel were mixed with 673 mg $Al(lac)_3$ and individual fractions of approx. 20 g set to different pH values by the addition of NaOH (1 M). The rheological data were obtained and processed with the rSpace software. The pH of the gel was monitored and recorded before and after the rheology measurement to verify that the system was at equilibrium.

8 References

[1] Gordalla, B. C.; Ewers, U.; Frimmel, F. H. *Environmental Earth Sciences* **2013**, *70*, 3875–3893.

[2] Long, N. J. *Angewandte Chemie International Edition in English* **1995**, *34*, 21–38.

[3] Malik, M. A.; Afzaal, M.; 'O Brien, P. *Chemisry Reviews* **2010**, *110*, 4417–4446.

[4] Malpass, D. B.; Band, E. I. In *Introduction to Industrial Polypropylene: Properties, Catalysts Processes*; John Wiley & Sons: Hoboken, NJ, USA, 2012; Chapter 3, pp 59–74.

[5] Torborg, C.; Beller, M. *Advanced Synthesis and Catalysis* **2009**, *351*, 3027–3043.

[6] Janiak, C.; Meyer, H. J.; Gudat, D.; Alsfasser, R. *Riedel - Moderne Anorganische Chemie*, 4th ed.; De Gruyter: Göttingen, 2012.

[7] Crabtree, R. H. *The Organometallic Chemistry of the Transition Metals*, 2005; Vol. 18.

[8] Wei, Y.; Wang, S.; Zhou, S. *Dalton Transactions* **2016**, *45*, 4471–4485.

[9] Abel, E. W.; Wilkinson, G.; Stone, G. In *Comprehensive organometallic Chemistry II: A review of the literature 1982-1994*, 1st ed.; Pergamon: New York, 1995.

[10] Sitzmann, H.; Lappert, M. F.; Dohmeier, C.; Schnöckel, H. *Journal of Organometallic Chemistry* **1998**, *561*, 203–208.

[11] Minasian, S. G.; Arnold, J. *Chemical Communications* **2008**, 4043–4045.

[12] Hudson, R. L.; Roberts, B. P. *J. Chem. Soc., Chem. Commun.* **1986**, 1194–1195.

[13] Young, J. D.; Khan, M. A.; Wehmschulte, R. J. *Organometallics* **2004**, *23*, 1965–1967.

[14] Linti, G.; Schnöckel, H. *Coordination Chemistry Reviews* **2000**, *206207*, 285–319.

[15] Atwood, J. L.; Butz, K. W.; Gardiner, M. G.; Jones, C.; Koutsantonis, G. A.; Raston, C. L.; Robinson, K. D. *Ignore. Chem.* **1993**, *32*, 3482–3487.

[16] Gardiner, M. G.; Raston, C. L. *Coordination Chemistry Reviews* **1997**, *166*, 1–34.

[17] Fischbach, A.; Herdtweck, E.; Anwander, R.; Eickerling, G.; Scherer, W. *Organometallics* **2003**, *22*, 499–509.

[18] Saboungi, M.-L.; Howet, M. A.; Price, D. L. *Molecular Physics* **1993**, *79*, 847–858.

[19] Palmer, K. J.; Elliott, N. *Journal of the American Chemical Society* **1938**, *60*, 1852–1857.

[20] Ketelaar, J. A. A.; MacGillavry, C. H.; Renes, P. A. *Recueil des Travaux Chimiques des Pays-Bas* **1947**, *66*, 501–512.

[21] Hollemann; Wiberg *Lehrbuch der Anorganischen Chemie*, 102nd ed.; Walter de Gruyter: Berlin, 2008.

[22] Mcgrady, G. S.; Turner, J. F. C.; Ibberson, R. M.; Prager, M. *Organometallics* **2000**, *19*, 4398–4401.

[23] Malone, J. F.; Mcdonald, W. S. *Chemical Communications* **1967**, *270*, 444–445.

[24] Smith, M. B. *Journal of Organometallic Chemistry* **1970**, *22*, 273–281.

[25] Lewiński, J.; Wheatley, A. E. H. In *Topics in Organometallic Chemistry*; Springer: Berlin, Heidelberg, 2013; Chapter 41, pp 1–58.

[26] Robinson, G. H.; Sangokoya, S. A. *Journal of the American Chemical Society* **1988**, *110*, 1494–1497.

[27] A. Papoian, G.; Hoffmann, R. *Angewandte Chemie International Edition* **2000**, *39*, 2408–2448.

[28] Munzarová, M. L.; Hoffmann, R. *Journal of the American Chemical Society* **2002**, *124*, 4784–4795.

[29] Ziegler, K.; Gellert, H. â.; Martin, H.; Nagel, K.; Schneider, J. *Justus Liebigs Annalen der Chemie* **1954**, *589*, 91–121.

[30] Ziegler, K.; Koster, R.; Lehmkuhl, H.; Reinert, K. *Liebigs Annalen der Chemie* **1960**, *629*, 33–49.

[31] Ziegler, K.; Holzkamp, E.; Breil, H.; Martin, H. *Angew. Chem.* **1955**, *67*, 426.

[32] Parvez, M. A.; Rahaman, M.; Suleiman, M. A.; Soares, J. B. P.; Hussein, I. A. *International Journal of Polymer Science* **2014**, 1–10.

[33] Bawn, C. E. H. *Biographical Memoirs of Fellows of the Royal Society* **1975**, *21*, 569–584.

[34] Behr, A. In *Ullmann's Encyclopedia of industrial Chemistry*; Wiley VCH Verlag GmbH & Co. KGaA: Weinheim, 2005; Chapter Ziegler Pr.

[35] Ziegler, K.; Holzkamp, E.; Breil, H.; Martin, H. *Angewandte Chemie* **1955**, *67*, 541–547.

[36] Noweck, K.; Grafahrend, W. In *Ullmann's Encyclopedia of Industrial Chemistry*; Wiley-VCH Verlag GmbH & Co. KGaA: Weinheim, Germany, 2006; Chapter Fatty Alco, pp 117–141.

[37] Washecheck, P. H. In *ACS Symposium Series*, 1981; Chapter 159, pp 87–100.

[38] Fischer, K.; Jonas, K.; Misbach, P.; Stabba, R.; Wilke, G. *Angewandte Chemie (International ed. in English)* **1973**, *12*, 943–1026.

[39] Ziegler, K.; Gellert, H.-G.; Zosel, K.; Holzkamp, E.; Schneider, J.; Söll, M.; Kroll, W.-R. *Justus Liebigs Annalen der Chemie* **1960**, *629*, 121–166.

[40] Cossee, P. *JOURNAL OF CATALYSIS* **1964**, *3*, 80–88.

[41] Arlman, J.; Cossee, P. *JOURNAL OF CATALYSIS* **1964**, *3*, 99–104.

[42] Arlman, E. J. *Journal of Catalysis* **1964**, *3*, 89–98.

[43] Resconi, L.; Bossi, S.; Abis, L. *Macromolecules* **1990**, *23*, 4489–4491.

[44] Brintzinger, H. H.; Fischer, D.; Mülhaupt, R.; Rieger, B.; Waymouth, R. M. *Angewandte Chemie International Edition in English* **1995**, *34*, 1143–1170.

[45] Chen, E. Y.-X.; Marks, T. J. *Chemical Reviews* **2000**, *100*, 1391–1434.

[46] Zijlstra, H. S.; Harder, S. *European Journal of Inorganic Chemistry* **2015**, *2015*, 19–43.

[47] Andresen, A.; Cordes, H.-G.; Herwig, J.; Kaminsky, W.; Merck, A.; Mottweiler, R.; Pein, J.; Sinn, H.; Vollmer, H.-J. *Angewandte Chemie International Edition in English* **1976**, *15*, 630–632.

[48] Sinn, H.; Kaminsky, W.; Vollmer, H.-J.; Woldt, R. *Angewandte Chemie International Edition in English* **1980**, *19*, 390–392.

[49] Watkins, K. *Chemical & Engineering News* **2001**, *79*, 30–42.

[50] Harlan, C. J.; Mason, M. R.; Barron, A. R. *Organometallics* **1994**, *13*, 2957–2969.

[51] Harlan, C. J.; Bott, S. G.; Barron, A. R. *J. Am. Chem. Soc.* **1995**, *117*, 6465–6474.

[52] Ystenes, M.; Eilertsen, J. L.; Liu, J.; Ott, M.; Rytter, E.; Stï¿½vneng, J. A. *Journal of Polymer Science Part A: Polymer Chemistry* **2000**, *38*, 3106–3127.

[53] Ghiotto, F.; Pateraki, C.; Tanskanen, J.; Severn, J. R.; Luehmann, N.; Kusmin, A.; Stellbrink, J.; Linnolahti, M.; Bochmann, M. *Organometallics* **2013**, *32*, 3354–3362.

[54] Linnolahti, M.; Collins, S. *ChemPhysChem* **2017**, *18*, 3369–3374.

[55] Benn, R.; Rufinska, A.; Lehmkuhl, H.; Janssen, E.; Krüger, C.; Rufińska, A.; Lehmkuhl, H.; Janssen, E.; Krüger, C. *Angewandte Chemie International Edition in English* **1983**, *22*, 779–780.

[56] Sinn, H. *Macromol. Symp.* **1995**, *97*, 27–52.

[57] Mason, M. R.; Smith, J. M.; Bott, S. G.; Barron, A. R. *J. Am. Chem. Soc.* **1993**, *115*, 4971–4984.

[58] Imhoff, D. W.; Simeral, L. S.; Sangokoya, S. A.; Peel, J. H. *Organometallics* **1998**, *17*, 1941–1945.

[59] Giannetti, E.; Nicoletti, G. M.; Mazzocchi, R. *Journal of Polymer Science: Polymer Chemistry Edition* **1985**, *23*, 2117–2134.

[60] Zijlstra, H. S.; Collins, S.; McIndoe, J. S. *Chemistry - A European Journal* **2018**, *24*, 5506–5512.

[61] Zijlstra, H. S.; Linnolahti, M.; Collins, S.; McIndoe, J. S. *Organometallics* **2017**, *36*, 1803–1809.

[62] Manasevit, H. M. *J. Electrochem. Soc.: Solid State Science* **1971**, *118*, 647–650.

[63] Cheng, C.-W.; Apostolopoulos, G.; Fitzgerald, E. A. *Journal of Applied Physics* **2011**, *109*, 023714–1 – 023714–8.

[64] Bent, B. E.; Nuzzo, R. G.; Dubois, L. H. *Journal of the American Chemical Society* **1989**, *111*, 1634–1644.

[65] Fujita, S.; Oda, M.; Kaneko, K.; Hitora, T. *Japanese Journal of Applied Physics* **2016**, *55*, 1202A3–1 – 1202A3–9.

[66] Bludau, W.; Onton, A.; Heinke, W. *Journal of Applied Physics* **1974**, *451*, 1846–2924.

[67] Yim, W. M.; Stofko, E. J.; Zanzucchi, P. J.; Pankove, J. I.; Ettenberg, M.; Gilbert, S. L. *Journal of Applied Physics* **1973**, *44*, 1237–3851.

[68] Nepal, N.; Li, J.; Nakarmi, M. L.; Lin, J. Y.; Jiang, H. X. *Citation: Appl. Phys. Lett. Applied Physics Letters Journal of Applied Physics Journal of Applied Physics Journal of Applied Physics Journal of Applied Physics Journal of Applied Physics* **2005**, *87*, 242104–151907.

[69] Foronda, H. M.; Laurent, M. A.; Yonkee, B.; Keller, S.; Denbaars, S. P.; Speck, J. S. *Semiconductor Science and Technology* **2016**, *31*, 1–5.

[70] Tebbe, F. N.; Parshall, G. W.; Reddy, G. S. *Journal of the American Chemical Society* **1978**, *100*, 3611–3613.

[71] Pine, S. H.; R, Z.; Evans, D. A.; Grubbs, R. H. *Journal of the American Chemical Society* **1980**, *102*, 3270–3272.

[72] Thompson, R.; Nakamaru-ogiso, E.; Chen, C.-h.; Pink, M.; Mindiola, D. J. *Organometallics* **2014**, *33*, 429–432.

[73] Saito, S.; Yamamoto, H. *Chemical Communications* **1997**, 1585–1592.

[74] Yamamoto, H.; Saito, S. *Pure and Applied Chemistry* **1999**, *71*, 239–245.

[75] Yamamoto, H. *Proceedings of the Japanese Academie, Series B* **2008**, *84*, 134–146.

[76] Larsen, M. F.; Liu, A. Z.; Bishop, R. L.; Hecht, J. H. *Geophysical Research Letters* **2003**, *30*, 1375–1379.

[77] Hallwachs, W.; Schafarik, A. *Liebigs Annalen der Chemie* **1859**, *109*, 206–209.

[78] Bowdler Buckton, G.; Odling, W. *Proceedings of the Royal Society of London* **1865**, *14*, 19–21.

[79] Elschenbroich, C. *Organometallics*, 3rd ed.; Wiley VCH Verlag GmbH & Co. KGaA: Weinheim, Germany, 2006.

[80] Ziegler, K.; Koester, R.; *Production of Aluminiu Hydrocarbons*; 1958.

[81] Tsudera, T.; Tanaka, S.; Iwai, D.; Nishiwali, H.; Honma, T.; *High-Purity*

Trimethylaluminum and Purification Method of Crud Trimethylaluminum - US Patent 7,179,931 B2; 2007.

[82] Robin, M. B. *Inorganic Chemistry* **1962**, *1*, 337–342.

[83] Buser, H. J.; Schwarzenbach, D.; Petter, W.; Ludi, A. *Inorganic Chemistry* **1977**, *16*.

[84] Werner, A. *Zeitschrift für Anorganische und Allgemeine Chemie* **1893**, *3*, 267–330.

[85] Robinson, G. H.; Sangokoya, S. A. *J. Am. Chem. Soc.* **1987**, *109*, 6852–6853.

[86] Trost, B. M.; Van Vranken, D. L. *Chemical Reviews* **1996**, *96*, 395–422.

[87] Trost, B. M.; Crawley, M. L. *Chemical Reviews* **2003**, *103*, 2921–2944.

[88] Slinker, J.; Bernards, D.; Houston, P. L.; Abruña, H. D.; Bernhard, S.; Malliaras, G. G. *Chemical Communications* **2003**, 2392–2399.

[89] Schmitz, C.; Schmidt, H.-W.; Thelakkat, M. *Chemistry of Materials* **2000**, *12*, 3012–3019.

[90] Hoppe, D.; Hense, T. *Angewandte Chemie International Edition* **1997**, *36*, 2282–2316.

[91] Vogler, A.; Paukner, A.; Kunkely, H. *Coordination chemistry Reviews Elsevier Science Publishers B.V* **1990**, *97*, 285–297.

[92] Dotsenko, A. A.; Shcheka, O. L.; Vovna, V. I. *Journal of Structural Chemistry* **2017**, *58*, 1090–1100.

[93] Abdalla, J. A. B.; Riddlestone, I. M.; Tirfoin, R.; Aldridge, S. *Angewandte Chemie International Edition* **2015**, *54*, 5098–5102.

[94] Chen, J.; Falivene, L.; Caporaso, L.; Cavallo, L.; Chen, E. Y.-X. *Journal of the American Chemical Society* **2016**, *138*, 5321–5333.

[95] Langford, C. H.; Gray, H. B. *Ligand Substitution Processes*; W. A. Benjamin, Inc.: New York, 1965.

[96] Hugi-Cleary, D.; Helm, L.; Merbach, A. E. *Helvetica Chimica Acta* **1985**, *68*, 545–554.

[97] Saito, K. *Poiyhedron* **1990**, *93*, 215–222.

[98] Orvig, C. In *Coordination Chemistry of Aluminum*; Robinson, G. H., Ed.; VCH Verlagsgesellschaft mbH: Weinheim, 1993; pp 85–122.

[99] Bertsch, P. M.; Anderson, M. A. *Anal. Chem* **1989**, *61*, 535–539.

[100] Johanson, G. *Acta Chem. Scand.* **1960**, *14*, 771–773.

[101] Johanson, G. *Acta Chem. Scand.* **1962**, *16*, 403–420.

[102] Martin, R. B. *Journal of Inorganic Biochemistry* **1986**, *28*, 181–187.

[103] Mclachlan, D. R. C. *Neurobiology qlAcing* **1986**, *7*, 525–532.

[104] Crumbliss, A. L.; Garrison, J. M. *Comments Inorg. Chem.* **1988**, *8*, 1–26.

[105] Krewski, D.; Yokel, R. A.; Nieboer, E.; Borchelt, D.; Cohen, J.; Harry, J.; Kacew, S.; Lindsay, J.; Mahfouz, A. M.; Rondeau, V. *Journal of Toxicology and Environmental Health, Part BOnline) Journal Journal of Toxicology and Environmental Health, Part B* **2007**, *10*, 1093–7404.

[106] Rogers, M. A. M.; Simon, D. G. *Age and Ageing* **1999**, *28*, 205–209.

[107] Sorenson, J. R. J.; Campbell, I. R.; Tepper, L. B.; Lingg, R. D. *Environmental Health Perspectives* **1974**, *8*, 3–95.

[108] Driscoll, C. T. *Environmental Health Perspectives* **1985**, *63*, 93–104.

[109] Tam, S. C.; Williams, R. J. P. *Journal of Inorganic Biochemistry* **1986**, *26*, 35–44.

[110] Bertrand, P.; Jonas, A.; Laschewsky, A.; Legras, R. *Macromolecular Rapid Communications* **2000**, *21*, 319–348.

[111] Hdu, K. R. R. G.; Goodyear, C.; Control, I. *Technology and Culture* **2010**, *51*, 357–387.

[112] Awaja, F.; Gilbert, M.; Kelly, G.; Fox, B.; Pigram, P. J. *Progress in Polymer Science* **2009**, *34*, 948–968.

[113] Huang, Z.-M.; Zhang, Y.-Z.; Kotaki, M.; Ramakrishna, S. *Composites Science and Technology* **2003**, *63*, 2223–2253.

[114] Ioelovich, M. *BioResources* **2008**, *3*, 1403–1418.

[115] Syrbe, A.; Bauer, W. J.; Klostermeyer, H. *International Dairy Journal* **1998**, *8*, 179–193.

[116] Sauter, D.; Taoufik, M.; Boisson, C.; Sauter, D. W.; Taoufik, M.; Boisson, C. *Polymers* **2017**, *9*, 185.

[117] Hearle, J. W. S. *International Journal of Biological Macromolecules* **2000**, *27*, 123–138.

[118] Padamwar, M. N.; Pawar, A. P. *Journal of Scientific & Industrial Research* **2004**, *63*, 323–329.

[119] Qi, Y.; Wang, H.; Wei, K.; Yang, Y.; Zheng, R.-Y.; Kim, I. S.; Zhang, K.-Q.; Hardy, J. G.; Holland, C. *International Journal of Molecular Sciences* **2017**, *18*, 237–258.

[120] Hon, D. N.-S.; Srinivasan, K. S. V. *Journal of Applied Polymer Science* **1983**, *28*, 1–10.

[121] Deopura, B. L.; Alagirusam, R.; Joshi, M.; B, G. *Polyesters and Polyamides*; Elsevier B.V, 2008.

[122] Hu, J.; Chen, S. *Journal of Materials Chemistry* **2010**, *20*, 3346–3355.

[123] Puglia, D.; Manfredi, L. B.; Vazquez, A.; Kenny, J. *Polymer Degradation and Stability* **2001**, *73*, 521–527.

[124] Reghunadhan Nair, C. P. *Progress in Polymer Science* **2004**, *29*, 401–498.

[125] Witten, T. A.; Cohen, M. H. *Macromolecules* **1985**, *18*, 1915–1918.

[126] Koyama, Y.; Taniguchi, A. *Journal of Applied Polymer Science* **1986**, *31*, 1951–1954.

[127] Eldridge, E.; Ferry, D. *The Journal of Physical Chemistry* **1954**, *58*, 992–995.

[128] Winter, H. H. *Polymer Engineering and Science* **1987**, *27*, 1698–1702.

[129] Liu, H.; Ramsden, L.; Corke, H. *Starch - Stärke* **1999**, *51*, 249–252.

[130] Fernandez-Lafuente, R.; Rosell, C.; Rodriguez, V.; Guisan, J. *Enzyme and Microbial Technology* **1995**, *17*, 517–523.

[131] Förster, N.; Pöppler, A.-C.; Stalke, D.; Vana, P. *Polymers* **2013**, *5*, 706–729.

[132] Asmussen, E.; Peutzfeldt, A. *European Journal of Oral Sciences* **2001**, *109*, 282–285.

[133] Takeichi, T.; Kano, T.; Agag, T. *Polymer* **2005**, *46*, 12172–12180.

[134] Stevens, M. P. *Polymer Chemistry - An Introduction*; Oxford University Press: New York, Oxford, 1999.

[135] Oku, T.; Furusho, Y.; Takata, T. *Angewandte Chemie* **2004**, *116*, 984–987.

[136] Shirai, M. *Polymer Journal* **2014**, *46*, 859–865.

[137] Kwolleck, S. L.; *Wholly aromatic carbocyclic polycarbonamide fiber having orientation... - US 3819587 A - IP.com*; 1971. http://ip.com/pat/US3819587.

[138] Gabara, V. In *Ullmann's Encyclopedia of industrial Chemistry*, 2015; pp 1–21.

[139] Tanner, D.; Fitzgerald, J. A.; Phillips, B. R. *Angewandte Chemie International Edition in English* **1989**, *28*, 649–654.

[140] Tillet, G.; Boutevin, B.; Ameduri, B. *Progress in Polymer Science* **2010**, *36*, 191–217.

[141] Gibbons, W. A. *Industrial & Engineering Chemistry* **1939**, *31*, 1199–1209.

[142] Krejsa, M. R.; Koenig, J. L. *Rubber Chemistry and Technology* **1993**, *66*, 376–410.

[143] Nieuwenhuizen, P. J.; Reedijk, J.; van Duin, M.; McGill, W. J. *Rubber Chemistry and Technology* **1997**, *70*, 368–429.

[144] Seguela, R. *Journal of Polymer Science Part B: Polymer Physics* **2005**, *43*, 1729–1748.

[145] Séguéla, R. *Macromolecular Materials and Engineering* **2007**, *292*, 235–244.

[146] Fakirov, S. *Stoyko Fakirov Fundamentals of Polymer Science for Engineers*; Wiley-VCH Verlag GmbH & Co. KGaA, 2017.

[147] Nicholson, J. W. In *The Chemistry of Polymers*, 3rd ed.; Royal Society of Chemistry: Cambridge, 2006; pp 54–56.

[148] Flory, P. J. *Journal of the American Chemical Society* **1962**, *84*, 2857–2862.

[149] Morrison, F. A. *Understanding Rheology*; Oxford University Press: New York, Oxford, 2001.

[150] Sandolo, C.; Matricardi, P.; Alhaique, F.; Coviello, T. *Food Hydrocolloids* **2009**, *23*, 210–220.

[151] Montgomery, C. In *Effective and Sustainable Hydraulic Fracturing*; Bunger, A. P.; McLennan, J.; Jeffrey, R., Eds.; InTech, 2013; Vol. 3, Chapter 1.

[152] Li, L.; Al-Muntasheri, G. A.; Liang, F. *Petroleum* **2016**, *2*, 313–323.

[153] Palisch, T. T.; Vincent, M. C.; Handren, P. J. *SPE Production & Operations* **2010**, *25*, 327–344.

[154] Veatch, R. W.; Moschovidis, Z. A.; Fast, C. R. In *Recent Advances in Hydraulic*

Fracturing; SPE Monograph Series: Richardson, Texas, 1989; Chapter 1, pp 1–38.

[155] Montgomery, C. T.; Smith, M. B. *Journal of Petroleum Technology* **2010**, *62*, 26–40.

[156] Engelder, T.; Howarth, R. W. *Nature* **2011**, *477*, 271–275.

[157] Finkel, M. L.; Hays, J. *Journal of Epidemiology and Community Health* **2016**, *70*, 221–22.

[158] Finkel, M. *Nature* **2016**, *540*, 39–39.

[159] Inman, M. *Nature* **2016**, *531*, 22–24.

[160] *Hydraulic Fracturing: The Process | FracFocus Chemical Disclosure Registry - accessed 09/10/2017*. https://fracfocus.org/hydraulic-fracturing-how-it-works/hydraulic-fracturing-process.

[161] King, G. E. *SPE Hydraulic Fracturing Technology Conference* **2012**, 1–80.

[162] Stringfellow, W. T.; Kay, M.; Domen, J. K.; Sandelin, W. L.; Varadharajan, C.; Jordan, P. D.; Reagan, M. T.; Cooley, H.; Heberger, M. G.; Birkholzer, J. T. *Environmental Pollution* **2017**, *220*, 413–420.

[163] *Hydraulic Fracturing - accessed 11/09/2014*; 2014. http://www.umweltbundesamt.de/themen/wasser/gewaesser/grundwasser/nutzung-belastungen/fracking.

[164] Stringfellow, W. T.; Domen, J. K.; Camarillo, M. K.; Sandelin, W. L.; Borglin, S. *Journal of hazardous materials* **2014**, *275*, 37–54.

[165] Aminto, A.; Olson, M. S. *Journal of Natural Gas Science and Engineering* **2012**, *7*, 16–21.

[166] McIlvaine, R.; James, A. *World Pumps* **2010**, 16–18.

[167] Zhang, D.; Ranjith, P. G.; Perera, M. S. A. *Journal of Petroleum Science and Engineering* **2016**, *143*, 158–170.

[168] Smeltz, K. C.; *Organic Titanium Compositions And Their Use As Cross-Linkers - US Patent - 4,609,479*; 1986.

[169] Shaver, P. E.-p. F.; *Zirconium Chelates and Their Use For Cross-Linking - US Patent - 4,798,902*; 1989.

[170] Hodge, R. M.; *Hydraulic Fracturing Method Using Delayed Crosslinker Composition - US Patent - 4,657,081*; 1987.

[171] England, K. S. T. C.; *Hydraulic Fracturing Method - US Patent - 6,776,235 B1*; 2004.

[172] Agency, E. C.; *Candidate List of Substances of Very High Concern for Authorisation - accessed 11/10/2017*; 2017. https://echa.europa.eu/web/guest/candidate-list-table.

[173] Vengosh, A.; Kondash, A.; Harkness, J.; Lauer, N.; Warner, N.; Darrah, T. H. *Procedia Earth and Planetary Science* **2017**, *17*, 21–24.

[174] Rahm, D. *Energy Policy* **2011**, *39*, 2974–2981.

[175] Meng, Q. *Science of the Total Environment* **2016**, *580*, 953–957.

[176] Christenson, D. P.; Goldfarb, J. L.; Kriner, D. L. *Energy Policy* **2017**, *105*, 407–417.

[177] Wheatley, A. E. H. *Chemical Society Reviews* **2001**, *30*, 265–273.

[178] Aldridge, S. *Organometallic Chemistry* **2007**, *33*, 102–155.

[179] Ziegler, K. *Angewandte Chemie* **1952**, *64*, 323–329.

[180] Welch, G. C.; San Juan, R. R.; Masuda, J. D.; Stephan, D. W. *Science (New York, N.Y.)* **2006**, *314*, 1124–6.

[181] Stephan, D. W. *Organic and Biomolecular Chemistry* **2008**, *6*, 1535–1539.

[182] Stephan, D.; Erker, G. *Angewandte Chemie International Edition* **2010**, *49*, 46–76.

[183] Stephan, D. W. *Accounts of Chemical Research* **2015**, *48*, 306–316.

[184] Stephan, D. W. *Journal of the American Chemical Society* **2015**, *137*, 10018–10032.

[185] Stephan, D. W.; Erker, G. *Phil. Trans. R. Soc. A* **2017**, *375*, 1–2.

[186] Appelt, C.; Westenberg, H.; Bertini, F.; Ehlers, A. W.; Slootweg, J. C.; Lammertsma, K.; Uhl, W. *Angewandte Chemie* **2011**, *123*, 4011–4014.

[187] McMahon, C. N.; Bott, S. G.; Barron, A. R. *Journal of the Chemical Society, Dalton Transactions* **1997**, *0*, 3129–3138.

[188] Lewiński, J.; Zachara, J.; Justyniak, I. *Organometallics* **1997**, *16*, 4597–4605.

[189] Jeffery, E. A.; Mole, T. *Australian Journal of Chemistry* **1968**, *21*, 2683–2686.

[190] Drew, D. A.; Haaland, A.; Weidlein, J. *Zeitschrift für anorganische und allgemeine Chemie* **1973**, *398*, 241–248.

[191] Healy, M. D.; Wierda, D. A.; Barron, A. R. *Organometallics* **1988**, *7*, 2543–2548.

[192] Petrie, M. A.; Olmstead, M. M.; Power, P. P. *Journal of the American Chemical Society* **1991**, *113*, 8704–8708.

[193] Dagorne, S.; Atwood, D. A. *Chemical Reviews* **2008**, *108*, 4037–4071.

[194] Lewiński, J.; Zachara, J.; Starowieyski, K. B. *Journal of the Chemical Society, Dalton Transactions* **1997**, *0*, 4217–4222.

[195] Lewiński, J.; Bury, W.; Kopeć, T.; Tratkiewicz, E.; Justyniak, I.; Lipkowski, J. *European Journal of Inorganic Chemistry* **2005**, *2005*, 3414–3417.

[196] Lewiński, J.; Gos, P.; Kopec, T.; Lipkowski, J.; Luboradzki, R. *Inorganic Chemistry Communications* **1999**, *2*, 374–377.

[197] Leman, J. T.; Barron, A. R. *Organometallics* **1989**, *8*, 1828–1829.

[198] Schiff, H. *Justus Liebigs Annalen der Chemie.* **1832**, *131-132*, 118–119.

[199] Atwood, D. A.; Harvey, M. J. *Chemical Reviews* **2001**, *101*, 37–52.

[200] Zhang, W.; Loebach, J. L.; Wilson, S. R.; Jacobsen, E. N. *Journal of the American Chemical Society* **1990**, *112*, 2801–2803.

[201] Gurian, P. L.; Cheatham, L. K.; Zillerb, J. W.; Barron, A. R. *Journal of the Chemical Society, Dalton Transactions* **1991**, 1449–1456.

[202] Dzugan, S. J.; Goedken, V. L. *Inorganic Chemistry* **1986**, *25*, 2858–2864.

[203] Atwood, D. A.; Hill, M. S.; Jegier, J. A.; Rutherford, D. *Organometallics* **1997**, *16*, 2659–2664.

[204] Lewiński, J.; Zachara, J.; Justyniak, I.; Drank, M. *Coordination Chemistry Reviews* **2005**, *249*, 1185–1199.

[205] Ovitt, T. M.; Coates, G. W. *Journal of the American Chemical Society* **2002**, *124*, 1316–1326.

[206] Rutherford, D.; Atwood, D. A. *Organometallics* **1996**, *15*, 4417–4422.

[207] Thompson, E. J.; Myers, T. W.; Berben, L. A. *Angewandte Chemie International Edition* **2014**, *53*, 14132–14134.

[208] Kareiva, A.; Harlan, C. J.; MacQueen, D. B.; Cook, R.; Barron, A. R. *Chemistry of Materials* **1996**, *8*, 2331–2340.

[209] Lewiński, J.; Bury, W.; Justyniak, I.; Lipkowski, J. *Angewandte Chemie* **2006**, *118*, 2938–2941.

[210] Morita, H.; Yamane, H.; Kimura, Y.; Kitao, T. *Journal of Applied Polymer Science* **1990**, *40*, 753–767.

[211] Bury, W.; Chwojnowska, E.; Justyniak, I.; Lewiński, J.; Affek, A.; Zygadło-

Monikowska, E.; Bąk, J.; Florjańczyk, Z. *Inorganic Chemistry* **2012**, *51*, 737–745.

[212] Bethley, C. E.; Aitken, C. L.; Harlan, C. J.; Koide, Y.; Bott, S. G.; Barron, A. R. *Organometallics* **1997**, *16*, 329–341.

[213] Dickie, D. a.; Choytun, D. D.; Jennings, M. C.; Jenkins, H. a.; a.C Clyburne, J. *Journal of Organometallic Chemistry* **2004**, *689*, 2186–2191.

[214] Branch, C. S.; Lewiński, J.; Justyniak, I.; Bott, S. G.; Lipkowski, J.; Barron, A. R. *Journal of the Chemical Society, Dalton Transactions* **2001**, *0*, 1253–1258.

[215] Lewiński, J.; Justyniak, I.; Zachara, J.; Tratkiewicz, E. *Organometallics* **2003**, *22*, 4151–4157.

[216] Lewiński, J.; Zachara, J.; Justyniak, I. *Organometallics* **1997**, *16*, 3859–3862.

[217] Lewiński, J.; Zachary, J.; Justyniak, I. *Inorganic Chemistry* **1998**, *37*, 2575–2577.

[218] Redshaw, C.; Elsegood, M. R. J. *Chemical Communications* **2001**, *833*, 2016–2017.

[219] de Laeter, J. R.; Böhlke, J. K.; De Bièvre, P.; Hidaka, H.; Peiser, H. S.; Rosman, K. J. R.; Taylor, P. D. P. *Pure and Applied Chemistry* **2003**, *75*, 683–800.

[220] Farrell, K. *Comprehensive Nuclear Materials* **2012**, *5*, 143–175.

[221] Akitt, J. W. *Progress in NMR Spectroscopy* **1989**, *21*, 1–149.

[222] Haouas, M.; Taulelle, F.; Martineau, C. *Progress in Nuclear Magnetic Resonance Spectroscopy* **2016**, *94-95*, 11–36.

[223] Aramini, J. M.; Saponja, J. A.; Vogel, H. J. *Coordination Chemistry Reviews* **1996**, *149*, 193–229.

[224] Andre, P.; Macke, H. *Journal of Inorganic Biochemistry* **2003**, *97*, 315–323.

[225] Shapiro, P. J. *Coordination Chemistry Reviews* **1999**, *189*, 1–17.

[226] Pinkas, J.; Roesky, H. W. *Journal of Fluorine Chemistry* **2003**, *122*, 125–150.

[227] Tian, D.; Liu, B.; Gan, Q.; Li, H.; Darensbourg, D. J. *ACS Catalysis* **2012**, *2*, 2029–2035.

[228] Serna, C. J.; White, J. L.; Hem, S. *Soil Science Society of America* **1977**, *41*, 1009–1013.

[229] Barron, A. R. *Comments on Inorganic Chemistry* **1993**, *14*, 123–153.

[230] Pasynkiewicz, S. *Polyhedron* **1990**, *9*, 429–453.

[231] Atwood, J. L.; Hrncir, D. C.; Priester, R. D.; Rogers, R. D. *Organometallics* **1983**, *2*, 985–989.

[232] Koide, Y.; Barron, A. R. *Organometallics* **1995**, *14*, 4026–4029.

[233] Lewiński, J.; Zachara, J.; Goś, P.; Grabska, E.; Kopeć, T.; Madura, I.; Marciniak, W.; Prowotorow, I. *Chemistry - A European Journal* **2000**, *6*, 3215–3227.

[234] Barati, R.; Liang, J.-T. T. *Journal of Applied Polymer Science* **2014**, *131*, n/a–n/a.

[235] Funkhouser, G. P.; Norman, L. R. *International Symposium on Oilfield Chemistry* **2003**, 1–6.

[236] Thombare, N.; Jha, U.; Mishra, S.; Siddiqui, M. Z. *International Journal of Biological Macromolecules* **2016**, *88*, 361–372.

[237] *Organometallic Crosslinked Fluids*; 2013. http://www.halliburton.com/public/pe/contents/Data{_}Sheets/web/H/H05667.pdf.

[238] England, K. W.; Parris, M. D. *Society of Petroleum Engineers International* **2011**, *140400*, 1–13.

[239] Moorhouse, R.; Matthews, L. E.; *United States Patent - US 6,737,386 B1*; 2004.

[240] Kesavan, S.; Prud'homme, R. K. *Macromolecules* **1992**, *25*, 2026–2032.

[241] Parris, M. D.; Mackay, B. A.; Rathke, J. W.; Klingler, R. J.; Gerald Ii, R. E. *Macromolecules2* **2008**, *41*, 8181–8186.

[242] Wang, X.; Qu, Q.; McCarthy, S.; Null, J.; Bowen, K.; Neumann, L. F. *Society of Petroleum Engineers International* **2002**, *73789*, 1–7.

[243] HARRY, D. N.; MOORHOUSE, R.; MATTHEWS, L.; CHEN, G. In *SPE International Symposium on Oilfield Chemistry*; pp 669–674. http://cat.inist.fr/?aModele=afficheN{&}cpsidt=6241854.

[244] Weijers, L.; Griffin, L. G.; Sugiyama, H.; Shimamoto, T.; Takada, S.; Chong, K. K.; Terracina, J. M.; McDaniel, B. W.; Wright, C. A. *SPE - Asia Pacific Oil and Gas Conference* **2002**, 183–196.

[245] Altomare, A.; Cascarano, G.; Giacovazzo, C.; Guagliardi, A. *Journal of Applied Crystallography* **1994**, *27*, 435.

[246] Sheldrick, G. M. *Acta Crystallographica. Section A, Foundations of Crystallography* **2008**, *64*, 112–122.

[247] Jemil, S.; Fatemi, A.; Williamson, D. J.; Moore, G. R. *Journal of Inorganic Biochemistry* **1992**, *46*, 35–40.

[248] Babushkin, D. E.; Semikolenova, N. V.; Panchenko, V. N.; Sobolev, A. P.; Zakharov, V. A.; Talsi, E. P. *Macromolecular Chemistry and Physics* **1997**, *198*, 3845–3854.

[249] Florjanczyk, Z.; Bury, W.; Zygadlo-Monikowska, E.; Justyniak, I.; Balawender, R.; Lewinski, J.; Zygadzo-Monikowska, E.; Justyniak, I.; Balawender, R.; Lewinski, J. *Inorganic Chemistry* **2009**, *48*, 10892–10894.

[250] Justyniak, I.; Prochowicz, D.; Tulewicz, A.; Bury, W.; Goś, P.; Lewinski, J. *Dalton Transactions* **2017**, *46*, 669–677.

[251] Sim, G. A.; Robertson, J. M.; Goodwin, T. H. *Acta Crystallographica* **1955**, *8*, 157–164.

[252] Butterhof, C.; Martin, T.; Milius, W.; Breu, J. *Zeitschrift für anorganische und allgemeine Chemie* **2013**, *639*, 2816–2821.

[253] Hendershot, D. G.; Barber, M.; Kumar, R.; Oliver, J. P. *Organometallics* **1991**, *10*, 3302–3309.

[254] Schumann, H.; Frick, M.; Heymer, B.; Girgsdies, F. *Journal of Organometallic Chemistry* **1996**, *512*, 117–126.

[255] Uhl, W.; Molter, J.; Koch, R. *European Journal of Inorganic Chemistry* **1999**, *1999*, 2021–2027.

[256] Uhl, W.; Molter, J.; Saak, W. *Zeitschrift für anorganische und allgemeine Chemie* **1999**, *625*, 321–328.

[257] Eiden, P.; Liu, Q.; Zein, S.; Abedin, E.; Endres, F.; Krossing, I. *Chemistry - A European Journal* **2009**, *15*, 3426–3434.

[258] Keepers, J. W.; James, T. L. *Journal of Magnetic Resonance (1969)* **1984**, *57*, 404–426.

[259] Keeler, J. *Understanding NMR spectroscopy*, 2nd ed.; John Wiley & Sons: Chichester, UK, 2010.

[260] Vögeli, B. *Progress in Nuclear Magnetic Resonance Spectroscopy* **2014**, *78*, 1–46.

[261] Mei, X.; August, A. T.; Wolf, C. *Journal of Organic Chemistry* **2006**, *71*, 142–149.

[262] Schmitt, A.-L.; Schnee, G.; Welter, R.; Dagorne, S. *Chemical Communications* **2010**, *46*, 2480–2482.

[263] Wang, X.-M.; Sun, H.-S.; Wang, S.-X.; Huang, X.-Y.; Yotf, X.-Z. *J. Cryst. Growth J. Phys. Chem. Acta Cryst. Acta Cryst. Acta Cryst* **1996**, *43*, 213–223.

[264] Hogerheide, M. P.; Wesseling, M.; Jastryebski, J. T. B. H.; Boersma, J.; Kooijman, H.; Spek, A. L.; Van Koten, G. *Organometallics* **1995**, *14*, 4483–4492.

[265] Zaworotko, M. J.; Rogers, R. D.; Atwood, J. L. *Organometallics* **1982**, *1*, 1179–1183.

[266] Martell, A. E.; Motekaitis, R. J.; Smith, R. M. *Polyhedron* **1990**, *9*, 171–187.

[267] Atheaux, I.; *Personal Communication by Isabelle Atheaux, SGR*; 2018.

[268] Sokhanvarian, K.; Nasr-El-Din, H. A.; Harper, T. L. In *SPE Asia Pacific Unconventional Resources Conference and Exhibition*; Society of Petroleum Engineers; pp 1–16. http://www.onepetro.org/doi/10.2118/176837-MS.

[269] Armstrong, D. R.; Davies, R. P.; Linton, D. J.; Schooler, P.; Shields, G. P.; Snaith, R.; Wheatley, A. E. H. *Journal of the Chemical Society, Dalton Transactions* **2000**, 4304–4311.

[270] Naka, H.; Morey, J. V.; Haywood, J.; Eisler, D. J.; McPartlin, M.; García, F.; Kudo, H.; Kondo, Y.; Uchiyama, M.; Wheatley, A. E. H. *Journal of the American Chemical Society* **2008**, *130*, 16193–16200.

[271] Institute for Occupational Safety and Health of the German Social Accident Insurance; *Isobutane Safety Data Sheet*; 2017. http://gestis-en.itrust.de/nxt/gateway.dll/gestis{_}en/025040.xml?f=templates{\protect\T1\textdollar}fn=default.htm{\protect\T1\textdollar}3.0.

[272] Rao, C. N. R.; Natarajan, S.; Vaidhyanathan, R. *Angewandte Chemie International Edition* **2004**, *43*, 1466–1496.

[273] Brown, G. M.; Chidambaram, R. *Acta Crystallographica Section B* **1973**, *29*, 2393–2403.

[274] Woehler, S. E.; Wittebort, R. J.; Oh, S. M.; Kambara, t.; Hendrickson, D. N.; Inniss, D.; Strouse, C. E. *Journal of the American Chemical Society* **1987**, *109*, 1063–1072.

[275] Qin, J.; Liao, Y.; Chen, X. Y.; Qian, C. X.; Zuo, J. L.; You, X. Z. *Journal of Organometallic Chemistry* **2012**, *716*, 275–280.

[276] Micklitz, W.; Bott, S. G.; Bentsen, J. G.; Lippard, S. J. *Journal of the American Chemical Society* **1989**, *111*, 372–374.

[277] Hubert-Pfalzgraf, L. G. *Coordination Chemistry Reviews* **1998**, *178-180*, 967–997.

[278] Grunova, E.; Roisnel, T.; Carpetier, J.-F. *Dalton Transactions* **2009**, 9010–9019.

[279] Lewiński, J.; Dutkiewicz, M.; Lesiuk, M.; Śliwiński, W.; Zelga, K.; Justyniak, I.; Lipkowski, J. *Angewandte Chemie International Edition* **2010**, *49*, 8266–8269.

[280] Bury, W.; Justyniak, I.; Prochowicz, D.; Rola-Noworyta, A.; Lewinki, J. *Inorganic Chemistry* **2012**, *51*, 7410–7414.

[281] Wróbel, Z.; Pietrzak, T.; Justyniak, I.; Lewiński, J. *Chemical Communications* **2017**, *53*, 10808–10811.

[282] Chen, M.-T.; Chen, C.-T. *Dalton Transactions* **2017**, *46*, 10181–10184.

[283] Lewiński, J.; Śliwiński, W.; Dranka, M.; Justyniak, I.; Lipkowski, J. *Angewandte Chemie International Edition* **2006**, *45*, 4826–4829.